Brain Dynamics as Confirmatory Biomarker of Dementia with Lewy Bodies Versus Alzheimer's Disease - an Electrophysiological Study

Ramtin Mehraram

Thesis submitted for the degree of Doctor of Philosophy

Newcastle University Translational and Clinical Research Institute

September 2020

Abstract

Introduction

Dementia with Lewy bodies (DLB), Parkinson's disease dementia (PDD) and Alzheimer's disease dementia (AD) are associated with different pathologies. Nevertheless, symptomatic overlap between these conditions may lead to misdiagnosis. Resting-state functional connectivity features in DLB as assessed with electroencephalography (EEG) are emerging as diagnostic biomarkers. However, their pathological significance is still questioned. This study aims to further investigate this aspect and to infer functional and structural sources of EEG abnormalities in DLB.

Methods

Graph theory analysis was first performed to assess EEG network differences between healthy controls (HC) and dementia groups. Source localisation and Network Based Statistics (NBS) were used to infer EEG cortical network and dominant frequency (DF) alterations in DLB compared with AD. Further analysis aimed to assess the subnetwork associated with visual hallucination (VH) symptom in DLB and PDD, i.e. LBD, compared with not-hallucinating (NVH) patients. Finally, probabilistic tractography was performed on diffusion tensor imaging (DTI) data between cortical regions, thalamus, and basal forebrain (NBM). Correlation between structural and functional connectivity was tested.

Results

EEG α-band (7-13.5 Hz) network features were affected in LBD compared with HC, whilst DLB β-band network (14-20.5 Hz) was weaker and more segregated when compared with AD. This scenario replicated in the source domain. DF was significantly lower in DLB compared with AD, and positively correlated with structural connectivity strength between NBM and the cortex. Functional visual ventral network connectivity and cholinergic projections towards the cortex were affected in VH compared with NVH, and significantly correlated in NVH.

Conclusions

Functional connectivity as assessed with EEG is more affected in DLB compared with AD. Moreover, the visual ventral network is functionally altered in VH compared with NVH. Results

from structural analysis provide empirical evidence on the role of cholinergic dysfunctions in DLB and PDD pathology and corresponding functional correlates.

Acknowledgements

First, I would like to thank my supervisors Prof Marcus Kaiser and Prof John-Paul Taylor for their important support, guidance, and encouragement throughout my PhD project. I would especially like to thank my former supervisor Dr Luis Peraza for believing in me and giving me such an incredible opportunity, patiently supporting me through every step of my research, and providing me with his precious help through my (first) first authored publication, which is also reported in this thesis.

I am thankful to all the people involved in the design and data collection for the CATFieLD and VEEG-Stim studies, which were analysed in the present thesis. Thanks to their important work I could start my research project focusing directly on data analysis.

I owe my gratitude to the members of the Lewy body lab and the ICO_2S research groups for their support and exchange of ideas which made my research more proficient. I would like to specifically thank Dr Sean Colloby for his valuable and prompt help with MRI data, Dr Julia Schumacher for her advice and technical help throughout my project, and Dr Michael Firbank for his help and advice with DTI data. I wish to thank the members of my research panel Dr Yujiang Wang and Prof Ian McKeith for their advice throughout my project development. Additionally, I would like to thank Prof Li Su and his research group for their advice and brainstorm during the final part of my PhD project.

I also appreciated the incredible opportunities offered by Newcastle University, which allowed me to improve my personal skills and become a TEDx speaker, and deliver a public lecture within the Newcastle University INSIGHTS Public Lectures program as winner of the speakers competition.

Finally, I wish to thank my family, friends, colleagues, and whoever supported me throughout this experience and helped me to make it incredibly enjoyable.

Funding body. The NIHR Newcastle Biomedical Research Centre (BRC) is a partnership between Newcastle Hospitals NHS Foundation Trust and Newcastle University, funded by the National Institute for Health Research (NIHR). The research presented in this thesis was funded by the National Institute for Health Research (NIHR) Newcastle Biomedical Research Centre (BRC). The views expressed are those of the author and not necessarily those of the

NIHR or the Department of Health and Social Care. The study—participant recruitment and data collection—was funded by an intermediate clinical Wellcome Trust Fellowship (WT088441MA) to J.-P.T.

Declaration

I have not taken part in participants recruitment, nor data collection, for the analyses presented in this thesis. People involved in these processes are members of the Lewy Body Lab at Newcastle University, and comprise Dr Ruth Cromarty, Dr Sara Graziadio, Alison Killen, Dr Nicholas Murphy, Dr Michael Firbank, and Prof John-Paul Taylor. Segmentation of structural images and cortical thickness extraction in Chapter 6 were performed and provided by Dr Sean Colloby; in the same chapter, subcortical volume values were computed by Dr Julia Schumacher. Any other analysis, statistics, and thesis writing work were produced entirely by me.

The study presented in Chapter 3 is also reported in the following publication:

Mehraram, R., Kaiser, M., Cromarty, R., Graziadio, S., O'Brien, J.T., Killen, A., Taylor, J.P. and Peraza, L.R. (2019) 'Weighted network measures reveal differences between dementia types: An EEG study', *Hum Brain Mapp*.

Table of Contents

List of Figures

List of Tables

Abbreviations

AChEI - Acetylcholinesterase inhibitor

AD – Alzheimer's disease dementia

ANCOVA – Analysis of covariate

ANOVA – Analysis of variance

ANTs – Advanced Normalisation Tools

ASL – Arterial spin labelling

AUROC – Area under receiver operating characteristic

BCT – Brain connectivity toolbox

C – Clustering coefficient

CAF – Clinical Assessment of Fluctuation

CAMCOG – Cambridge Cognitive Examination

CATFieLD – Cognitive and Attentional Function in Lewy Body Diseases

CSF – Cerebrospinal fluid

CTh – Cortical thickness

DAN – Dorsal attentional network

DCM – Dynamic casual modelling

DF – Dominant (power-spectrum) frequency

DFV – Dominant frequency variability

DLB – Dementia with Lewy bodies

DMN – Default mode network

DTI – Diffusion tensor imaging

EEG – Electroencephalography

eLORETA – Exact low-resolution brain electromagnetic tomography

EPI – Echo-planar imaging

ERP – Event-related potential

FA – Fractional anisotropy

FIR – Finite impulse response

fMRI – functional magnetic resonance imaging

FWER – Family wise error rate

GABA - γ-aminobutyric acid

GM – Grey matter

HC – Healthy controls

ICA – Independent component analysis

iEEG – Intracranial electroencephalography

IPSP – Inhibitory post synaptic potential

IT – Inferior-temporal cortex

K – Node degree

L – Average characteristic path length

LB – Lewy bodies

LBD – Lewy body dementia (DLB + PDD)

LEDD – Levodopa equivalent daily dose

LFP – Local field potential

LN – Lewy neurites

MAPE – Mean absolute percentage error

MCI – Mild cognitive impairment

MD – Mean diffusivity

MEG – Magnetoencephalography

MMSE – Mini-Mental State Examination

MNE – Minimum norm estimate

MNI – Montreal Neurological Institute

MPRAGE - Magnetisation prepared rapid gradient echo

MRI – Magnetic resonance imaging

MST – Minimum spanning tree

NBM – Nucleus basalis of Meynert

NBS – Network Based Statistics

NPI – Neuropsychiatric Inventory

NPV – Negative predictive value

NVH – Without visual hallucination

ODFAS – One-day fluctuations scale

PAD – Perception and attention deficit

PD – Parkinson's disease

PDD – Parkinson's disease dementia

PET – Positron emission tomography

PFC – Prefrontal cortex

PLI – Phase lag index

PPV – Positive predictive value

PSG – Polysomnography

PT% - Threshold percentage

PTE – Phase transfer entropy

Q – Modularity

qEEG – Quantitative electroencephalography

RBD – Rapid eye movement sleep behaviour disorder

RD – Radial diffusivity

REM – Rapid eye movement

ROI – Region of interest

sLORETA – Standardized low-resolution brain electromagnetic tomography

SPECT – Single Photon Emission Computed Tomography

SPM – Statistical Parametric Mapping

SPSS – Statistical Package for Social Sciences

SSE – Sum of squares error

TMS – Transcranial magnetic stimulation

$\mathbf{t_{th}}$ – Test statistics threshold

UPDRS – Unified Parkinson's Disease Rating Scale

V – Volume

VAN – Ventral attentional network

VBM – Voxel-based morphometry

VEEG-Stim – Visual hallucinations: an EEG and non-invasive Stimulation

VH – Visual hallucinations

WM – White matter

WPLI – Weighted phase lag index

σ – Small-worldness

Chapter 1. Introduction

1.1. Dementia with Lewy Bodies

Dementia with Lewy bodies (DLB) is the second most common form of dementia, following Alzheimer's disease dementia (AD), accounting from 4% up to 10% of clinically diagnosed dementia cases (McKeith *et al.*, 2007; Vann Jones and O'Brien, 2014; Walker *et al.*, 2015). A diagnosis of dementia is generally associated with progressive cognitive decline significantly affecting social and occupational functions (World Health Organisation, 2012). People with DLB also develop specific core symptoms, as reported in the most recent diagnostic criteria for DLB (McKeith *et al.*, 2017):

- Cognitive fluctuations: people with DLB present at least one alteration experience in cognitive functions, such as attention and arousal (Walker *et al.*, 2000; Ballard *et al.*, 2001a; McKeith *et al.*, 2005), which can also include daytime drowsiness and disorganised speech (Bradshaw *et al.*, 2004).
- Rapid eye movement (REM) sleep behaviour disorder (RBD): 76% of DLB patients present altered REM sleep atonia (Ferman *et al.*, 2011; Ferini-Strambi *et al.*, 2014; Chan *et al.*, 2018), and may move repeatedly while dreaming (Boeve *et al.*, 2007).
- Parkinsonism: at later stages of the pathology, over 85% of DLB patients develop variable parkinsonian features, including postural and gait disorder (Louis *et al.*, 1995; Burn *et al.*, 2003; Hershey and Irwin, 2018).
- Complex visual hallucinations: being one of the most common symptoms, hallucinations to different degrees occur in 80% of DLB patient (Collerton *et al.*, 2005; McKeith, 2007a; Mosimann *et al.*, 2008). Hallucinatory phenomena feature people, children and/or animals. This symptom is described in detail in section 1.2.

Other clinical symptoms which are frequently associated with DLB include autonomic dysfunction, anxiety, and delusions.

An effective disease modifying treatment for DLB does not exist yet. However, different forms of medication have been shown to produce positive effects on the symptoms. These include acetylcholinesterase inhibitors and memantine, which are used to attenuate attentional

deficits and visual hallucinations (Aarsland *et al.*, 2009; Burghaus *et al.*, 2012; Wang *et al.*, 2015). Parkinsonism in generally treated with levodopa (Bonelli *et al.*, 2004; Molloy *et al.*, 2005; Taylor *et al.*, 2020).

1.1.1. Pathology

At later stages, DLB pathology and symptoms are the same as those in Parkinson's disease dementia (PDD) (McKeith, 2007b). In fact, both syndromes are associated with the development of a Lewy body disease (Kosaka *et al.*, 1984) and belong to the Lewy body dementia (LBD) umbrella definition. The aetiology of LBD is likely to be a progressive build-up of alpha-synuclein protein bodies, known as Lewy bodies (LB), and thread-like Lewy neurites (LN) across the brain (Baba *et al.*, 1998; Mattila *et al.*, 1998; Braak *et al.*, 2003). As described in the Braak stages (Braak *et al.*, 2003), Parkinson's disease (PD) is initially associated with a high number of LN, outnumbering LB, over the dorsal motor nucleus of the medulla oblongata and within intermediate reticular area. As the pathology progresses, LN and LB spread across the medulla oblongata towards projection neurons of the raphe nuclei and the reticular formation, also affecting the brainstem and the coeruleus-subcoeruleus complex in the pontine tegmentum. As LB number increases, the midbrain is also affected, and protein bodies spread across the substantia nigra and the basal forebrain. Dopaminergic cells of the pars compacta are then affected, as well as the mesocortex and allocortex. Olfactory areas become severely damaged as the pathology spreads across the neocortex and its pyramidal cells, involving sensory association areas, the insular fields, the anterior cingulate cortex, and prefrontal areas. Primary areas are lastly affected. Dementia from PD is thought to be driven by LB density in the neocortex at the latest stage of the pathology (de Vos *et al.*, 1995; Tsuboi *et al.*, 2007), although the role of α-synuclein pathology in disease development is still a matter of speculation (Schapira and Jenner, 2011; Weil *et al.*, 2017).

On the other hand, many DLB cases are associated predominantly with cortical presence of LB rather than in lower brain regions (Kosaka, 1978; Harding *et al.*, 2002; Frigerio *et al.*, 2011). Although DLB is also associated with the extent of LB burden throughout the brain (Beach *et al.*, 2009) and dopaminergic degeneration (Walker *et al.*, 2002; O'Brien *et al.*, 2004), it may also coexist with AD (McKeith *et al.*, 2005; Weisman *et al.*, 2007). In this latter case,

discrimination depends on the extent to which AD-type pathology co-exists with the presence of LB (McKeith *et al.*, 2005). DLB symptoms have been also shown to be specifically associated with reduced cholinergic activity and dopaminergic deficit throughout the brain (Perry *et al.*, 1991; Tiraboschi *et al.*, 2000; Tiraboschi *et al.*, 2002; Lemstra *et al.*, 2003; Delli Pizzi *et al.*, 2015b).

1.1.2. Symptomatic overlap and difference with other dementia types

Pathological inconsistency between conditions also emerges at symptomatic level. In fact, people with DLB first develop cognitive disorders, followed by parkinsonism at later stages. According to the "one-year rule" (McKeith *et al.*, 2005; McKeith, 2007b), DLB patients develop bradykinesia, tremor and rigidity (Hornykiewicz and Kish, 1987; Gaig and Tolosa, 2009) one year after the onset of cognitive impairment. In PDD instead, as already stated above, cognitive symptoms develop at the advanced stage of PD. Although AD shows slower rate of cognitive decline compared with DLB (Blanc *et al.*, 2017) as well as more severe memory impairment (Hamilton *et al.*, 2004; Ricci *et al.*, 2009), symptomatic overlap exists between the two conditions at early stages, and is a major contributor to the misdiagnosis of DLB (Palmqvist *et al.*, 2009). Over the recent years, the diagnostic criteria for DLB (McKeith *et al.*, 1996; McKeith *et al.*, 2005; McKeith *et al.*, 2017) aimed to improve discrimination accuracy between DLB and AD (Vann Jones and O'Brien, 2014; Rizzo *et al.*, 2018). The latest guidelines recommend probable DLB diagnosis when two or more core clinical features are present (McKeith *et al.*, 2017). Biomarkers are also included and classified as indicative and supportive. In fact, probable DLB is also diagnosed when an indicative biomarker exists with at least one core clinical feature. Indicative biomarkers include:

- Reduced dopaminergic Ioflupane (commercially known as DaT) uptake in basal ganglia as assessed with Single Photon Emission Computed Tomography (SPECT) (Brigo *et al.*, 2015; McCleery *et al.*, 2015; Shimizu *et al.*, 2017). This has been reported to provide with sensitivity of 77.7% and specificity of 90.4% (McKeith *et al.*, 2007).
- Reduced uptake on ^{123}Iodine-MIBG myocardial scintigraphy (Watanabe *et al.*, 2001; Hanyu *et al.*, 2006; Kobayashi *et al.*, 2009). This is a non-invasive technique used to assess cardiac nerve damage (Glowniak *et al.*, 1989), a common pathological outcome

in LBD. Sensitivity and specificity are respectively 69% and 89%, with higher percentages in milder cases (Yoshita *et al.*, 2015).

- RBD confirmation through Polysomnography (PSG), which has been shown to be associated with high probability of synucleinopathy in people with dementia (Boeve *et al.*, 2008; Boeve *et al.*, 2013; Pao *et al.*, 2013; Bugalho *et al.*, 2019).

Supportive biomarkers do not show high specificity. Nevertheless, they provide useful information in the diagnostic context. These include:

- Reduced medial temporal lobe atrophy in DLB compared with AD, as assessed with MRI or CT scan (Barber *et al.*, 2000b; Burton *et al.*, 2009). Accuracy of 66% was reported for this biomarker in a multicentre study based on autopsy confirmation (Harper *et al.*, 2016).
- Reduced uptake on SPECT and positron emission tomography (PET) metabolism scan is associated with reduced activity over the occipital cortex in DLB (Higuchi *et al.*, 2000; Lobotesis *et al.*, 2001; Shimizu *et al.*, 2005).
- Dominant power spectrum frequency (DF) revealed with electroencephalography (EEG) reduced over the occipital lobe and other altered patterns in DLB and its prodromal stage, correlating with clinical scores (Bonanni *et al.*, 2008; Peraza *et al.*, 2018).

Due to its portability and low-cost (Lee and Tan, 2006), EEG is emerging as a promising diagnostic tool for several conditions including epilepsy (Smith, 2005; Acharya *et al.*, 2012; Mirandola *et al.*, 2017) and AD (Rodriguez *et al.*, 1999; Bennys *et al.*, 2001; Moretti *et al.*, 2004). However, research on DLB has not been extensive to date (Law *et al.*, 2020), and existing studies are discussed in the next sections. The main scope of this thesis project was to detect differential EEG biomarkers to discriminate DLB versus AD. Due to their high specificity in DLB discrimination against DLB and coexisting pathology cases with prominent AD (Tiraboschi *et al.*, 2006; Jicha *et al.*, 2010; Toledo *et al.*, 2013; Yoshizawa *et al.*, 2013), visual hallucinations were also a matter of interest in this thesis; investigation on functional and structural correlates of this clinical feature is reported in Chapter 6.

1.2. Visual Hallucinations in Lewy Body Dementia

Single experiences of visual perception not matching with reality are quite common phenomena (McKellar, 1957; Ohayon, 2000), in some cases felt as either neutral or comforting (Grimby, 1993; Paulson, 1997; Collerton *et al.*, 2005). However, they can be disturbing in pathological conditions as misperceptions and visual hallucinations (VH) become a recurrent and complex condition.

Generally speaking, VH differ from misperceptions and illusions, as they are not necessarily triggered by non-environmental stimuli (Asaad and Shapiro, 1986; Brasić, 1998; Collerton *et al.*, 2005). Collerton and colleagues proposed a definition for complex VH as "repetitive involuntary images […] experienced as real […] for which there is no objective reality" (Collerton *et al.*, 2005). VH were already described during the ninth-century in the Persian literature (Gorji and Ghadiri, 2002), and later became a matter of interest in different disorders, such as epilepsy, migraine (Panayiotopoulos, 1994), schizophrenia (Stefan *et al.*, 1989; Oertel *et al.*, 2007), Charles Bonnet syndrome (Howard *et al.*, 1998; Hanoglu *et al.*, 2016) and dementia (Burn *et al.*, 2006; Onofrj *et al.*, 2019). In fact, LBD is among the syndromes associated with highest rates of complex VH. As opposed to simple VH, complex hallucinations may include unrecognised as well as familiar images, mostly featuring people and animals, but also inanimate objects (Aarsland *et al.*, 2001; Burghaus *et al.*, 2012). Hallucinatory episodes tend to be short, and mostly occur at night or in reduced environmental brightness (Fénelon *et al.*, 2000; Barnes and David, 2001; Holroyd *et al.*, 2001). This latter aspect resonates with evidence that the eye condition may also be a risk factor for VH, as also reported for Charles Bonnet Syndrome, where VH is associated with eye disease-related vision impairment (Schultz and Melzack, 1991; Teunisse *et al.*, 1996).

1.2.1. Pathology

The pathological mechanisms associated with VH in LBD are not clear yet. Early studies speculated that VH might be a consequence of dopaminergic treatment (Fénelon *et al.*, 2000; Collerton *et al.*, 2005; Williams and Lees, 2005), due to evidence of levodopa or clozapine induced hallucinatory experience (Devanand and Levy, 1995; Cannas *et al.*, 2001). However,

the majority of studies do not report any correlation between medication and VH characteristics (Goetz *et al.*, 1998; Harding *et al.*, 2002; Williams and Lees, 2005). In fact, VH are thought to be associated with LBD-related impairment of cholinergic and dopaminergic systems (Ballard *et al.*, 2000; Harding *et al.*, 2002; Diederich *et al.*, 2005; Shine *et al.*, 2011; Shine *et al.*, 2014; Onofrj *et al.*, 2019). Autopsy studies have also reported higher LB burden within the ventral visual network, i.e. occipital and temporal cortical lobes, in LBD patients (Harding *et al.*, 2002; Williams and Lees, 2005; Gallagher *et al.*, 2011). The involvement of the cholinergic system in VH physiology is suggested by the ability of cholinergic drugs to suppress VH (Perry and Perry, 1995). This hypothesis is also supported by recent studies demonstrating greater burden of LB and damaged white matter (WM) fibre tracts within the nucleus basalis of Meynert (NBM) in LBD with VH (Hepp *et al.*, 2017a; Sakai *et al.*, 2019). The NBM is located in the basal forebrain (Heimer *et al.*, 1999), and is in fact the primary source of cholinergic innervations projecting to the cerebral cortex (Mesulam, 1990; Selden *et al.*, 1998; Hepp *et al.*, 2017a).

1.2.2. Computational models

Multiple attempts have been pursued during the recent years to implement computational models describing VH phenomenology in multiple disorders. Based on a previous study (Horowitz, 1975), Collerton and colleagues proposed the Perception and Attention Deficit (PAD) model, based on VH in DLB (Collerton *et al.*, 2005). According to this model, recurrent complex VH are a consequence of disrupted visual perception of objects and impaired attentional processes, which in the context of scene representation lead to wrong objects representation. This implementation builds on previous psychology models, which represent visual perception as a result of an interaction between attentional-mnemonic top-down neuronal processes and bottom-up sensory input. These two streams are thought to involve respectively the prefrontal cortex (PFC) and inferior-temporal cortex (IT), and the occipital region and IT. The PAD model combines the psychological perspective with DLB pathology and manipulation of cholinergic system. Hence, disrupted cholinergic projection might affect the interaction between the top-down and bottom-up streams, being the underlying driver of VH in DLB (Angela and Dayan, 2002; Collerton *et al.*, 2005).

The idea of a mismatch between top-down attentional network and bottom-up sensory stream in VH nicely resonates with most of the literature describing the visual system. Both information flows are thought to exist in the so called ventral visual network, which has a major role in object recognition (Bar, 2003). As mentioned above, this network comprises the lower-level visual areas, which project towards the IT and to the PFC. According to existing models, a rough version of visual information is rapidly sent from the primary visual area to the PFC, which based on information already stored in memory and scene context, produces a range of predictions. These are projected back to the IT and, together with contextual and emotional response originating respectively in the hippocampus and amygdala, are matched with the information later provided through the bottom-up sensory stream. A successful matching will produce a correct object perception (Bar, 2003; Bar *et al.*, 2006; Chaumon *et al.*, 2009; Gamond *et al.*, 2011; Chaumon *et al.*, 2014; O'Callaghan *et al.*, 2017).

In a recently developed model of VH in DLB based on these assumptions, authors showed that wrong visual perception is associated with both disrupted projection from the occipital to the PFC and impaired communication between occipital and temporal areas. This might lead to altered communication between the PFC and the IT, hence the mismatch between the two visual processing streams (Tsukada *et al.*, 2015) as proposed in the PAD model. Shine *et al.* (2011) proposed a more complex perspective through a model of VH phenomenology in PD. This model assumes that attentional networks are involved in processing visual perception, and VH are due to over activation of default mode network (DMN) and ventral attentional network (VAN) relatively to the dorsal attentional network (DAN). DMN consists of synchronised activation of temporal, prefrontal and parietal regions which occurs in resting-state, i.e. during mind wandering (Binder *et al.*, 1999; Mazoyer *et al.*, 2001; Raichle, 2015). The VAN comprises lateral and inferior PFC, temporoparietal junction and ventral areas, and is associated with stimulus driven attentional processes (Corbetta and Shulman, 2002; Menon and Uddin, 2010), whilst DAN involves sustained activation of frontoparietal areas and is associated with top-down cognitive control of attentional focus (Kastner *et al.*, 1999; Shulman *et al.*, 1999; Corbetta *et al.*, 2000; Siegel *et al.*, 2008; DiQuattro and Geng, 2011; Simpson *et al.*, 2011). Similarly to the model developed by Tsukada *et al.* (2015) and the PAD model (Collerton *et al.*, 2005), interaction between bottom-up and top-down attentional streams is proposed to be affected, as DAN is wrongly engaged by DMN and VAN, making internal

imagery prevail over actual perception. On the other hand, it is proposed here that visual processing impairment alone is not sufficient to describe VH symptom and its related pathological mechanisms, and more extensive network alterations should be taken in account.

1.2.3. Experimental evidence supporting VH-related models

Consistency of developed models was partly confirmed by empirical results. In a recent work, authors used voxel-based morphometry (VBM) and found major grey matter atrophy over the frontal gyri, as well as insula and caudate nucleus in DLB with VH (Pezzoli *et al.*, 2019). Glucose hypometabolism was also reported in LBD with VH over the occipital and temporal areas compared with the control group (Pasquier *et al.*, 2002; Gasca-Salas *et al.*, 2016). This finding was also confirmed in a recent study with arterial spin labelling (ASL) magnetic resonance imaging (MRI) (Taylor *et al.*, 2012), which is a technique that allows for the measurement of tissue blood flow using labelled arterial blood water protons as intrinsic tracer (Petcharunpaisan *et al.*, 2010). In addition, Taylor *et al.* (2012) also reported reduced cortical activation in DLB with VH during a visual task over higher level visual areas, including V5, MT and lateral occipital cortex, as assessed with functional MRI (fMRI). Supporting these findings, significantly greater grey matter atrophy was also found in PD with VH compared with PD without VH (NVH), as well as reduced occipital activity assessed with γ-aminobutyric acid (GABA) levels, detected with magnetic resonance spectroscopy (MRS) (Firbank *et al.*, 2018). MRS GABA level reflects GABAergic activity, which is thought to be associated with synchronisation of inhibitory interneurons by perisomatic postsynaptic potentials (Lytton and Sejnowski, 1991; Buzsáki and Wang, 2012).

In support of PD-VH model developed by Shine *et al.* (2011), one recent study investigated brain fMRI response in a task featuring bistable, i.e. ambiguous, and monostable, i.e. well defined, images in PD patients with and without VH (Shine *et al.*, 2012; Shine *et al.*, 2014). In either type of images, VH group showed reduced activation of DAN regions, associated with lower task performance score. Reduced activation of DAN during the task was significantly associated with reduced resting state functional connectivity between attentional networks. Moreover, reduced resting state connectivity between VAN and DMN was detected in VH, and functional alterations were associated with reduced grey matter (GM) volume within the

anterior insula (Shine *et al.*, 2014). These findings are in line with other fMRI studies reporting DMN over-activation associated with VH in LBD (Yao *et al.*, 2014; Franciotti *et al.*, 2015). Another work found significant reduction of functional connectivity across the whole brain in PD-VH compared with controls, as well as in areas belonging to attentional networks. However, no significant differences were found between PD-VH and PD-NVH (Hepp *et al.*, 2017b).

1.3. Electroencephalography

Electroencephalography (EEG) is progressively emerging in research and clinical framework due to its low cost (Lee and Tan, 2006), efficiency and portability. It consists of the recording of the electrical activity of the brain from the scalp using a wearable cap made of sensors (Berger, 1929). The outcome of the recording consists of as many voltage signals as sensors available in the cap. Recorded signals reflect the current flowing in pyramidal neuron populations, located over the external layer of the cerebral cortex and normally oriented with respect to the scalp (Lopes da Silva, 2013).

1.3.1. Frequency bands

The physiological interpretation of the recorded signals depends on their activity at different oscillation frequencies. In fact, brain electrical activity ranges between infraslow and very fast oscillations. Save for variability across studies, EEG oscillatory activity has been conventionally classified in frequency bands, which can be associated with specific physiological mechanisms depending on where in the brain the activity occurs. Generally, lower frequency bands have a spatial integration role, whilst higher range activity is involved in information transfer within discrete neuronal populations (Lopes da Silva, 2013). In detail:

- **Delta (δ) band.** Delta (δ) band ranges between about 0.2 to 3.5 Hz. Signal waves within the δ-band become prominent all over the cerebral cortex during sleep, and they are thought to have an active role in memory consolidation (Tononi and Cirelli, 2003; Walker and Stickgold, 2006; Rasch and Born, 2013). Correlation between δ-band activity and memory consolidation during sleep emerges using transcranial magnetic

stimulation (TMS) induced low frequency waves; it has been reported that participant receiving TMS stimulation during non-REM sleep presented better memory retention compared with participants receiving higher frequency stimulation (Marshall *et al.*, 2006). In line with this hypothesis, lower δ activity during sleep has been reported in patients with amnestic mild cognitive impairment (MCI), a condition involving impaired memory, that can potentially progress towards AD (Barabash *et al.*, 2009). Prominent δ activity was also found to be a specific feature in patients who had an ischemic stroke (Jordan, 2004; Finnigan *et al.*, 2016) and, when localised, to be associated with white matter lesions (GLOOR *et al.*, 1977).

- **Theta (θ) band.** Similarly, theta (θ) band also seems to have major role in memory processes (Klimesch *et al.*, 1994; Doppelmayr *et al.*, 1998; Kirov *et al.*, 2009). In fact, θ-band activity was also observed over the hippocampus and connected regions using intracranial EEG (iEEG) (Buzsáki, 2002; Lega *et al.*, 2012). Enhanced θ rhythms are typically reported in diverse pathological conditions, including brain tumour (Decker and Knott, 1972), schizophrenia (Kirino, 2007) and sickle cell disease (Case *et al.*, 2017). The θ-band is conventionally defined within 4 - 7.5 Hz (Lopes da Silva, 2013).

- **Alpha (α) band.** Alpha (α) rhythm is the most prominent EEG activity, ranging between 8 and 13.5 Hz. A physiological EEG power spectrum shows a positive peak within this range, whose corresponding frequency value shows some variability across subjects (Valdes-Hernandez *et al.*, 2010; Goljahani *et al.*, 2012), and is conventionally referred to as the dominant frequency (DF) (Prinz and Vitiell, 1989; Goel *et al.*, 1996), individual alpha frequency (Grandy *et al.*, 2013) or α-peak frequency (Valdes-Hernandez *et al.*, 2010). α-band activity is prominent over the occipital region, is regulated by the cholinergic system (Feige *et al.*, 2005; Lopes da Silva, 2013; Wan *et al.*, 2019) and is associated with attentional and visual perception processes (Mulholland and Runnals, 1962; Klimesch *et al.*, 1998; Benedek *et al.*, 2014). Nevertheless, several evidences suggest that these mid-range cortical oscillations likely originate in the thalamus nuclei, as initially proposed by the inventor of EEG (Berger, 1933). For instance, a study reported positive correlation between occipito-parietal α-band power recorded at awake rest and thalamus glucose metabolism as revealed with positron emission tomography (PET) (Schreckenberger *et al.*, 2004). In previous studies, α-band rhythms

have been recorded both in the thalamic nuclei and the cerebral cortex in dogs and cats (Lopes da Silva *et al.*, 1973; Schürmann *et al.*, 2000). Moreover, the lateral geniculate nuclei (LGN) of the thalamus are highly involved in the visual network, as they receive the visual information from the optical nerves and project it towards the primary visual area (V1) within the occipital lobe (Reinagel *et al.*, 1999; Kveraga *et al.*, 2007). Simulations have shown that DF is inversely proportional to the period of thalamo-cortico-thalamic loop, being reduced for more marked delays in the synchronous activity between thalamus and cortex (Robinson *et al.*, 2001; Roberts and Robinson, 2008; Valdes-Hernandez *et al.*, 2010). Hence, most computational models aiming to study α-band activity in healthy and pathological condition are built on this loop network architecture (Bhattacharya *et al.*, 2011; Onofrj *et al.*, 2019). Also, α-band power modulation over the occipital region is associated with perception of visual stimuli. This phenomenon is called α-band reactivity and likely reflects synchronisation of the corresponding neuronal population. With eyes open, local neuronal population is disinhibited, and this reflects into neuronal desynchronization, i.e. lower α-band power. Inhibition mechanism occur with eyes closed, in order to avoid any noisy perception and optimise signal-to-noise ratio (Chapman *et al.*, 1962; Jensen and Mazaheri, 2010; Wan *et al.*, 2019). α-band activity is also referred to as mu (μ) rhythm when recorded from the sensori-motor area (Bernier *et al.*, 2014).

- **Beta (β) band.** Beta (β) band modulation is also prominent over the sensori-motor cortex during movement. β activity is conventionally bounded between 14 and 30 Hz (Lopes da Silva, 2013). In fact, several studies have shown that arm reaching movements are associated with desynchronization, i.e. reduced power with a negative peak at the highest movement speed, followed by synchronisation, i.e. increase of power at the end of the movement. Like α-band reactivity, this phenomenon seems to reflect the disinhibition followed by feedback mechanism driven by the sensory area after a movement. This mechanism was found to be affected in PD (Pfurtscheller, 2000; Nelson *et al.*, 2017; Ricci *et al.*, 2019; Tatti *et al.*, 2019). β-band activity has also been associated with alertness (Kamiński *et al.*, 2012) and cognitive and emotional processing (Ray and Cole, 1985). Specifically, higher parietal β emerged during cognitive tasks, with greater lateralisation for verbal tasks, whilst higher parietal and

temporal β were revealed in positive tasks compared with sad emotional tasks (Ray and Cole, 1985). In recent studies, increased β-band power was also found over the occipital area during attentional tasks involving visual cues when correct responses were provided by participants (Gola *et al.*, 2013; Güntekin *et al.*, 2013). Moreover, in a study involving patients with cerebral stroke, generalised reduced β-band power was reported for patients with cognitive impairment compared with patients without (Wang *et al.*, 2013b). In this thesis, early β-band will be considered, i.e. 14-20.5 Hz, as corresponding EEG activity is less likely affected by muscular artifacts (Whitham *et al.*, 2007; Stylianou *et al.*, 2018).

- **Gamma (γ) band.** Gamma (γ) was initially used to refer to the range within 30 – 45 Hz (Jasper and Andrews, 1938). However, today it is usually considered lower bounded on 30 Hz and can include frequencies of up to 600 Hz (Gaona *et al.*, 2011; Buzsáki and Wang, 2012; Lopes da Silva, 2013). From the cellular perspective, γ-band oscillations are thought to be related to GABAergic activity associated with inhibitory post-synaptic potentials (IPSPs) in pyramidal cells driven by interneurons (Traub *et al.*, 1997; Whittington and Traub, 2003; Bartos *et al.*, 2007; Buzsáki and Wang, 2012). In fact, two computational models describe the likely cooperating mechanisms of generation of γ rhythms consisting respectively of 1) synchronous IPSPs generated by coupling of inhibitory interneurons and 2) phase delay between spikes of interconnected excitatory pyramidal neurons and inhibitory interneurons (Buzsáki and Wang, 2012). It has been shown that γ activity can be modulated by slower rhythms, i.e. θ oscillations, when occurring in memory-related processes, e.g. in the hippocampus, frontal and parietal cortex. This mechanism might be involved in information transfer between the hippocampus and the cortex, and strength of cross-frequency coupling seems to depend on task demand (Caplan *et al.*, 2003; Raghavachari *et al.*, 2006; Axmacher *et al.*, 2010; Fujisawa and Buzsáki, 2011).

1.3.2. The inverse problem

Pyramidal neurons generating the EEG signals are arranged in parallel to each other, building an intermediate layer between the cortical surface and the scalp. Sources of signals recorded

with each EEG cap sensor correspond to neuronal population potentials, known as local field potential (LFP). LFPs result from post-synaptic longitudinal currents which add to each other across neurons (Hämäläinen *et al.*, 1993). However, intermediate tissues hamper the route between sources and scalp, distorting the travelling signals. From the mathematical perspective, transforming source potential to its corresponding sensor signal requires solving the forward problem. Assuming that sources are submerged in a linear medium, for N sensors and L sources and a specific time point, the forward problem can be formulated as follows (Van Veen *et al.*, 1997; Grech *et al.*, 2008):

$$\boldsymbol{x} = \sum_{i=1}^{L} \boldsymbol{H}(\boldsymbol{q}_i) \cdot \boldsymbol{m}(\boldsymbol{q}_i) + \boldsymbol{n} \tag{1.1}$$

$$\boldsymbol{m}(\boldsymbol{q}_i) = \boldsymbol{Q}(\boldsymbol{q}_i) \cdot d_i \tag{1.2}$$

where**:**

- $\boldsymbol{x}$ = surface potentials [V] (N x 1)
- $\boldsymbol{H}$ = leadfield vector $\left[\frac{V}{C \cdot m}\right]$ (N x 3)
- $\boldsymbol{q}_i$ = *i*-dipole spatial coordinates [m] (3 x 1) (*i* = 1, 2, …, *L*-1, *L*)
- $\boldsymbol{m}(\boldsymbol{q}_i)$ = *i*-dipole current [C · m] (3 x 1)
- $\boldsymbol{Q}(\boldsymbol{q}_i)$ = *i*-dipole charge [C] (3 x 1)
- d_i = distance between *i*-dipole charges [m]
- $\boldsymbol{n}$ = perturbation [V] (N x 1).

The leadfield (***H***) contains the signal transformation between source and sensor domains. This is the solution to the forward problem, and is obtained by solving Maxwell's equations with quasi-static assumption (Hämäläinen *et al.*, 1993). It depends on source and sensor locations as well as anatomical properties, e.g. geometry of head anatomy and electromagnetic properties of the tissues between the cortex and the scalp. For accurate modelling, the leadfield matrix should be based on individual anatomical head model rather than head template, and surface recording should be performed with high-density EEG cap (Cho *et al.*, 2015; Song *et al.*, 2015; Dattola *et al.*, 2020).

The forward problem relies on computing the leadfield matrix and providing with a univocal signal for each electrode (Nunez, 1988; de Munck, 1989; Van Veen *et al.*, 1997). On the other hand, inferring the location and intensity of the sources generating the recorded EEG signals is an ill posed problem, known as inverse problem. In fact, it is an optimisation problem, as additional constraints are needed to obtain a univocal analytical solution (Helmholtz, 1853).

To date, several approaches have been developed to solve the inverse problem, known as source localisation techniques. In such approaches, brain sources are modelled as current dipoles, whose intensity and orientation are in general unknown. These techniques can be grouped in two main categories, depending on whether a priori assumption of the number of source dipoles is made or not. Fixed distribution of sources is chosen in non-parametric methods, whilst no a priori choice is made when using parametric techniques (Grech *et al.*, 2008). In non-parametric methods sources are expected to extend over multiple cortical areas, whereas a concentrated source is searched for with parametric methods. Hence, the choice of the localisation technique is dependent on the scope of the study, as it may have a significant impact on the outcome of source domain analysis (Hincapié *et al.*, 2017). The minimum norm estimates fall within the first category (Gorodnitsky *et al.*, 1995; Pascual-Marqui, 1999b; Pascual-Marqui, 2002; Grave de Peralta Menendez *et al.*, 2004), whereas beamformers and subspace techniques are within the second group (Van Veen and Buckley, 1988; Mosher *et al.*, 1992). Methodologies in this thesis project include one non-parametric technique, which is reported in detail below.

1.3.3. Standardised low-resolution brain electromagnetic tomography (sLORETA)

The minimum norm estimate (MNE) was the first developed non-parametric source localisation technique (Hämäläinen and Ilmoniemi, 1984). However, this method is known to be biased towards the most external cortical areas and wrongly localise deepest sources (Fuchs *et al.*, 1999; Pascual-Marqui, 1999b; Hauk *et al.*, 2011). Pascual-Marqui (2002) proposed an improvement to this approach through standardising the obtained solution by the variance of the estimated source current density. It is assumed that the forward model is defined up to a constant value depending on the arbitrary reference for the leadfield and EEG measurement. That is, in equation (1.1), we choose $n = c\mathbf{1}$, being $\mathbf{1}$ the identity vector and c

an arbitrary constant. In a brain without lesions, sources can be assumed to be normal to the cortical surface, i.e. source orientation is known. The equation can then be written as follows:

$$\boldsymbol{x} = \boldsymbol{Hm} + c\mathbf{1} \tag{1.3}$$

where:

- $\boldsymbol{x}$ = surface potentials (N x 1)
- $\boldsymbol{H}$ = leadfield matrix, based on known dipole orientations [N x L]
- $\boldsymbol{m}$ = source current densities [L x 1]
- c = constant (reference arbitrariness).

To obtain an optimal solution, the following functional must be minimised:

$$F = \left|\left|\boldsymbol{x} - \boldsymbol{Hm} - c\mathbf{1}\right|\right|^2 + \alpha\left|\left|\boldsymbol{m}\right|\right|^2 \tag{1.4}$$

In functional (*1.4*), $\alpha \geq 0$ is a regularisation parameter which reflects the variance of noise in the measurement. It can be estimated with a cross-validation method (Pascual-Marqui, 1999a; Dale *et al.*, 2000). To obtain an optimal solution, notation is here simplified by assuming that the signal at both sensor and source is average referenced, i.e. $c = 0$. The solution to the minimisation problem corresponds to the MNE solution:

$$\boldsymbol{m}_{MNE} = \boldsymbol{Kx} \tag{1.5}$$

$$\boldsymbol{K} = \boldsymbol{H}^T[\boldsymbol{HH}^{\boldsymbol{T}} + \alpha\boldsymbol{D}]^+ \tag{1.6}$$

where $\boldsymbol{D}$ is a N x N centring matrix, and *T* is the transpose operator. According to the Bayesian formulation of the inverse problem (Tarantola, 2005), actual source variance corresponds to an L x L identity matrix:

$$\boldsymbol{S_m} = \boldsymbol{I} \tag{1.7}$$

Instead, sensor variance is affected by measurement noise variance:

$$\boldsymbol{S_x^{noise}} = \alpha\boldsymbol{D} \tag{1.8}$$

Sensor noise and actual source variances are assumed to be uncorrelated. Linear relationship between sensor variance and actual source variance can then be formulated, based on (1.5) with average reference:

$$\boldsymbol{S_x} = \boldsymbol{HH}^T + \boldsymbol{S_x^{noise}} \tag{1.9}$$

Using (1.5), estimated source variance is:

$$\boldsymbol{S_{m_{MNE}}} = \boldsymbol{KS_xK}^T = \boldsymbol{H}^T[\boldsymbol{HH}^T + \alpha \boldsymbol{D}] \tag{1.10}$$

The sLORETA estimation for the *i*-source is then obtained by standardising the MNE solution (1.5) by the estimated source variance (1.10):

$$m_{sLORETA_i} = \frac{\left(m_{MNE_i}\right)^2}{\left[S_{\boldsymbol{m}_{MNE_i}}\right]_{ii}} \tag{1.11}$$

1.4. Electroencephalography and Dementia with Lewy Bodies

The use of EEG as a supporting diagnostic tool for dementia is becoming widespread in research. In fact, it is commonly used to obtain direct inference of cortical activity alteration in DLB in either task or resting state experimental protocols, with attempts to link any abnormalities to known pathological features and clinical development of DLB.

1.4.1. Task protocols

As attentional processes are generally affected in dementia, several studies investigated alteration of event-related potentials (ERPs) (Makeig and Onton, 2011) associated with attentional tasks. P300 occurs within 300 ms to 500 ms after a stimulus and is the most prominent ERP component. It has been shown to reflect perception- and cognition-related processes (Donchin *et al.*, 1978; Luck, 2014). In fact, few studies reported higher latency of P300 component associated with auditory stimuli in AD (Goodin *et al.*, 1978; Pokryszko-

Dragan *et al.*, 2003) and more severely in DLB (Bonanni *et al.*, 2010), in which it correlated with cognitive fluctuation severity. Sensory gating mechanism was also shown to be affected in DLB. In other words, people with DLB show less efficient pre-attentional filtering of sensory input. EEG activity associated with sensory gating is known as prepulse inhibition (PPI), consisting of N100/P200 component suppression due to P50 auditory stimuli paradigm (Wan *et al.*, 2008). In fact, PPI was found to be reduced in DLB compared with AD and HC, and thought to be linked to DLB-related cortico-thalamic network alteration (Perriol *et al.*, 2005). Recent research is also using the visual Attention Network Test (ANT) (Fan *et al.*, 2002) to investigate whether attentional subnetworks are affected in DLB. When tested with this protocol, patients lacked post-stimulus θ overall synchronisation, which emerged instead in AD and HC; this feature positively correlated with the Clinical Assessment of Fluctuation (CAF) score (see section 2.1 for details on this clinical score) (Cromarty, 2016).

Two methodologies used to obtain quantitative EEG (qEEG) metrics in resting state consist of time-frequency and functional connectivity analysis. The first involves assessing power and frequency shifts across the physiological power spectrum, and how these are associated with the clinical condition (Oken and Chiappa, 1988; Salinsky *et al.*, 1991). In the second case, EEG sensors – or sources – are used as network nodes, connectivity between nodes is assessed using a chosen metric, and network properties are extracted, depending on the type of network analysis and hypothesis of interest (Schoffelen and Gross, 2009).

1.4.2. Resting state: time-frequency analysis

The most consistent feature emerging from comparing DLB with AD and healthy condition is a negative shift of DF over specific cortical regions. Early studies already reported α rhythm slowing in AD compared with healthy controls (HC) (Penttilä *et al.*, 1985; Soininen and Riekkinen, 1992), as also confirmed in more recent studies (Jackson and Snyder, 2008). However, Briel *et al.* (1999) found marked generalised reduced α activity in DLB compared with AD, as well as transient slow wave activity over the temporal area. This latter feature correlated with temporary loss of consciousness in DLB patients. In another study, authors could not find any significant difference in EEG activity between AD and DLB, but a differential trend for generalised EEG slowing. Nevertheless, EEG alteration correlated with Mini-Mental

State Examination (MMSE) score (see section 2.1 for details on this clinical score), suggesting that it could be associated with disease severity (Barber *et al.*, 2000a). The common speculation across studies on the origin of these abnormal changes is an impairment of the cholinergic system. In line with this hypothesis, early research showed that AD patients with more prominent low frequency power had reduced cell density within the NBM (Riekkinen *et al.*, 1991). Furthermore, a few studies reported that α slowing in DLB was restored towards physiological values due to acetylcholinesterase inhibitor treatment (Agnoli *et al.*, 1983; Balkan *et al.*, 2003; Kai *et al.*, 2005). DF shift, increase of θ activity and, generally, α-band rhythm slowing in DLB was consistently reported in several other studies, with diagnostic classifiers yielding an area under the receiver operating characteristic (AUROC) curve above 80% (Andersson *et al.*, 2008; Bonanni *et al.*, 2008; Peraza *et al.*, 2018; Stylianou *et al.*, 2018). However, some inconsistency exists in reporting DF variability (DFV). Two studies reported higher DFV in AD compared with HC, DLB and PDD (Peraza *et al.*, 2018; Stylianou *et al.*, 2018), in contrast with one study reporting highest DFV in DLB (Bonanni *et al.*, 2008). This is due to different definitions of DFV, which has been defined as standard deviation in the first case, and frequency of variability in the second one. It has been suggested that EEG variability in DLB might be associated with cognitive fluctuation (Andersson *et al.*, 2008). In fact, a recent study explored association between EEG microstates dynamics and cognitive fluctuation in patients with DLB (Schumacher *et al.*, 2019). Authors reported that microstates duration correlated positively with cognitive fluctuation clinical score, and negatively with connectivity between thalamic nuclei and cortex (Schumacher *et al.*, 2019), supporting the idea of cortico-thalamic network's relevant role in regulating the cortical activity recorded with EEG. A few studies also reported reduced variability in α-power modulation, i.e. α reactivity, in LBD compared with AD (Franciotti *et al.*, 2006), and its correlation with reduced NBM volume in PDD (Schumacher *et al.*, 2020b). However, no correlation was found between α reactivity and clinical measures, suggesting that alteration of this mechanism might be associated with the presence but not severity of the disease.

1.4.3. Resting state: functional connectivity

Cerebral dysfunction associated with dementia and specifically DLB emerges as alteration of physiological connectivity between brain areas. Brain networks can be assessed at both structural and functional levels. In the first case, axons are responsible for connecting brain regions, hence white matter anisotropic properties are an index of structural connectivity integrity (Moseley *et al.*, 1990; Basser, 1995; Jbabdi *et al.*, 2015). In the second context, areas do not need to be structurally linked to be connected, as long as they show some form of temporal dependence in their activity (Aertsen *et al.*, 1989; van den Heuvel and Hulshoff Pol, 2010). EEG is a suitable tool to assess functional brain connectivity, as several studies have shown (Astolfi *et al.*, 2007; Sakkalis, 2011; Haufe *et al.*, 2013; Lee and Hsieh, 2014).

EEG connectivity abnormalities also emerge in dementia. In line with task-related studies, results on resting state connectivity also seem to suggest affected attentional processes, which rely on ventral and dorsal frontoparietal networks (Corbetta and Shulman, 2002). Causal interaction between network nodes can be assessed with phase transfer entropy (PTE); specifically, given X_t and Y_t two signals recorded at time t from two nodes, PTE measures positive contribution of signal X_t to Y_t on predicting Y_{t+1} (Lobier *et al.*, 2014). Dauwan *et al.* (2016) used PTE to investigate network alterations in DLB and AD. From their analysis, posterior-to-anterior PTE gradient was significantly reduced in DLB within the α-band compared with HC. Differences between DLB and AD in PTE causality drivers (Hillebrand *et al.*, 2016) emerged over occipital and centrotemporal channels within the α-band network, but only for the centrotemporal channels within the β-band network. Moreover, stronger connectivity lead from occipital region in posterior/anterior information flow in DLB negatively correlated with cognitive fluctuations (Dauwan *et al.*, 2016). This last finding resonates with disrupted EEG occipital activity in DLB reported in time-frequency studies, as well as with fMRI studies showing such impairment (Peraza *et al.*, 2014). A way to build brain network graphs consists of minimum spanning tree (MST), i.e. fully connected network with minimum number of strongest edges without cycling paths (Graham and Hell, 1985). A graph theory study based on MST reported reduced hubness, i.e. functional centrality of network nodes, in DLB compared with HC (van Dellen *et al.*, 2015), in line with previous fMRI study (Peraza *et al.*, 2015). DLB showed also reduced connectivity compared with AD within the α range, whilst no differences were found in other frequency ranges. Furthermore, network

efficiency measures correlated with cognitive performance as assessed with MMSE and Trail Marking Test (TMT) (Reitan, 1958; van Dellen *et al.*, 2015). However, these findings partially contrast with another study based on MST, which did not report any difference between AD and DLB within the α-band network (Peraza *et al.*, 2018). In fact, authors reported reduced connectivity in all dementia groups, i.e. AD, DLB and PDD, within the α-band, and DLB connectivity lower than AD in the β-band and high-θ-band. In addition, they found higher randomisation in the MST for LBD within α-band and θ-band networks. They also investigated whether DF functional network was affected in the disease, reporting no differences between dementia and HC groups. Authors suggest that similarly to DF negative shift, connectivity alteration might reflect compensatory mechanisms associated with over recruitment of neural tissues, as also proposed in other studies with diverse modalities (Reuter-Lorenz and Cappell, 2008; Frantzidis *et al.*, 2014). Both mentioned MST studies measured EEG connectivity using the Phase Lag Index (PLI). Different from correlation measures, PLI accounts for synchronisation between signals, i.e. to which extent phase difference between signals is fixed over time; this measure is not sensitive to volume conduction, which is a common issue in EEG measurements (Stam *et al.*, 2007b; Peraza *et al.*, 2012).

In a recent study, connectivity patterns have been analysed at the source level, using Exact LORETA (eLORETA) source localisation technique (Pascual-Marqui, 2007). DLB patients had higher interhemispheric connectivity over occipital and temporal areas compared with AD within the α-band, but no significant intrahemispheric connection differences were found (Babiloni *et al.*, 2018). In line with other studies, authors speculate that abnormal activity within this range in dementia might be associated with alteration of cortico-thalamic circuits, known to be generators of EEG α-band rhythms as described in section 1.3.1.

1.5. Electroencephalography and Visual Hallucinations in Lewy Body Dementia

Most EEG studies on VH in LBD consistently reported delayed visual ERPs in VH compared with NVH patients and healthy condition. In fact, when presented with checkerboard stimuli, PD patients with VH showed delayed P100 component, compared with NVH group (Matsui *et al.*, 2005). In another study with facial recognition paradigm, P300 visual ERP was significantly delayed in LBD-VH group over the parietal area compared with HC, whilst this was not

reported for the LBD-NVH group. In addition, the study also involved an auditory stimulus, for which auditory P300 latency was measured. Ratio between visual and auditory P300 latencies predicted VH condition with AUROC = 73% ± 11% (Kurita *et al.*, 2005; Kurita *et al.*, 2010). These results were also confirmed in a more recent study, which reported PD-VH patients showing delayed P300 compared with HC, with 6% higher risk of having VH for each millisecond delay (Chang *et al.*, 2016). In line with other studies' speculations, authors suggested these alterations to be associated with cholinergic dysfunction.

Nevertheless, the literature on VH in dementia is lacking resting state EEG studies, as they mostly consist of case reports, whose findings include abnormal synchronous discharges (Sun *et al.*, 2014a; daSilva Morgan *et al.*, 2018). To the best of author's knowledge, only three studies investigated M/EEG spectral and connectivity correlates of VH in AD, DLB and PDD at rest. Specifically, two of these studies found that DF was reduced in VH compared with NVH (Dauwan *et al.*, 2018; Dauwan *et al.*, 2019). Also, VH had lower β-band power compared with NVH. In addition, β-band connectivity over the right temporal area, discriminated between hallucinating AD and DLB as well as between non-hallucinating AD and hallucinating DLB. Coherent with existing literature, authors speculated that the cholinergic system must have a major role in VH-related EEG alteration (Dauwan *et al.*, 2018; Dauwan *et al.*, 2019). A more recent study found increased δ-band activity in DLB with VH compared to NVH, and higher α-band activity in PDD-VH compared to NVH (Babiloni *et al.*, 2020). Authors believed that dysfunctions of dopaminergic system might be associated with reported EEG differences between conditions (Babiloni *et al.*, 2020). To date, no M/EEG studies focused on functional connectivity differences between VH and NVH condition at rest, specifically in LBD.

1.6. White Matter Abnormalities in Dementia with Lewy Bodies

Several studies investigated structural abnormalities in DLB compared with AD and HC. As mentioned in sections 1.1.2 and 1.2.3, few studies consistently reported preserved medial temporal lobe in DLB compared to AD (Barber *et al.*, 2000b; Burton *et al.*, 2009; Mak *et al.*, 2014) as well as abnormalities within the visual cortex in DLB (Taylor *et al.*, 2012). A meta-analysis including seven studies on VBM reported reduced grey matter within the right lateral

temporal/insular cortex and left lenticular nucleus/insular cortex in DLB compared to HC (Zhong *et al.*, 2014).

Other studies focused on abnormal changes in white matter fibres. As mentioned in section 1.4.3, white matter tracts' anisotropy can be used to measure connectivity between brain regions. White matter distribution can be assessed using diffusion tensor imaging (DTI). With DTI, water molecules diffusion is measured as a diffusion tensor, which contains information on magnitude, degree, and orientation of diffusion anisotropy. The most common way to obtain a DTI registration is through a single-shot echo-planar imaging (EPI) MRI protocol (Mansfield, 1984; Alexander *et al.*, 2007). One can then either look at the fibres' integrity by measuring properties such as mean diffusivity (MD) and fractional anisotropy (FA) or obtain extrinsic brain structural pathways by running tractography (Sotiropoulos and Zalesky, 2019). Greater MD or reduced FA reflect loss of anisotropy, i.e. connectivity efficiency. Specifically, MD is associated with cell membrane pathological damages, whilst FA reduces with less organised fibre bundles, which is the case in demyelination or axonal degradation. Radial diffusivity (RD) as index of demyelination is also measured in some studies, although its interpretation is controversial (Johansen-Berg and Behrens, 2013; Delli Pizzi *et al.*, 2015a).

Delli Pizzi *et al.* (2015a) found higher MD within thalamus subregions projecting towards PFC and parieto-occipital cortex in DLB compared with HC, but no differences with AD were reported, contrasting another study which reported lower FA over the left thalamus in DLB compared with AD (Watson *et al.*, 2012). The impairment of these two subregions was suggested to be associated respectively with affected consciousness (and alertness) and visual perception processes in DLB. In the same study, increased total choline was found within the right thalamus in DLB compared with AD, which correlated with cognitive fluctuation severity. The cingulum-cingulate gyrus and the uncinate fasciculus also presented higher MD and RD in DLB as compared to HC, whilst the inferior longitudinal fasciculus had reduced FA in both AD and DLB, in agreement with a previous work (Ota *et al.*, 2009). Alteration of the uncinate fasciculus correlated with frontal thinning in DLB. In contrast, AD group showed affected mnemonic networks. Based on previous literature on the role of these networks (Bonnelle *et al.*, 2012; Leech and Sharp, 2014), authors suggested that white matter alteration in DLB might be associated with affected attentional networks, and reduced cholinergic innervation of the thalamus (Delli Pizzi *et al.*, 2015a; Delli Pizzi *et al.*, 2015b). Another study also found

correlation between presence of visual hallucinations and reduced inferior longitudinal fasciculus FA in DLB (Kantarci *et al.*, 2010). This structure connects the amygdala with occipital and temporal areas (Catani *et al.*, 2003), hence its degeneration in DLB with VH fits with the idea of bottom-up visual stream disruption as described in computational models (section 1.2) (Kantarci *et al.*, 2010). Considering that VH symptom is shared with PD/D, this result somehow contrasts with another study which failed to report any difference between PDD with and without VH after controlling for cognitive function (Firbank *et al.*, 2018). Nevertheless, DLB showed higher amygdala MD, whereas AD presented higher MD within the hippocampus. Authors speculated that amygdala structural abnormalities might be associated with microvacuolation in DLB (Kantarci *et al.*, 2010). Similarly, another study found reduced FA in LBD over frontal, parietal and posterior areas (Lee *et al.*, 2010a). In addition, DLB showed more affected visual association areas, i.e. occipital and lateral regions, compared with PDD. Authors suggested that this latter finding might be reflecting more affected visual recognition memory in DLB compared to PDD (Lee *et al.*, 2010a), despite similar pathology. Consistently, affected posterior white matter in DLB compared with HC was also reported in other studies, as well as less damaged parahippocampal white matter compared with AD (Firbank *et al.*, 2007; Watson *et al.*, 2012; Nedelska *et al.*, 2015).

1.6.1. Functional and structural interdependence

Quantitative evidence in literature showed that functional and structural mechanisms in the brain are strictly related. In fact, directly structurally connected regions are likely to be also functionally connected. However, the inverse might not be true, in which case indirect structural connectivity should be taken in account (Guye *et al.*, 2003; Greicius *et al.*, 2008; Bullmore and Sporns, 2009; Damoiseaux and Greicius, 2009; Honey *et al.*, 2009; Deco and Jirsa, 2012; Stam *et al.*, 2016). Although most studies on this aspect involve fMRI as a functional measure, M/EEG evidence has also been reported.

In a recent study involving seven patients with different diseases, EEG-MNE sources were computed, and functional EEG connectivity was measured (Chu *et al.*, 2015). Source network nodes were used as regions of interest (ROIs) to perform probabilistic tractography. With probabilistic tractography, probability that any couple of voxels is connected to each other is

measured, i.e. proportion of fibres passing from one voxel that cross the other (Behrens *et al.*, 2007). Results showed similarities between functional and structural network, which were more evident within higher EEG frequency bands (Chu *et al.*, 2015). One MEG study reported positive correlation between α-band amplitude of regions within the "posterior α-network" (Hindriks *et al.*, 2015) and structural connections between these regions and V1. Source activity was estimated through a beamforming algorithm, whilst structural connectivity was assessed through probabilistic tractography (Hindriks *et al.*, 2015). One EEG study found positive and negative correlation between respectively left and right inferior longitudinal fasciculus FA and EEG-DF over the occipital area (Valdes-Hernandez *et al.*, 2010). However, the strongest correlation was found between DF and interhemispheric commissural fibres of the Corpus Callosum connecting the occipital lobes, being positive for superior fibres and negative for the inferior ones. This study showed white matter asymmetry as well as dependence of DF on interhemispheric white matter myelination over the posterior areas (Valdes-Hernandez *et al.*, 2010).

1.6.2. Does functional alteration reflect white matter changes in DLB?

Few attempts have been pursued to infer structural drivers of functional alteration in dementia and, specifically, AD. One study involving MCI patients showed that structural network strength defined from fMRI network components predicted conversion from MCI to AD (Hahn *et al.*, 2013); structural connectivity was assessed with deterministic tractography, which methods "provide a point estimate of the path of least hindrance to diffusion between two points" (Sotiropoulos and Zalesky, 2019). In line with these results, one EEG study found a positive correlation between diffusivity measures over posterior areas and α-band coherence in MCI (Teipel *et al.*, 2009), whilst another one found reduced source domain δ-band network integration associated with lower FA within the Corpus Callosum in MCI (Vecchio *et al.*, 2015). Affected Corpus Callosum in MCI was also reported in another study which also found correlation with higher θ-band activity over frontal areas in MCI and AD compared with HC (Scrascia *et al.*, 2014). However, to date, no studies have investigated the relationship between EEG and structural alteration in DLB.

1.7. Aims and Hypothesis

According to the current literature, EEG is a suitable candidate to become a diagnostic tool for dementia. Specifically, many studies highlighted its potential to be a discriminative biomarker for DLB against AD, whose symptomatic phenotype tend to overlap at early pathological stage. From the cortical activity perspective, task based studies consistently reported ERP abnormalities in DLB compared with AD and HC (Wan *et al.*, 2008; Bonanni *et al.*, 2010). However, DF negative shift in the EEG spectrum at rest over occipital regions has been so far the most discriminative biomarker (Bonanni *et al.*, 2008; Peraza *et al.*, 2018; Stylianou *et al.*, 2018). At the same time, recent studies have investigated alteration of functional network as assessed with EEG connectivity. There is a consensus around the idea that DLB network shows lower hubness as well as more affected attentional networks compared with AD and HC (Dauwan *et al.*, 2016; Peraza *et al.*, 2018). Most studies speculated that EEG activity abnormalities in DLB are due to affected cholinergic system throughout the brain and its primary source, i.e. the NBM (Riekkinen *et al.*, 1991; Kai *et al.*, 2005), as well as an impaired cortico-thalamic network (Perriol *et al.*, 2005).

In fact, the source of EEG abnormalities in DLB is still a matter of speculation, as no direct evidence has been reported as of yet on their origin. Although few studies were source domain focused, they often involved the use of low-density EEG caps, which have been shown to be suboptimal. In the case of functional network analysis, network graph architecture in DLB was investigated only with MST graphs. Furthermore, no investigation of affected cortical network topological patterns in the source domain has been reported yet.

This project focused on investigating the following aspects:

1) Network architecture differences as defined in sensor domain between dementia types, i.e. AD, DLB and PDD, by means of a Graph Theory study based on proportional thresholding. An exploratory study has been performed, and significant differences in network measures between dementia groups were expected.
2) Replication of Graph Theory analysis in the source domain. Results were expected to resonate with sensor domain analysis outcome. Correlation between α-band topographical alterations and DF shift over the posterior regions in AD and DLB was

also tested, to investigate whether network and posterior activation abnormalities are associated with the same pathological mechanisms.

3) Discrimination between AD and DLB: source localisation of differences in EEG functional network measures as detected in sensor domain analysis. It was hypothesised that connectivity paths matching with attentional networks should be differentially affected between the two conditions. Correlation between disease-related DF shift and structural connectivity between NBM, thalamus and cortex was tested. This analysis aimed to investigate whether cholinergic dysfunctions in DLB may be driving DF negative shift, supporting previous speculations and models.
4) EEG and structural network in VH and NVH condition in LBD (DLB + PDD): source localisation of affected functional network component and corresponding functionally weakened regions. The aim was to produce an empirical evidence of the hypotheses of existing computational models and clinical based speculations, i.e. affected visual subnetworks in VH as compared with NVH. Correlation between functional features and GM volumes over cortical and subcortical regions was also tested in both groups. Thalamus and NBM were expected to show neuronal loss associated with VH. Correlation between EEG functional and structural network measures in VH and NVH groups was tested to investigate whether structural connectivity between NBM, thalamus and cortex may be driving functional connectivity VH-related alterations, supporting previous speculations and models on the role of the cholinergic system in VH development.

Chapter 2. General Methods

In this chapter shared methodologies across analyses reported in this thesis are outlined. Materials and methods which are specific for each analysis are reported in the respective chapter.

2.1. Clinical Scores and Participants

Participant recruitment was performed prior to this research project as part of the Cognitive and Attentional Function in Lewy Body Diseases (CATFieLD) study at Newcastle University (Cromarty, 2016), funded by the Wellcome Trust. Diagnoses were delivered by two experienced clinicians, based on diagnostic criteria for DLB (McKeith *et al.*, 2017), criteria for PDD (Emre *et al.*, 2007) and National Institute on Ageing-Alzheimer's Association criteria for AD (McKhann *et al.*, 2011). To this purpose, a battery of neuropsychological and neuropsychiatric tests has been collected from all participants:

- **Mini-Mental State Examination (MMSE).** The MMSE is widely used to assess cognitive function and its impairment in diverse conditions, including ageing and dementia (de Folstein, 1975; Brayne *et al.*, 1998). This examination covers aspects of the condition including short term memory, language processing and orientation. MMSE score ranges from 0 to 30, and MMSE ≤ 24 is usually associated with pathological conditions. For this thesis, any patient with MMSE score < 12 and healthy subjects with MMSE score < 26 were excluded, which resulted in not including one PDD patient with MMSE = 8 in the cohort.

- **Cambridge Cognitive Examination (CAMCOG).** The CAMCOG is a cognitive test which was developed to capture subtle cognitive alterations emerging in mild dementia (Roth *et al.*, 1988; Huppert *et al.*, 1995). It assesses several cognitive subdomain states, including orientation, language, memory, attention, praxis, calculation, abstract thinking, and perception (Huppert *et al.*, 1995). Threshold between dementia and healthy condition is a score of 80 out of 105.

- **Neuropsychiatric Inventory (NPI).** The NPI is provided by the patient's informants and reflects the severity of typical dementia patient symptoms (Cummings, 1997). These include "delusions, hallucinations, agitation, dysphoria, anxiety, apathy, irritability, euphoria, disinhibition, aberrant motor behaviour, night-time behaviour disturbances, and appetite and eating abnormalities" (Cummings, 1997). For each behavioural domain, a severity score is obtained from the questionnaire. In this thesis, NPI hallucination (NPI-hall) score will be only related to visual hallucinations.

- **Trail Making Test (A).** This is a visuomotor control test, consisting of 25 numbered circles on a paper sheet in a random spatial distribution, which patients are asked to connect by drawing a continuous line. Higher cognitive impairment is associated with longer time to complete the task (Reitan, 1958).

- **Phonemic verbal fluency (FAS) and animal naming test.** These tests are specifically aimed to assess language processing, respectively verbal and semantic fluency. The FAS test consists of asking patients to write as many words as possible beginning with the letters F, A and S in one minute (Bechtoldt *et al.*, 1962), whilst in the latter patients are asked to write names of animals (Kertesz, 1982).

- **Unified Parkinson's Disease Rating Scale part III (UPDRS III).** Part III of the UPDRS consists of motor examination. Sections of this form concern several aspects of motor behaviour, such as speech, tremor, and rigidity. Total score is obtained by adding up single section scores. UPDRS score ≥ 8 is associated with parkinsonism.

Participants cohort with EEG recording comprised 18 HC (11 males, 7 females), 32 AD (22 males, 10 females), 25 DLB (20 males, 5 females) and 21 PDD (20 males, 1 females). Most patients were on an acetylcholinesterase inhibitor medication (AChEI), and LBD patients were also taking levodopa. From the latter, levodopa equivalent daily dose (LEDD) data was collected. Participants did not report any other neurological or psychiatric condition apart from dementia and provided written informed consent before taking part of the study. The CATFieLD study was approved by the Northumberland Tyne and Wear NHS Trust and Newcastle ethics committee. Complete demographics are reported in Table 2.1; statistics

were performed using MATLAB 9.2 (The MathWorks Inc., Natick, MA, 2017) and Statistical Package for Social Sciences (SPSS) (version 24).

	HC (N=18)		AD (N=32)		DLB (N=25)		PDD (N=21)		p-value
Age	76.28	±5.50	76.63	±7.72	76.16	±6.24	73.38	±5.89	df=3, p-value=0.228ǂ
Male/Female	11/7		22/10		20/5		20/1		df=3, p-value=0.055ǂ
MMSE	29.17	±0.86	20.16	±4.30	22.68	±4.32	23.43	±3.49	df=3; p-value<0.001ǂ
CAMCOG total	96.67	±3.68	66.22	±15.87	74.84	±12.78	75.86	±10.80	df=3; p-value<0.001ǂ
NPI hall	0	0	0.03	±0.18	1.71	±1.88	2.19	±1.99	p-value=0.312Ŧ
CAF total	0	0	0.58	±1.39	4.13	±4.13	6.63	±4.27	p-value=0.045Ŧ
Animal naming	20.72	±5.54	10.66	±4.97	10.80	±3.88	11.38	±4.14	df=3; p-value<0.001ǂ
UPDRS	1.28	±1.49	2.77	±3.11	16.20	±7.52	24.52	±6.71	p-value<0.001Ŧ
FAS Verbal fluency	44.89	±16.07	26.43	±16.23	18.28	±10.60	20.86	±13.66	df=3, p-value<0.001ǂ
Trail making test A	36.43	±10.25	79.16	±52.55	109.88	±68.84	167.35	±107.11	df=3, p-value<0.001ǂ
AChEI (yes/no)	0/18		29/3		22/3		17/3^		df=4, p-value=0.537*
LEDD	0	0	0	0	176.88	±230.44	805.90	±392.70	df=44, p-value<0.001Ŧ

Table 2.1 – Demographic data and clinical scores. ǂ χ2 test four groups, Ŧ Unpaired Mann-Whitney U test (DLB vs PDD), ǂ Kruskal-Wallis four groups, * χ2 test three groups (AD, DLB, PDD). ^ One PDD patient was on Memantine.

2.2. Experimental Protocol

EEG recordings were obtained in a resting-state paradigm; participants were asked to sit in a dim-lit room with eyes closed for ~ 2.5 minutes, relax, mind wander, and refrain from moving. To avoid any effect of drowsiness on the recorded data, participants were instructed to stay awake, and the researcher conducting the recording session watched them and checked for possible slowing (δ-waves) on the ongoing EEG signal. The one-day fluctuations scale (ODFAS) was also obtained from all participants. If this was particularly marked, the patient was not tested on that day. EEG Waveguard cap (ANT Neuro, The Netherlands) with 128 sintered Ag/AgCl electrodes (also referred to as channels) with 10-5 derivation system (Oostenveld and Praamstra, 2001) was used (Figure 2.1). Recordings were performed at 1024 Hz sampling frequency, with sensor/scalp impedance below 5 kΩ and ground channel attached to the right clavicle. Reference channel at recording was Fz.

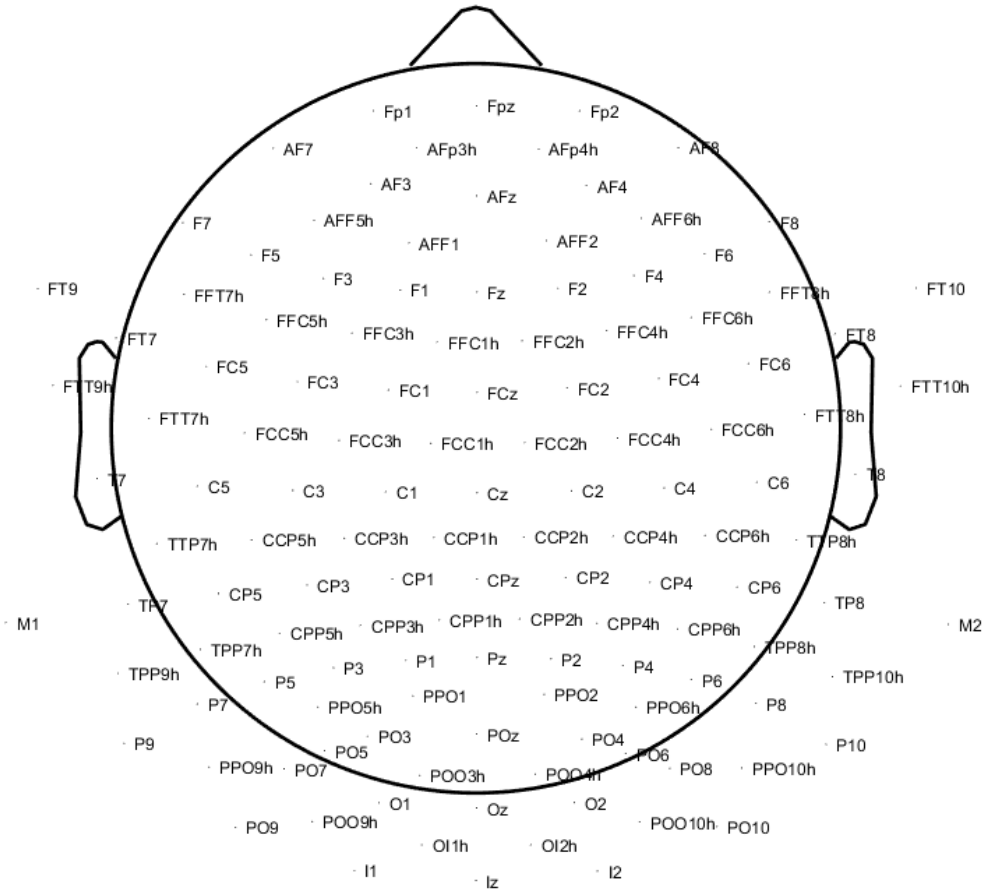

Figure 2.1 – EEG cap channels distribution on scalp, 10-5 derivation system. Figure obtained with EEGLAB toolbox for MATLAB.

2.3. Electroencephalography Data Pre-processing

EEG signals can generally be affected by artefacts. In fact, EEG also captures non-neurogenic activity generated by facial muscle contraction, breathing, heartbeat, eye movement, amplifier voltage bumps, and power line noise (Corby and Kopell, 1972; Muthukumaraswamy, 2013; Urigüen and Garcia-Zapirain, 2015). Therefore, it is crucial to implement a pre-processing pipeline to minimise artefactual contributions to the signal as much as possible before performing any further analysis. There is currently no consensus on how to perform such cleaning process; in this project, author's choice fell on a protocol he obtained familiarity with in previous research projects (Ricci *et al.*, 2019; Tatti *et al.*, 2019). The pipeline was implemented using EEGLAB toolbox version 14 (Delorme and Makeig, 2004) on MATLAB 9.2 (The MathWorks Inc., Natick, MA, 2017).

2.3.1. Filtering and "epoching"

Frequency bands of interest in this project span from θ-band to β-band, up to 20.5 Hz. A Hamming windowed sinc finite impulse response (FIR) filter was applied between 0.5 Hz and 80 Hz to remove very low and high frequency oscillation signal. This latter is likely affected by muscular artefacts (Muthukumaraswamy, 2013) which are only partially attenuated through filtering, whereas slow oscillations and baseline shifts are likely associated with breathing, swatting and electrode shifts on the skin (Anderer *et al.*, 1999; Fisch and Spehlmann, 1999). Attenuation of this non-neurogenic affected activity aims to increase signal-to-noise (SNR) ratio. Furthermore, a notch filter was applied on 50 Hz to remove powerline noise (Figure 2.2). Time-series were then segmented in two-seconds time intervals, from here referred to as epochs.

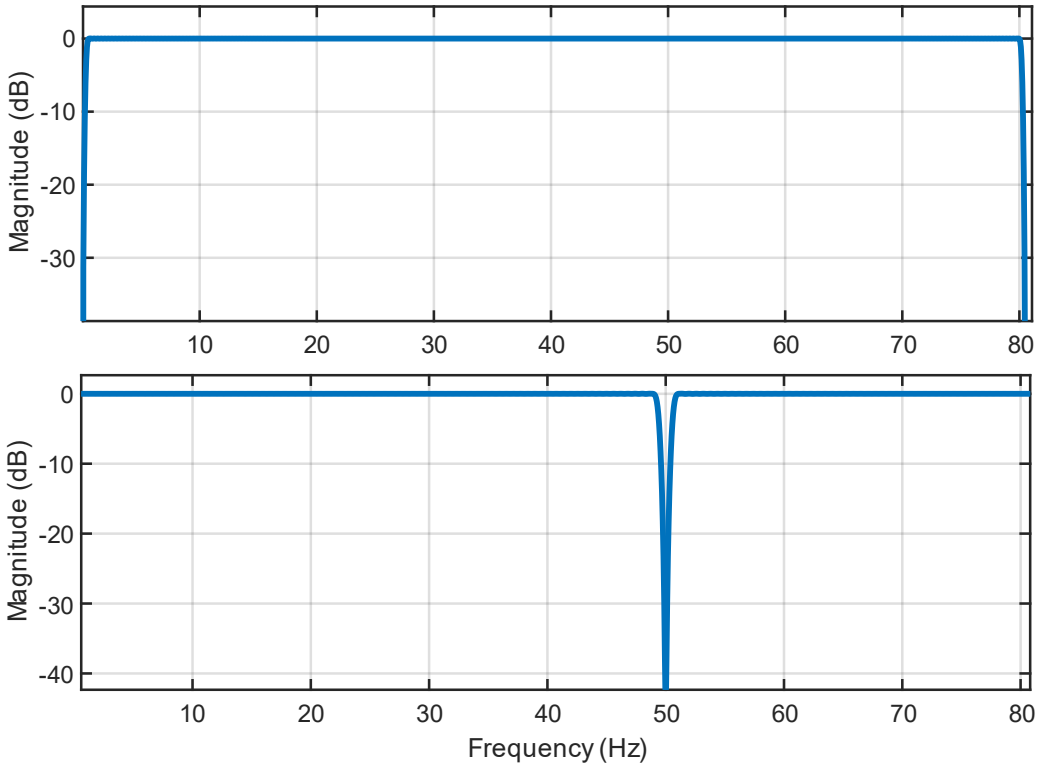

Figure 2.2 – FIR filters. Top: bandpass filter [0.5 Hz – 80 Hz]; bottom: notch filter [50 Hz].

2.3.2. Visual inspection for artefact

Filtered signals were visually inspected to detect non-systematic noise as well as badly connected channels. Typical sources of the first type of artefacts are sudden isolated muscular contractions or voltage bumps. Disconnected channels are a common issue which in high-density caps mostly emerge for most external channels, due to head anatomy (Nelson *et al.*, 2017; Stylianou *et al.*, 2018). Sporadic artefacts were removed by removing the corresponding 2-seconds epochs for all channels, whilst systematically disconnected channels were removed from the whole recording. An example of EEG recording before visual inspection is shown in Figure 2.3.

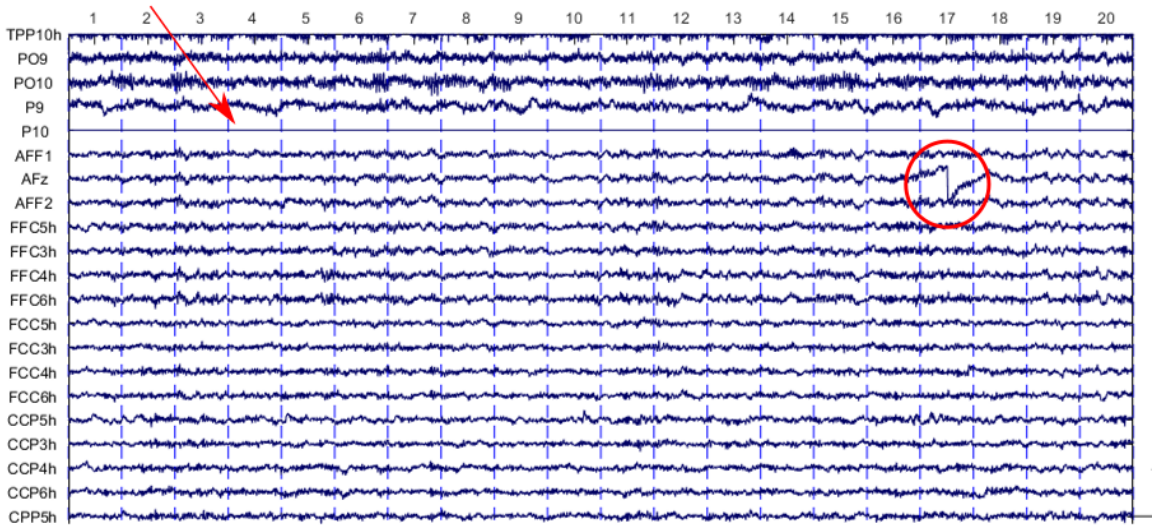

Figure 2.3 – Sporadic artifacts detected by visual inspection. Red arrow: P10, disconnected channel; red circle: voltage bump. Numbers on top indicate 2-seconds consecutive epochs.

2.3.3. Artefactual component detection: independent component analysis

Following visual cleaning, systematic noise must be removed from signals. These include eye blinks, systematic muscle contractions, and heartbeat. Independent component analysis (ICA) is an effective method to detect EEG systematic patterns, which include neurogenic and artefactual activity (McMenamin *et al.*, 2010; Muthukumaraswamy, 2013). ICA is a mathematical method that consists of decomposing a series of signals and obtaining their independent features (Comon, 1994; Hyvärinen and Oja, 2000). In general, for N channels and L epochs, the mathematical formulation can be expressed as follows (Viola *et al.*, 2010):

$$\boldsymbol{A} \simeq \boldsymbol{WX} \tag{2.1}$$

where:

- X = EEG data [N x L]
- W = matrix of weights [N x N]; this is estimated by the ICA algorithm
- A = independent components time-series [N x L]

Once artefactual components are rejected, a new matrix of weights (***Z***) is generated, and cleaned time-series are obtained:

$$\boldsymbol{X_{clean}} = \boldsymbol{ZA_{clean}} \tag{2.2}$$

To date, diverse implementations have been proposed to compute $\boldsymbol{W}$ (Xu *et al.*, 1998; Hyvarinen, 1999; Theis *et al.*, 2003; Lin *et al.*, 2007). In this project, we relied on the Infomax algorithm, due to its good performance and stability with high-dimensional data (Amari *et al.*, 1996; Delorme and Makeig, 2004; Langlois *et al.*, 2010). Briefly, the algorithm starts with random $\boldsymbol{W(0)}$, and runs the following step until convergence:

$$\boldsymbol{W}(t+1) = \boldsymbol{W}(t) + \eta(t)(\boldsymbol{I} - f(\boldsymbol{A})\boldsymbol{A}^T)\boldsymbol{W}(t) \quad (2.3)$$

where:

- t is the iteration step
- $\eta(t)$ specifies step sizes
- $f(\boldsymbol{A})$ is a nonlinear function depending on the type of distribution.

ICA is based on certain assumptions. Components to be extracted must be independent, must not have Gaussian probability density function, and be the only source of stochasticity; there must not be any systematic offset in the data; $\boldsymbol{W}$ must be square and full rank (Langlois *et al.*, 2010). These assumption are likely to be met in high-density EEG recordings (Delorme and Makeig, 2004; Ullsperger and Debener, 2010).

Inspection of independent components is performed by checking their topography, power spectrum, temporal distribution, and pattern waveform. In resting state recordings, neurogenic component's spectrum should resemble physiological EEG spectrum, i.e. prominent activity over lower frequency bands, and progressive decrease towards higher frequencies. Topographies should reflect physiologically meaningful areas, e.g. occipital areas are associated with α-band components, frontal areas with θ-band patterns. Dipolar localised high frequency components with pattern of burst are generally associated with muscular artifacts. Examples of independent components are shown in Figure 2.4**.**

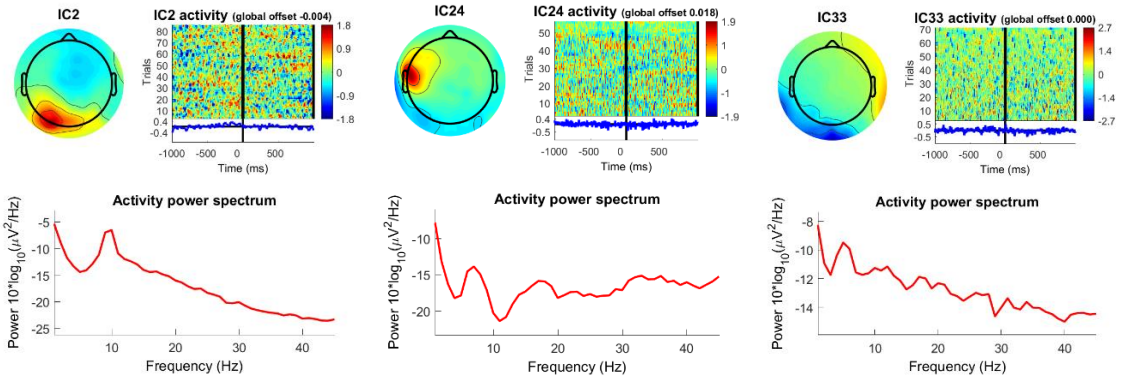

Figure 2.4 – Examples of independent components from the study sample; from left to right: neurogenic, muscular artefact, heartbeat.

ICA outcome consisted of as many components as EEG channels. To identify stable components despite short (about two minutes) recordings, principal component analysis (PCA) was performed on the data before running ICA in order to reduce data dimension to half number of channels preserved at the visual inspection step (Delorme and Makeig, 2004; Ricci *et al.*, 2019).

2.3.4. Channel interpolation and average referencing

After rejection of artefactual components, channels that have been removed during visual inspection were replaced with spherical spline interpolation of neighbouring channels. Eventually, channels were referenced to spatial average. Choice of reference depends on analysis aim, and a sensible choice should rely on a region of no interest (Hagemann *et al.*, 2001; Lei and Liao, 2017). Average reference is preferable when the analysis involves the whole scalp and it can be assumed that EEG activity is not event related, as in resting state (Bertrand *et al.*, 1985).

2.4. Functional Connectivity

To analyse brain network characteristics, a connectivity measure must be chosen. As mentioned in section 1.4.3, EEG connectivity can be assessed by different means, depending on analysis aim. In general, connectivity should assess the extent to which the EEG activity at

any couple of nodes shows temporal interdependence. A commonly used measure is phase coherence, which for *N* discrete time points is defined as follows (Mormann *et al.*, 2000):

$$R = \langle e^{i\Delta\phi} \rangle = \left| \frac{1}{N} \sum_{k=0}^{N-1} e^{i\Delta\phi}(t_k) \right| \tag{2.4}$$

where $\Delta\phi$ is the phase difference between signals and t_k is the time step. Phase coherence is bounded between 0, i.e. no connectivity, and 1, full connectivity. Higher values of *R* are associated with higher synchronisation between signals, i.e. lower variability of $\Delta\phi$ across time. However, the scenario in which $\Delta\phi \simeq 0$, i.e. almost identical signals, falls within the case of maximum coherence. In high-density EEG caps where electrodes are close to each other, this scenario is likely to be due to volume conduction, i.e. current associated with one EEG signal being conducted between electrodes due to head tissues conductivity (Holsheimer and Feenstra, 1977; van den Broek *et al.*, 1998). PLI was proposed to overcome this issue (Stam *et al.*, 2007b), as it measures asymmetry of phase difference distribution across time between two signals. It is an instantaneous measure, based on Hilbert transform. For discrete time steps, its formulation is:

$$PLI = |\langle sign[\Delta\phi(t_k)] \rangle|, sign[\Delta\phi] = \begin{cases} -1, \Delta\phi < 0 \\ 0, \Delta\phi = 0 \\ 1, \Delta\phi > 1 \end{cases} \tag{2.5}$$

where *sign* is the signum function. PLI equals zero when two signals are perfectly overlapping. However, it is still sensitive to almost zero-lagging signals, i.e. when $\Delta\phi \simeq 0$. In fact, this can occur when weak noisy conducting sources contribute to the signal. In this thesis, connectivity was measured using weighted PLI (WPLI). Given two signals $Z_1$and Z_2, WPLI consist of PLI weighted by the imaginary part of the cross-spectrum (*X*) between the two signals (Vinck *et al.*, 2011):

$$WPLI = \frac{|\langle Im(X) sign[\Delta\phi(t_k)] \rangle|}{\langle |Im(X)| \rangle} \tag{2.6}$$

$$X = Z_1 Z_2^* = A\, \mathrm{e}^{i\Delta\phi} = A[(cos\Delta\phi) + i(sin\Delta\phi)] \tag{2.7}$$

where Z_2^* is the complex conjugate of Z_2, and *A* is the magnitude of the cross-spectrum. $|Im(X)|$ spans between 0 and 1 as $|\Delta\phi|$ ranges between 0 and $\frac{\pi}{2}$. Hence, WPLI attenuates signals with shorter time delay. Although false negatives could be generated when two signals are generated from the same source (Colclough *et al.*, 2016), this measure is sensitive to linear and non-linear mutual activity between regions (Imperatori *et al.*, 2019), and shows inter-subject reliability and repeatability (Hardmeier *et al.*, 2014). WPLI was computed for θ-band (4-7.5 Hz), α-band (8-13.5 Hz) and β-band (14-20.5 Hz) networks (Mehraram *et al.*, 2019) as implemented in the Fieldtrip toolbox for MATLAB (Oostenveld *et al.*, 2011) after transforming EEG time-series to the time-frequency domain through Windowed Fourier Transform (3-10 cycles adaptive windows width, 0.5 Hz frequency step). To emphasise those connections which consistently maintain the same direction across time and within each frequency band, signed WPLI values were first averaged across time and frequency bins, then absolute values were computed on the obtained matrices.

After measuring connectivity, obtained connectomes (Sporns *et al.*, 2005) were represented as network graphs, and network features were analysed. The chosen strategy to obtain graphs depended on the analysis. Part of this project related to this methodological aspect and is reported in Chapter 3.

2.5. Connectivity Strength Difference Between Conditions

For each frequency band of interest, average connectivity strength over the whole network was computed and compared between groups with non-parametric tests (Kruskal-Wallis with Mann-Whitney U post hoc tests, $p<0.05$, Holm-Bonferroni corrected (Holm, 1979)). Furthermore, network topological differences between groups were assessed with Network Based Statistics (NBS) (Zalesky *et al.*, 2010). This approach consists of assessing network components which are most consistently different between groups. This is pursued by first testing all connections for the hypothesis of interest. Test statistic threshold (t_{th}) is chosen, and connections with t-value overcoming t_{th} are candidates to be part of a significant connected network component, i.e. a connection cluster with $p<0.05$ from testing between groups. In fact, the null-hypothesis is tested at the component level rather than single connection, by computing the corresponding family wise error rate (FWER) corrected p-value.

The size of the detected significant component is computed, and data are permuted between groups. Component size can be measured as the extent, i.e. number of connections, or intensity, i.e. sum of t-values. This process iterates thousands of times, and the largest component sizes are recorded. The FWER-corrected p-value for each component is obtained as a ratio between number of iterations at which the largest component was of the same size of it or greater and total number of permutations. A weak point of this method is the arbitrariness of t_{th} choice. In the reported analyses, t_{th} was chosen to pursue clarity in network topographies and highlight most consistently affected motifs.

2.6. Graph Theory

Spatial organisation of brain connections determines network topology. Graph theory (Diestel, 1997) is a well-established mathematical approach to extract brain network topological features, in both structural and functional context (Iturria-Medina *et al.*, 2007; Bullmore and Sporns, 2009; Rubinov and Sporns, 2010; van Wijk *et al.*, 2010; Kaiser, 2011). Geometrically, a binary graph is made of nodes and edges. In brain network context, nodes correspond to brain regions, and an edge between any couple of nodes is traced if a connection exists between the corresponding regions. Edges can also feature connection intensity, in which case weighted graphs are obtained. Graph theory involves implementation of measures associated with different network features depending on connectivity distribution across the network. In brain network studies, this set of features is compared between subjects to assess any association with physiological mechanisms or pathological condition, such as epilepsy, autism, and dementia (de Haan *et al.*, 2009; Zhou *et al.*, 2014; Bernhardt *et al.*, 2015). Graph measures are defined for both binary and weighted graphs. In this project, they were computed as implemented in the Brain Connectivity Toolbox (BCT) for MATLAB (Rubinov and Sporns, 2010).

2.6.1. Local network measures

Local graph features are measured for each node individually and averaged over ROIs. Measures of interest in this thesis included node degree (K) and clustering coefficient (C) (Watts and Strogatz, 1998).

Node degree (K). K of a node is an index of centrality of the corresponding brain region and consists of the number of edges connected to the node. Hence, higher K is associated with higher number of direct connections involving that specific node, i.e. more neighbouring nodes. In weighted graphs, weighted node degree (W-K or K_W), or node strength, is obtained by summing weights of directly connected edges (Opsahl *et al.*, 2010). Since WPLI values span between 0 and 1, for the same network, it is true that: $W\text{-}K \leq K$.

Clustering coefficient (C). C is the ratio between number of edges between neighbours (ε) and number of potential edges between neighbours (Kaiser, 2011). For an *i*-node, it is defined as follows:

$$C_i = \frac{\varepsilon_i}{K_i(K_i - 1)} \tag{2.8}$$

It is a simple measure of network segregation, which is generally associated with higher efficiency. The weighted variant (W-C or C_w) is also influenced by weights of connections. Weaker connections between neighbours and the node itself have a lowering impact on W-C value. In fact, W-C is obtained by weighting C by the average intensity (I) of triangles formed by edges connecting the node with every two other neighbours, where *I* is the geometrical mean of connections forming each triangle. Mathematically, for N triangles, W-C of an *i*-node can be expressed as follows (Onnela *et al.*, 2005):

$$W\text{-}C_i = \frac{2}{K_i(K_i - 1)} \sum_{j,k}^{N} (w_{ij} w_{jk} w_{ki})^{\frac{1}{3}} = I_i C_i \tag{2.9}$$

where *w* values are the weights normalised by the largest weight of the graph. As per definition, both C and W-C are bounded between 0 (neighbours not connected to each other) and 1 (neighbours fully connected to each other).

2.6.2. Global network measures

Global features are computed at whole network level, as they reflect the overall organisation of the network. Measures included in this project analyses are average characteristic path length (L), small-worldness (σ) and modularity (Q).

Average characteristic path length (L). L is a measure of network integration. The characteristic path length between any couple of nodes is the number of intermediate nodes belonging to the shortest paths connecting the two nodes. Values for all couple of nodes are averaged across the whole network to obtain L (Watts and Strogatz, 1998). A lower L is associated with a more efficient network architecture. To compute L for weighted matrices (W-L or L_w), paths are obtained assuming that connection length is inversely related to weights between nodes (Dijkstra, 1959; Newman, 2001). In both binary and weighted computation, the shortest path between two *i*-*j*-nodes is obtained with the Dijkstra algorithm (Dijkstra, 1959), which consists of the following steps:

1) *i*-node is set as current node.
2) Distances are computed with all neighbouring nodes. Nodes that are not neighbours are marked with infinite distance from *i*-node.
3) Obtained distances are marked as shortest paths from current node.
4) Neighbour node whose shortest path from current node is the lowest is marked as the current node.
5) Step 2 is performed for the current node.
6) Obtained distances between current and neighbour nodes are summed with the shortest path from *i*-node to the current node.
7) The result is compared with previously detected distances between *i*-node and the new neighbour nodes. The lowest value is marked as shortest path between *i*-node and the new node.
8) Algorithm iterates from step 4 until *j*-node is reached by the shortest path from *i*-node.

Small-worldness (σ). σ measures the compromise between segregation and integration of the network as compared with a random network. By definition, a small-world network shows higher clustering coefficient and similar characteristic path length compared with a random

network with the same number of nodes and edges (Watts and Strogatz, 1998; Humphries and Gurney, 2008). The mathematical formulation of σ is:

$$\sigma = \frac{\frac{C}{C_{rand}}}{\frac{L}{L_{rand}}} \tag{2.10}$$

where "rand" subscripts indicate that the measure is obtained on a random graph. In this thesis, random surrogates were obtained as average across 40 equivalent random networks obtained preserving the node degree distribution of the original networks (Milo *et al.*, 2002; Sporns and Zwi, 2004). A small-world network shows $\sigma > 1$ (Humphries and Gurney, 2008), where this value scales linearly with network size. Whether the human brain shows a small-world organisation is still a matter of debate (Achard *et al.*, 2006; Hilgetag and Goulas, 2016). In fact, although different studies report small-world properties of the cerebral cortex (Sporns and Zwi, 2004; Stam *et al.*, 2007a; van den Heuvel *et al.*, 2008), some evidence suggests that the brain might rather be closer to a more regular scale-free network, i.e. node degree follows a power law distribution (Eguiluz *et al.*, 2005; Kaiser *et al.*, 2007; Lee *et al.*, 2010b).

Modularity (Q). Q measures the extent to which the network is organised in modules. It is obtained as the difference between fraction of within-module edges and expected fraction of randomly distributed edges. Hence, nodes within the same module are more connected than nodes belonging to different modules. For a network with *l* edges, its mathematical formulation is (Newman, 2006):

$$Q = l^{-1} \sum_{i,j \in N} \left[a_{ij} - l^{-1}\left(K_i K_j\right) \right] \delta_{m_i m_j} \tag{2.11}$$

where $\mathrm{m_i}$ is the module containing the *i*-node, $\mathrm{a_{ij}}$ equals 1 if *i*-node and *j*-node are connected, and $\delta_{\mathrm{m_i m_j}}$ is the Kronecker delta function. Q (and its weighted variant W-Q or Q_w) can either be positive or negative, where higher values indicate higher segregation. In fact, Q is not associated with the number of modules existing in the network community structure.

Chapter 3. Sensor Domain Analysis Across Dementia Types

3.1. Summary

Early diagnosis of DLB versus AD can be difficult due to similar symptomatic phenotypes. EEG is an inexpensive and non-invasive method which may provide additional diagnostic information. Previous studies reported alteration in AD functional network compared with healthy condition; however, similar studies including DLB and PDD are still not numerous. In this chapter, EEG network connectivity patterns were compared across conditions, and differential network biomarkers were inferred. In addition, the hypothesis that weighted graphs may lead to more reliable network measures by preserving topological information was tested. Outcome of this study shows that connectivity is reduced in dementia groups in the α-band network, whilst DLB shows affected posterior-anterior patterns in the β-band and higher network segregation within the θ-band compared to AD. Higher consistency across network densities emerged for weighted graphs, and network properties alterations reflected changes in connectivity strength. In conclusion, β- and θ-band network features result in suitable diagnostic biomarkers for DLB vs AD, whilst α-band network properties are similarly affected in LBD (DLB + PDD) compared with HC. Detected network alterations may be associated with impairment of attentional networks in Parkinsonian diseases.

Content of this chapter is also reported in detail in the publication titled “Weighted network measures reveal differences between dementia types: an EEG study” in Human Brain Mapping journal (Mehraram *et al.*, 2019).

3.2. Introduction

As reported in Chapter 1, diagnosis of DLB versus AD can be difficult especially at early pathological development due to their similar symptoms, and biomarkers may provide additional information for this purpose. At the same time, at later stages DLB shows a symptomatic spectrum similar to PDD, which is why researchers tend to group together DLB and PDD as LBD when aiming to assess diagnostic biomarkers (Lippa *et al.*, 2007). However, symptomatic differences at early stages as well as higher burden of amyloid in DLB compared

to PDD (Edison *et al.*, 2008) make the assessment of different physiological correlates between these two conditions a further matter of research, as it might provide additional pathological insights (Stylianou *et al.*, 2018).

EEG resting state network studies reported parietal-frontal connectivity patterns affected in DLB compared with AD and HC (Lemstra *et al.*, 2014; Dauwan *et al.*, 2016). In fact, these pathways are known to be involved in attentional processes (Corbetta and Shulman, 2002). A study based on MST reported reduced hubness within α-band in DLB compared with AD, associated with more severe cognitive impairment in DLB (van Dellen *et al.*, 2015). A recent study showed reduced interhemispheric connectivity in dementia compared with HC, with reduced connectivity in AD compared with DLB over posterior and temporal regions within the α frequency range (Babiloni *et al.*, 2018); no differences were found between DLB and PDD, likely due to pathological similarities between these two conditions (Babiloni *et al.*, 2018). Another work based on MST reported the α-band to be discriminative between HC and dementia, whilst PLI was significantly lower in DLB compared with AD within the β-band (15-30 Hz) (Peraza *et al.*, 2018). Hence, authors suggested that β-band network might be a potential candidate as a diagnostic biomarker for DLB.

To date, no EEG studies on DLB used proportional thresholding to obtain network graphs. As mentioned in section 2.4, diverse strategies can be implemented to obtain a graph once connectivity is assessed. Generally, a threshold value is chosen, and connections above this value are preserved, whilst the remaining ones are replaced with zeros. Then, the obtained matrix may be either binarised, i.e. surviving edges are set to 1, or edge weights may be preserved. Graph thresholding is still a matter of debate among researchers (van Wijk *et al.*, 2010; Langer *et al.*, 2013; Garrison *et al.*, 2015; Jalili, 2016), who proposed different approaches with respective rationales. In fact, the thresholding approach is currently arbitrary. An EEG network study with schizophrenic patients showed that preserving edge weights yielded more prominent differences between conditions in terms of network properties (Rubinov *et al.*, 2009). However, no further quantitative evidence has been produced so far to assess whether edge weights in graphs in dementia studies might enhance differentiation between conditions and improve consistency of the analysis outcomes across network densities.

3.2.1. Objective

In this chapter, an exploratory investigation on EEG network feature differences between dementia types is reported. A graph theory analysis based on proportional thresholding was performed to assess disease-related differences between groups. Additional analysis aimed to find evidence to support the hypothesis that weighted graphs lead to more consistent results by including additional topological information.

3.3. Methods

Part of methods implemented in this analysis are reported in detail in Chapter 2. Briefly, the study sample comprised 18 HC, 32 AD, 25 DLB and 21 PDD. Clinical information for all participants was collected through a battery of tests, which included MMSE, CAMCOG, Trail Making Test A, Animal naming, FAS verbal fluency, UPDRS III, CAF and NPI (see Table 2.1). EEG was recorded in eyes-closed resting state with high-density sensor cap (128 electrodes). Recorded signals were pre-processed (section 2.3), and connectivity was measured with WPLI (section 2.4) generating three connectivity matrices representing each frequency band for each participant. An example of an estimated connectivity matrix from a HC participant within the β-band is shown in Figure 3.1**.**

3.3.1. Connectivity strength

The first part of the analysis consisted of investigating any bias that might have been introduced to network topology due to group-specific functional connectivity strength. WPLI values were averaged across connections and compared between groups. Moreover, edges were grouped in four ranges based on their inter-node Euclidean distance (very short: <57 mm; short: 57-114 mm; long: 115-170 mm; very long: 171-227 mm) and average WPLI was computed for each group at each range.

3.3.2. Proportional thresholding

To compute graph theory measures, connectivity matrices were thresholded and weighted graphs were obtained. Proportional thresholding was applied as implemented in threshold_proportional.m function included in the BCT (Rubinov and Sporns, 2010), with network densities (PT%) spanning between 3% and 60% in steps of 1%. To reflect underlying structural network properties, PT%=40 as highest density would already be effective (Kaiser, 2011; Bohr *et al.*, 2013). Nevertheless, some studies included larger density ranges (Giessing *et al.*, 2013) and in consequence, the choice in this study aimed to cover most of the range choices made in previous research. A wider range was also necessary to effectively assess any dependence of network measures on network density (section 3.3.5). For each density, the corresponding weighted graph was obtained by setting to 0 any edge weights below the respective threshold; corresponding binary graphs were obtained by replacing all weights with 1. Network features were computed at each network density and averaged across densities.

3.3.3. Network measures

Topology of binary and weighted EEG networks was assessed computing graph theory local and global features using BCT. Specifically, computed measures and their weighted variants (W-) included node degree (K), clustering coefficient (C), characteristic path length (L), small-worldness (σ) and modularity (Q) (see section 2.6 for detailed description on these measures). Computation of both binary and weighted measures was aimed to prove that weighted graphs yielded stronger preservation of network topology. Weighted measures were computed after normalising all WPLI values by the highest weight within each matrix. This step also aimed to remove any bias from network features associated with group-dependent functional connectivity strength (Onnela *et al.*, 2005).

3.3.4. Statistical analysis: connectivity strength

Comparisons between groups were performed using MATLAB. Specifically, topographical differences were assessed with the NBS toolbox, version 1.2 (see section 2.5 for detailed description on this approach). For analysis of variance (ANOVA) tests, t_{th} was set to 8, whilst

3.8 was chosen for the post hoc one tail t-tests, as the analysed data topographies showed enough clarity with these settings (Zalesky *et al.*, 2010). FWER was controlled by performing a permutation test (5000 permutations), and differences were considered significant at p-value < 0.05, with Bonferroni correction for post hoc tests (12 comparisons). Topographies were visualised with the BrainNet Viewer (Xia *et al.*, 2013). Average WPLI was compared across groups for each frequency band with Kruskal-Wallis tests ($p < 0.05$) followed by post hoc two-tailed Mann-Whitney U tests ($p < 0.05$) with Holm-Bonferroni correction (six-comparisons). Average WPLI was also computed at different Euclidean connection distance ranges, as described in section 3.3.1. Differences across groups were assessed with Kruskal-Wallis tests ($p < 0.05$, Holm-Bonferroni correction for number of distance ranges, four tests) followed by two-tailed Mann-Whitney U post hoc tests ($p < 0.05$, Holm-Bonferroni correction, six comparisons). Correlation between average WPLI and clinical scores was tested for each group and frequency band with Spearman rank correlation test ($p < 0.05$, uncorrected).

3.3.5. Dependence of network topology on thresholding level

Spearman rank correlation was tested ($p < 0.05$) between graph density and network features regardless of group or frequency band. False-positive correlation likely due to high number of observations (60 density values for each of the three frequency ranges and four participant groups) was avoided by applying bootstrapping with 5000 permutations, and a correlation distribution was obtained. A relation between network density and measure was considered significant if within the 0.025% of the empirical null distribution tails ($|\rho|<0.025\%$, i.e. double sided). Between-group differences of network measures at each PT% were tested by first performing a Mack-Skill test (Mack and Skillings, 1980) ($p < 0.05$) for each frequency range. When the test was significant, Kruskal-Wallis test ($p < 0.05$, Holm-Bonferroni, 60 tests) was performed followed by two-tailed Mann-Whitney U post hoc tests ($p < 0.05$, Holm-Bonferroni correction, six comparisons).

A model fitting approach was pursued (Bradley *et al.*, 2007; Fjell *et al.*, 2010) to confirm the outcome of this correlation. A power law model of network measure-versus-PT% curves was fitted using the Curve Fitting toolbox (version 3.5.5) in MATLAB. The first derivative of the obtained curve, i.e. dependence of network measure on graph density, was compared

between binary and weighted graphs. The choice of a power law rather than other fitting models such as exponential, linear, or polynomial, was driven by the lowest fitting error as revealed by the sum of squares error (SSE). Results of this analysis are reported in section 3.4.2 for clustering coefficient from the HC group in the β-band.

3.3.6. Differences between groups in weighted matrices

For each frequency band, network measures were averaged across thresholds and compared between groups. Kruskal-Wallis test ($p < 0.05$) was first performed, followed by post hoc two-tailed Mann-Whitney U tests ($p < 0.05$) with Holm-Bonferroni correction (six comparisons). Following the approach pursued in Stylianou *et al.* (2018) study, local measures were also tested regionally within frontal, temporal, central and posterior regions; selected regions are shown in Figure 3.1. In this case, group comparison was preceded by repeated measures ANOVA with region as within subject factor and group as between subject factor. Whether any interaction was found, Kruskal-Wallis followed by post hoc Mann-Whitney U tests were performed, as described before. Rank correlation was eventually tested between network measures and clinical scores for each group and frequency band with Spearman tests ($p < 0.05$, uncorrected).

3.3.7. Scale-free behaviour of the network

To further assess disease-related alteration of EEG network architecture, hubness changes were investigated. Hubness indicates existence of nodes with high degree. In general, a network with high hubness is less resistant to targeted node attack, i.e. iterative removal of connections from high towards low degree nodes. This procedure was applied to weighted matrices as described in previous studies (Barabasi and Albert, 1999; Kaiser *et al.*, 2007; Stam *et al.*, 2009). Nodes with highest degree were progressively removed, and average weight-based characteristic path length (W-L) was computed on the resulting network at each iteration and plotted with respect to the percentage of removed nodes. As reported in previous studies, in such a plot the network measure is expected to show an increasing trend, reach a peak of global maximum, and decrease towards zero as nodes are progressively

removed. In scale-free networks, this peak occurs earlier when compared with small-world or random networks (Kaiser *et al.*, 2007), due to their lower resistance to targeted attack. As mentioned in section 2.6.2, some evidence suggests that healthy brains networks show scale-free properties (Eguiluz *et al.*, 2005). Accordingly, W-L in HC was expected to show an earlier peak in the targeted removal plots compared with dementia groups.

3.3.8. Diagnostic accuracy

In this study, diagnostic potential of graph theory network measures in EEG between conditions was also tested. To this purpose, a random forest classifier was implemented using the Scikit-Learn framework in Python (version 0.20.1), and the Imbalanced-Learn library for Python (version 0.4.3); cross-validation was performed with six-fold, ten repetitions. All network variables in all frequency bands were used to train the classifier, and mean accuracy, F_1 score, sensitivity, specificity, and AUROC curve were obtained. A classifier was built for each group comparison scenario associated with significant differences in network measures. Results from six-fold cross-validation are reported here, but similar results are obtainable when using five-fold or seven-fold (see Appendix A).

3.3.9. Connectivity and network measures: 10-20 system

In order to explore clinical suitability of these methodologies, additional investigation aimed to assess whether these yielded the same results with a standard EEG 10-20 derivation system, i.e. the EEG setup normally used in the clinical framework. This was obtained by preserving only nodes belonging to 10-20 system in connectivity matrices and extracting network features from resulting low-density networks. Since any difference in clustering coefficient and characteristic path length was expected to reflect in small-worldness, this measure was not further computed for this investigation.

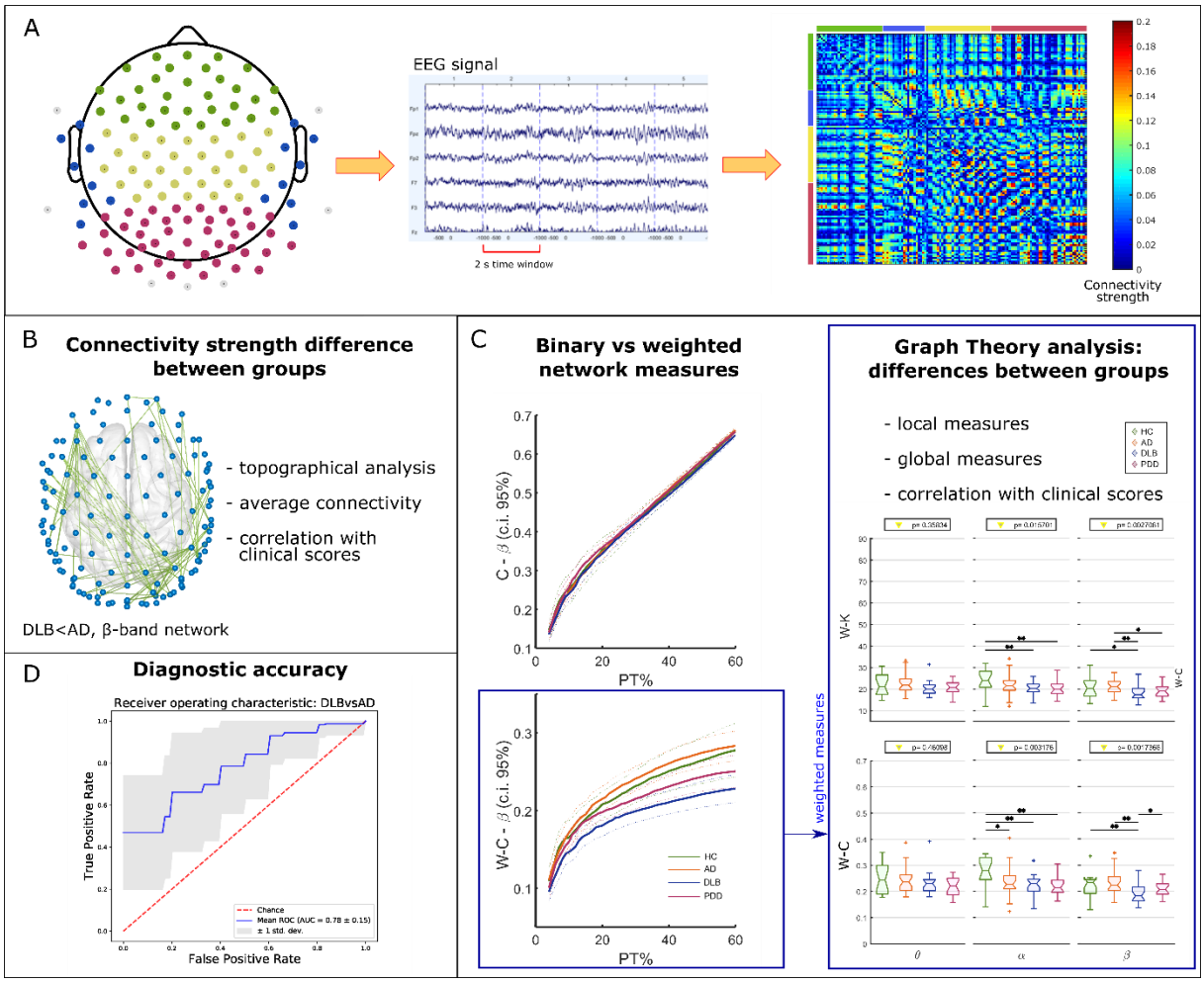

Figure 3.1 – Methodological workflow (Mehraram *et al.*, 2019). A) From left to right: distribution of the 128 EEG electrodes in the 10-5 system. Grey electrodes were deemed noisy, hence were excluded in all network analyses. An example of EEG recording from a healthy participant and a connectivity matrix computed on one HC subject in the β-band network are reported. Colours span across connectivity (defined as weighted phase lag index, or WPLI, as reported in detail in the Methods section) values between 0 and 0.2. Coloured bars on the sides of the connectivity matrix and colour of the electrodes define scalp regions. Green: frontal region; blue: lateral region; yellow: central region; purple: posterior region. B) Topography showing significantly weakened connections in DLB compared with AD within the β-band network; C) Left: binary and weighted clustering coefficient values across (β-band) network densities, reported here as an example; right: average weighted node degree and weighted clustering coefficient, t-tests across groups (Kruskal-Wallis value on top, *p<0.05, **test survives multiple comparison correction); D) Receiver operating characteristic curve obtained with random forest classifier, testing DLB vs AD discrimination.

3.4. Results

3.4.1. Connectivity strength comparison between groups

Differences in average edge weights between groups are shown in Figure 3.2. Connectivity strength was reduced in the α-band in all dementia groups compared with HC, whilst it was lower in LBD compared with HC and lower in DLB compared with AD in the β-band (Figure 3.2a). Long connections were mostly affected within the α-band, whereas all distance ranges showed altered connectivity strength in the β-band (Figure 3.2b). Differences in average WPLI were not detected within the θ-band network.

NBS revealed a missing right-occipital network cluster within the α-band network in AD, as well as reduced posterior-anterior connectivity and weakened frontal connections (Figure 3.3). Topographical differences between DLB and HC included affected parietal-frontal connectivity. For the β-band network, occipital-central patterns and connections over the right-temporal areas were weaker in LBDs vs HC. Left occipital-frontal connectivity patterns and left temporal area were lower in DLB compared with AD.

Average WPLI in DLB correlated negatively with severity of visual hallucinations as assessed with NPI hallucination score within the α and β bands (Figure 3.4). No other significant correlations were found between connectivity strength and other clinical scores.

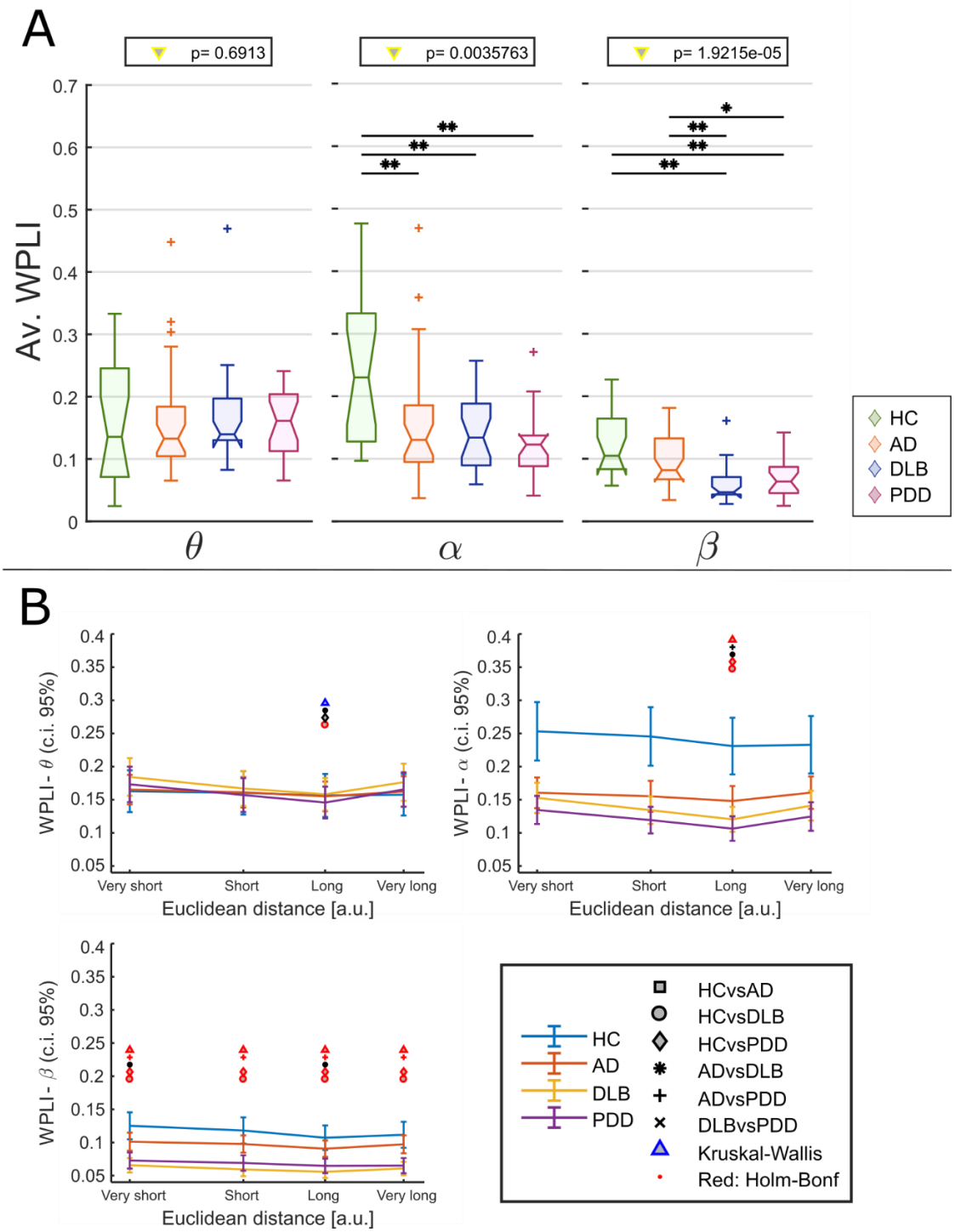

Figure 3.2 – Results from the connectivity strength analysis (Mehraram *et al.*, 2019). (A) Average WPLI for each group and frequency band; values on top indicate the result of the one-way ANOVA ($p<0.05$); *significant two tailed Mann-Whitney U test post hoc test ($p<0.05$); **post hoc test survives Holm-Bonferroni correction (6 comparisons). (B) Distance analysis. WPLI values are averaged by edge length ranges; very short: < 57 mm; short: 57 – 114 mm; long: 115 – 170 mm; very long: 171 – 227 mm. Different markers were used to indicate significant results from one-way Kruskal-Wallis ($p<0.05$) and two-tailed Mann-Whitney U test post hoc test ($p<0.05$) as described in the legend on the right side. Red marker: test survives Holm-Bonferroni correction (Kruskal-Wallis: 4 ranges; post hoc: 6 comparisons). Error bars represent 95% confidence interval.

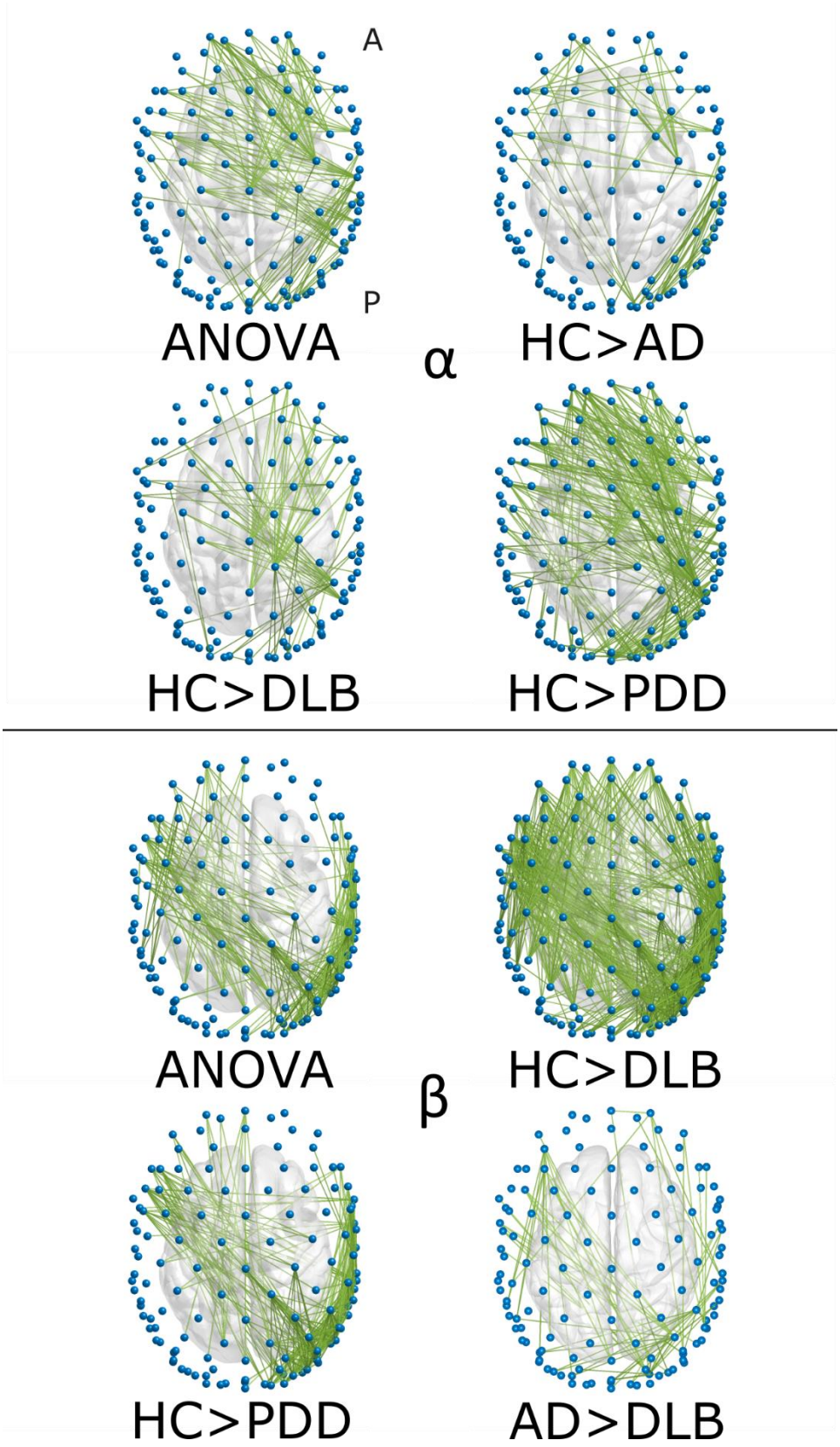

Figure 3.3 - Results from the two-tailed t-tests (5000 permutations) with the NBS (Mehraram *et al.*, 2019) (Network Based Statistics, ANOVA F-threshold = 8, $p<0.0042$; post hoc t-threshold = 3.8, $p<0.0042$) respectively in α (top) and β (bottom) range. A: anterior; P: posterior. No significant differences were found in θ band.

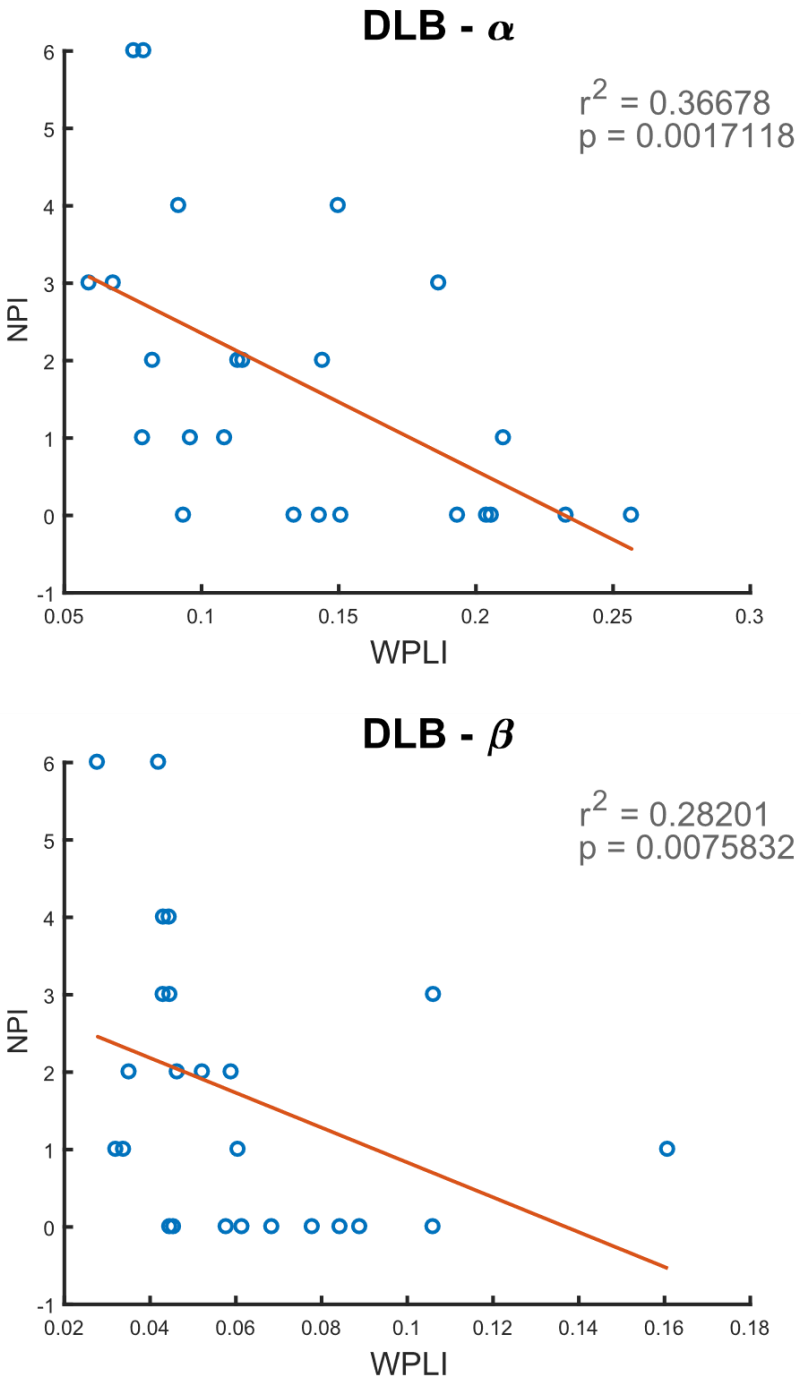

Figure 3.4 - Significant Spearman's test correlation between WPLI and NPI score in DLB at α and β frequency bands (Mehraram *et al.*, 2019).

3.4.2. Weighted vs binary graphs after proportional thresholding

Before estimating graph theory measures, proportional threshold was applied on WPLI matrices, obtaining a range of matrices with density spanning between 3% and 60%.

Dependency of C and L on PT% was compared between weighted and binary graphs, and was lower when weights were preserved, as assessed with Spearman rank correlation test ($p = 0, \rho_{C_b} = 0.9666, \rho_{C_w} = 0.6765, \rho_{L_b} = -0.9692, \rho_{L_w} = -0.0665$). Normalised metrics were less influenced by preservation of weights compared with not normalised ones ($p = 0, \rho_{C_{b_{norm}}} = 0.5134, \rho_{C_{w_{norm}}} = 0.4673, \rho_{L_{b_{norm}}} = -0.7981, \rho_{L_{w_{norm}}} = 0.1022$). Metric-versus-density trends for C and L in the β range and statistical tests at each PT% are shown respectively in Figure 3.5 and Figure 3.6**.**

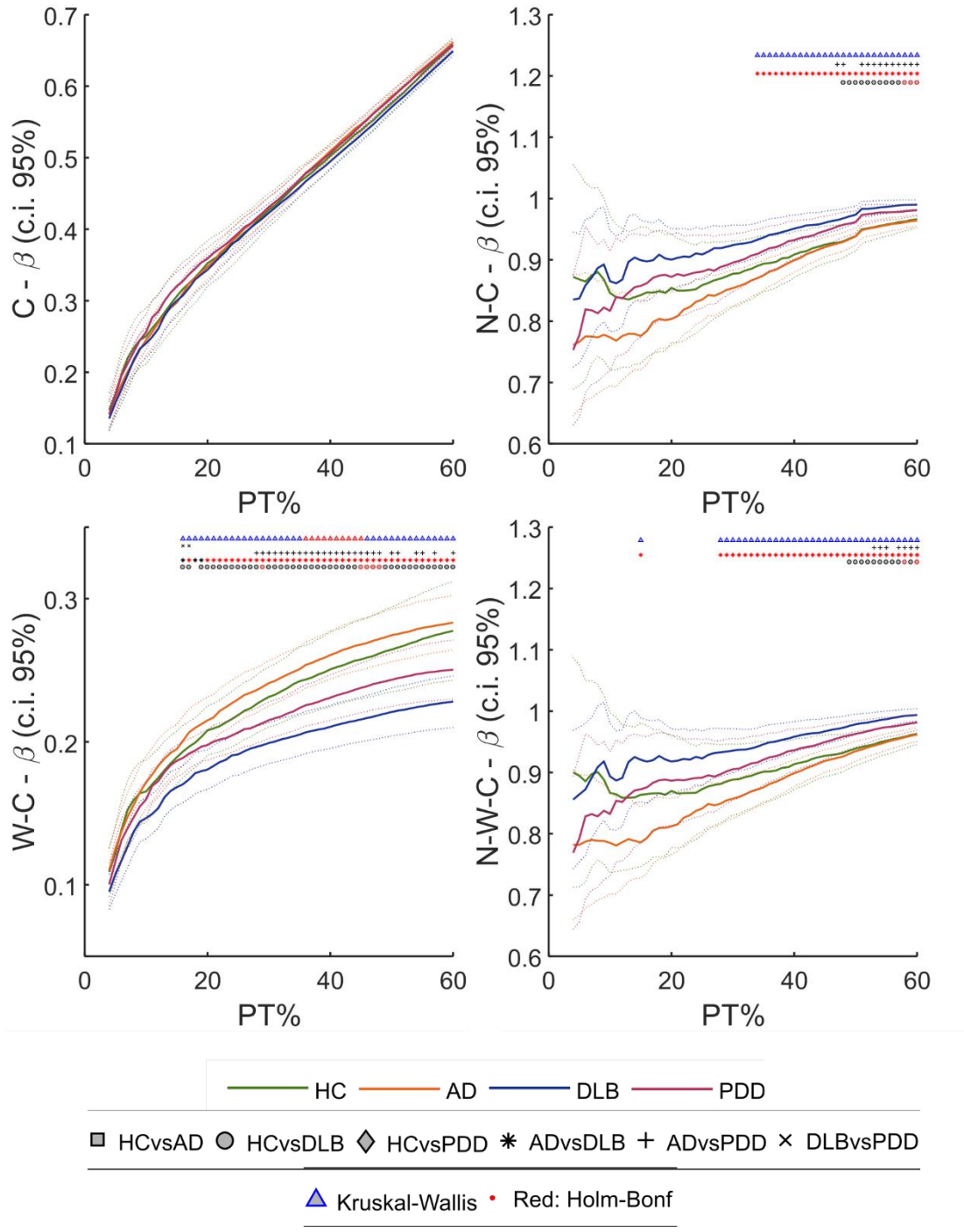

Figure 3.5 – Dependence of clustering coefficient on connectivity matrix thresholding level (PT%) (Mehraram *et al.*, 2019). Horizontal axis: PT% (range within 3-60); vertical axis: network measure. Markers on top represent results of one-way Kruskal-Wallis ($p<0.05$) and two-tailed Mann-Whitney U post hoc tests ($p<0.05$) performed at each PT% as described in the legend on side. Red marker: test survives Holm-Bonferroni correction (Kruskal-Wallis: 60 tests; post hoc test: 6 comparisons). Dotted lines of the same colour delineate 95% confidence interval for each group. From top-left to bottom-right: average clustering coefficient (C), average normalized clustering coefficient (N-C), average weighted clustering coefficient (W-C), average normalized weighted clustering coefficient (N-W-C).

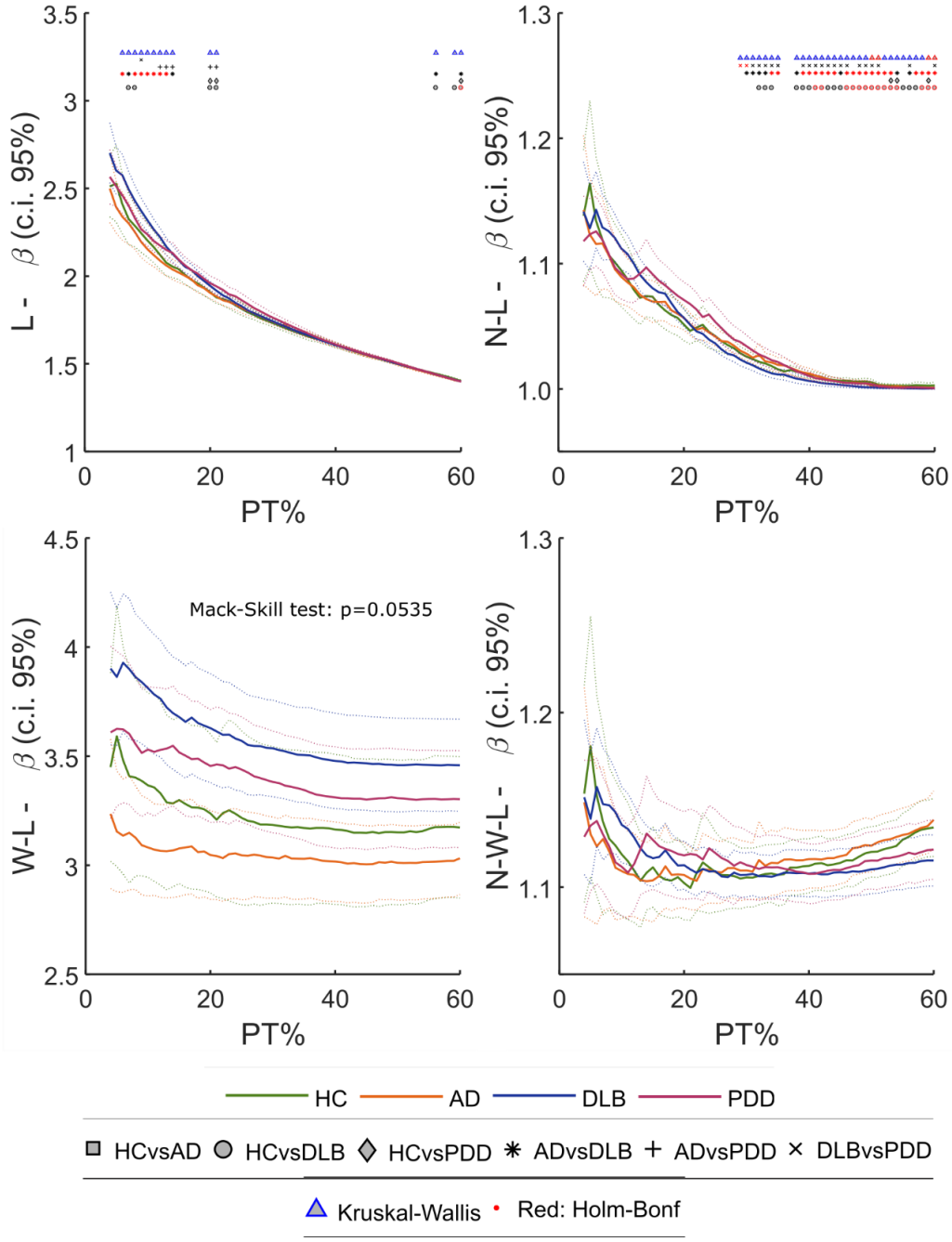

Figure 3.6 - Dependence of characteristic path length on connectivity matrix thresholding level (PT%) (Mehraram *et al.*, 2019). Horizontal axis: PT% (range within 3-60); vertical axis: network measure. Markers on top represent results of one-way Kruskal-Wallis ($p<0.05$) and two-tailed Mann-Whitney U post hoc tests ($p<0.05$) performed at each PT% as described in the legend on side. Red marker: test survives Holm-Bonferroni correction (Kruskal-Wallis: 60 tests; post hoc test: 6 comparisons). Dotted lines of the same colour delineate 95% confidence interval for each group. From top-left to bottom-right: average characteristic path length (L), normalised average characteristic path length (N-L), weight-based average characteristic path length (W-L), weight-based normalized average characteristic path length (N-W-L).

Differences between groups at each PT% were tested only if Mack-Skill test revealed an effect of PT% on network measure. As resulting from correlation tests, curves obtained from weighted measures show reduced slope, that is, reduced dependency on threshold axis, PT%. For C (Figure 3.5), tests were significant only in the weighted case (Kruskal-Wallis: $p < 0.05$ with Holm-Bonferroni correction). Notably, W-C was significantly lower in DLB when compared with AD for PT% > 15; normalised (W-)C showed similar results, with differences between AD and DLB at PT% > 33 in the binary case and PT% > 27 for the weighted measure. Moreover, dependence of L on PT% was strongly reduced in the weighted case (W-L) (Figure 3.6). In fact, Mack-Skill test did not result in any significant PT% effect on W-L ($p = 0.0535$). DLB had higher binary L compared with AD for PT% < 15, whilst the normalised measure revealed differences between DLB and AD as well as between DLB and HC for PT% > 28. No differences between groups were found for normalised W-L. Correlation curves for other network features are reported in Appendix A**.**

To investigate the attenuation effect of graph weights on measure – density relation, network-versus-threshold curves were modelled as first order power law equations. The analysis for C in HC within β-band network is reported below, but similar results are obtained with L (see Appendix A). Binary and weighted measures were modelled respectively as $\mathrm{C_b} = \mathrm{ft^g} + \mathrm{h}$ and $\mathrm{C_w} = \mathrm{mt^n} + \mathrm{q}$, with *t*=PT%, with b and w standing for binary and weighted measures. Model fitting yielded the following coefficients (with 95% confidence interval shown in brackets): *f* = 0.8065 [0.7941; 0.8189]; *g* = 0.6718 [0.6269; 0.7161]; *h* = 0.072 [0.05228; 0.09172]; *m* = 0.9912 [0.6306; 1.352]; *n* = 0.06905 [0.04059; 0.09751]; *q* = -0.6802 [-1.043; -0.3175]. Goodness of fit is described by SSE: $SSE_b = 0.003371$, $SSE_w = 0.0002147$.

The first derivative of the fitting equations with respect to *t* is associated with curve dynamics, that is, curve slopes. A derivative closer to zero reflects a steady behaviour. For binary and weighted C derivatives are: $\frac{\mathrm{dC_b}}{\mathrm{dt}} = \mathrm{fgt^{g-1}}$ and $\frac{\mathrm{dC_w}}{\mathrm{dt}} = \mathrm{mnt^{n-1}}$. Values of *t* were searched for which the weighted measure showed lower dependence on PT% compared with the binary one. Mathematically:

$$\frac{dC_w}{dC_b} < 1; 0 < t \leq 1 \tag{3.1}$$

Solving inequation (3.1) yielded $0.0322 < t \leq 1$. Hence, dependence of C on PT% in HC is lower in weighted graphs than in binary graphs for almost all PT%.

Remaining results of this study are reported for weighted graphs only, since these have been proved to lead to more sable results compared with binary ones. Same statistics for binary metrics, as well as network measures computed on non-thresholded weighted matrices, are reported in Appendix A.

3.4.3. Network properties alterations

Hypothesis of this analysis is that EEG network architecture at rest is affected depending on dementia subtypes. Results from comparison of network measures between groups are shown in Figure 3.7. Differences within the θ-band emerged only for small-worldness and modularity. LBD (DLB and PDD) showed increased network segregation when compared with AD. These two measures significantly correlated with cognitive scores (MMSE and CAF) and NPI-hall score in the same frequency band in PDD, but not in DLB. All measures (except for a trend in small-worldness) were significantly different between LBD and HC within the α-band network. Network integration was also reduced in dementia groups as reflected by higher characteristic path length and modularity. Average clustering coefficient and characteristic path length respectively in DLB and PDD correlated with the Animal naming test, whilst node degree and average characteristic path length in DLB showed significant correlation with verbal fluency (FAS) test score. The strongest difference was found within the β-band network, and consisted of greater general alteration of network measures in DLB compared with AD. Specifically, DLB showed weaker connectivity and more segregated network compared with AD. Subtle differences with PDD and HC were also found. Complete results from correlation with clinical score tests are shown in Table 3.1 and Figure 3.8**.**

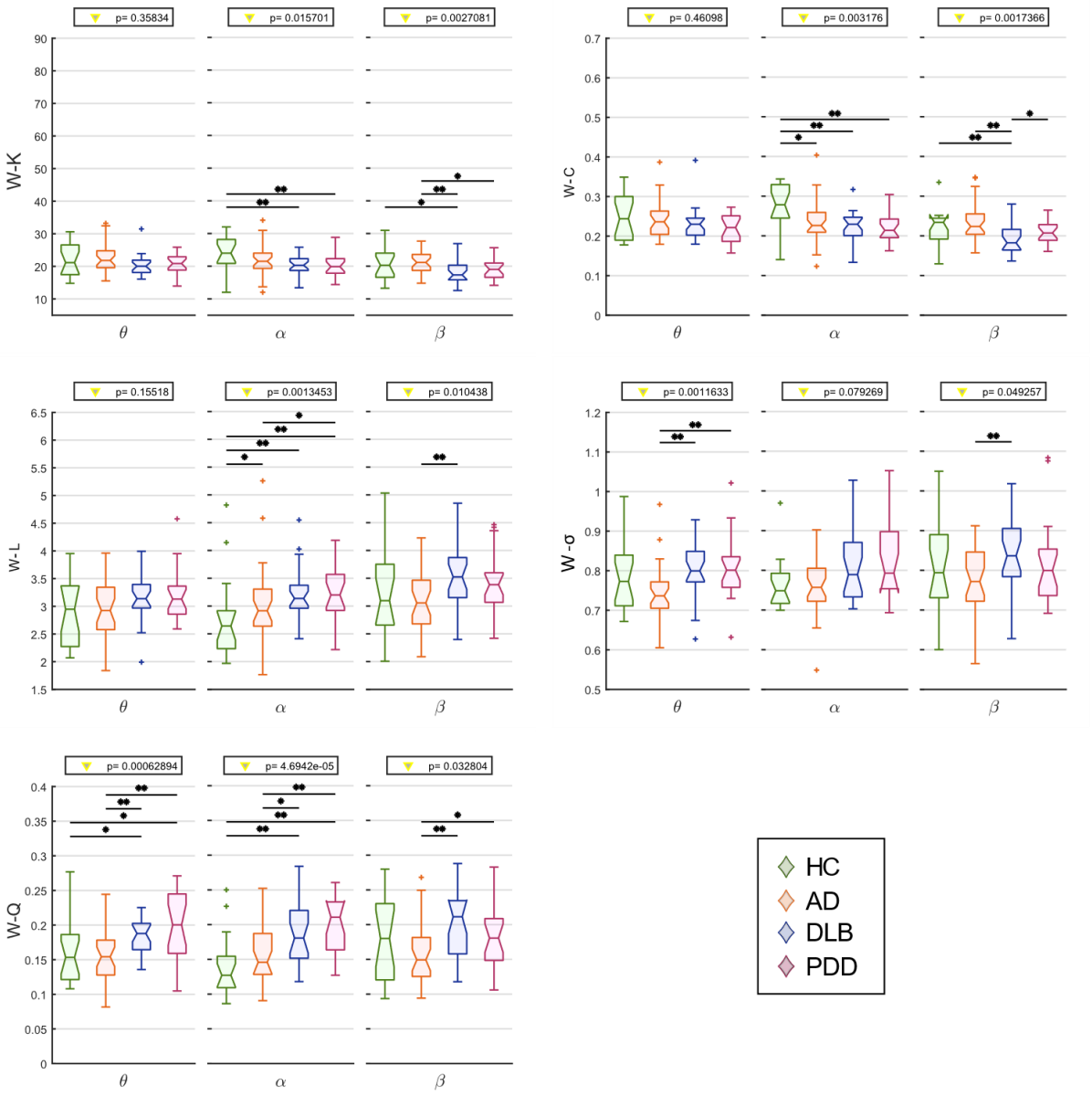

Figure 3.7 – Results from the graph theory analysis on the average weight-based network measures. Vertical axis: network measure. W: weighted. K: node degree; C: clustering coefficient; L: characteristic path length; σ: small-worldness; Q: modularity. Horizontal axis: frequency band of interest (θ: 4-7.5 Hz, α: 8-13.5 Hz, β: 14-20.5 Hz). Values on top indicate the result from the one-way Kruskal-Wallis test ($p<0.05$); *significant two-tailed Mann-Whitney U test post hoc test ($p<0.05$); **post hoc test survives Holm-Bonferroni correction (6 comparisons).

		HC			AD			DLB			PDD		
		θ	α	β	θ	α	β	θ	α	β	θ	α	β
WPLI	*NPI*	-	-	-	-	-	-	-0.29 (0.165)	**-0.61 (0.002)**	**-0.53 (0.008)**	0.02 (0.936)	-0.21 (0.362)	-0.23 (0.325)
W-K	*FAS*	-0.01 (0.974)	-0.35 (0.154)	-0.44 (0.070)	0.07 (0.705)	0.03 (0.886)	-0.13 (0.493)	-0.26 (0.215)	**-0.46 (0.020)**	-0.36 (0.081)	-0.10 (0.666)	-0.19 (0.400)	-0.26 (0.250)
W-C	*Animals*	-0.46 (0.056)	-0.18 (0.465)	0.14 (0.578)	-0.06 (0.740)	0.32 (0.073)	-0.18 (0.315)	-0.10 (0.639)	**-0.44 (0.028)**	-0.13 (0.524)	-0.12 (0.617)	-0.43 (0.050)	-0.11 (0.627)
W-L	*FAS*	0.04 (0.871)	0.34 (0.173)	0.42 (0.086)	-0.06 (0.734)	-0.00 (0.981)	0.17 (0.384)	0.30 (0.147)	**0.44 (0.030)**	0.36 (0.073)	0.06 (0.781)	0.16 (0.499)	0.28 (0.215)
	Animals	0.38 (0.115)	0.09 (0.733)	-0.28 (0.270)	0.06 (0.742)	-0.16 (0.388)	0.32 (0.075)	0.12 (0.553)	0.39 (0.057)	0.18 (0.380)	0.24 (0.300)	**0.45 (0.041)**	0.15 (0.504)
W-σ	*MMSE*	-0.36 (0.142)	-0.09 (0.724)	-0.44 (0.070)	0.21 (0.254)	-0.25 (0.160)	0.12 (0.508)	-0.06 (0.782)	0.12 (0.571)	0.14 (0.501)	**-0.62 (0.003)**	-0.37 (0.101)	-0.01 (0.968)
	CAF	-	-	-	-	-	-	0.09 (0.691)	-0.31 (0.138)	-0.09 (0.684)	**0.56 (0.014)**	0.43 (0.064)	0.06 (0.818)
	NPI	-	-	-	-	-	-	0.22 (0.292)	0.17 (0.428)	0.37 (0.077)	**0.49 (0.025)**	0.32 (0.151)	-0.16 (0.499)
	UPDRS	0.02 (0.949)	-0.18 (0.478)	-0.17 (0.497)	-0.20 (0.290)	0.11 (0.547)	0.04 (0.844)	**0.40 (0.049)**	-0.04 (0.842)	-0.17 (0.421)	0.31 (0.165)	0.38 (0.093)	-0.16 (0.476)
W-Q	*MMSE*	-0.17 (0.491)	-0.04 (0.869)	-0.31 (0.217)	0.19 (0.287)	-0.26 (0.157)	0.06 (0.746)	-0.17 (0.425)	0.27 (0.196)	0.16 (0.440)	**-0.74 (0.0001)**	-0.37 (0.102)	-0.07 (0.777)
	CAF	-	-	-	-	-	-	0.21 (0.328)	-0.19 (0.371)	0.06 (0.770)	**0.69 (0.001)**	0.40 (0.092)	-0.02 (0.951)
	FAS	0.003 (0.99)	**0.52 (0.026)**	0.33 (0.177)	0.34 (0.063)	0.02 (0.932)	0.13 (0.495)	-0.22 (0.286)	0.31 (0.137)	0.03 (0.891)	-0.09 (0.711)	-0.03 (0.913)	0.01 (0.982)

Table 3.1 – Correlations between network measures and clinical scores as assessed by Spearman test ($p<0.05$, uncorrected). *ρ* and p values are shown whether any correlation for that network measure and clinical variable was found for any diagnosis group and frequency band. Significant correlations are highlighted in bold.

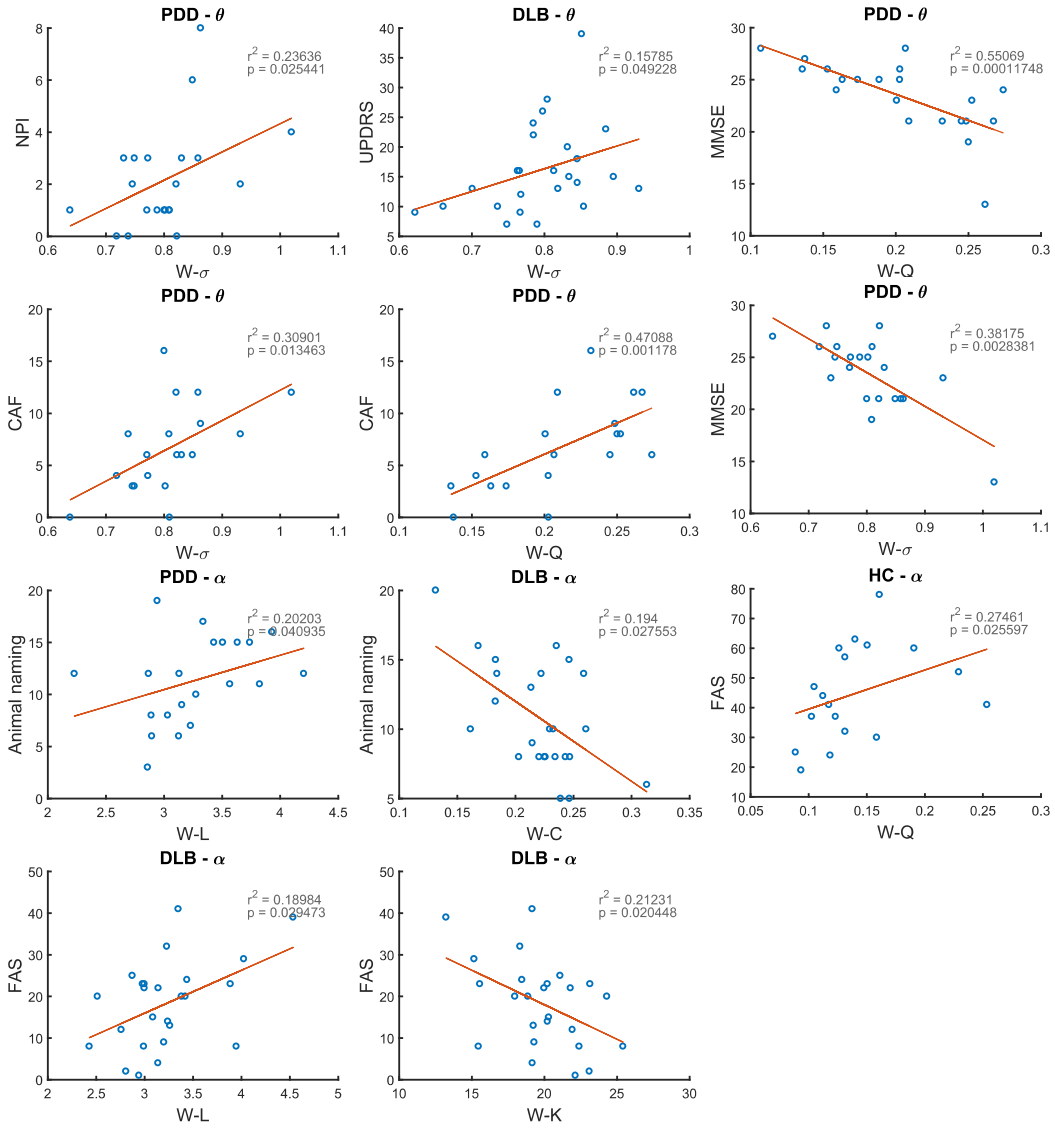

Figure 3.8 – Significant correlations between weight-based network measures and clinical scores assessed by Spearman test ($p < 0.05$, uncorrected). For each correlation, r^2 and p-value are shown.

Regional differences in local measures (average node degree and clustering coefficient) were also investigated (Figure 3.9). Node degree was not locally different between groups in the α-band network, whilst differences in DLB compared with AD within the β-band were driven by the occipital region ($p < 0.01$), although frontal regions also presented significant differences ($p < 0.05$). Clustering coefficient was significantly lower in DLB compared with AD in the β-band over frontal and posterior areas. For both measures, lateral areas were not differently

affected by the disease. Local changes of node degree and clustering coefficient reflect connectivity patterns which are associated with network disruption (see section 3.4.1).

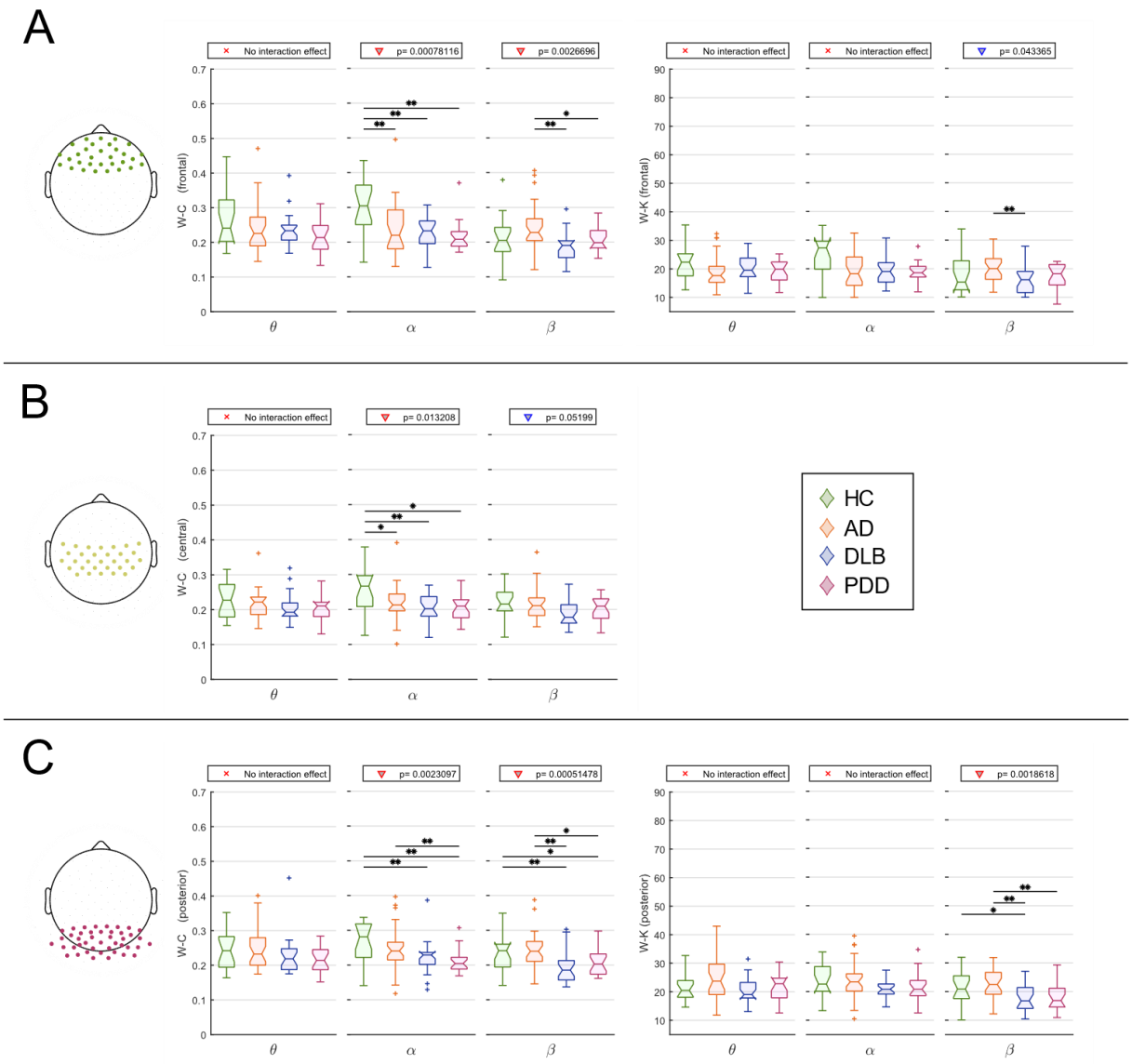

Figure 3.9 – Results from local graph theory analysis through average local weight-based network measures. Y-axis: local network measure; x-axis: frequency band of interest (θ: 4-7.5 Hz, α: 8-13.5 Hz, β: 14-20.5 Hz). If any interaction was found in the repeated measures ANOVA (within subjects: areas; between subjects: group), the result of the one-way Kruskal-Wallis test ($p<0.05$) is indicated on top of each plot. Red triangle: Kruskal-Wallis test survives Holm-Bonferroni correction (4 areas); *significant two-tailed Mann-Whitney U test post hoc test ($p<0.05$); **post hoc test survives Holm-Bonferroni correction (6 comparisons). A: frontal area. B: central area. C: posterior area. No significant differences between groups were found in the lateral area and for the node degree in the central area.

3.4.4. Targeted node attack outcome

Figure 3.10 shows the outcome of the network node attack analysis at network density of 15%. The clearest result is a delayed peak of LBD in the α-band compared with HC. No clear differences between groups in terms of peak position emerged in other frequency bands. Similar outcome is obtained at network density of 10% and 20%, as reported in Appendix A.

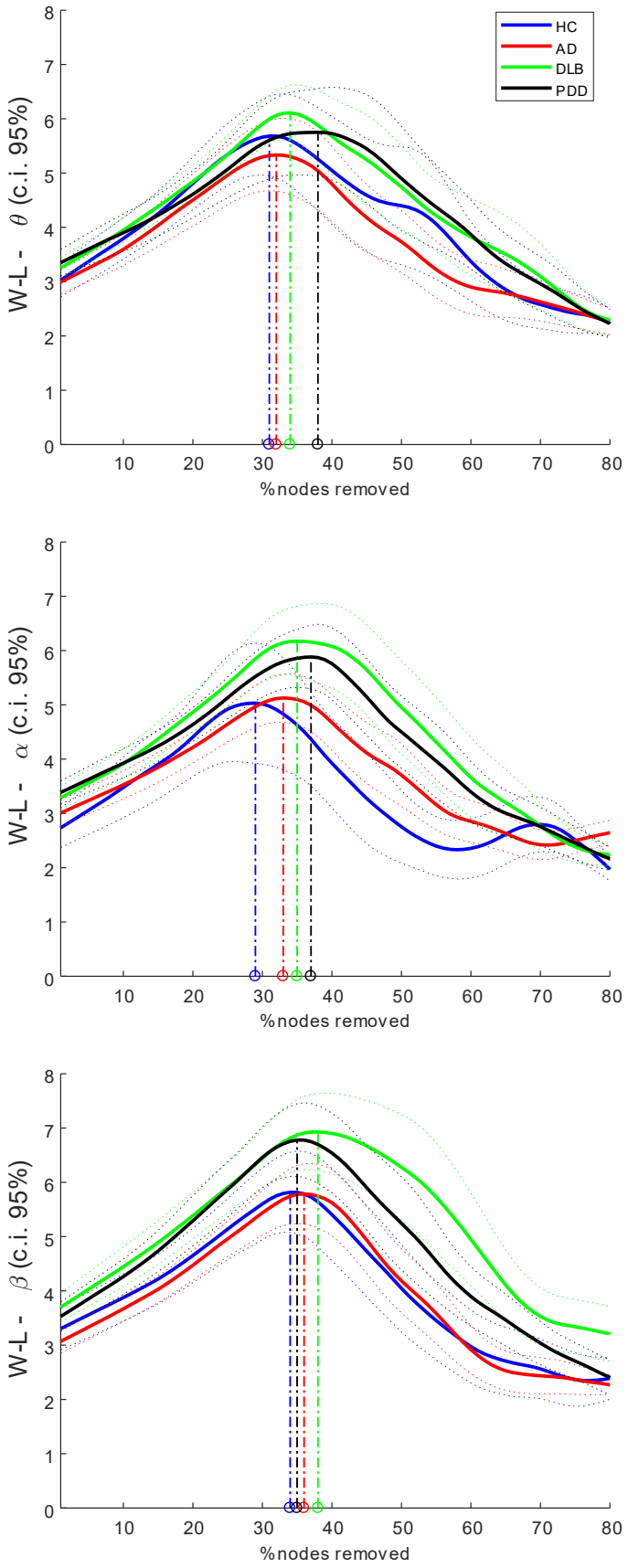

Figure 3.10 – Results of targeted node attack (edge density = 15%). Y axis is the weight-based characteristic path length, x axis is the percentage of removed nodes.

3.4.5. Diagnostic accuracy

From statistical analysis, two scenarios emerged for which significant differences between groups were found for most network features: DLB versus AD and LBD versus HC. Results for other scenarios are reported in Appendix A. All weighted network measures were used to train a random-forest classifier, from which ROC curves shown in Figure 3.11 were obtained. For each scenario, mean variable importance ranking was obtained. DLB vs AD classifier yielded mean accuracy of 66% (± 13%), mean F_1 score of 65% (± 13%), mean positive predictive value (PPV) of 66% (± 22%), mean negative predictive value (NPV) of 71% (± 13.04%), optimal sensitivity and specificity respectively of 47 and 100%, and AUROC of 78% (± 15%). The four most important variables based on classifier ranking were WPLI in the β-band, modularity in the θ-band, node degree in the β-band, and small-worldness in the θ-band. LBD and HC were classified with mean accuracy and F_1 score of 76% (± 12%), mean PPV of 88% (± 10%), mean NPV of 59% (± 21%), optimal sensitivity and specificity respectively of 59 and 100% and AUROC of 82% (± 14%). The four most important variables were the WPLI in the β-band, modularity, characteristic path length and clustering coefficient in the α-band.

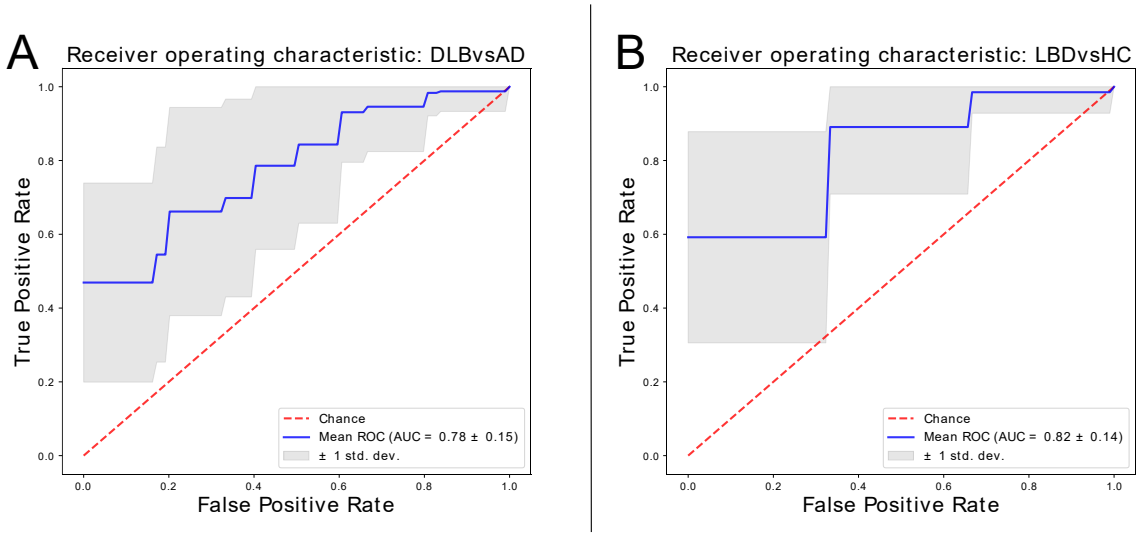

Figure 3.11 – Receiver operating characteristic (ROC) curves obtained with random forest classifier and computed for each of the defined scenarios. All (weighted) network measures were used to train the classifier. A: DLB vs AD, mean accuracy: 66% (± 13), optimal sensitivity and specificity respectively of 47% and 100%; B: LBD vs HC, mean accuracy: 76% (± 12%), optimal sensitivity and specificity respectively of 59% and 100%.

3.4.6. Effect of EEG cap density on connectivity and graph measures

Spatial subsample of EEG recordings did not lead to significant differences in network features. In fact, connectivity strength difference patterns were not affected by subsampling, whilst some topological differences between groups were less prominent (Figure 3.12).

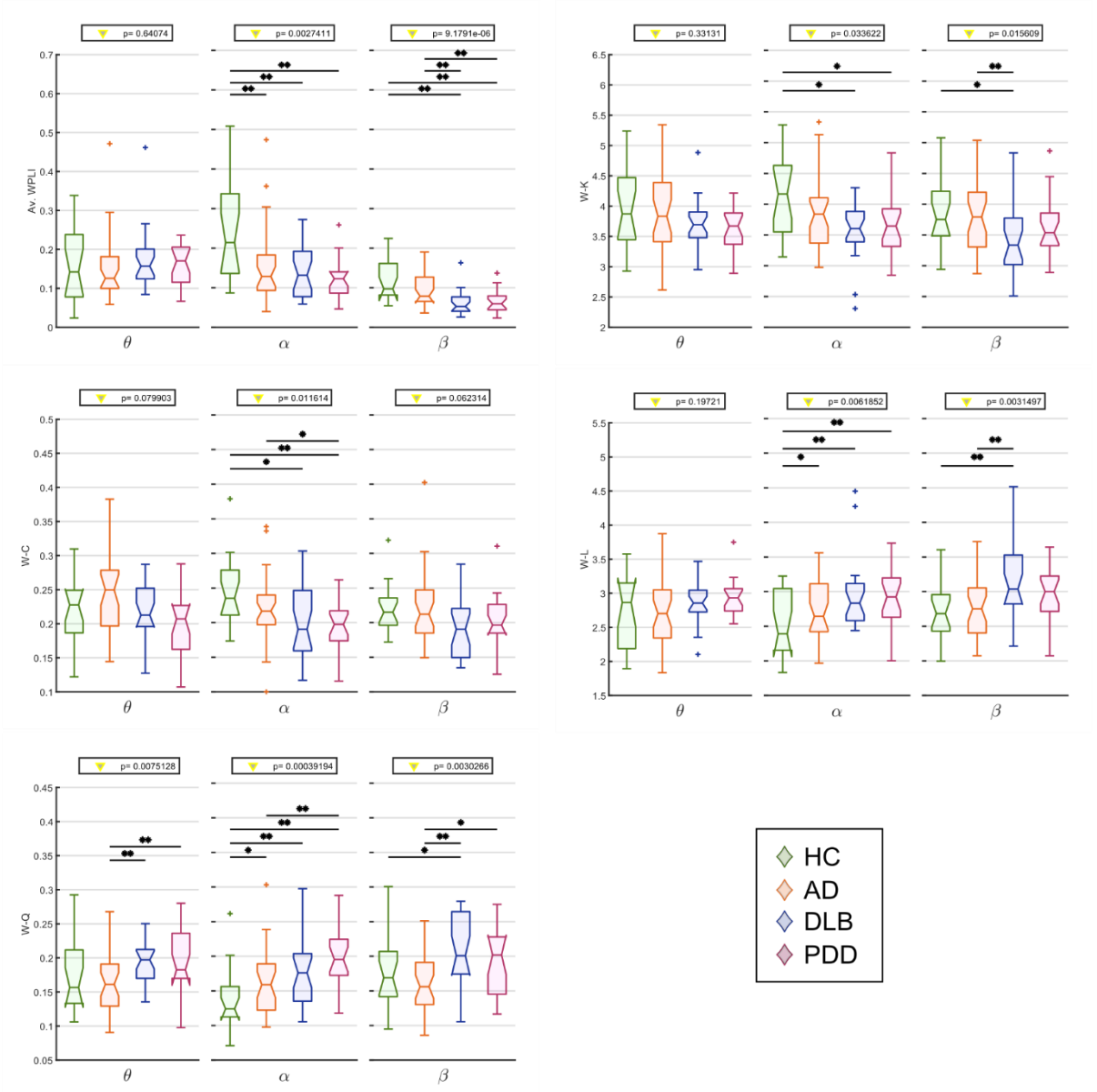

Figure 3.12 - Connectivity and network measures obtained with EEG 10-20 system. y-axis: measure; x-axis: frequency band of interest (θ: 4-7.5 Hz, α: 8-13.5 Hz, β: 14-20.5 Hz). The result of the one-way Kruskal-Wallis test ($p < 0.05$) is indicated on top. *significant two-tailed Mann-Whitney U test post hoc test ($p < 0.05$); **post hoc test survives Holm-Bonferroni correction (6 comparisons). Small-worldness is not reported here, as it can be obtained from C and L.

3.5. Discussion

The primary hypothesis of this study was that different dementia subtypes are associated with differential alterations in EEG network features. Connectivity strength was lower in dementia groups compared with HC within α-band network and reduced in DLB compared with AD in the β-band. These differences could potentially introduce a bias in network measures (van den Heuvel *et al.*, 2017), hence weighted graphs were normalised before extracting network features. Results from the present work supported the proposition that weighted graph measures are consistent across graph densities, and these measures were significantly altered in DLB compared with AD within the β-band. In addition, in Lewy body dementia (LBD) groups, i.e. DLB and PDD, network properties were significantly altered compared to HC and were more segregated than AD network. Classification between DLB and AD based on random forest approach was driven by connectivity strength and node degree in the β-band as well as segregation measures in the θ-band. For LBD, differentiation from HC was mostly due to connectivity strength in β-band network and graph features in α-band.

Patients in this study were on a range of medications. As mentioned in section 1.4.2, this likely partially restored EEG activity and network properties towards normative values (Agnoli *et al.*, 1983; Balkan *et al.*, 2003) making group differences less distinct. Nevertheless, significant alterations across patient group emerged and resonated with previous findings (Stam *et al.*, 2009; Peraza *et al.*, 2018).

3.5.1. Average connectivity is reduced in dementia

Statistical analysis revealed lower WPLI in dementia compared with HC within the α-band network. Also, overall β-band network connectivity was weakened for all groups, and significantly lower in LBD compared with HC. Notably, connectivity analysis revealed that β-band might potentially be a biomarker for differentiation of DLB vs AD. This latter finding is supported by previous M/EEG network studies (Stam *et al.*, 2009; Dauwan *et al.*, 2016; Engels *et al.*, 2017; Peraza *et al.*, 2018), and may reflect network randomisation in LBD (Peraza *et al.*, 2018). Distance analysis outcome in α- and β-band reproduced the scenario of a previous fMRI study, where authors found a decreasing trend of connectivity strength towards longer connections (Peraza *et al.*, 2015). WPLI values correlated negatively with visual hallucination

frequency and severity as assessed with NPI-hall score in DLB for both α- and β-band. This correlation is in line with a previous study which pursued a modelling approach to associate visual hallucinations with impairment of attentional networks in LBD (Shine *et al.*, 2011), and might reflect the role of EEG α- and β-band frequency activity respectively in visuo-attentional and cognitive mechanisms (Anderson and Ding, 2011; Bauer *et al.*, 2012; Lopes da Silva, 2013).

3.5.2. Topographical connectivity patterns are altered in dementia

NBS analysis revealed that most affected connections in AD and DLB compared with HC comprised posterior-anterior pathways, in agreement with previous findings (Lemstra *et al.*, 2014; Dauwan *et al.*, 2016). This also matches with the outcome from NBS, which detected affected long connections in both α- and β-band networks (Figure 3.3). A possible speculation is that weakening of these pathways is associated with impairment of attentional networks, which are thought to be affected in AD and DLB (Corbetta and Shulman, 2002; Cromarty *et al.*, 2018). In fact, disruption of the occipital cortical network may play a role in alteration of information flow towards frontal areas in DLB (Briel *et al.*, 1999; Bonanni *et al.*, 2008; Peraza *et al.*, 2014).

Results of this analysis partially contrast with a recent EEG connectivity study which reported differences between dementia groups in the α-band, but no differences in the β-band (van Dellen *et al.*, 2015). This apparently contrasting finding may be due to methodological differences in the analysis. For instance, PLI might omit significant differences between groups in scenarios when the overall connectivity is low, such as we found in the β-band, and uncorrelated noise might affect connectivity (Vinck *et al.*, 2011).

3.5.3. Weighted measures preserve topological information

Preservation of graph weights prevents loss of topological network information. In line with previous research on schizophrenia (Rubinov *et al.*, 2009), in this analysis more prominent differences between patient groups emerged in weighted than in binary measures. Contrary to what has been stated in other studies (Li *et al.*, 2009; Ponten *et al.*, 2009; van Wijk *et al.*, 2010), the outcome of the analysis was influenced by graph weights. In fact, in Ponten *et al.*

(2009) analysis was performed with only network measures normalised by random surrogates when comparing binary and weighted graphs. Normalised measures as reported in section 3.4.2 were less dependent on graph weights. However, normalisation may be associated with a bias accentuating size effect on the measures (van Wijk *et al.*, 2010). Furthermore, the strategy pursued to obtain normalised metrics may influence their dependence on network size, as discussed below.

3.5.4. Normalised clustering coefficient shows an unexpected trend

In order to compute small-worldness, (weighted) clustering coefficient and characteristic path length were normalised by the same measures obtained on random matrices (see section 2.6.2). According to most network studies, small-world networks show a clustered organisation which is in between random and regular networks, i.e. normalised clustering coefficient is above 1, and decays linearly as network density increases (Humphries and Gurney, 2008; Telesford *et al.*, 2011; Sun *et al.*, 2014b; Peraza *et al.*, 2015). However, an inverse trend was obtained in this study, i.e. normalisation yielded values lower than 1, which increased towards higher network density (Figure 3.5). Further investigation revealed that this outcome is due to the choice of preserving node degree distribution when randomising connectivity matrices. This approach was preferred to a complete random edge shuffling as it takes into account differences in degree distribution between groups which might influence network clustering (Milo *et al.*, 2002; Sporns and Zwi, 2004). In addition, this approach is comparable with previous dementia studies (Stam *et al.*, 2007a; Peraza *et al.*, 2018). In fact, if randomisation is performed by shuffling edges (in either binary or weighted graphs) regardless of node degree distribution, i.e. by generating equivalent Erdős–Rényi networks as proposed by Humphries and Gurney (2008), the obtained trend is in line with previous studies, as shown in Figure 3.13. To the best of author's knowledge, the analysis presented in this thesis is the only one to date based on WPLI in which network measure trends with respect to network density are investigated. Hence, speculation on the source of this apparently unexpected outcome cannot be based on direct comparison with existing literature. Previous studies based on (W)PLI did actually rely on Erdős–Rényi random surrogates rather than degree-conservative matrices, and results matched with the criterium for which (W-)$C>C_{rand}$ (Stam *et al.*, 2009; Hardmeier *et al.*, 2014), although Stam *et al.* (2009) also found relatively low values

compared with other studies. A possible explanation to this phenomenon as suggested by Stam *et al.* (2009) is that spurious connectivity due to volume conduction captured by other connectivity strength measures might generate spurious clusters throughout the network, which are absent in PLI-based graphs. This attenuation is likely even more enhanced in WPLI, and preserving node degree while randomising WPLI-based graphs might generate spurious clustering, which leads to N-C < 1. Instead, a complete randomisation destroys graph structure, preventing this phenomenon and leading to N-C > 1. Therefore, unlike other connectivity measures, it seems to be crucial in WPLI network graphs to take the degree distribution in account when assessing network motifs to correctly interpret associated analyses and results.

Nevertheless, even in this case recommendation proposed in this study on the use of weighted measures without normalisation holds true all the more for this reason. In fact, topological information is lost after normalisation and no differences between groups emerge anymore (Figure 3.13). Moreover, dependence of normalised measure on PT% is higher than of W-C ($\rho_{N\text{-}W\text{-}C}$ = -0.8898). This latter aspect is discussed in the section below.

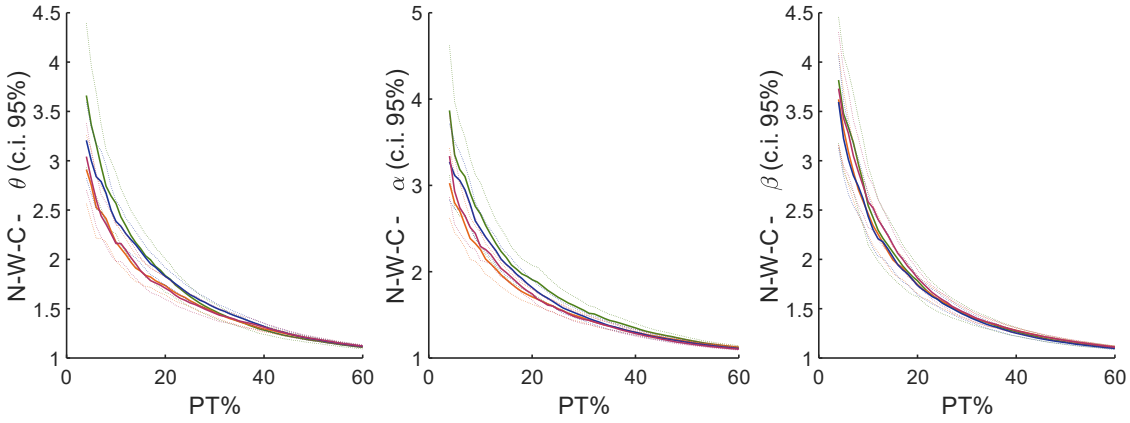

Figure 3.13 – Normalised clustering coefficient (N-W-C) vs graph density (PT%). Normalisation of W-C is computed with equivalent Erdős–Rényi random surrogates. Similar outcome is obtained with binary clustering coefficient.

3.5.5. Weighted measures are less dependent on network density

Dependence of network measures on edge density is a well reported issue (van Wijk *et al.*, 2010; Langer *et al.*, 2013). With the analysis presented in this chapter, a rationale has been proposed for using thresholded weighted graphs rather than binary ones in graph theory studies. In fact, weighted network measures are more consistent across densities than their binary counterpart. Alternative may be to consider full non-thresholded weighted matrices, in which case interpretation of connectivity measures would change. In fact, node degree would instead be a measure of nodal strength, i.e. total involvement of the node in the network, rather than number of connected edges (Opsahl *et al.*, 2010). Network thresholding preserving graph weights is here recommended as a reasonable compromise. MST constructed graphs are also another strategy to avoid dealing with thresholding arbitrariness. As mentioned in section 1.4.3, MST leads to fully connected weighted graphs (Stam *et al.*, 2014), i.e. full sized networks. Peraza *et al.* (2018) performed an EEG study based on MST with the same cohort of participants. Although differences in connectivity strength are comparable with findings of the analysis reported in this chapter, MST approach does not provide local alterations within network architecture, which in the present study were found significant in patient groups.

However, the approach pursued in this study presents with some limitations. In fact, these results are limited to the context of EEG connectivity analysis. Further investigation will be required to reproduce these results with other methodologies. The choice of WPLI as connectivity measure may also have influenced the analysis outcome. Attenuation of quasi-zero lag connections (Vinck *et al.*, 2011) likely introduces higher number of weak edges which weakly influence the whole network when introduced as the network density increases.

3.5.6. Brain functional network is segregated in dementia

Dementia groups showed higher segregation and lower integration in the EEG brain network. Reduced integration reflects in higher characteristic path length, as also found in a previous EEG study (Stam *et al.*, 2007a). Longer path length is thought to be associated with reduced interaction between cortical areas (Sporns and Zwi, 2004), although this contrasts with another study where path length in AD group was shorter than in HC (de Haan *et al.*, 2009). In

fact, different thresholding strategy and connectivity measure might play a role in interpreting the contrasting results. In de Haan *et al.* (2009) three arbitrary threshold values were chosen to obtain network graphs, whilst in the present study a wide range of graph densities was considered, which might have led to the inclusion of more network topological information. In addition, their study was only based on normalised binary network features. Contrasting results in normalised values may be due to normalisation approach, as discussed in section 3.5.4. However, they suggest that their results are associated with loss of hubness and more randomised network topology in AD, in agreement with other studies (de Haan *et al.*, 2012a; Stam, 2014) and results presented in this study, as discussed in the next section (3.5.7).

Network segregation in LBD emerged within the θ-band, i.e. higher small-worldness and modularity, in line with a previous fMRI study on the same participant cohort (Peraza *et al.*, 2015). As suggested in that study, this phenomenon is likely associated with the presence of a larger number of short-range connections, altogether with weaker long-range connections in dementia groups, as we also found in the distance analysis (Figure 3.2). This might have led to higher normalised clustering coefficient and consequently higher small-worldness in LBD. Network segregation within θ-band in LBD significantly correlated with cognitive performance (MMSE and CAF scores) in PDD. It has been reported that θ-band activity has a role in memory consolidation processes, modulation of information transfer and integration across neuronal populations (Lopes da Silva, 2013). One may then speculate that these processes are affected in PDD, but not in DLB. However, further analysis is needed to assess why such correlation did not emerge in DLB, and to interpret significant correlations between graph measures and Animal naming and FAS tests reported in section 3.4.3 and Table 3.1.

3.5.7. Network hubness is reduced in dementia

LBD also present reduced node degree and clustering coefficient in the α-band, whilst these measures are lower in DLB compared with AD in the β-band. As also reported in another study, this finding may be interpreted as reduced network hubness associated with the pathology (Engels *et al.*, 2015), driven by posterior and frontal regions (Figure 3.9), resonating with disrupted topological patterns reported in section 3.4. This interpretation is also supported by the outcome of targeted node attack (see section 3.4.4). As expected, robustness to targeted

node attack as measured through characteristic path length (Figure 3.10) was higher in LBD compared to HC, suggesting that pathological condition is associated more with a small-world or random rather than a scale-free organisation of functional brain network (Kaiser *et al.*, 2007). In fact, as mentioned in section 2.6.2, whether the human brain is a scale-free network is still controversial (Eguiluz *et al.*, 2005; Kaiser *et al.*, 2007). Due to their higher hubness as compared with small-world and random networks, in a targeted node attack process scale-free networks show a peak in characteristic path length at an earlier percentage of removed nodes (Barabasi and Albert, 1999). In the reported analysis, this peak was delayed in LBD compared with HC, suggesting that hubness is affected in the pathological condition. Slight differences also emerged between groups within θ- and β-bands. As described in section 1.3.1, EEG α- and β-band activities are known to be involved respectively in attentional (Anderson and Ding, 2011) and cognitive processes (Ray and Cole, 1985). This leads to speculate that impairment of corresponding networks may emerge as alteration of connectivity features. However, in the α-band network, node degree was not locally affected, and the clustering coefficient showed a reduction over the central nodes regions in DLB.

3.5.8. LBD versus HC classification yields high accuracy

The most accurate discrimination obtained with random forest classifier was between LBD and HC groups (AUROC = 0.82 ± 0.14). Results obtained from classifier training reflect the outcome of graph theory analysis, as β- and α-band network measures were the most important for classification. Notably, WPLI in the β-band was the strongest driver of discrimination. As mentioned above, randomisation of the network in LBD might be specifically associated with network abnormalities in pathological groups (Peraza *et al.*, 2018).

3.5.9. Higher segregation and reduced hubness discriminate DLB from AD

Importance of WPLI within the β range in discriminating LBD also emerges in DLB versus AD scenario (AUROC = 0.78 ± 0.15). Important features for classification also comprise segregation of θ-band network as well as node degree in the β-band. These results are in line with the outcome of statistical tests between groups discussed in previous paragraphs and

suggest that EEG network features within θ- and particularly β-band network may be potential biomarkers for DLB versus AD differentiation. Outcome of classification analysis further confirms that higher randomisation and reduced hubness of EEG network in DLB are prominent features, suggesting that DLB may be described as a more severe disconnection syndrome compared with AD (Delbeuck *et al.*, 2003; de Haan *et al.*, 2009).

3.5.10. The optimal working point of the classifier yields maximum specificity

Notably, the optimal point of the classifier corresponded to highest specificity (100%) and lowest sensitivity (47% and 59%, respectively, for the two scenarios). In this work, the optimal point was computed as the point on the ROC curve at which the difference between true and false positive values was the highest (Fluss *et al.*, 2005; Perkins and Schisterman, 2005). Choice of the optimal point is a matter of debate among researchers, as alternative methods are being proposed whose choice might be more clinically relevant (Zou *et al.*, 2013; Rota and Antolini, 2014). In the presented work the most common strategy was pursued. However, the discrete sample size as well as imbalanced distribution of observations between groups might have introduced a bias to the outcome of the classification (Brereton, 2006; Sun *et al.*, 2009).

3.5.11. Connectivity strength is the most discriminatory variable

Higher relevance of connectivity strength as compared with other network measures for discrimination between types of neurological disease was also reported in previous studies (Xu *et al.*, 2016; Peraza *et al.*, 2018). In fact, findings of the present study provide further evidence that simple measures such as connectivity strength are likely accurate enough for diagnostic purposes. Consistency of connectivity strength difference between conditions also emerged after spatial subsampling, as shown in Figure 3.12. Suitability of EEG features as diagnostic biomarkers is strengthened by this aspect. Nevertheless, graph features abnormalities might be associated with the severity of the disease. Future studies involving prodromal and larger participant cohorts shall investigate whether similar network alteration may be detected at earliest stages of disease development and be suitable as predictive biomarkers.

3.6. Conclusions

Main findings of this study include reduced connectivity and node degree, as well as increased network segregation in the β- and θ-band in DLB compared with AD. These differential features provide accurate classification of DLB cases versus AD. In addition, network measures obtained in the α-band were significantly altered in LBD compared to HC. Further, it was demonstrated that weighted thresholded graphs yield more consistent network features across graph densities. A rationale was then provided for choosing this approach rather than binarise connectivity matrices, as this latter choice would suppress topological information stored in graph weights. These findings altogether with advantageous properties of EEG support its use as a suitable diagnostic tool for dementia and, particularly, DLB.

Chapter 4. Cortical Source Alterations in Dementia with Lewy Bodies

4.1. Summary

The graph theory study reported in the previous chapter revealed significant differences in network features between dementia types; these consisted of altered α-band network in LBD compared to HC, and differences in β-θ-band between AD and DLB. Although already clinically relevant, this information does not provide direct inference on possible pathological mechanism associated with abnormal functional changes. In the present chapter, source localisation was used to assess whether EEG graph differential features between DLB and other groups emerge at the cortical level with a source domain analysis. Furthermore, affected α-band network topographical patterns in AD and DLB were assessed, and correlation with EEG slowing over the posterior cortex was tested. Outcome of the graph theory analysis showed that scalp and source domain are equally affected in DLB, which validated EEG scalp measure as a reliable methodological approach. Affected patterns in AD and DLB within the α-band included attentional and default mode networks, in line with speculations suggesting that efficiency of such networks may be affected in dementia. Moreover, average strength across affected pathways was associated with reduced DF over the occipital lobe in DLB, but not in AD; this may lead to speculate that DF slowing and connectivity alteration could originate from the same pathological mechanisms in DLB.

4.2. Introduction

The sensor domain analysis reported in Chapter 3 showed that EEG functional connectivity between brain regions is significantly affected in dementia, depending on its type. Specifically, β-band connectivity and α-band network features are affected in LBD (DLB and PDD) as compared with HC (AUROC = 82% ± 14%), whilst β- and θ-band networks are discriminative between DLB and AD (AUROC = 78% ± 15%). No differences emerge between DLB and PDD. As discussed in section 3.5, these outcomes are supported by previous investigations on dementia-related functional alterations based on EEG and other modalities. However, whether EEG sensor domain abnormalities in DLB are associated with similar patterns at the source level is still a matter of research. Existing source domain studies involving DLB either

relied on low-density EEG recordings (Babiloni *et al.*, 2018; Babiloni *et al.*, 2020) or used a standard template as a head model to solve the inverse problem (Babiloni *et al.*, 2017).

As mentioned in section 1.4.2, the most specific EEG feature associated with DLB is a negative DF shift as compared with HC and AD (Andersson *et al.*, 2008; Bonanni *et al.*, 2008; Peraza *et al.*, 2018; Stylianou *et al.*, 2018), most prominent over posterior areas (Bonanni *et al.*, 2015; Babiloni *et al.*, 2017; Stylianou *et al.*, 2018). To date, no studies have investigated whether any correlation exists between weakening of connectivity in DLB network and DF shifting. This information would provide further insight into functional processes associated with the pathology and disease severity.

4.2.1. Objective

The first part of this chapter aimed to assess whether network features which showed abnormalities in DLB compared with HC and AD in the sensor domain are also significantly altered at the source level. In second part of the presented analysis α-band network differential topographical patterns and DF changes in DLB and AD compared to HC were obtained, and correlation between these two features was tested in both conditions.

4.3. Methods

Details on experimental protocol, EEG acquisition and measured network features are reported in Chapter 2. Since individual MRI recordings were needed to perform source localisation, a subsample of the original cohort with available MRI was selected for this analysis; this comprised 18 HC, 28 AD, and 21 DLB (see Table 4.1). EEG was recorded in eyes-closed resting state with a high-density sensor cap (128 electrodes). Recorded signals were pre-processed (section 2.3) (number of removed channels: 15 ± 13; number of removed epochs: 14 ± 10; number of removed ICA components: 39 ± 10), source localised (section 4.3.2 below) and connectivity between cortical sources was measured with WPLI (section 2.4).

	HC (N=18)	AD (N=28)	DLB (N=21)	p-value
Age	76.28 ±5.50	76.71 ±7.52	76.52 ±6.21	df=2, p-value=0.878ǂ
Male/Female	11/7	20/8	16/5	df=2, p-value=0.580ǂ
MMSE	29.17 ±0.86	20.82 ±3.83	22.90 ±4.45	df=2; p-value<0.001ǂ
CAMCOG total	96.67 ±3.68	69.07 ±13.46	74.71 ±13.36	df=2; p-value<0.001ǂ
NPI hall	0 0	0 0	1.71 ±1.95	/
CAF total	0 0	0 0	3.67 ±3.92	/
Animal naming	20.72 ±5.54	11.50 ±4.65	10.81 ±3.91	df=2; p-value<0.001ǂ
UPDRS	1.28 ±1.49	2.39 ±2.17	16.62 ±8.14	/
Angle discrimination	19.65 ±0.86	18.71 ±2.27	15.35 ±5.27	df=2, p-value=0.003ǂ
FAS Verbal fluency	44.89 ±16.07	27.39 ±16.39	19.29 ±10.70	df=2, p-value<0.001ǂ
Trail making test A	36.43 ±10.25	77.14 ±53.31	109.57 ±69.97	df=2, p-value<0.001ǂ
ACheI (yes/no)	0/18	26/2	19/2	df=1, p-value=0.763*
LEDD	0 0	0 0	182 ±243	/

Table 4.1 - Demographic data (subsample) and clinical scores. ǂ χ2 test three groups, ǂ Kruskal-Wallis three groups, * χ2 test two groups (AD, DLB).

4.3.1. Magnetic resonance imaging recording and processing

To perform source localisation, individual MRI recordings were obtained. Acquisitions were performed on a 3-T Philips Intera Achieva scanner with magnetisation prepared rapid gradient echo (MPRAGE) sequence, sagittal acquisition, echo time 4.6 ms, repetition time 8.3 ms, inversion time 1250 ms, flip angle=8°, SENSE factor = 2, in-plane field of view 240x240 mm^2 with slice thickness 1.0 mm, yielding voxel size of 1.0 x 1.0 x 1.0 mm^3 (Peraza *et al.*, 2014; Schumacher *et al.*, 2020b). Pre-processing and segmentation of acquired T1 weighted images were performed by Dr Sean Colloby using FreeSurfer (version 5.1, http://surfer.nmr.mgh.harvard.edu/) (Dale *et al.*, 1999; Fischl and Dale, 2000) as in previous analyses which included part of the cohort of this thesis and were reported in their respective publications (Colloby *et al.*, 2011; Blanc *et al.*, 2015). The automated processing pipeline involved intensity non-uniformity correction, Talairach registration, removal of non-brain tissue (i.e. skull stripping), white matter (WM) and subcortical grey matter (GM) segmentation, tessellation of GM-WM boundary, and surface deformation following GM-

Cerebrospinal fluid (CSF) intensity gradients for optimal placing of GM-WM and GM-CSF borders. Modelling of cortical surface was followed by surface inflation, transformation to spherical atlas and parcellation into regions according to the atlas developed by Destrieux *et al.* (2010). This parcellation consists of 148 cortical areas and is entirely based on anatomical information. Respective network nodes are obtained as mass centroids across each region vertices. Cortex parcellation and coordinates of network nodes in the Montreal Neurological Institute (MNI) reference space are reported respectively in Figure 4.1 and in Appendix B. Resulting images from each processing step were visually inspected and, were required, manually corrected to ensure accurate segmentation (Blanc *et al.*, 2015).

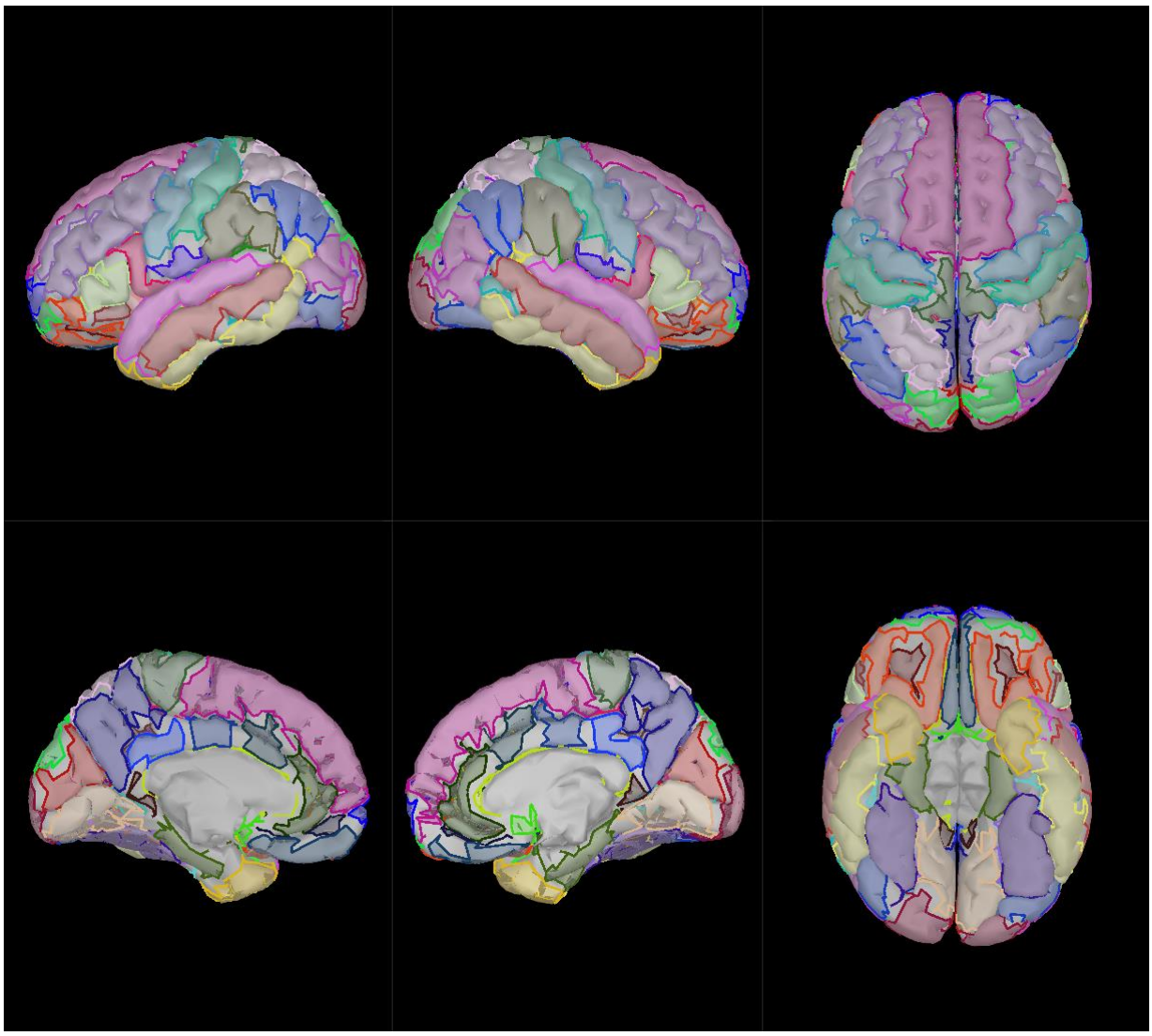

Figure 4.1 – Destrieux parcellation on MNI ICBM152 template. Cortical surface and parcellation were visualised with Brainstorm toolbox for MATLAB. Views from top-left to bottom-right: left, right, dorsal, internal left, internal right, ventral. Network nodes corresponded to mass centroids of segmented regions.

4.3.2. Cortical source localisation

Cortical source estimation from EEG signals was obtained through sLORETA technique (Pascual-Marqui, 2002) implemented in the Brainstorm toolbox for Matlab (Tadel *et al.*, 2011) and described in section 1.3.3. This method has been proven to be the most accurate compared with other existing non-parametric methods in literature (Grech *et al.*, 2008), and suitable for connectivity analysis (Hincapié *et al.*, 2017). Since digitised sensor localisation was unavailable, EEG sensors distribution was manually co-registered over the scalp for each participant using the Brainstorm toolbox (Stropahl *et al.*, 2018) before performing any further

step. An example of co-registration outcome from one subject is shown in Figure 4.2. Head model based on the individual anatomical data was obtained with boundary element method (BEM) as implemented in OpenMEEG (Kybic *et al.*, 2005; Gramfort *et al.*, 2010). Noise covariance was set to an identity matrix as recommended in the Brainstorm's tutorial for not available baseline recording, cortical sources were reconstructed with assumption of normal dipole orientations with respect to cortical surface, and resulting time-series were averaged within each of the 148 regions defined with the Destrieux atlas (Destrieux *et al.*, 2010). Channels which were removed and interpolated during the pre-processing step were excluded from source localisation to reduce the risk of false positives. Signs of opposite sources within each region were flipped to match the main orientation and averaged. Before any analysis, source activity from all subjects was projected back to the ICBM152 template (Mazziotta *et al.*, 2001) using Shepard's interpolation method (Shepard, 1968).

Validation of the implemented pipeline was performed using data collected for a different study involving active motor task, where participants were asked to maintain isometric contraction by opposition of thumb and index (Graziadio *et al.*, 2010). Four subjects were randomly chosen, respective EEG task data were pre-processed, source localised, and power-spectrum topographies generated. For the source localisation pipeline being deemed correct, prominent power activation across time points within the β-band over sensory-motor areas was expected, as described in section 1.3.1. This was in fact the case, as shown in Figure 4.3.

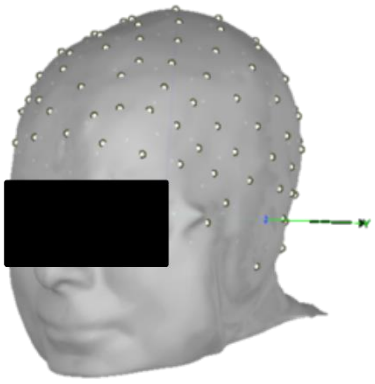

Figure 4.2 – MRI – EEG cap co-registration. White dots correspond to EEG cap sensors. Outcome produced with Brainstorm toolbox.

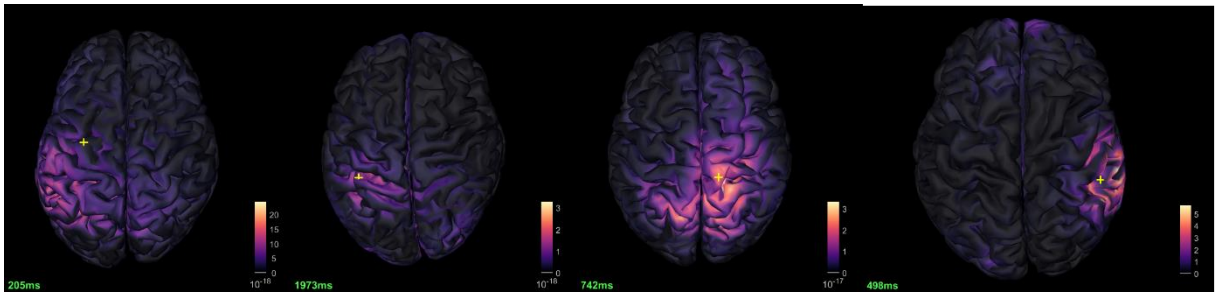

Figure 4.3 – Instantaneous β-band power activation during motor task in four participants. Prominent activation emerges over either left or right sensori-motor areas.

4.3.3. Graph theory

Connectivity between localised cortical sources was computed with WPLI, whose implementation is described in detail in section 2.4. As described in section 3.3.2, obtained graphs were proportionally thresholded at densities spanning between 3% and 60%, weighted network features were computed for all participants and averaged across thresholding values. In this case, comparison between DLB and other groups was only performed for scenarios which were found to be significant in the sensor domain analysis as reported in the previous chapter. Mann-Whitney U tests were carried out for each scenario (one-tail, $p < 0.05$) as listed in Table 4.2. Small-worldness was not extracted in this analysis as its value is directly dependent on C_w and L_w.

vs	**DLB**
HC	α-band: WPLI, K_w, C_w, L_w, Q_w β-band: WPLI, C_w
AD	θ-band: Q_w β-band: WPLI, K_w, C_w, L_w, Q_w

Table 4.2 – Tested network metrics. Only measures which were significantly different between DLB and the other groups in Chapter 3 were extracted. Subscript W = weighted measure.

4.3.4. Topographical differences

To test the correlation between connectivity strength and DF in DLB and AD, analysis was restricted to α-band. Specifically, affected topological network patterns in DLB and AD against HC were obtained with NBS (Zalesky *et al.*, 2010), of which implementation is described in detail in section 2.5. One-tailed t-tests were performed for AD < HC and DLB < HC scenarios at $t_{th} = 3.5$; FWER was controlled by performing a permutation test (5000 permutations), components were deemed significant at $p < 0.025$, and were visualised with the BrainNet Viewer (Xia *et al.*, 2013). Average strength across connections belonging to NBS component ($WPLI_{NBS}$) was computed for all the subjects.

4.3.5. Dominant frequency

DF and DFV in all groups over the occipital lobe were computed. Sources belonging to the occipital lobe were first selected from the parcellation as shown in Figure 4.4; these included: parieto-occipital sulcus, anterior occipital sulcus, occipital inferior gyrus and sulcus, occipital superior and transverse sulcus, occipital superior gyrus, middle occipital gyrus, middle occipital gyrus and Lunatus, transverse collateral posterior sulcus, lingual gyrus, calcarine sulcus, cuneus and occipital pole. EEG source time-series were transformed to the time-frequency domain using Windowed Fourier Transform (3-10 cycles adaptive windows width, 0.5 Hz frequency step), and power-spectrum for each 2-s epochs of each subject was obtained. Lowest number of clean epochs across subjects was extracted from all recordings, which resulted in selecting 40 epochs from each subject. DF of each epoch was measured by obtaining the frequency value corresponding to the maximum power peak between 4-13 Hz. Mean DF for each subject was then obtained by averaging DF across epochs (Bonanni *et al.*, 2008), whilst DFV was computed as standard deviation (Peraza *et al.*, 2018). Differences in DF and DFV values across groups were assessed with Kruskal-Wallis test ($p < 0.05$) followed by post hoc Mann-Whitney U tests; test tails were chosen with prior hypothesis based on DF and DFV findings reported in previous publications (Peraza *et al.*, 2018; Stylianou *et al.*, 2018) ($p < 0.05$, DF tests: HC > AD, HC > DLB, AD > DLB, one-tailed; DFV tests: one-tailed for HC < AD and AD > DLB, two-tailed for HC vs DLB; Holm-Bonferroni corrected).

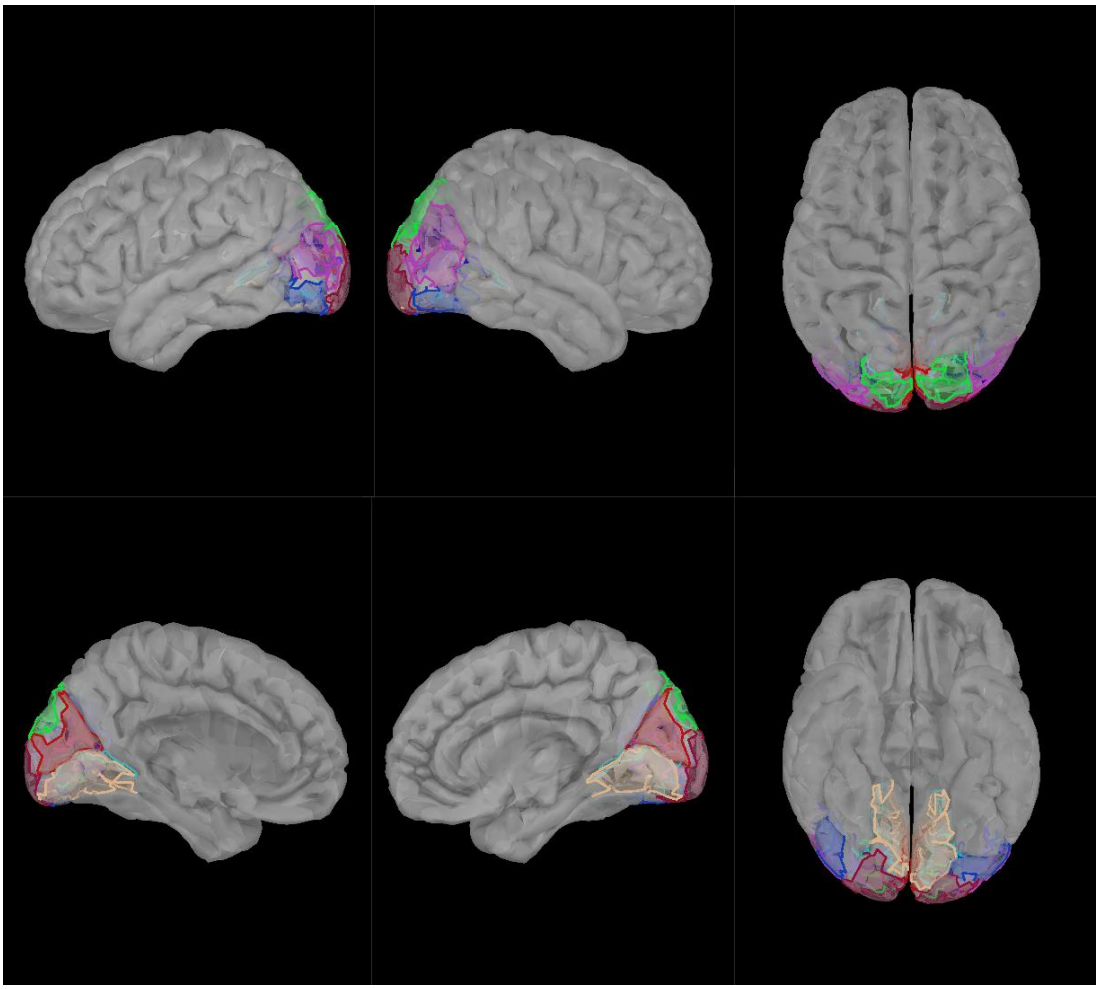

Figure 4.4 – Regions belonging to the occipital lobe (ICBM152 template). 22 regions were selected from Destrieux parcellation. Views from top-left to bottom-right: left, right, dorsal, internal left, internal right, ventral.

4.3.6. Correlation between connectivity and dominant frequency

Connectivity values were averaged across network edges belonging to NBS components, and correlation between averaged connectivity and DF was tested in both AD and DLB as well as within HC group for both NBS networks with Spearman rank correlation test ($p < 0.05$, one-tailed, Holm-Bonferroni corrected for two NBS tests). If any positive correlation was found between the two measures, a random forest regressor was implemented to compute prediction accuracy of DF from NBS average strength. To this purpose the Scikit-Learn framework in Python (version 0.20.1) was used. Cross-validation was implemented with k-folds algorithm (10 folds), and prediction accuracy was obtained as $[100 \cdot (1 - MAPE)]\%$,

where MAPE is the mean absolute percentage error, computed as $\frac{1}{n}\sum_n \left|\frac{DF_{predicted}-DF_{true}}{DF_{true}}\right|$ (De Myttenaere *et al.*, 2016), where *n* is the number of participants of the tested group.

4.4. Results

4.4.1. Network alterations in DLB

Alteration of connectivity strength and weighted graph features in DLB compared with AD and HC also emerged in the source domain, as all Mann-Whitney U test results were significant ($p < 0.05$), as shown in Figure 4.5. WPLI in DLB group was lower than HC in both α- and β-band, whilst DLB and AD were significantly different in the β-band. Node degree and clustering coefficient were lower than HC and AD respectively in the α- and β-band, and the latter measure was also reduced in the β-band compared with HC. Characteristic path length and modularity were higher compared with HC and AD respectively in the α- and β-band networks, and modularity was also higher than AD in the θ-band.

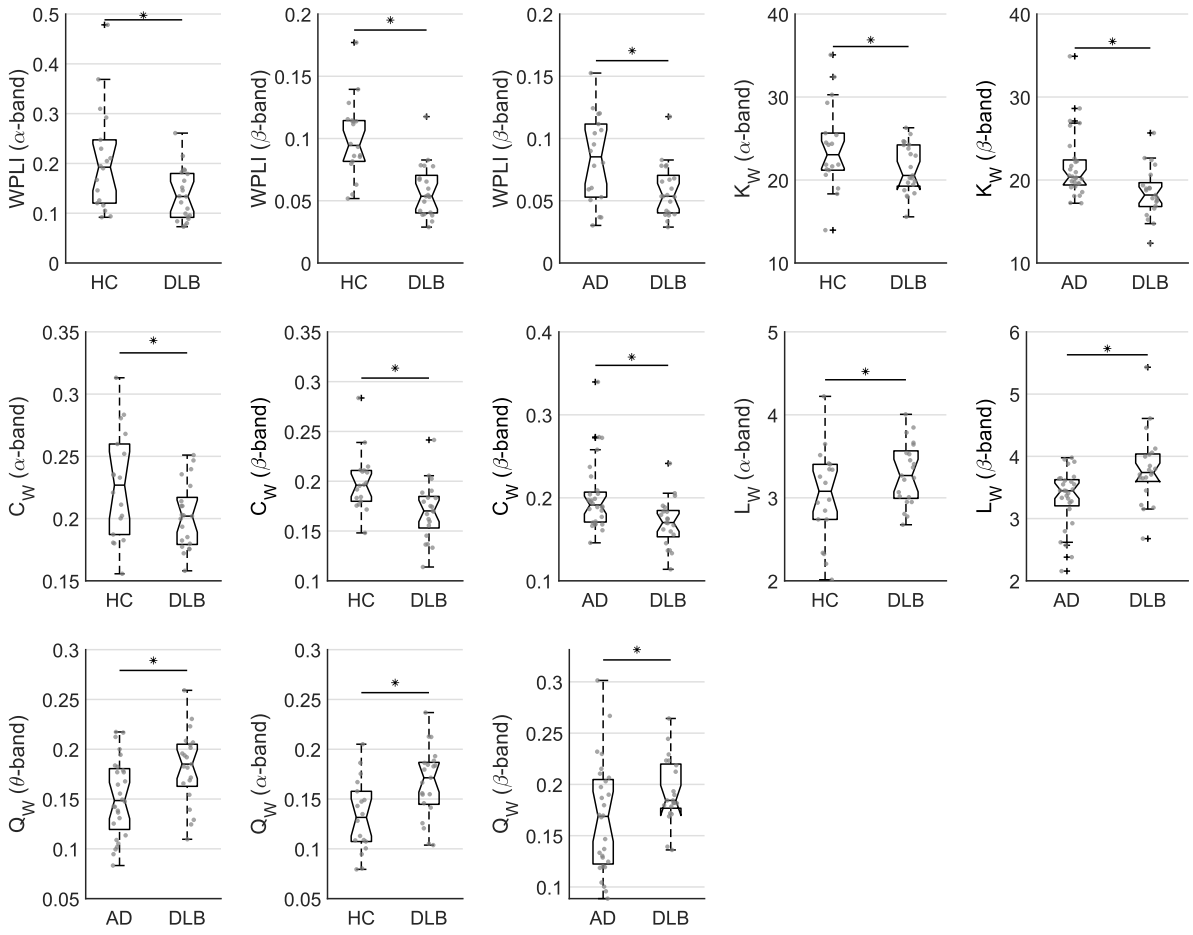

Figure 4.5 – Graph theory measure comparisons in the source domain. Outcome of comparisons in the sensor domain emerges identically in the source domain. Small-worldness was not computed as directly dependent on C_w and L_w. *significant Mann-Whitney U test ($p < 0.05$, one-tail).

4.4.2. NBS components (α-band) vs DF: outcome of correlation analysis

Outcome of NBS tests are shown in Figure 4.6**.** AD < HC test yielded one network component comprising 43 nodes and 54 edges ($p = 0.024$), whilst DLB < HC resulted in one component with 59 nodes and 85 edges ($p = 0.013$). In both scenarios, affected components comprised posterior-anterior patterns, including areas belonging to attentional networks. AD group showed affected dorsal network over the right hemisphere, whilst weaker connectivity emerged between left insula and cingulate cortex. Similarly, connections over dorsal regions were weaker in DLB within the right hemisphere, although affected connectivity within ventral regions including occipital cortex, inferior temporal cortex, cingulate, insula, and ventral PFC

was more prominent than in AD. In both conditions, affected patterns were lateralised over the right hemisphere. Reduced inter-hemispheric connectivity also emerged in both groups.

DF over the occipital lobe was reduced in both disease groups compared to HC, and lower in DLB than in AD. DFV was significantly higher in AD as compared with both HC and DLB. As shown in Figure 4.7, all tests survived Holm-Bonferroni correction.

Outcome of correlation tests is shown in Figure 4.8. Correlation between $WPLI_{NBS}$ and DF was significant for DLB group (ρ = 0.483, p = 0.014), whilst only a trend towards significance emerged in AD group (ρ = 0.250, p = 0.099). Hence, weaker functional connectivity between NBS detected areas corresponded to more pronounced DF negative shift in DLB, but not significantly in AD. For each differential component, correlation between $WPLI_{NBS}$ and DF in HC group was also tested, and no significant results emerged. Random forest regressor was then trained with $WPLI_{NBS}$ values from DLB < HC test, and DF values of DLB subjects were predicted with accuracy of 88.58%.

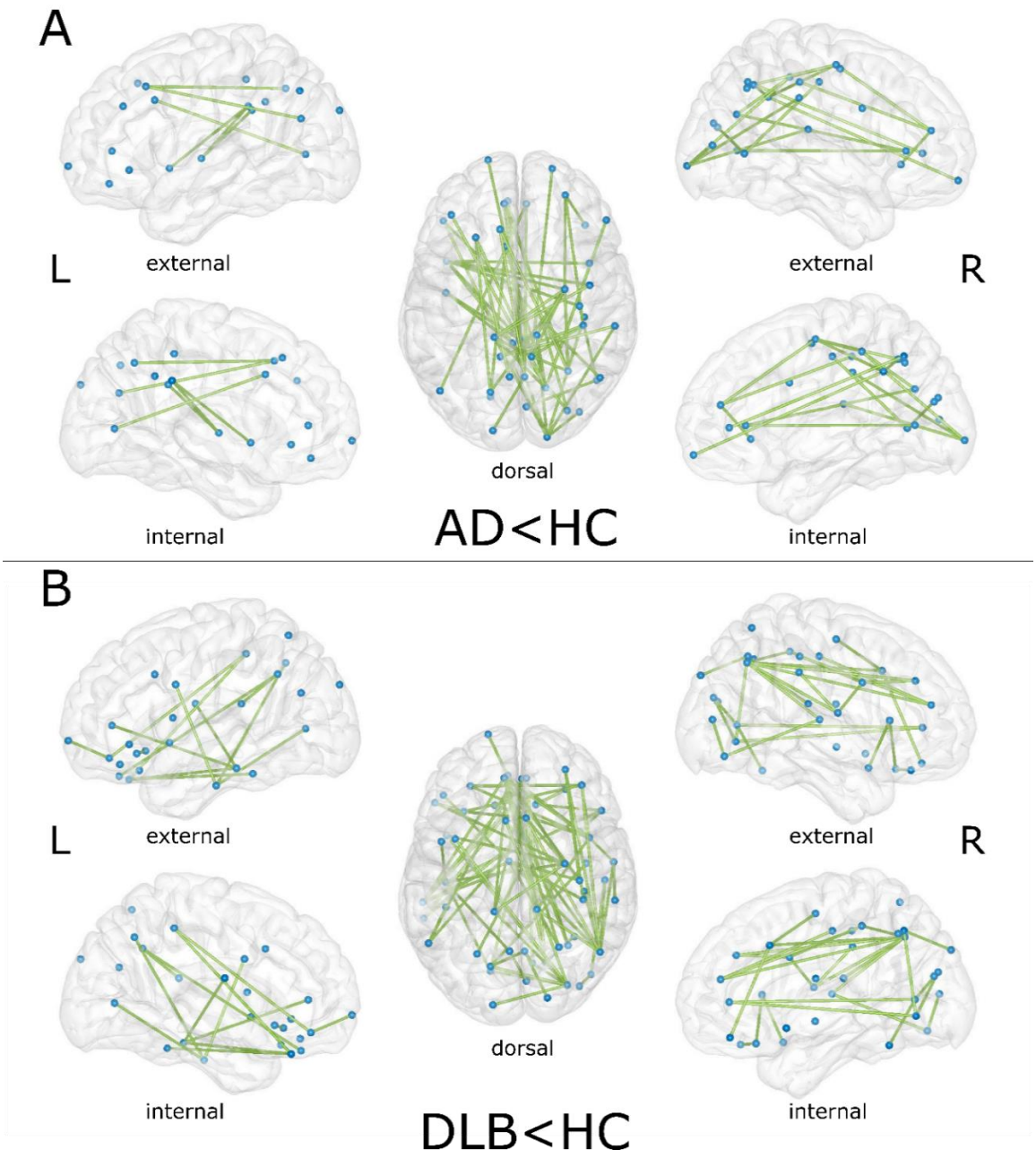

Figure 4.6 – Outcome of NBS analysis within the α-band in the source domain. Green lines represent edges belonging to a significantly affected network component. Both groups show affected attentional networks, and DLB also shows weakened visual ventral network. A: AD < HC; B: DLB < HC.

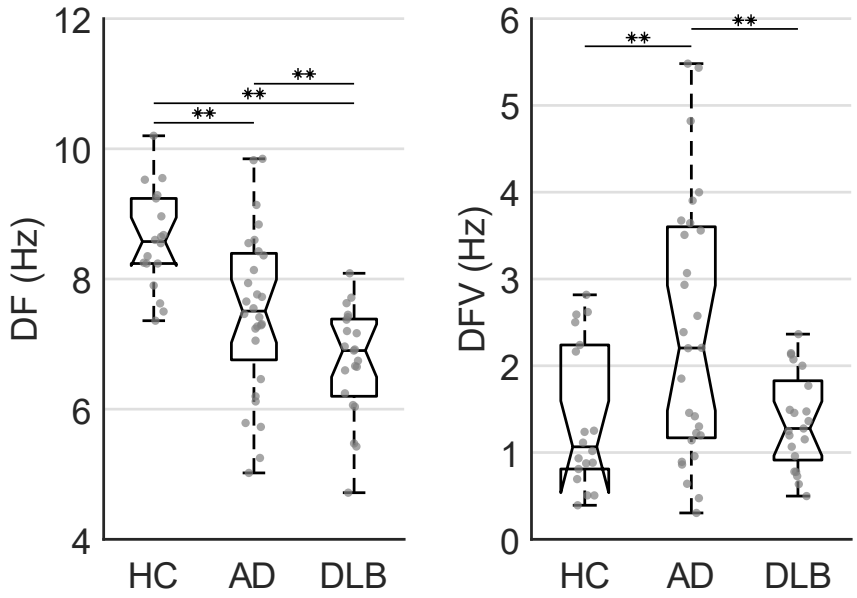

Figure 4.7 – DF and DFV over the occipital lobe. DF was lower in patient groups compared to HC, and lower in DLB as compared with AD. DFV was higher in AD compared to HC and DLB. **significant Mann-Whitney U test surviving Holm-Bonferroni correction (three tests for each measure).

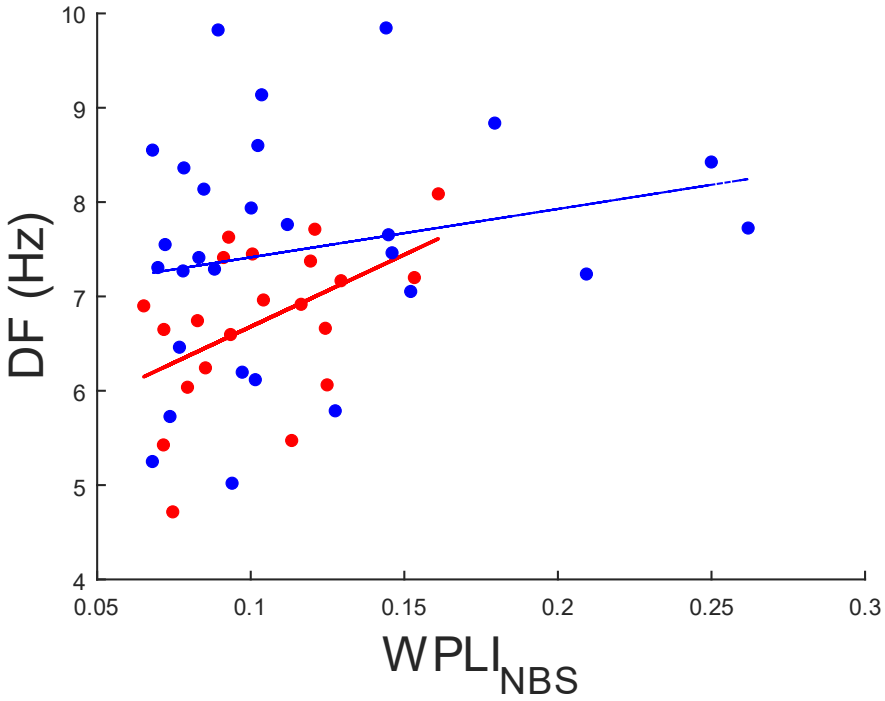

Figure 4.8 – $WPLI_{NBS}$ vs DF: linear fitting for AD and DLB. Significant correlation emerges from Spearman rank test for DLB, but not for AD. Thicker line represents significant correlation trend. Blue: AD (ρ = 0.250); red: DLB (ρ = 0.483).

4.5. Discussion

In this chapter network graph features measured in the source domain were compared between DLB, AD and HC. The analysis focused on those measures which were significantly differential between groups at the sensor level as reported in Chapter 3, to assess whether any resonance exists between the sensor and the source domains. As a result, differential trends in the source domain matched with the ones obtained with sensor domain analysis, suggesting that differences which emerged with the latter approach can be deemed reliable and not influenced by non-cortical sources. The NBS analysis within the α-band revealed that attentional networks are affected in both AD and DLB, in line with speculations from previous studies based on EEG and fMRI. DF differences between groups over posterior regions showed the pattern DLB < AD < HC, consistently with previous EEG studies. Reduced average connectivity within NBS component in DLB was associated with more pronounced DF reduction, suggesting that DF changes in DLB might be as well associated with impairment of attentional processing at rest.

4.5.1. Graph measures are equally altered in DLB at source and sensor level

Differences between DLB and other groups were tested for those graph measures which were significantly altered in DLB at the sensor domain. Specifically, comparisons included: reduced connectivity strength and clustering coefficient in DLB compared to HC in the α- and β-band, and compared to AD in the β-band; lower node degree and higher characteristic path length against HC and AD respectively in α- and β-band; higher modularity compared to HC and AD respectively in α-band and θ-β-band. Notably, both connectivity strength and graph measures differential trends resonated between the two domains, as all statistical test results were significant. This result supports the idea that for diagnostic purposes the methodological approach, i.e. scalp or source analysis, does not introduce significant variability into the analysis. However, this idea partially contrasts with recent studies comparing network measures at source, i.e. iEEG or source localised, and scalp level (Snyder and Smith, 2015; Lai *et al.*, 2018; Snyder *et al.*, 2018). For instance, Lai *et al.* (2018) compared EEG connectivity strength and graph features between the two domains using diverse source localisation techniques, including sLORETA, and connectivity measures. They found that connectivity

strength strongly correlated between the two domains, whereas for graph features only moderate correlation emerged in the best case, i.e. when connectivity was assessed with metrics insensitive to volume conduction. A number of methodological aspects might explain this partially contrasting outcome. First, their study was based on MST graphs; such approach might omit local topological organisation of the network which would instead emerge through graph proportional thresholding, as discussed in section 3.5.5. Second, source localisation in the present study was based on individual MRI recordings, which likely yielded more accurate source reconstruction as compared with their use of standard template (Cho *et al.*, 2015). Third, in their study binary graph measures were used, whilst the present analysis is based on weighted network measures, which have been proven in Chapter 3 to be more consistently associated with network topology. On the other hand, in the reported study comparison between sensor and source level was performed only at the group level. Hence, individual variances leading to potential inconsistency between sensor and source domain might be attenuated. Similarity of between-group graph differences across source and scalp domains supports EEG as a reliable diagnostic tool from a clinical perspective. However, whilst scalp recordings may therefore be robust enough for clinical purposes, source reconstructed measures can potentially provide additional insights into topological distribution of functionally affected cortical areas, as discussed in the next sections.

4.5.2. Attentional networks are affected in DLB

Another objective in this chapter was to assess whether DF shifts over occipital regions in DLB are associated with connectivity alteration. As discussed in section 1.4.2, DF has been consistently reported as a reliable differential parameter for DLB against AD and HC (Bonanni *et al.*, 2008; Peraza *et al.*, 2018; Stylianou *et al.*, 2018). The aim of this analysis was to provide further informative elements supporting speculation on associated pathological mechanisms. To this purpose, most consistently affected connectivity patterns in DLB and AD were spatially assessed using NBS. Comparison of the two groups against HC yielded differential network components which included parietal and frontal regions, as well as affected connectivity between cingulate and insular cortex. These areas are known to be part of the default mode and attentional networks, as assessed in previous studies with different modalities (Corbetta and Shulman, 2002; Fox *et al.*, 2006; Vossel *et al.*, 2014; Raichle, 2015; Jimenez *et al.*, 2016).

As initially proposed by Corbetta and Shulman (2002), top-down cognitive driving of attention is likely associated with dorsal-frontoparietal information flow, whilst sensitivity to external and unexpected stimuli is processed by a ventral-frontoparietal stream. Task-based fMRI (Kastner *et al.*, 1999; Shulman *et al.*, 1999; Corbetta *et al.*, 2000; DiQuattro and Geng, 2011) and M/EEG (Siegel *et al.*, 2008; Simpson *et al.*, 2011) studies have reported consistent activations of above mentioned areas during visual clue detection tasks; sustained dorsal areas activation was observed, whilst ventral areas were triggered by unexpected clues, and interaction emerged between the two streams. Studies based on resting-state paradigms were also successful in reporting such segregation. For instance, an fMRI study by Fox *et al.* (2006) reported higher correlation between areas belonging to one or the other attentional network, and Morillas-Romero *et al.* (2015) found lower frontal and parietal resting-state EEG theta/beta ratio associated with better orienting abilities as well as higher parietal delta/beta ratio positively correlating with score of self-reported attention control questionnaire. AD and DLB are typically featured with attentional dysfunctions (Perry and Hodges, 1999; Foldi *et al.*, 2002; Bradshaw *et al.*, 2006; Ferman *et al.*, 2006), and functional alteration in fronto-parietal areas reported in previous task and resting-state studies have been in fact consistently associated with such impairment (Li *et al.*, 2012; Franciotti *et al.*, 2013; Peraza *et al.*, 2014; Kobeleva *et al.*, 2017). The data driven approach pursued in the present chapter provides further topographical evidence of attention-related functional impairment in AD and DLB. Also, altered connectivity between regions belonging to the default mode network at rest is in line with previous findings in fMRI studies (Galvin *et al.*, 2011; Franciotti *et al.*, 2013). NBS test between DLB and HC also produced affected pathways belonging to the visual ventral network, i.e. linking occipital and IT areas. This is likely due to the fact that part of the DLB cohort presents complex visual hallucinations, which are thought to be associated with affected information flow within visual networks (Collerton *et al.*, 2005; Tsukada *et al.*, 2015). This aspect is investigated in Chapter 6. Although differential features between AD and DLB were not detected in the α-band network, these emerged within the β-band, as reported in Chapter 3 with the sensor-domain investigation. Source domain topographical analysis in the β-band is presented in the next chapter.

4.5.3. Reduced DF is associated with lower functional connectivity in DLB

Comparison across groups of DF and DFV over the occipital lobe yielded the differential pattern DLB < AD < HC, in line with all previous findings (Briel *et al.*, 1999; Bonanni *et al.*, 2008; Jackson and Snyder, 2008; Roks *et al.*, 2008; Peraza *et al.*, 2018; Stylianou *et al.*, 2018). The source localisation approach pursued in the presented analysis allows for detailed focus on posterior cortical regions, which were significantly affected in the present study. As discussed in section 1.4.2, DF abnormalities in AD and DLB have been consistently associated with disruption of the cholinergic system (Perry *et al.*, 1991; Tiraboschi *et al.*, 2000; Tiraboschi *et al.*, 2002; Lemstra *et al.*, 2003; Delli Pizzi *et al.*, 2015b). However, there is no investigation to date assessing whether such alteration and functional connectivity abnormalities originate from the same disease-related process. Based on the results obtained from correlation analysis, this seems to be the case for DLB, but not for AD. Notably, DLB-DF values could be predicted based on $WPLI_{NBS}$ using a random forest regressor with accuracy close to < 90%. This suggests that in DLB both phenomena might depend on the same pathological mechanism. Correlation between $WPLI_{NBS}$ and DF in the HC group did not yield any significant result for either NBS components, strengthening the idea that such correlation may be associated with a DLB-specific pathological mechanism. From the functional perspective, establishing a causality relationship between the two biomarkers is challenging. It is possible that either affected communication between brain areas might cause the posterior EEG slowing, or that the posterior abnormal activity propagates through the attentional network altering its efficiency. This latter speculation would resonate with the fact that the EEG slowing is generally detected over the whole scalp, although less prominently (Peraza *et al.*, 2018; Stylianou *et al.*, 2018), including anterior regions (Franciotti *et al.*, 2020). Further disruption of the cholinergic system in DLB compared with AD might be generating a more severe functional alteration, which reflects in both DF slowing and connectivity reduction, whilst some degree of preservation in AD might let the two phenomenon still not be equally affected. To which extent cholinergic dysfunctions in the two conditions are associated with respective EEG alterations is still unanswered. This aspect will be investigated in the next chapter.

4.6. Conclusions

This chapter followed up on the sensor domain analysis reported in Chapter 3 by using source localisation. Network measures which were found to be differential at the sensor level between DLB and other groups were tested in the source domain. All tested network features were significantly different between groups, supporting EEG network analysis as robust diagnostic approach. Second aim of this analysis was to assess whether the well reported DF alteration in DLB is associated with detected functional connectivity changes. This hypothesis was valid as DF values in DLB, but not in AD, positively correlated with connectivity strength of most consistently affected pathways, which included attentional and default mode networks. Overall, the presented analysis further validated EEG capability as a diagnostic tool and provided a step forward towards association between disease phenotype and underlying pathological mechanisms in DLB. Direct comparison between AD and DLB functional network topographies at the cortical level as well as association between DF and cholinergic system is presented in the following chapter.

Chapter 5. Modular Segregation and Cholinergic Alteration in Dementia with Lewy Bodies

5.1. Summary

In Chapter 3 it was observed that the EEG β-band network comprised most of the differential features between AD and DLB, with average WPLI being the most discriminative variable. DLB network was also more segregated compared to AD. As discussed in the previous chapter, analysis in the source domain can provide further mechanistic insights into processes associated with functional abnormalities. The primary aim of the present chapter was to assess affected network patterns and modular distribution in DLB compared to AD at the cortical level using source localisation. In addition, integrity of the cholinergic system was measured by obtaining structural connectivity between the cholinergic cell group of the basal forebrain, thalamus, and occipital cortex, and comparing it between groups. Correlation with DF values in both groups was also tested to investigate any association between cholinergic system and posterior EEG α-band slowing. Modular analysis revealed that DLB group presents higher number of modules compared to AD, due to frontal and temporal connectivity disruption. Two main differential clusters emerged from NBS analysis, each comprising intrahemispheric connections, and connected by only one interhemispheric edge. The right temporal lobe was the most consistently affected, due to reduced connectivity between inferior temporo-occipital and prefrontal regions. Higher disruption of EEG source network in DLB also reflected into higher modularity, which positively correlated with better cognitive performance. Since lower modularity was associated with AD pathology, low modularity values within DLB groups associated with worst cognitive performance might be reflecting the presence of mixed AD-LB pathology cases within DLB cohort. This idea might also explain the fact that association between NBM-occipital cortex white matter tract integrity and DF over the occipital cortex emerged in both groups, but was less consistent in DLB, although still significant. Among EEG features, connectivity was the most discriminative variable between groups. Overall, these results provide further validation to EEG as a diagnostic tool for DLB and shows that its features may significantly reflect persistence of mixed-pathology condition.

5.2. Introduction

In the sensor domain analysis, most topological differences in EEG network between DLB and AD were detected in the β-band. As reported in Chapter 3, the best differential measure between conditions was connectivity strength, which was lower in DLB compared to AD. From a clinical perspective, this result is advantageous since computation and interpretation of connectivity strength is a more immediate measure compared to graph features estimation. In addition, it was shown in Chapter 4 that source localisation combined with NBS is an effective approach to infer cortical topographical differences between groups. The analysis reported in Chapter 3 also showed that EEG network in DLB is more segregated than in AD within the β-band network. Greater segregation in DLB is in agreement with an fMRI study (Peraza *et al.*, 2015) where it is suggested to reflect distribution of stronger connections within the network over shorter edges compared to AD topology, as also found in the EEG sensor domain analysis and shown in Figure 3.2b. Such distribution likely leads to higher disruption, hence segregation of the network. However, this aspect was not further investigated in other studies, and modular distribution in DLB and its differences with AD are still unknown.

In the previous chapter, it was also shown that DF is significantly lower in DLB than in AD over the occipital lobe, in line with previous investigations (Briel *et al.*, 1999; Bonanni *et al.*, 2008; Peraza *et al.*, 2018; Stylianou *et al.*, 2018). In addition, DF values were associated with reduced average strength of those α-band network pathways which were significantly weakened compared with HC. This latter result suggested that both DF and functional alterations in DLB might originate from the same disease-related mechanisms. As discussed in the first chapter, the most prevailing speculation in the literature regarding the source of these abnormalities is a dysfunction of the cholinergic system. Specifically, it has been speculated that DF slowing might be associated with neurodegeneration of cholinergic projection towards the occipital lobe (Babiloni *et al.*, 2017). This hypothesis is supported by several evidences which include degeneration of the basal forebrain in AD with prominent DF slowing (Riekkinen *et al.*, 1991) and in DLB (Hepp *et al.*, 2017a; Sakai *et al.*, 2019), as well as DF restoring capabilities of cholinergic treatment (Agnoli *et al.*, 1983; Balkan *et al.*, 2003; Kai *et al.*, 2005). However, existence of any direct correlation between DF slowing and degeneration of cholinergic projections has still not been investigated.

5.2.1. Objective

The first aim of this chapter was to investigate topographical differences between DLB and AD in the β-band; specifically, connectivity strength and modular distribution in the source domain were assessed and compared between groups. The second aim of this chapter was to assess whether cholinergic projections towards the cortex are more affected in DLB compared to AD, and whether in any of the groups any association between cholinergic pathways and EEG slowing emerges.

5.3. Methods

Details on experimental protocol, EEG acquisition and measured network features are reported in Chapter 2. A subsample with available EEG, MRI and DTI data was selected for this analysis. Also, stricter selection was performed based on the quality of structural recording, according to evaluation performed in a previous study including participants of the same cohort (Blanc *et al.*, 2015). The final subsample comprised 26 AD and 18 DLB (see Table 5.1). EEG was recorded in eyes-closed resting state with high-density sensor cap (128 electrodes). Recorded signals were pre-processed (section 2.3) (number of removed channels: 14 ± 10; number of removed epochs: 13 ± 10; number of removed ICA components: 41 ± 10), source localised and connectivity between cortical sources was measured with WPLI and averaged across time and frequency bins within the β-band (14-20.5 Hz). Modularity (Q_W) was computed on non-thresholded WPLI matrices and compared between groups with Mann-Whitney U test (one-tailed, $p < 0.05$).

	AD (N=26)		DLB (N=18)		p-value
Age	77.15	±7.50	76.28	±6.64	df=1, p-value=0.459Ŧ
Male/Female	20/6		14/4		df=1, p-value=0.947ǂ
MMSE	21.15	±3.71	23.00	±4.10	df=1; p-value=0.157Ŧ
CAMCOG total	69.88	±13.64	74.56	±13.61	df=1; p-value=0.599Ŧ
NPI hall	0	0	1.56	±1.79	/
CAF total	0	0	3.83	±3.92	/
Animal naming	11.62	±4.78	10.67	±3.71	df=1; p-value=0.254Ŧ
UPDRS	2.38	±2.21	15.50	±8.10	/
Angle discrimination	18.69	±2.35	15.82	±5.19	df=1, p-value=0.051Ŧ
FAS Verbal fluency	28.77	±16.18	20.28	±10.74	df=1, p-value=0.077Ŧ
Trail making test A	77.15	±55.20	110.82	±72.67	df=1, p-value=0.055Ŧ
AChel (yes/no)	24/2		17/1		df=1, p-value=0.782ǂ
LEDD	0	0	163	±213	/

Table 5.1 – Demographic data (subsample) and clinical scores. Ŧ Unpaired Mann-Whitney U test, ǂ χ2 test.

5.3.1. Magnetic resonance imaging recording

Individual MRI T1 recordings were obtained on a 3-T Philips Intera Achieva scanner with MPRAGE sequence, sagittal acquisition, echo time 4.6 ms, repetition time 8.3 ms, inversion time 1250 ms, flip angle=8°, SENSE factor = 2, in-plane field of view 240x240 mm^2 with slice thickness 1.0 mm, yielding voxel size of 1.0 x 1.0 x 1.0 mm^3 (Peraza *et al.*, 2014; Schumacher *et al.*, 2020b). Pre-processing and segmentation of acquired T1 weighted images was performed by Dr Sean Colloby using FreeSurfer software package (version 5.1, http://surfer.nmr.mgh.harvard.edu/) (Dale *et al.*, 1999; Fischl and Dale, 2000) as in the previous analyses which included part of the cohort of this thesis and were reported in their respective publications (Colloby *et al.*, 2011; Blanc *et al.*, 2015). The automated processing pipeline involved intensity non-uniformity correction, Talairach registration, removal of non-brain tissue (i.e. skull stripping), WM and subcortical GM segmentation, tessellation of GM-WM boundary, and surface deformation following GM-CSF intensity gradients for optimal placing of GM-WM and GM-CSF borders. Modelling of cortical surface was followed by surface inflation, transformation to spherical atlas and parcellation into regions according to the atlas

developed by Destrieux *et al.* (2010). Respective network nodes are obtained as mass centroids across each region vertices. Resulting images from each processing step were visually inspected and, where required, manually corrected to ensure accurate segmentation (Blanc *et al.*, 2015).

DTI recordings were performed with a 2-dimensional spin-echo, echo planar imaging diffusion-weighted sequence with 59 slices: TR = 6100 ms; TE = 70 ms; flip angle = 90°; field of view = 270 x 270 mm; pixel size= 2.1 x 2.1 mm; slice thickness = 2.1 mm. Images were diffusion weighted along 64 uniformly distributed directions (diffusion contrast b = 1000 $s \cdot mm^{-2}$), and six acquisitions did not have any diffusion weight applied (b = 0 $s \cdot mm^{-2}$) (Firbank *et al.*, 2007).

5.3.2. Cortical source localisation

The pipeline for EEG source reconstruction is reported in detail in section 4.3.2. Briefly, cortical source estimation from EEG signals was obtained through sLORETA technique (Pascual-Marqui, 2002) as implemented in the Brainstorm toolbox for Matlab (Tadel *et al.*, 2011) and described in section 1.3.3. EEG sensors distribution was manually co-registered over the scalp for each participant using the Brainstorm toolbox (Stropahl *et al.*, 2018) before performing any further steps. Head model based on the individual anatomical data was obtained with boundary element method (BEM) as implemented in OpenMEEG (Kybic *et al.*, 2005; Gramfort *et al.*, 2010). Noise covariance was set as identity matrix, cortical sources were reconstructed with assumption of normal dipole orientations with respect to cortical surface, and resulting time-series were averaged within each of the 148 regions defined with the Destrieux atlas (Destrieux *et al.*, 2010). Channels which were removed and interpolated during the pre-processing step were excluded from source localisation to reduce the risk of false positives. Signs of opposite sources within each region were flipped to match the main orientation and averaged. Before any analysis, source activity from all subjects was projected back to the ICBM152 template (Mazziotta *et al.*, 2001) using Shepard's interpolation method (Shepard, 1968).

5.3.3. Topographical differences

Differential topographical network patterns between DLB and AD were obtained using NBS (Zalesky *et al.*, 2010), of which implementation is described in detail in section 2.5. One-tailed t-tests were performed (DLB < AD) at two different t_{th} values, i.e. $t_{th_1} = 3.3$ and $t_{th_2} = 3.5$; FWER was controlled by performing a permutation test (5000 permutations), network differential components were deemed significant at $p < 0.05$, and were visualised with the BrainNet Viewer (Xia *et al.*, 2013). Average strength across connections belonging to the NBS components ($WPLI_{NBS}$) was computed and compared between groups (one-tailed Mann-Whitney U test, $p < 0.05$).

Modular distribution was obtained for both groups using routines implemented in the BCT. First, for each EEG network, the optimal community structure was obtained and each node was assigned to a module; an agreement matrix was obtained for each group, where each element a_{ij} indicates the number of networks in the group for which i-node and j-node belong to the same module; elements of the agreement matrix were then converted to probabilities according to the formulation $\frac{a_{ij}}{n}$, where *n* is the number of networks of each group; the agreement matrix was thresholded preserving probabilities above 60%; eventually, modular distribution was obtained as consensus matrix, whose computation was based on the algorithm developed by Lancichinetti and Fortunato (2012). Obtained modular distribution was visualised with the BrainNet Viewer, by marking nodes belonging to the same module with the same colour. For each group, proportion of within-module NBS connections was obtained based on the group's modular distribution. This measure was computed as a ratio between number of within-module NBS connections and total number of NBS connections.

5.3.4. Correlation between EEG network measures and cognitive performance

Correlation between network metrics ($WPLI_{NBS}$ and Q_w) and MMSE in DLB group was tested with Spearman rank correlation test ($p < 0.05$, Holm-Bonferroni corrected, two tests). If any significant correlation was found, prediction accuracy was tested by implementing a random forest regressor using the Scikit-Learn framework in Python (version 0.20.1). Cross-validation was implemented with k-folds algorithm (10 folds), and prediction accuracy was obtained as

$[100 \cdot (1 - MAPE)]\%$, where MAPE is the mean absolute percentage error, computed as $\frac{1}{n}\sum_n \left|\frac{MMSE_{predicted} - MMSE_{true}}{MMSE_{true}}\right|$ (De Myttenaere *et al.*, 2016), where *n* is number of DLB participants.

5.3.5. Dominant frequency

DF and DFV in DLB and AD groups over the occipital lobe were computed, as performed in Chapter 4 with the larger subsample. Sources belonging to the occipital lobe were first selected from the parcellation as shown in Figure 4.4. EEG source time-series were transformed to the time-frequency domain using Windowed Fourier Transform (3-10 cycles adaptive windows width, 0.5 Hz frequency step), and power-spectrum for each 2-s epochs of each subject was obtained. Lowest number of clean epochs across subjects was extracted from all recordings, which resulted in selecting 40 epochs from each subject. DF of each epoch was measured by obtaining the frequency value corresponding to the maximum power peak between 4-13 Hz. Mean DF for each subject was then obtained by averaging DF across epochs, whilst DFV was computed as standard deviation. Differences in DF and DFV values between groups were assessed with Mann-Whitney U tests ($p < 0.05$, one-tailed).

5.3.6. Probabilistic tractography and correlation with EEG

Integrity of white matter fibre tracts connecting the occipital lobe, NBM and thalamus was compared between AD and DLB, by testing whether number of fibres was lower in DLB compared to AD for each of the three tracts of interest (Mann-Whitney U test, one-tailed, $p < 0.05$). Tractography pipeline was implemented with the FMRIB's Diffusion Toolbox (Jenkinson *et al.*, 2012). DTI recordings were first corrected for eddy current distortion, movement and motion-induced signal dropout using the eddy package (Andersson *et al.*, 2016; Andersson and Sotiropoulos, 2016), preserving the original gradient directions. Local probability distribution of fibre direction was then assessed at each voxel with automatic detection of number of fibres per voxel (Behrens *et al.*, 2003a; Behrens *et al.*, 2007). Probabilistic tractography algorithm (Behrens *et al.*, 2003a; Behrens *et al.*, 2007) was eventually used to track white matter fibres connecting the defined ROIs. Probability between voxels was

estimated as proportion of connecting fibres over 5000 sampled fibres per voxels. ROI masks defining the occipital lobe, thalamus and NBM, were used as tractography seeds, and connections passing any of the other two ROIs was candidate to be deemed valid. No minimum fibre-length was set as termination threshold, whilst streamlines were terminated after 2000 steps (i.e. 1 metre), if they turned by more than 80 degrees, if they looped back on themselves, or if they left the brain. Any streamline either crossing the ventricles, not being contained within the WM, not reaching any other ROI or with a volume fraction of subsidiary fibres lower than 0.01 was considered invalid and discarded. The outcome of tractography was a structural connectivity matrix of dimension 3 (seed masks) x 3 (target masks). Connectivity strength was measured as number of streamlines connecting two different regions. Previous studies suggested that streamline count may be a biased measure of connectivity, as number of streamlines is directly proportional to ROI sizes and to straightness, shortness and simplicity of connection path (Jones, 2010; Jones *et al.*, 2013). Other methods which rely on WM properties rather than fibre count have been proposed as indices of connectivity, including FA, MD and RD (Conti *et al.*, 2017; Messaritaki *et al.*, 2019; Yeh *et al.*, 2020). However, principal interest of the present analysis was to infer between-group differential connectivity features, rather than assessing individual network properties. Hence, it was assumed that any bias associated with the connectivity measure would have equally affected the analysed groups, and that any condition-related difference would have emerged. Streamlines' directionality could not be assessed, hence each connectivity matrix **S** was symmetrised by replacing each $s_{i,j}$ element with average between itself and $s_{j,I}$ (Cabral *et al.*, 2011).

NBM ROI in the MNI space, limited specifically to the Ch4 cholinergic group (Liu *et al.*, 2015), was generated with Statistical Parametric Mapping (SPM) Anatomy Toolbox for MATLAB (Eickhoff *et al.*, 2005), whilst thalamus MNI ROI was selected from the Harvard-Oxford subcortical atlas included in the FMRIB Software Library (Jenkinson *et al.*, 2012). Subcortical ROIs were transformed to the subject space using affine and non-linear transformations as implemented in the Advanced Normalisation Tools (ANTs) software (Avants *et al.*, 2009). Occipital lobe for each subject was defined generating a ROI mask comprising region volumes from the Destrieux parcellation as listed in section 4.3.5 and shown in Figure 4.4, i.e. regions within which DF was computed. Before performing tractography, ROI masks were transformed from subject space to the diffusion space. To this purpose, a linear

transformation matrix for each subject was generated with the FLIRT package (Jenkinson *et al.*, 2002) using as origin and target respectively a FA map and brain-extracted T1 MRI image. Subcortical ROIs as defined in the MNI space are shown in Figure 5.1**.**

Association between white matter degeneration and altered EEG activation was also investigated. Spearman rank correlation tests ($p < 0.05$, one-tailed) were performed between DF and number of fibre tracts connecting respectively NBM-occipital lobe, NBM-thalamus and thalamus-occipital lobe for both AD and DLB groups.

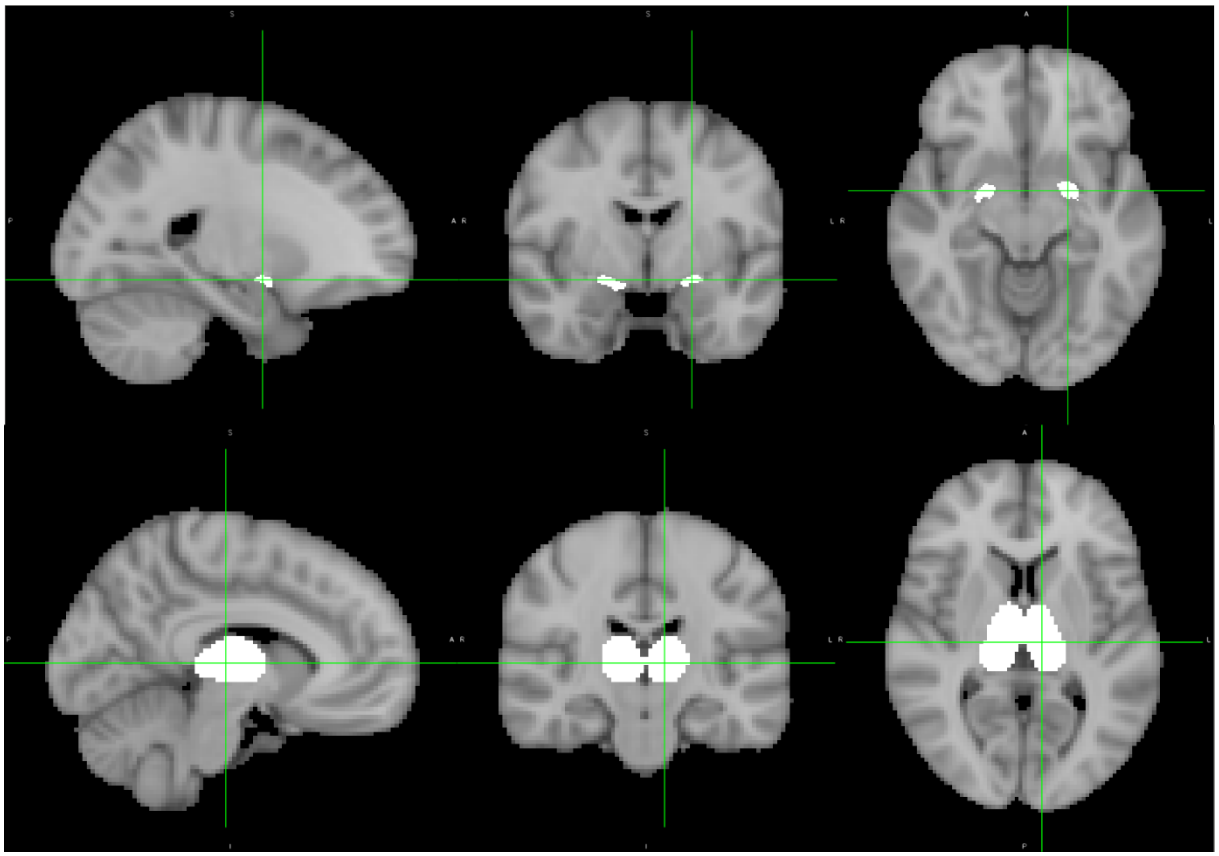

Figure 5.1 – NBM (top) and thalamus (bottom) masks on ICBM152 brain. NBM was generated with SPM toolbox, whilst thalamus definition is from the Harvard-Oxford atlas. Figure generated with FSLeyes tool (https://doi.org/10.5281/zenodo.1470761).

5.3.7. Diagnostic accuracy: $WPLI_{NBS}$ vs Q_w vs DF

Accuracy of group classification was obtained for EEG connectivity strength, modularity, and dominant frequency. A random forest classifier was implemented using the Scikit-Learn framework in Python (version 0.20.1) and the Imbalanced-Learn library for Python (version 0.4.3). To perform cross-validation, each group was randomly split in 80% training and 20%

test subsets. NBS component and respective $WPLI_{NBS}$ were obtained on the training subsample and obtained values together with Q_w and DF were used to train the classifier. Predictions were tested on the remaining 20% subjects. This procedure was performed 60 times, and mean accuracy, F_1 score, sensitivity, specificity, and AUROC curve were obtained. Iterations for which no significant NBS component was detected were excluded from classifier training.

5.4. Results

5.4.1. Differential topographical patterns

Modular distribution in both groups is shown in Figure 5.2. In AD group, optimal community structure yielded four modules, of which two comprised respectively left and right temporal and occipital regions, one included the right PFC, part of the right IT and nodes belonging to left parietal regions, and one included left prefrontal areas as well as two nodes belonging respectively to parietal and occipital regions. Compared to AD group, DLB showed general alteration of modular organisation of the network leading to six modules, driven by disruption of left prefrontal and temporal area, and right inferior temporal lobe.

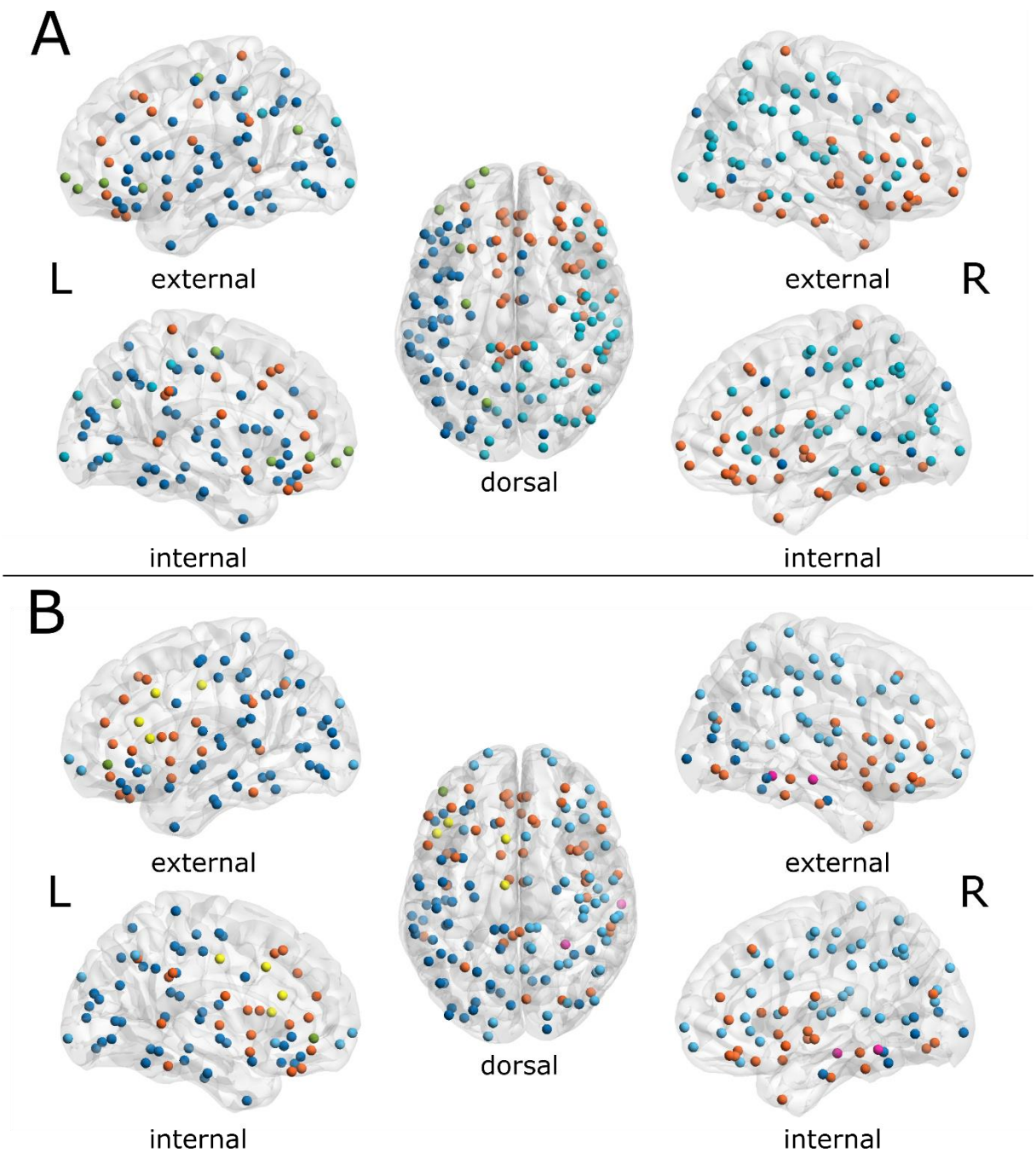

Figure 5.2 – Modular distributions. A: AD, four modules; B: DLB, six modules. Nodes marked with the same colour belong to the same module. DLB shows higher network disruption compared to AD.

Outcome of NBS analysis is shown in Figure 5.3. The less conservative primary statistical threshold, i.e. $t_{th_1} = 3.3$, produced one network component comprising 43 nodes and 48 edges (p = 0.013). This included two ventral intrahemispheric clusters connected with one only

interhemispheric edge between the inferior part of the right precentral sulcus and the left transverse temporal sulcus. Differentially altered connections within the left hemisphere were between occipito-temporal areas and PFC, whilst affected pattern in the right hemisphere included connections between occipital, inferior-temporal and superior temporal lobe, and PFC. Both hemispheres showed differential patterns comprising the cingulate and the insula. With stricter thresholding, i.e. $t_{th_2} = 3.5$, only a significant pattern of six nodes and six edges within the right hemisphere survived (p = 0.017), which comprised connections between inferior temporal and occipital lobe, and superior and inferior pre/central regions, as shown in Figure 5.4.

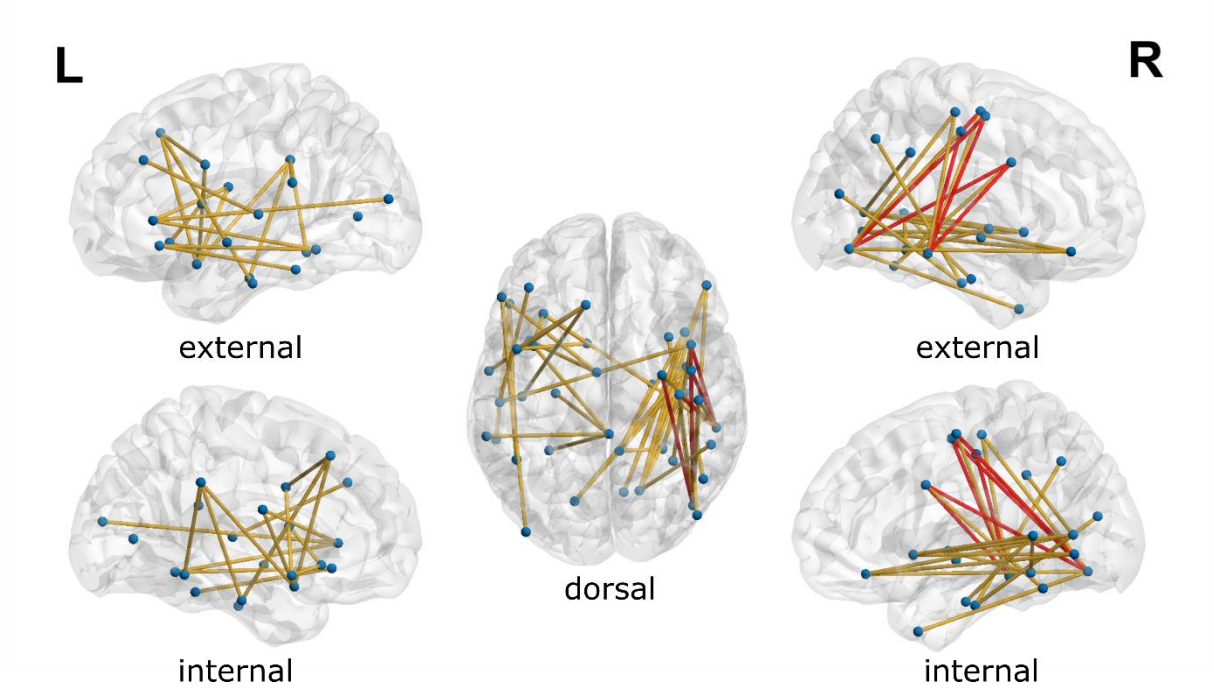

Figure 5.3 – NBS outcome for DLB < AD test (t_{th} = 3.3). Affected pathways comprise two ventral intrahemispheric clusters. Red edges: NBS outcome for t_{th} = 3.5.

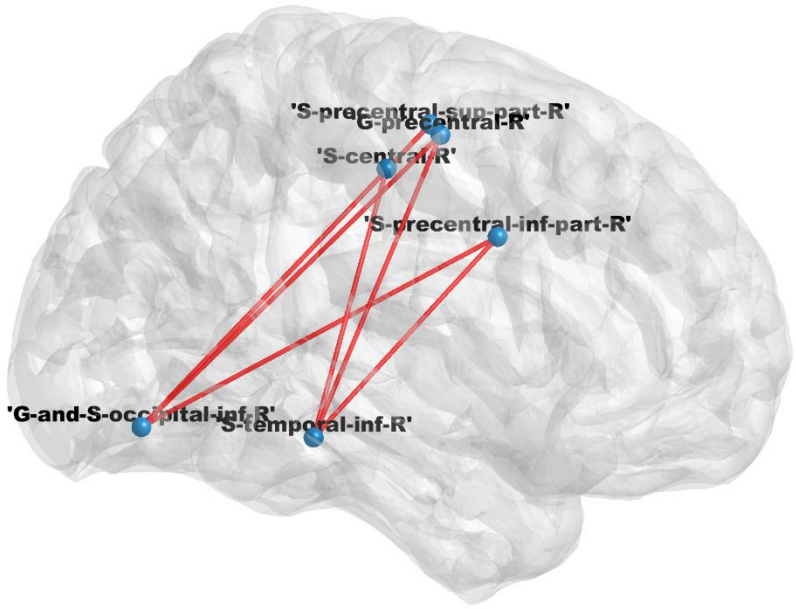

Figure 5.4 – NBS outcome for DLB < AD test (t_{th} = 3.5). Resulting component included right hemisphere temporal and parietal regions. Nodes are labelled according to the Destrieux atlas (S = sulcus; G = gyrus, R = right).

Distribution of connections belonging to the NBS component (t_{th} = 3.3) across modules in AD and DLB is shown in Figure 5.5. In the AD group, 27.08% of NBS edges were connecting nodes belonging to the same module, whilst in DLB, i.e. the group in which connections detected with NBS were more affected, this was the case for only 8.33%. This resulted in 18.75% of NBS connections being associated with higher modular disruption in DLB.

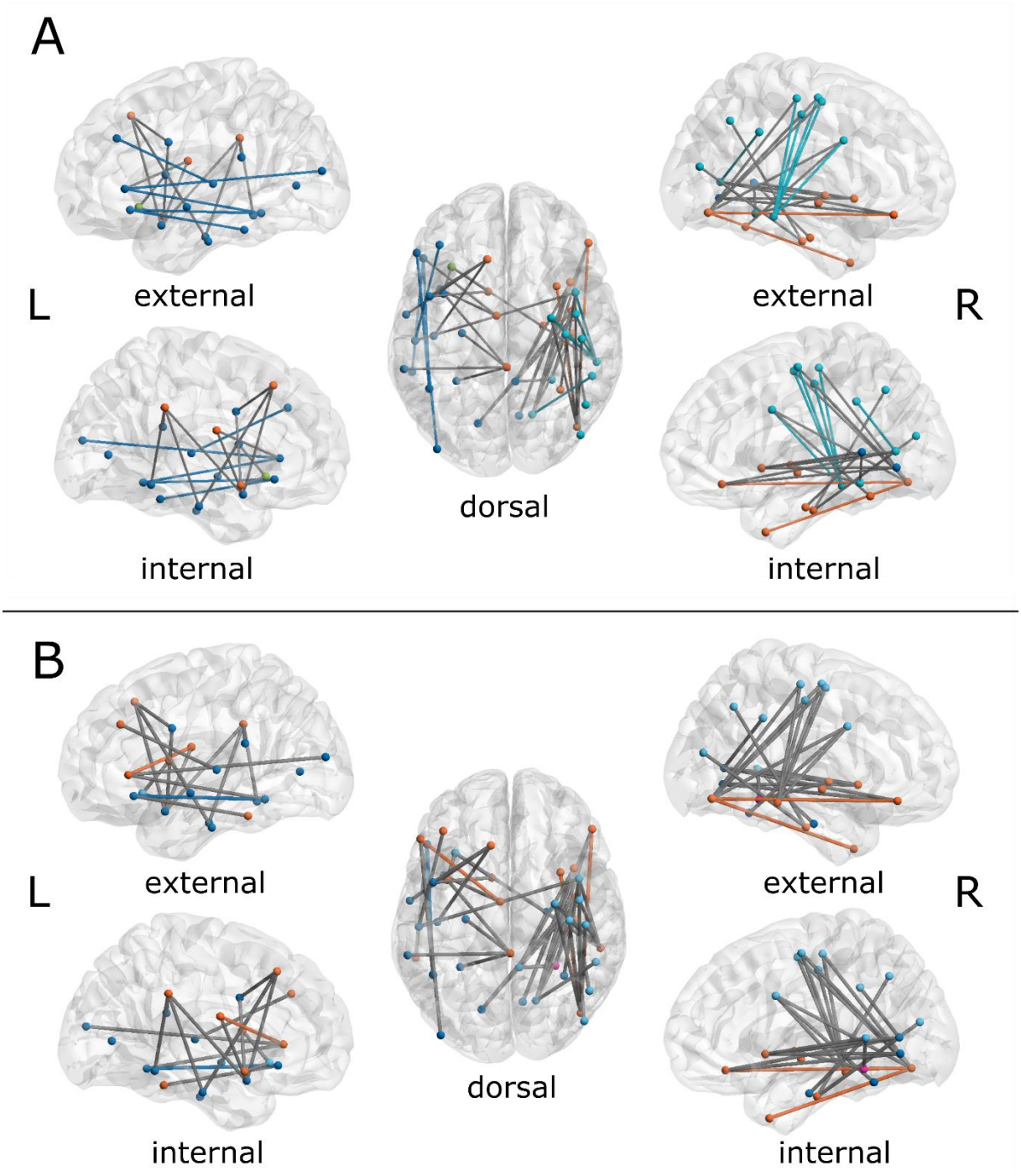

Figure 5.5 – Modular distribution of NBS component. A: AD group, 27.08% within-module edges; B: DLB group, 8.33% within-module edges. Within-module edges are marked with the same colour as the module the connected nodes are part of, based on Figure 5.2. Between-module edges are marked in grey.

5.4.2. Connectivity strength and modularity differences

Distribution within groups of average connectivity of NBS component ($WPLI_{NBS}$) and Q_w values are shown in Figure 5.6. Compared to the NBS component associated with t_{th_1}, NBS connections in AD for t_{th_2} were overall higher, leading to a more consistent difference with DLB. Modularity (Q_w) was significantly higher in DLB compared with AD ($p < 0.001$).

Among network measures, only Q_w in DLB group showed significant correlation with MMSE ($\rho = 0.55$, $p = 0.018$), as shown in Figure 5.7. Random forest regressor with cross-validation predicted MMSE values from Q_w with accuracy of 81.66%.

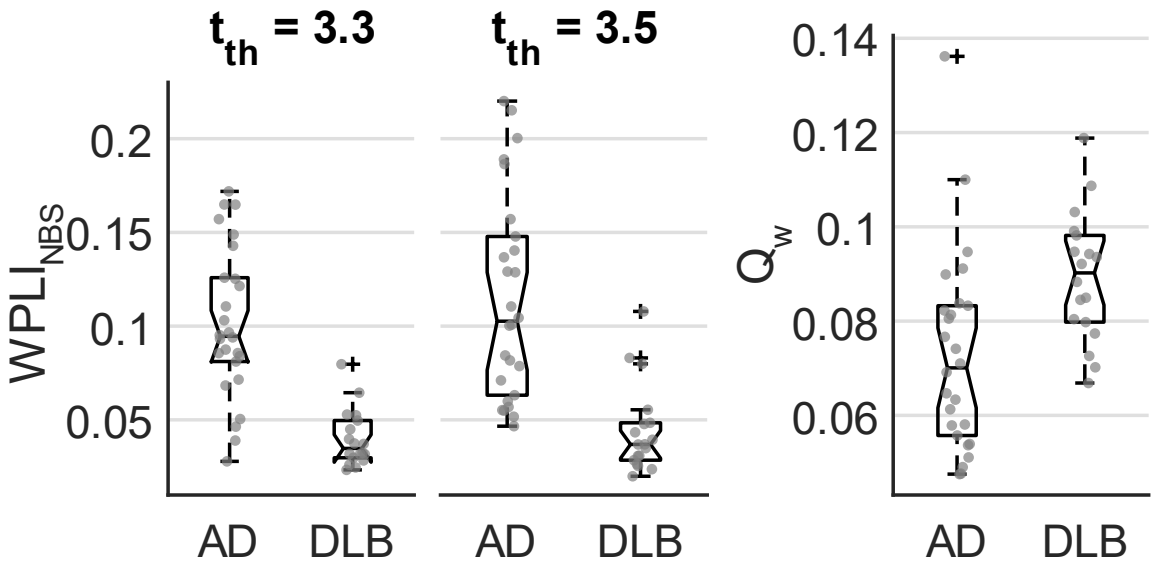

Figure 5.6 – $WPLI_{NBS}$ and modularity (Q_w) distributions. Both measures are significantly more affected in DLB compared with AD.

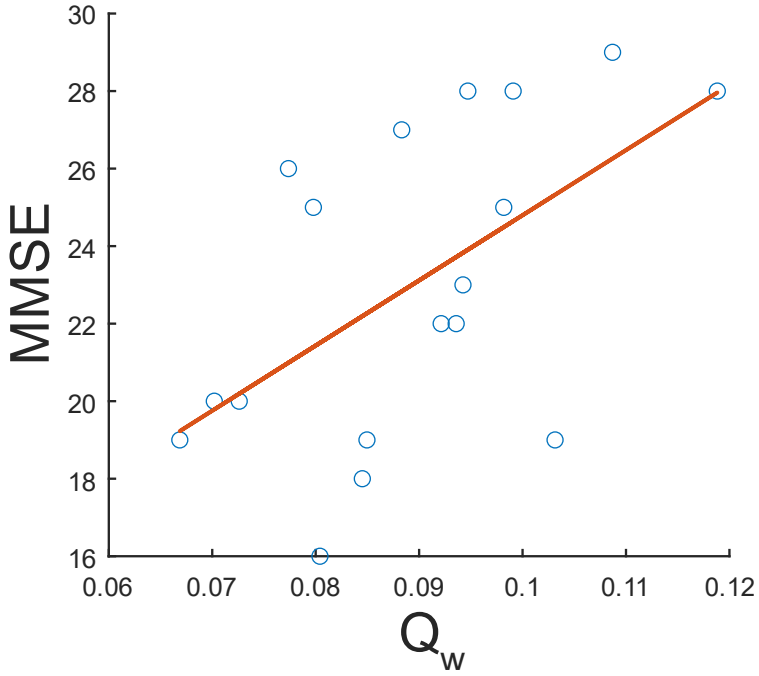

Figure 5.7 – Linear fitting for Q_w-MMSE trend in DLB. Spearman rank correlation test yielded significant positive correlation (ρ = 0.55, p = 0.018), and random forest regressor yielded accuracy of 81.66%.

5.4.3. Structural connectivity vs DF: outcome of correlation analysis

Replication of DF and DFV analysis pursued in Chapter 4 with a smaller subsample produced the same outcome, i.e. both measures were lower in DLB compared to AD, as shown in Figure 5.8.

Comparison of number of white matter (WM) fibres between groups did not produce any significant outcome in any of the three tracts of interest, which included NBM-occipital cortex, NBM-thalamus, and thalamus-occipital cortex. However, significant correlation was found between average structural connectivity in the NBM-occipital tract and DF values in AD and DLB as a whole group (ρ = 0.40, p = 0.004), as well as within the single groups, although more consistently in AD (ρ = 0.43, p_{AD} = 0.015, p_{DLB} = 0.039). WM-DF trends are shown in Figure 5.9.

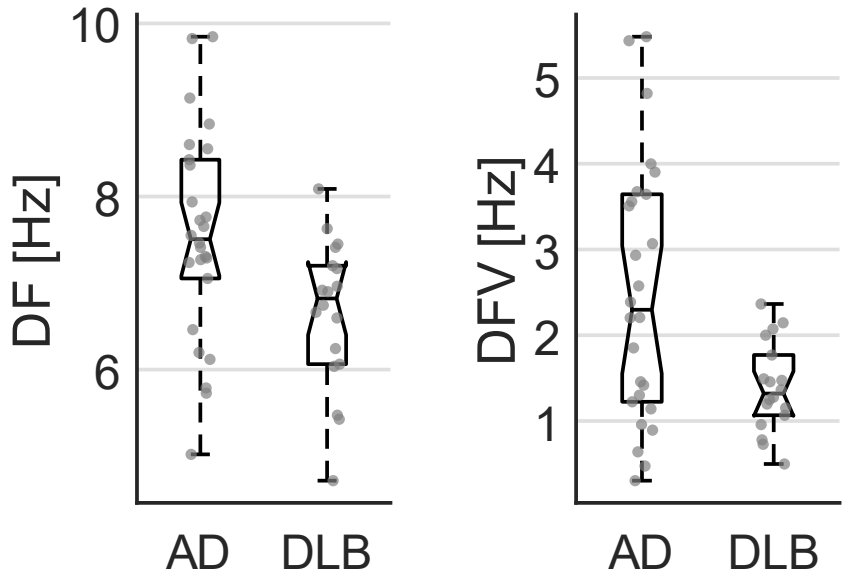

Figure 5.8 – DF and DFV over the occipital lobe. DF and DFV were significantly lower in DLB as compared with AD.

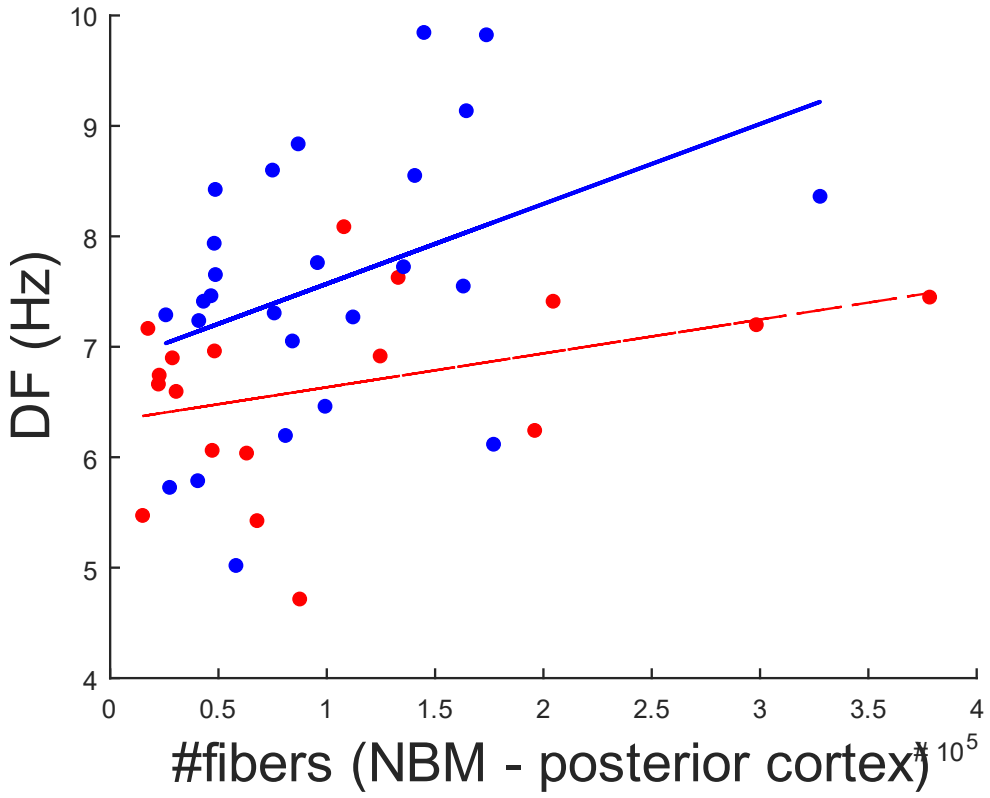

Figure 5.9 – Structural connectivity (NBM – occipital) vs DF: linear fitting for AD and DLB. Significant correlation emerges from Spearman rank test in both groups together (ρ = 0.40) and within each group (ρ_{AD} = ρ_{DLB} = 0.43). Thicker line represents significant correlation trend. Blue: AD; red: DLB.

5.4.4. EEG features: diagnostic accuracy

Random forest classifier discriminated between DLB and AD with an accuracy of 71.26% ± 11.48%, F1 score 69.73% ± 12.37%, optimal sensitivity 0.46, optimal specificity 1.00, mean PPV 77.00% ± 20.32%, mean NPV 72.00% ± 11.07%, AUROC 72% ± 13% (Figure 5.10). Variables were ranked based on their importance with first $WPLI_{NBS}$ (0.4938 ± 0.0287) followed by Q_w (0.2718 ± 0.0248) and DF (0.2344 ± 0.0239).

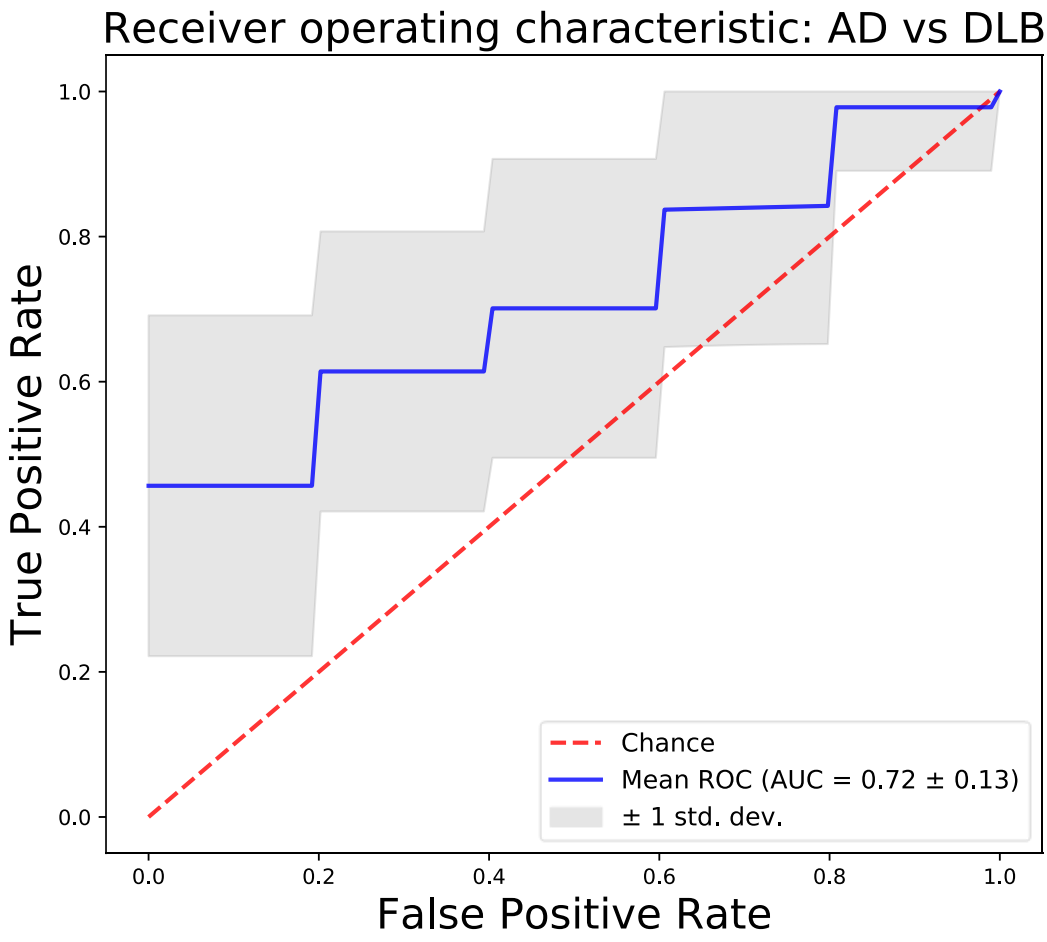

Figure 5.10 – ROC curve obtained with random forest classifier, AD vs DLB. Most predictive variable was $WPLI_{NBS}$.

5.5. Discussion

The analysis presented in this chapter aimed to directly compare structural and functional features between the DLB and AD groups. Since in Chapter 3 significant differences between the groups in the sensor domain emerged within the β-band network, differential EEG source network features were investigated in the presented analysis within that frequency band. Topographical analysis showed that ventral pathways including prefrontal, temporo-occipital and parietal areas were more affected in DLB compared to AD. 18.75% NBS connections were associated with higher network disruption in DLB, as evidenced by a higher number of modules and greater modularity, and where this latter measure positively correlated with cognitive performance as assessed with MMSE score, with 81.66% prediction accuracy. Despite a lack of difference in structural connectivity, fibre tract integrity between basal forebrain and occipital lobe was positively associated with DF values in both groups, although more consistently in AD. EEG features yielded discrimination between groups with accuracy of 71.26% ± 11.48%, with $WPLI_{NBS}$ being the most predictive feature.

5.5.1. DLB network is more segregated than AD

In line with the sensor domain network, β-band source network was more segregated in DLB compared to AD. The optimal community structure obtained with 60% threshold on the agreement matrices consisted of four modules in AD and six modules in DLB. Difference in the number of modules was mainly driven by disruption of the left prefrontal and part of the right temporal modules, as well as redistribution of other modules. Higher propensity of DLB network to organise in modules emerged as higher modularity, as also found in the sensor domain analysis reported in Chapter 3 and in agreement with a previous fMRI study which included the same cohort (Peraza *et al.*, 2015). Outcome of NBS analysis concurs with the idea that impairment of long-range connections in DLB compared to AD may lead the network towards higher segregation. In fact, affected pathways consisted of posterior-anterior and ventral-dorsal projections, whilst short weakened edges did not emerge. Physiological brain dynamics have been shown to be also associated with transient modular organisation (Betzel *et al.*, 2012). Such dynamics were reported to be slowed in DLB compared to AD in a recent study on the same participants cohort (Schumacher *et al.*, 2019). Therefore, higher modularity

in DLB might be a consequence of disruption of physiological brain transient states, which leads the functional network towards a more segregated organisation. Interestingly, affected regions also included the insular cortex and cingulate, which in DLB have been found to show dopaminergic deficit (Pilotto *et al.*, 2019), reduced metabolism (Minoshima *et al.*, 2001) and enhanced α-synuclein pathology likely involving the von Economo neurons (Kosaka, 1978; Gómez-Tortosa *et al.*, 1999; Pletnikova *et al.*, 2005; Blanc *et al.*, 2016; Fathy *et al.*, 2019). These latter are known to be involved in fast assessment of complex situations (Allman *et al.*, 2005) and salience (Cauda *et al.*, 2013), both parts of physiological cognitive and attentional processes which are typically affected in DLB. Future studies combining autopsy and EEG might provide additional insights into these DLB-related features and their specificity for diagnosis purposes.

Moreover, the differential pattern within the right hemisphere was consistently weakened in DLB and comprised connections within a disrupted module (the teal coloured module in Figure 5.5). This network component consists of connections between dorsal and ventral areas, suggesting that interaction between attentional networks might be particularly affected in DLB over the right hemisphere, towards which the ventral network was proposed to be lateralised in healthy condition (Corbetta and Shulman, 2002; Corbetta *et al.*, 2008). Alternatively, it is possible that such consistent connectivity reduction within the right hemisphere is associated with emotional and cognitive features which typically emerge in DLB, such as delusion or depression (McKeith *et al.*, 2017). Supporting this speculation is that previous studies have attributed a major role in cognitive and emotional processing to the right hemisphere (Schwartz *et al.*, 1975; Liotti and Tucker, 1992; Spence *et al.*, 1996) which has also been associated with β-band activity (Ray and Cole, 1985; Wang *et al.*, 2013b), as described in section 1.3.1. However, MMSE was not significantly different between DLB and AD, as reported in Table 5.1. Therefore, perhaps only emotional alteration might be associated with such network abnormality. Right-hemisphere-related psychiatric features are reflected into the score of NPI questionnaire, as described in section 2.1. To explore the possible relationship between psychiatric dysfunctions and right-hemisphere connectivity disruption as speculated, Spearman rank correlation test (one-tailed) was performed between $WPLI_{NBS_{t_{th_2}}}$ and NPI total score in DLB group. Correlation test resulted in a trend towards significance (ρ = -0.34, p = 0.082), as shown in Figure 5.11, showing that right-hemisphere

psychiatric dysfunctions are at least partly associated with functional connectivity alteration. Tests for single subdomains revealed that the detected trend was driven by eating (p = 0.043, uncorrected) and sleep disorders (p = 0.075, uncorrected); however, whilst symptom severity values within NPI subdomains corresponding to high connectivity values were consistently low, weak $WPLI_{NBS}$ was overall associated with strong NPI values variability across subjects. This likely biased the correlation tests towards a not significant outcome. Further analysis with a larger DLB cohort will be needed to reliably assess which specific psychiatric domains as measured with NPI subsections are driving the detected correlation trend and are significantly associated with the detected connectivity strength weakening.

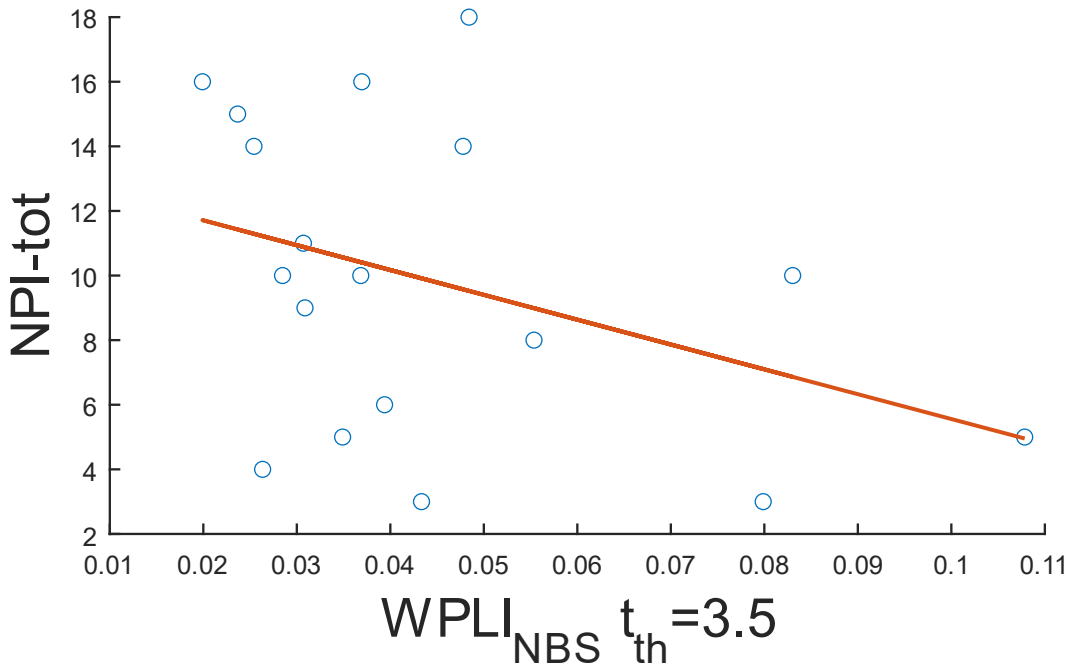

Figure 5.11 – Linear fitting between right-hemisphere functional connectivity and NPI total score in DLB. Only a trend towards significance emerged from Spearman rank correlation test (ρ = -0.34).

On the other hand, modularity in DLB showed positive correlation with MMSE, which could be predicted with an accuracy of 81.66%. Paradoxically, higher network disruption in DLB was associated with better cognitive performance, but not in AD. Any neurobiological explanation to this phenomenon remains speculative. Correspondence between 18.75% of differential pathways and disrupted modules as shown in Figure 5.5 may suggest that functional modular network organisation in DLB acts as a compensatory mechanism aimed to preserve cognitive functions, which would otherwise be more affected than in AD due to differences in connectivity strength. This speculation resonates with previously reported lower modularity associated with ageing (Meunier *et al.*, 2009; Onoda and Yamaguchi, 2013; Song *et al.*, 2014), a physiological condition which normally leads to cognitive decline (Gallagher and Colombo, 1995; Christensen, 2001; Deary *et al.*, 2009; Bishop *et al.*, 2010). Another possible explanation may rely on the fact that most DLB cases show coexisting AD pathology (McKeith *et al.*, 2005; Schneider *et al.*, 2007; Weisman *et al.*, 2007; Iizuka and Kameyama, 2016), which has been associated with low functional modularity using diverse modalities (de Haan *et al.*, 2012b; Wang *et al.*, 2013a; Peraza *et al.*, 2015; Jalili, 2017). Concurrence of pathological condition might more severely affect cognitive functions whilst prominence of AD component and lower LB pathology might result in a reduced segregation of the network, yielding significant correlation between the two features as obtained in this analysis.

5.5.2. Cholinergic system is associated with DF

Structural connectivity between thalamus, basal forebrain and occipital cortex was assessed with probabilistic tractography. Main scope of this analysis was to assess whether the cholinergic system shows any degeneration in one condition or the other. Although inclusion of the basal forebrain, i.e. the main source of cholinergic projections (Mesulam, 1990; Selden *et al.*, 1998; Hepp *et al.*, 2017a), among regions of interest might be enough for this purpose, the thalamus was also considered due to its cholinergic projections from the reticular formation (Yeo *et al.*, 2013) and pedunculpontine nucleus (French and Muthusamy, 2018), its regulatory role on EEG oscillations (Lopes da Silva *et al.*, 1973; Schürmann *et al.*, 2000; Robinson *et al.*, 2001; Roberts and Robinson, 2008) and its reported involvement in DLB clinical phenotype (Delli Pizzi *et al.*, 2015b; Onofrj *et al.*, 2019; Schumacher *et al.*, 2019). Unexpectedly, none of the considered white matter tracts were differentially affected

between conditions. This result apparently contrasts speculations which associate prominent cholinergic disruption with DLB pathology (Perry *et al.*, 1991; Tiraboschi *et al.*, 2000; Tiraboschi *et al.*, 2002; Lemstra *et al.*, 2003; Delli Pizzi *et al.*, 2015b). Notably, structural connectivity between NBM and occipital cortex was associated with DF values in both groups. This outcome introduces novel evidence that α-band activity over the occipital cortex might be directly driven by the cholinergic system originating from the NBM. However, in DLB group correlation was not as consistent as in AD, as emerges from the distributions showed in Figure 5.9 (p_{AD} = 0.015, p_{DLB} = 0.039). In fact, monotonic trend in DLB assessed with Spearman rank test appears to be mostly driven by those subjects with number of fibres above 10^5, whilst those below form a randomly distributed cluster. In contrast, a consistent increasing trend emerges in AD. As already proposed in the previous section for Q_w-MMSE correlation, DLB subjects which show an association between WM integrity and DF might again have developed coexisting pathology. It could be suggested that WM-DF association reflects control of cholinergic system over functional processes in the cortex; such mechanism is still intact in AD pathology and only partially affected in mixed pathology where AD component is prominent. Instead, in LB-prevalent cases, cholinergic system might be majorly disrupted, as also reflected into lower and less variable DF values over time, e.g. lower DFV. In addition, it is possible that in DLB a negative shift of DF involves other pathological mechanisms, which are worth of investigation in future studies. Interestingly, there was no correlation between any of the WM tracts including the thalamus and DF in either groups. It is possible that functional abnormalities associated with DLB persist in the thalamus, and their involvement in occipital DF slowing might be mediated by the above-mentioned pathological mechanisms. Implementation of EEG subcortical source localisation will be needed to explore this hypothesis.

One of the most specific clinical features of DLB is complex visual hallucinations (VH), which have been shown to effectively discriminate DLB from AD and AD-LB mixed pathology where AD component is prominent (Tiraboschi *et al.*, 2006; Jicha *et al.*, 2010; Toledo *et al.*, 2013; Yoshizawa *et al.*, 2013). The fact that part of the DLB cohort included here did not feature VH further suggests the existence of coexisting pathology in some subjects, which may introduce a level of variability in EEG and structural metrics within the group. To further investigate this aspect, the focus of the next chapter will be on this specific disease phenotype within Lewy body pathology, i.e. DLB and PDD.

5.5.3. Connectivity strength is the most discriminative EEG feature

The purpose of the research presented in this thesis is to further validate EEG and, specifically, EEG connectivity metrics as biomarkers for DLB against AD. Connectivity strength was the most discriminative variable between DLB and AD, in line with findings from the EEG scalp analysis, as well as previous EEG network studies also including other conditions (Xu *et al.*, 2016; Blinowska *et al.*, 2017; Peraza *et al.*, 2018). Overall, network features were more predictive than DF, suggesting that the first should be progressively introduced in a diagnostic framework beside EEG power frequency features and assessed indicative biomarkers. However, classification accuracy was not as high as reported in previous studies (Andersson *et al.*, 2008; Bonanni *et al.*, 2008; Peraza *et al.*, 2018; Stylianou *et al.*, 2018). This is likely due to two reasons. First, compared to the presented analysis, classifiers in those studies were trained with higher number of differential variables. Second, a conservative cross-validation approach was pursued in the presented analysis: $WPLI_{NBS}$ feature was obtained by performing NBS on 60 random subsamplings, and due to the relatively small sample with probable presence of outliers, few iterations did not yield any significant differential network components or, in the best case, produced inconsistent patterns. Performing the same analysis on a larger sample may reduce influence of outliers on the analysis, provide more consistent differential topographies and consequently lead to a better classification between groups.

5.6. Conclusions

This chapter investigated differential EEG features between AD and DLB in the source domain. Functional connectivity analysis within the β-band network resulted in higher segregation of DLB network compared to AD, as well as weaker connectivity patterns likely associated with affected cognitive and emotional processes. Modularity was associated with better cognitive performance in DLB, but not in AD. Investigation of cholinergic involvement in DF showed that the cholinergic system likely has a regulatory role over EEG activity. It was observed that white matter projections were not more significantly affected in DLB, but association between structural connectivity and DF in DLB was not as consistent as in AD. From the diagnostic perspective, EEG connectivity was the most discriminative variable, and it may be suggested

to be included as a supportive biomarker for DLB beside DF slowing. However, outcomes of the presented analysis suggest that pathological differences between AD and DLB may not consistently emerge if mixed pathology cases in DLB are not taken into account. This will be pursued in the next chapter by investigating functional and structural abnormalities associated with complex visual hallucinations in Lewy body dementias, i.e. DLB and PDD.

Chapter 6. Functional and Structural Alterations in Lewy Body Dementia with Visual Hallucinations

6.1. Summary

Visual hallucinations occur in most Lewy body dementia cases. Previous studies have shown that VH is highly specific in differentiating LBD from AD and AD-LB mixed pathology cases with prominent AD. Computational models proposed impairment of visual and attentional networks to be at the basis of VH symptomatology. However, there is still a lack of experimental evidence on functional and structural brain network abnormalities associated with VH in LBD. In this chapter, EEG source localisation and NBS were used to assess differential topographical patterns between VH and NVH participants; grey matter differences were also tested within functionally affected cortical areas belonging to the visual ventral network, thalamus and NBM. DTI was used to assess structural connectivity between subcortical regions of interest and cortical regions belonging to the functionally affected network component in VH, as assessed with NBS. Number of WM fibres within the cortex and between subcortical and cortical regions was compared between VH and NVH and correlated with average EEG source connectivity of the NBS component. Moreover, modular organisation of the EEG source network was obtained, compared between groups, and tested for correlation with structural connectivity. Network analysis showed that there is consistent weakened connectivity within visual ventral network, and between this network and DMN or VAN, but not between or within attentional networks. The cuneus was the most functionally disconnected region, although cortical thickness was preserved in VH and reduced in NVH, in this latter group comparable with thickness values in AD. Subcortical volumes were reduced in VH, although no significant correlation between GM and EEG connectivity strength emerged. Between-group comparison yielded significantly affected WM fibres between NBM and cortical regions in VH compared to NVH. Number of fibres in the tract correlated with cortical functional connectivity in NVH, but not in VH. Furthermore, significant negative correlation emerged between modularity and cholinergic innervation in the thalamus in NVH, and only a trend in VH. This study proposes for the first time differential topography of altered functional network between VH and NVH, and provides a validation of existing computational models. Specifically, outcome of the present study shows that VH condition is associated with

functional network segregation in LBD and confirms the involvement of the cholinergic system in LB pathology and, specifically, VH condition.

6.2. Introduction

Complex visual hallucinations (VH) are a common feature in Lewy body dementia (LBD), i.e. DLB and PDD, occurring in about 80% of clinically diagnosed cases (Collerton *et al.*, 2005; McKeith, 2007a; Mosimann *et al.*, 2008). As described in section 1.2, complex VH can feature people, animals, and inanimate objects (Aarsland *et al.*, 2001; Burghaus *et al.*, 2012), tend to have short duration and occur at low-light environment (Fénelon *et al.*, 2000; Barnes and David, 2001; Holroyd *et al.*, 2001). Due to their high specificity in discriminating LBD from AD and AD-LB mixed pathology cases (Tiraboschi *et al.*, 2006; Jicha *et al.*, 2010; Toledo *et al.*, 2013; Yoshizawa *et al.*, 2013), VH are a matter of interest in dementia research and, specifically, in this chapter of this thesis.

A consistent picture of the underlying pathology and associated functional dysfunctions in LBD-related VH has not been defined yet. Autopsy and clinical studies support the idea that dysfunction of the cholinergic and dopaminergic systems must have a relevant role in generation of VH by affecting brain areas involved in visual and attentional processing (Ballard *et al.*, 2000; Harding *et al.*, 2002; Diederich *et al.*, 2005; Shine *et al.*, 2011; Shine *et al.*, 2014; Onofrj *et al.*, 2019). Models by Collerton *et al.* (2005) and Tsukada *et al.* (2015) proposed mismatch of top-down and bottom-up affected visual networks to be associated with pathological mechanisms generating VH. This hypothesis is supported by evidence which includes GM atrophy over the frontal cortex (Pezzoli *et al.*, 2019), hypometabolism within occipital and temporal areas (Pasquier *et al.*, 2002; Gasca-Salas *et al.*, 2016), reduced activation over secondary visual areas (Taylor *et al.*, 2012) and lower occipital GABA levels (Firbank *et al.*, 2018). On the other hand, Shine *et al.* (2011) proposed a deranged interaction between DAN, DMN and VAN to be drivers of VH phenomenon; empirical evidence on this perspective includes reduced fMRI activation of DAN areas and lower connectivity between VAN and DMN associated with lower GM within the insula (Shine *et al.*, 2014), although another study did not report significant functional connectivity differences within attentional networks between VH and NVH in a PD cohort (Hepp *et al.*, 2017b). As discussed in section

1.5, EEG features on the topic remain under-researched. Recent works reported delayed ERP components associated with visual stimuli in LBD-VH (Kurita *et al.*, 2005; Matsui *et al.*, 2005; Kurita *et al.*, 2010; Chang *et al.*, 2016), lower resting state DF, β-band power and right-temporal connectivity (Dauwan *et al.*, 2018; Dauwan *et al.*, 2019) and higher δ-band and α-band activity (Babiloni *et al.*, 2020) compared to NVH and HC. As shown in Chapter 5, there appears to be partial loss of cholinergic regulation over cortical activity in DLB compared to AD. It was speculated that partial preservation of such control within DLB group was associated with reduced α-synuclein pathology in mixed AD-LB pathology cases, whilst EEG features in pure DLB cases might be significantly affected by cholinergic disruption. This aspect might be untangled by investigating such correlation in LBD-related VH, due to specificity of development of VH as a marker of purer α-synuclein pathology against mixed pathology condition (Tiraboschi *et al.*, 2006; Jicha *et al.*, 2010; Toledo *et al.*, 2013; Yoshizawa *et al.*, 2013).

6.2.1. Objective

In this chapter, EEG source localisation and NBS were used to assess network alteration patterns associated with VH in LBD. It was hypothesised that regions belonging to the visual network were significantly affected in VH condition, in line with existing computational models. Due to its well reported association with visual and attentional processing (Chapman *et al.*, 1962; Mulholland and Runnals, 1962; Klimesch *et al.*, 1998; Jensen and Mazaheri, 2010; Benedek *et al.*, 2014; Wan *et al.*, 2019), the analysis here focused on the α-band network. Regions which were functionally more disconnected were detected, and cortical thickness (CTh) in such regions which also belonged to the visual network was compared between groups. To obtain speculative elements on whether EEG and structural volume alterations share pathological mechanisms, correlation tests were performed in both groups. It was hypothesised here that abnormalities of cortical functional connectivity are associated with degeneration of cholinergic projections towards the cortex. To prove this hypothesis, volumes differences between groups of thalamus and NBM were first tested; moreover, following the approach pursued in Chapter 5, structural connectivity between basal forebrain, thalamus and functionally affected cortical areas was assessed, compared between groups, and correlated with EEG connectivity strength. In addition, for exploratory purposes, functional modular distribution in VH and NVH was obtained and compared between groups.

6.3. Methods

Details on the experimental protocol, EEG acquisition and measured network features are reported in Chapter 2. A subsample of DLB and PDD patients with available EEG and MRI data was selected and distributed in VH and NVH groups based on the NPI hallucination total score, respectively higher than zero and equal to zero. To reach a balanced distribution of DLB and PDD among groups, eight additional subjects were included from the "Visual hallucinations: an EEG and non-invasive Stimulation" (VEEG-Stim) study at Newcastle University (Murphy, 2016; Firbank *et al.*, 2018), which featured the same resting-state protocol as CATFieLD. Although the majority of VH patients presented complex hallucinations, four of them had only simple visual hallucinations. These have been included in the VH group since minor hallucinatory phenomena have been shown to be associated with progressive development of complex VH (Ffytche *et al.*, 2017) and have been suggested to be part of the same psychotic spectrum. The resulting sample comprised 26 VH (12 DLB and 14 PDD) and 17 NVH (7 DLB and 10 PDD) (see Table 6.1). EEG was recorded in eyes-closed resting state with high-density sensor cap (128 electrodes). Recorded signals were pre-processed (section 2.3) (number of removed channels: 16 ± 16; number of removed epochs: 10 ± 9; number of removed ICA components: 36 ± 13), source localised and connectivity between cortical sources was measured with WPLI and averaged across time and frequency bins within the α-band (8-13.5 Hz).

	VH (N=26)	NVH (N=17)	p-value
Age	73.88 ±6.32	74.88 ±6.53	df=1, p-value=0.737Ŧ
Male/Female	25/1	13/4	df=1, p-value=0.049ǂ
DLB/PDD	12/14	7/10	df = 1, p-value=0.748ǂ
MMSE	22.58 ±4.11	24.65 ±4.00	df=1; p-value=0.067Ŧ
NPI hall num.	1.73 ±1.00	0 0	/
NPI hall freq.	2.15 ±1.08	0 0	/
NPI hall sev.	1.15 ±0.37	0 0	/
NPI hall dis.	1.04 ±1.31	0 0	/
NPI hall TOT. (freq. x sev.)	2.65 ±1.96	0 0	/
Complex hall (yes/no)	22/4	/	/
ACheI (yes/no)	23/3	10/6*	df=2, p-value=0.065ǂ
LEDD	499 ±474	475 ±431	df=1, p-value=0.500Ŧ

Table 6.1 - Demographic data and clinical scores (CATFieLD + VEEG-Stim subsample with available EEG-MRI data). Ŧ Unpaired Mann-Whitney U test, ǂ χ2 test. * One PDD patient was on Memantine.

For the modularity and DTI analysis, a narrower subsample of DLB and PDD patients with available EEG, MRI and DTI data was selected. The resulting sample comprised 25 VH (11 DLB and 14 PDD) and 16 NVH (7 DLB and 9 PDD) (see Table 6.2). Modularity (Q_w) was computed on non-thresholded WPLI matrices and compared between groups with ANCOVA test corrected for MMSE ($p < 0.05$).

	VH (N=25)	NVH (N=16)	p-value
Age	73.88 ±6.17	74.31 ±6.29	df=1, p-value=0.820Ŧ
Male/Female	24/1	12/4	df=1, p-value=0.045ǂ
DLB/PDD	11/14	7/9	df=1, p-value=0.987ǂ
MMSE	23.04 ±3.78	24.69 ±4.13	df=1; p-value=0.098Ŧ
NPI hall num.	1.56 ±0.87	0 0	/
NPI hall freq.	2.08 ±1.04	0 0	/
NPI hall sev.	1.12 ±0.33	0 0	/
NPI hall dis.	0.92 ±1.22	0 0	/
NPI hall TOT. (freq. x sev.)	2.44 ±1.66	0 0	/
Complex hall (yes/no)	21/4	/	/
AChei (yes/no)	22/3	10/5*	df=2, p-value=0.121ǂ
LEDD	540 ±482	480 ±445	df=1, p-value=0.378Ŧ

Table 6.2 - Demographic data and clinical scores (CATFieLD + VEEG-Stim subsample with available EEG-MRI-DTI data). Ŧ Unpaired Mann-Whitney U test, ǂ χ2 test. * One PDD patient was on Memantine.

6.3.1. Magnetic resonance imaging recording

Individual MRI T1 recordings were obtained on a 3-T Philips Intera Achieva scanner with MPRAGE sequence, sagittal acquisition, echo time 4.6 ms, repetition time 8.3 ms, inversion time 1250 ms, flip angle=8°, SENSE factor = 2, in-plane field of view 240x240 mm^2 with slice thickness 1.0 mm, yielding voxel size of 1.0 x 1.0 x 1.0 mm^3 (Peraza *et al.*, 2014; Firbank *et al.*, 2018; Schumacher *et al.*, 2020b). Pre-processing and segmentation of acquired T1 weighted images was performed by Dr Sean Colloby using FreeSurfer software package (version 5.1, http://surfer.nmr.mgh.harvard.edu/) (Dale *et al.*, 1999; Fischl and Dale, 2000) as in previous analyses which included part of the cohort of this thesis and were reported in their respective publications (Colloby *et al.*, 2011; Blanc *et al.*, 2015). The automated processing pipeline involved intensity non-uniformity correction, Talairach registration, removal of non-brain tissue (i.e. skull stripping), WM and subcortical GM segmentation, tessellation of GM-WM boundary, and surface deformation following GM-CSF intensity gradients for optimal placing of GM-WM and GM-CSF borders. Modelling of cortical surface was followed by surface inflation, transformation to spherical atlas and parcellation into regions according to the atlas developed by Destrieux *et al.* (2010). Respective network nodes are obtained as mass centroids across each region vertices. Resulting images from each processing step were visually inspected and, were required, manually corrected to ensure accurate segmentation (Blanc *et al.*, 2015).

CTh (measured in mm) for each cortical region was obtained as the closest distance from GM-WM and GM-CSF boundaries at each vertex of the tessellated surface (Fischl *et al.*, 2004), and mapped to the inflated surface (Blanc *et al.*, 2015).

DTI recordings were performed with a 2-dimensional spin-echo, echo planar imaging diffusion-weighted sequence with 59 slices: TR = 6100 ms; TE = 70 ms; flip angle = 90°; field of view = 270 x 270 mm; pixel size= 2.1 x 2.1 mm; slice thickness = 2.1 mm. Images were diffusion weighted along 64 uniformly distributed directions (diffusion contrast b = 1000 $s \cdot mm^{-2}$), and six acquisitions did not have any diffusion weight applied (b = 0 $s \cdot mm^{-2}$) (Firbank *et al.*, 2007).

6.3.2. Subcortical ROIs definition for subcortical volume analysis

Subcortical volumes were computed by Dr Julia Schumacher. For subcortical volume analysis, thalamus and NBM (Ch4 cellular group) structures and respective ROI masks were obtained using the SPM Anatomy Toolbox for MATLAB (Eickhoff *et al.*, 2005). The thalamus mask was based on the Oxford thalamic connectivity atlas (Behrens *et al.*, 2003b), whilst the NBM was defined with a probabilistic anatomical map from microscopic delineation of ten post mortem human brains (Zaborszky *et al.*, 2008). Resulting masks in the MNI space are shown in Figure 6.1. Volumes were averaged across hemispheres and measured for each subject. Obtained values were normalised by total GM volume.

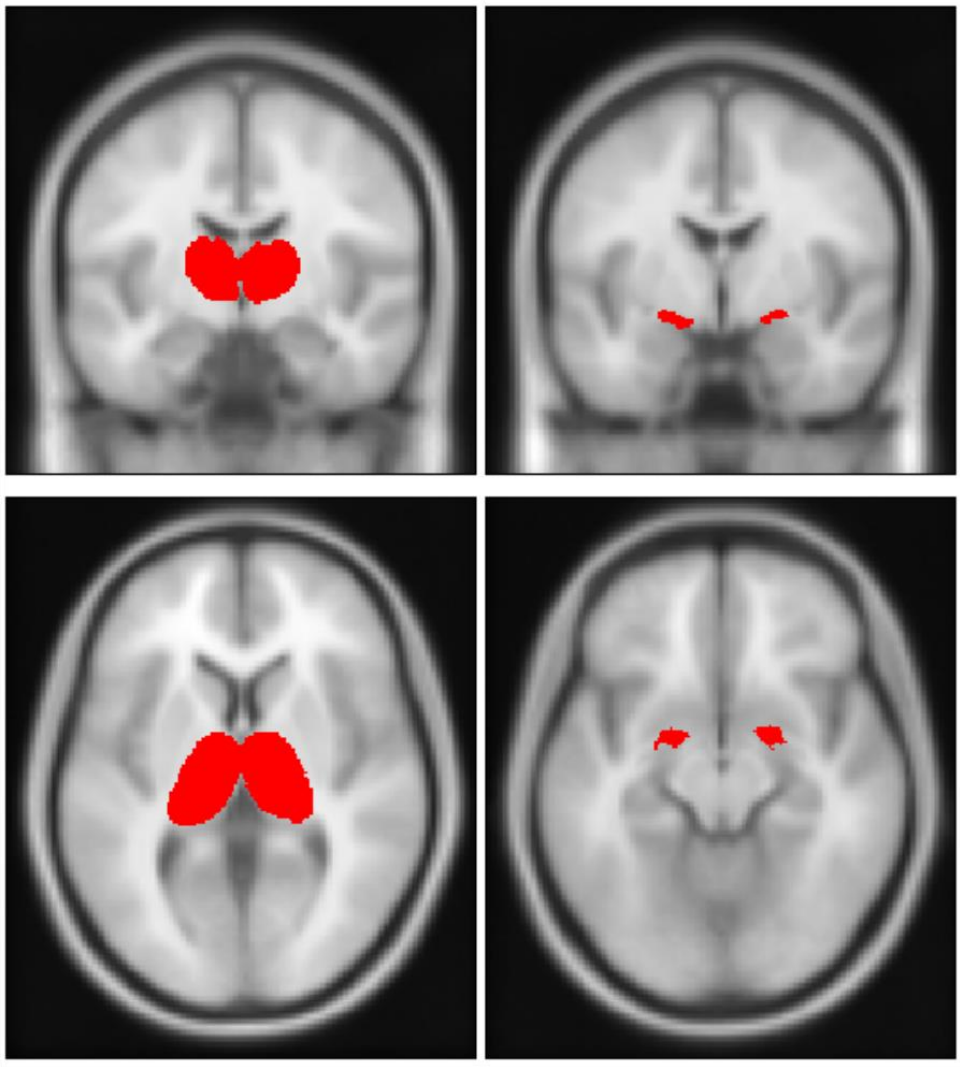

Figure 6.1 – Thalamus (left) and NBM (right) ROI masks in MNI space obtained with SPM anatomy toolbox for MATLAB.

6.3.3. Cortical source localisation

The pipeline for EEG source reconstruction is reported in detail in section 4.3.2. Briefly, cortical source estimation from EEG signals was obtained through sLORETA technique (Pascual-Marqui, 2002) as implemented in the Brainstorm toolbox for Matlab (Tadel *et al.*, 2011) and described in section 1.3.3. EEG sensors distribution was manually co-registered over the scalp for each participant using the Brainstorm toolbox (Stropahl *et al.*, 2018) before performing any further step. Head model based on the individual anatomical data was obtained with boundary element method (BEM) as implemented in OpenMEEG (Kybic *et al.*, 2005; Gramfort *et al.*, 2010). Noise covariance was set as identity matrix, cortical sources were reconstructed with assumption of normal dipole orientations with respect to cortical surface, and resulting time-series were averaged within each of the 148 regions defined with the Destrieux atlas (Destrieux *et al.*, 2010). Channels which were removed and interpolated during the pre-processing step were excluded from source localisation to reduce the risk of false positives. Signs of opposite sources within each region were flipped to match the main orientation and averaged. Before any analysis, source activity from all subjects was projected back to the ICBM152 template (Mazziotta *et al.*, 2001) using Shepard's interpolation method (Shepard, 1968).

6.3.4. Topographical differences: functional and structural alterations

Differential topographical network patterns between VH and NVH were obtained using NBS (Zalesky *et al.*, 2010), of which implementation is described in detail in section 2.5. F-test was performed at t_{th} = 13.8, and FWER was controlled by performing a permutation test (5000 permutations); network differential components were deemed significant at $p < 0.05$, and were visualised with the BrainNet Viewer (Xia *et al.*, 2013). Average strength across connections belonging to the NBS components ($WPLI_{NBS}$) was computed and compared between groups (two-tailed Mann-Whitney U test, $p < 0.05$). This analysis was performed in both the EEG-MRI available sample and the EEG-MRI-DTI subsample.

To detect the most functionally altered regions within NBS component, node strength (K_W) was computed for NBS nodes, and compared between groups by performing a Wilks' Lambda multivariate test as implemented in SPSS ($p < 0.05$), followed by post hoc Mann-Whitney U

tests as implemented in MATLAB ($p < 0.05$, Holm-Bonferroni corrected for number of NBS nodes). Before computing node strength, edge weights were divided by the maximum WPLI value across NBS edges (Onnela *et al.*, 2005). This analysis was performed on the EEG-MRI subsample.

CTh values in significantly altered nodes (including those not surviving multiple comparison correction) which were part of occipital cortex, IT or PFC, were compared between groups by performing a Wilks' Lambda multivariate test ($p < 0.05$), followed by post hoc Mann-Whitney U tests ($p < 0.05$, Holm-Bonferroni corrected for number of selected nodes). Association between node strength and CTh was tested for nodes which had significantly different CTh between groups with Spearman rank correlation tests ($p < 0.05$). This analysis was performed on the EEG-MRI subsample.

Modular distribution was obtained for both groups using routines implemented in the BCT, as described in detail in section 5.3.3. Briefly, for each EEG network, the optimal community structure was obtained, an agreement matrix was obtained for each group, the agreement matrix was thresholded preserving probabilities above 63%, and modular distribution was obtained as consensus matrix, whose computation was based on the algorithm developed by Lancichinetti and Fortunato (2012). Obtained modular distribution was visualised with the BrainNet Viewer. For each group, proportion of within-module NBS connections was obtained based on the group's modular distribution. This measure was computed as a ratio between number of within-module NBS connections and total number of NBS connections. This analysis was performed on the EEG-MRI-DTI subsample.

6.3.5. Subcortical alterations vs functional connectivity

Volume (V) differences between groups for both thalamus and NBM were tested with Wilks' Lambda multivariate test ($p < 0.05$), followed by post hoc analysis of covariate (ANCOVA) tests ($p < 0.05$); thalamus differences were tested in both directions (two-tails, $V_{VH} \lesseqgtr V_{NVH}$), whilst NBM was hypothesised to show higher degeneration in VH (one-tail, $V_{VH} < V_{NVH}$), based on previous evidence and speculations related to the role of cholinergic system dysfunction in VH, as discussed in section 1.2.1 (Ballard *et al.*, 2000; Harding *et al.*, 2002; Diederich *et al.*, 2005; Shine *et al.*, 2011; Shine *et al.*, 2014; Hepp *et al.*, 2017a; Onofrj *et al.*, 2019; Sakai *et al.*,

2019). Spearman rank correlation tests ($p < 0.05$) were performed between volume values of each subcortical region and $WPLI_{NBS}$ for both groups. This analysis was performed on the EEG-MRI subsample.

6.3.6. Probabilistic tractography and correlation with EEG

Tractography pipeline was implemented with the FMRIB's Diffusion Toolbox (Jenkinson *et al.*, 2012) and described in detail in section 5.3.6. Briefly, DTI recordings were first corrected for eddy current distortion, movement and motion-induced signal dropout using the eddy package (Andersson *et al.*, 2016; Andersson and Sotiropoulos, 2016). Local probability distribution of fibre direction was then assessed at each voxel with automatic detection of number of fibres per voxel (Behrens *et al.*, 2003a; Behrens *et al.*, 2007). Probabilistic tractography algorithm (Behrens *et al.*, 2003a; Behrens *et al.*, 2007) was eventually used to track white matter fibres connecting functionally affected cortical regions, thalamus and NBM. Probability between voxels was estimated as proportion of connecting fibres, over 5000 sampled fibres per voxels. The outcome of tractography was a structural connectivity matrix of dimension n+2 (seed masks) x n+2 (target masks), where n was the number of cortical regions detected with NBS. Each connectivity matrix **S** was symmetrised by replacing each $s_{i,j}$ element with an average between itself and $s_{j,I}$ (Cabral *et al.*, 2011).

NBM (Ch4 cellular group) ROI in the MNI space was generated with the SPM Anatomy Toolbox for MATLAB (Eickhoff *et al.*, 2005), whilst thalamus MNI ROI was selected from the Harvard-Oxford subcortical atlas included in the FMRIB Software Library (Jenkinson *et al.*, 2012). Subcortical ROIs were transformed to the subject space using affine and non-linear transformations as implemented in the ANTs software (Avants *et al.*, 2009). Cortical ROIs were defined as nodes detected from NBS, i.e. being part of a functionally affected network component. Corresponding volume masks were selected from the Destrieux parcellation among the regions shown in Figure 4.1. Before performing tractography, ROI masks were transformed from subject space to the diffusion space. To this purpose, a linear transformation matrix for each subject was generated with the FLIRT package (Jenkinson *et al.*, 2002) using as origin and target respectively a FA map and brain-extracted T1 MRI image. Subcortical ROIs as defined in the MNI space are shown in Figure 5.1**.**

Integrity of white matter fibres within the cortex, in cortex-NBM, cortex-thalamus, and NBM-thalamus tracts was compared between VH and NVH, by testing whether or not the number of fibres was lower in VH compared to NVH in each tract of interest (Mann-Whitney U test, one-tailed, $p < 0.05$). Association between white matter degeneration and altered EEG source network was also investigated. Spearman rank correlation tests ($p < 0.05$, one-tailed) were performed between EEG features, i.e. $WPLI_{NBS}$ (right-tailed) and Q_w (left-tailed), and average structural connectivity between cortical (NBS-detected) regions, number of NBM-thalamus WM fibres, and total number of WM fibres connecting cortical regions to respectively thalamus and NBM, for both VH and NVH groups.

This analysis was performed on the EEG-MRI-DTI subsample.

6.4. Results

6.4.1. Demographic data

Demographic information and clinical score comparison between groups are reported in Table 6.1 and Table 6.2. Groups were matched for age and diagnosis, however matching for gender was not achievable due to sample availability. Results could not be corrected for gender, as the number of female subjects was too low. Since there is no evidence in literature of gender effect on VH-related pathological and functional processes, it was assumed that results were not significantly affected by gender imbalance. A trend towards significance was found for MMSE, hence NBS test and subcortical volume comparisons were corrected for MMSE score to exclude any cognitive deficit effect. The majority of participants were on cholinergic medication and one NVH patient was on memantine, and distribution across groups was not significantly different. Daily intake of levodopa was not different between groups.

6.4.2. Topographical differences

Results of NBS analysis are shown in Figure 6.2. Comparison between groups yielded one significant component comprising 18 nodes and 18 edges ($p = 0.031$), which included areas belonging to occipital cortex, left and right IT, and PFC. Comparison of $WPLI_{NBS}$ and average

K_W between groups showed that NBS component consisted of weaker connectivity pattern in VH compared to NVH (Figure 6.3). Affected subnetwork included:

- connectivity between the right cuneus and both the right inferior occipito-temporal lobe and the right primary auditory cortex
- connections between the left orbitofrontal cortex and right IT, right cingulate, superior part of right PFC and left parieto-occipital region
- inter-hemispheric connections between temporal lobes
- connectivity between left occipital cortex and right cingulate.
- connections between left insula and right occipito-temporal areas.

Multivariate test for node strength comparison yielded p = 0.032, hence individual nodes differences were tested. 11 out of 18 node strengths were significantly different in VH compared to NVH, as highlighted in Figure 6.2**; i**ndividual nodes values were all lower in VH compared to NVH, as shown in Figure 6.4, but only right cuneus' strength comparison test survived Holm-Bonferroni correction (p = 0.0015).

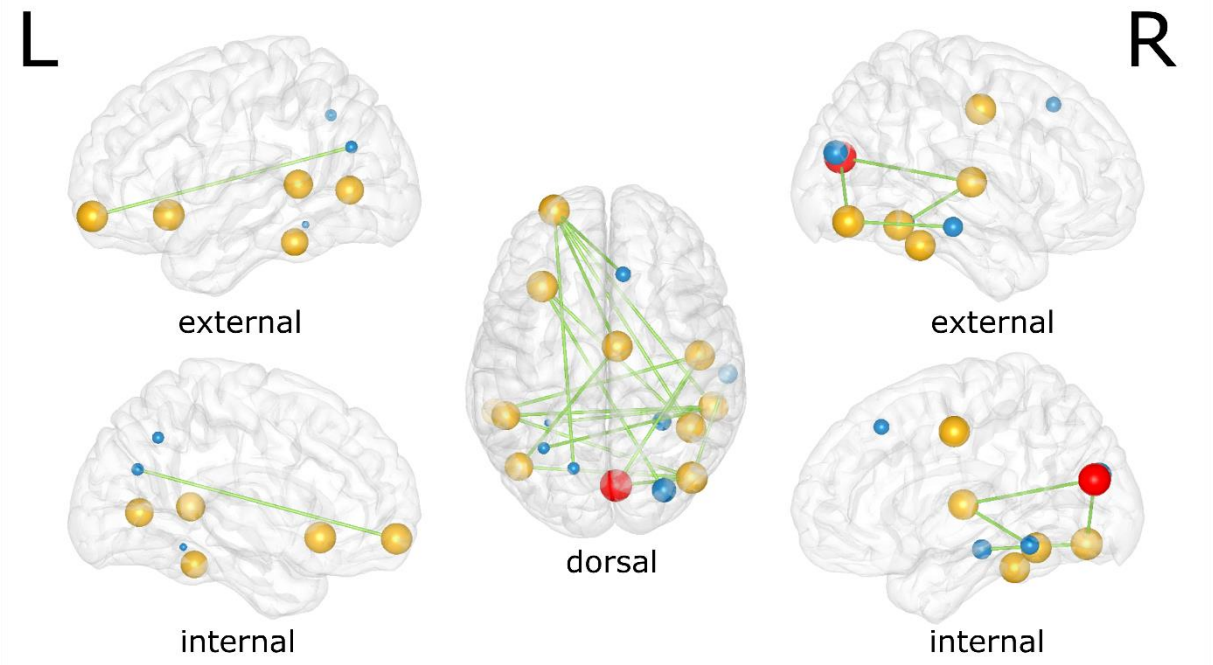

Figure 6.2 – NBS test outcome: VH vs NVH. Green lines represent network pattern affected in VH compared to NVH; these include interhemispheric connectivity, as well as occipital-temporal-frontal projections. Yellow nodes had lower strength in VH compared to NVH; red nodes, i.e. only right cuneus, survived multiple comparison correction. Node sizes are inversely proportional to respective p-values.

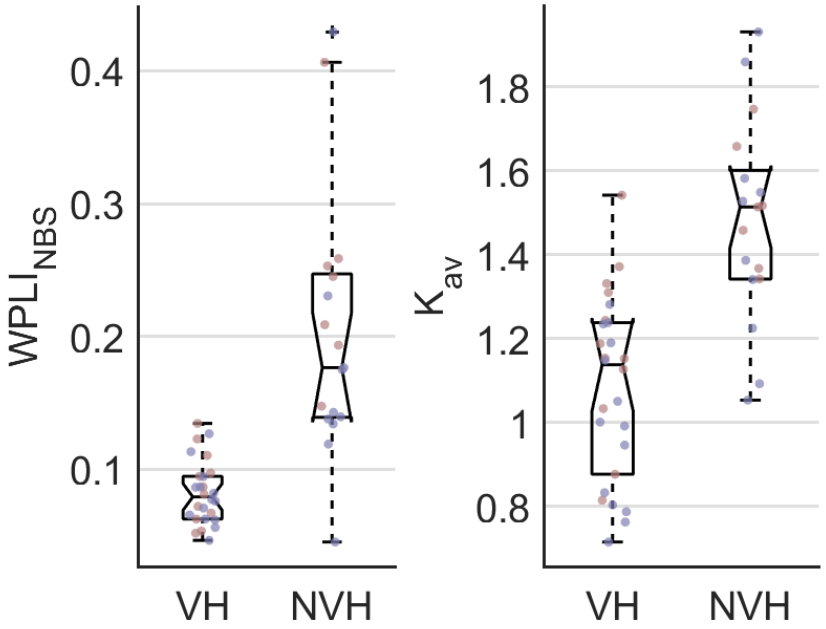

Figure 6.3 – Average connectivity and node strength within the NBS component: VH vs NVH. Functional source connectivity is weakened in VH compared to NVH. Red dots: DLB; blue dots: PDD.

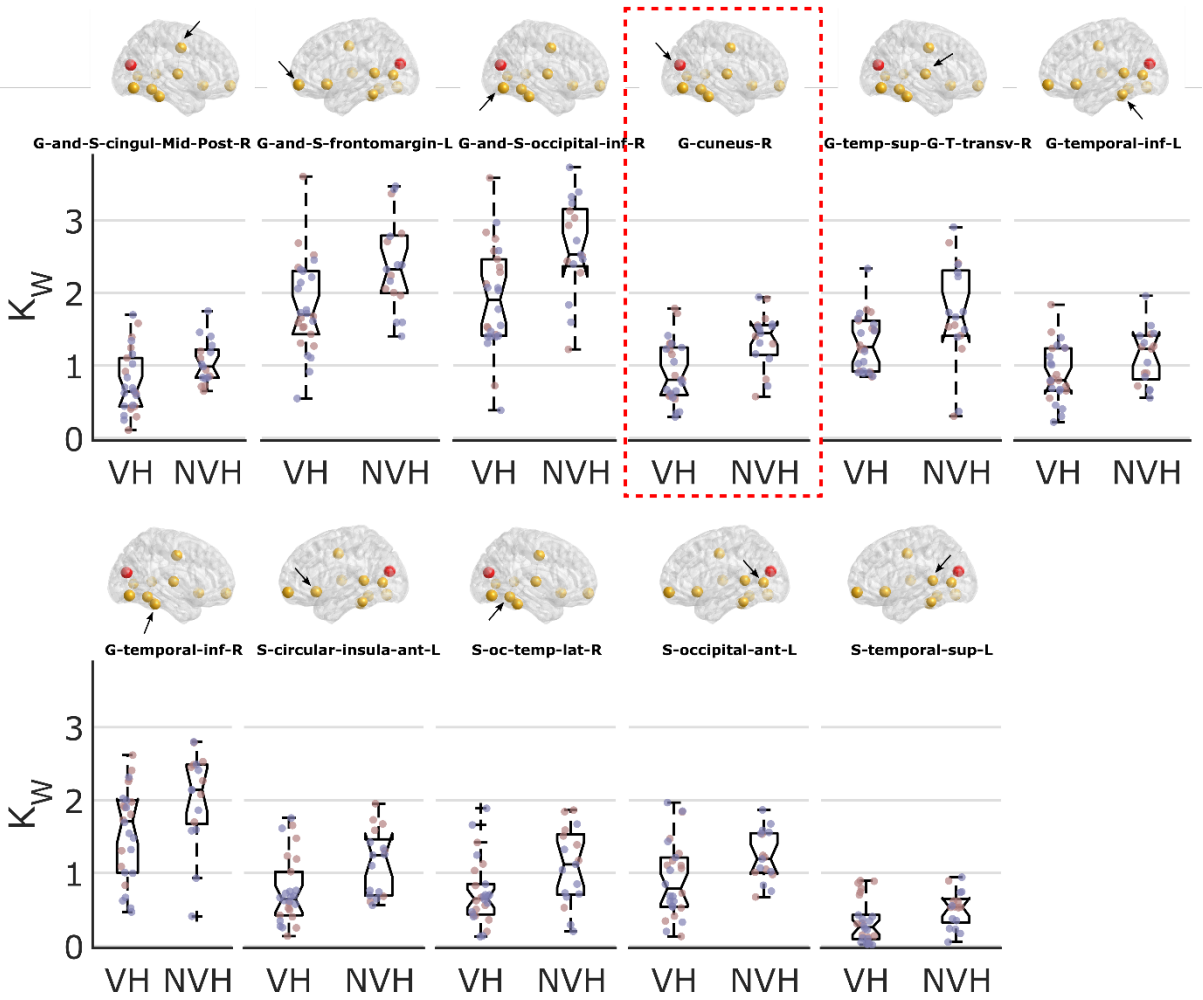

Figure 6.4 – Individual node strength distributions for significantly affected nodes. 11 out of 18 nodes were significantly weaker in VH compared to NVH, but only the right cuneus (highlighted in red) survived multiple comparison correction. L: left; R: right; G: gyrus; S: sulcus. Red dots: DLB; blue dots: PDD.

Modular distribution in VH and NVH networks is shown in Figure 6.5. The consensus matrix included four modules in VH, one including right and central frontal regions and right temporal pole, one comprising left frontal and temporal pole regions, and the other two mainly comprising respectively the left and the right temporal-parietal-occipital cortices. NVH modular organisation comprised three major modules over the left hemisphere, the right prefrontal region, and the right temporal-parietal-occipital areas; two further modules emerged which comprised respectively three nodes within the left temporal lobe and two nodes over the right temporal and prefrontal cortex.

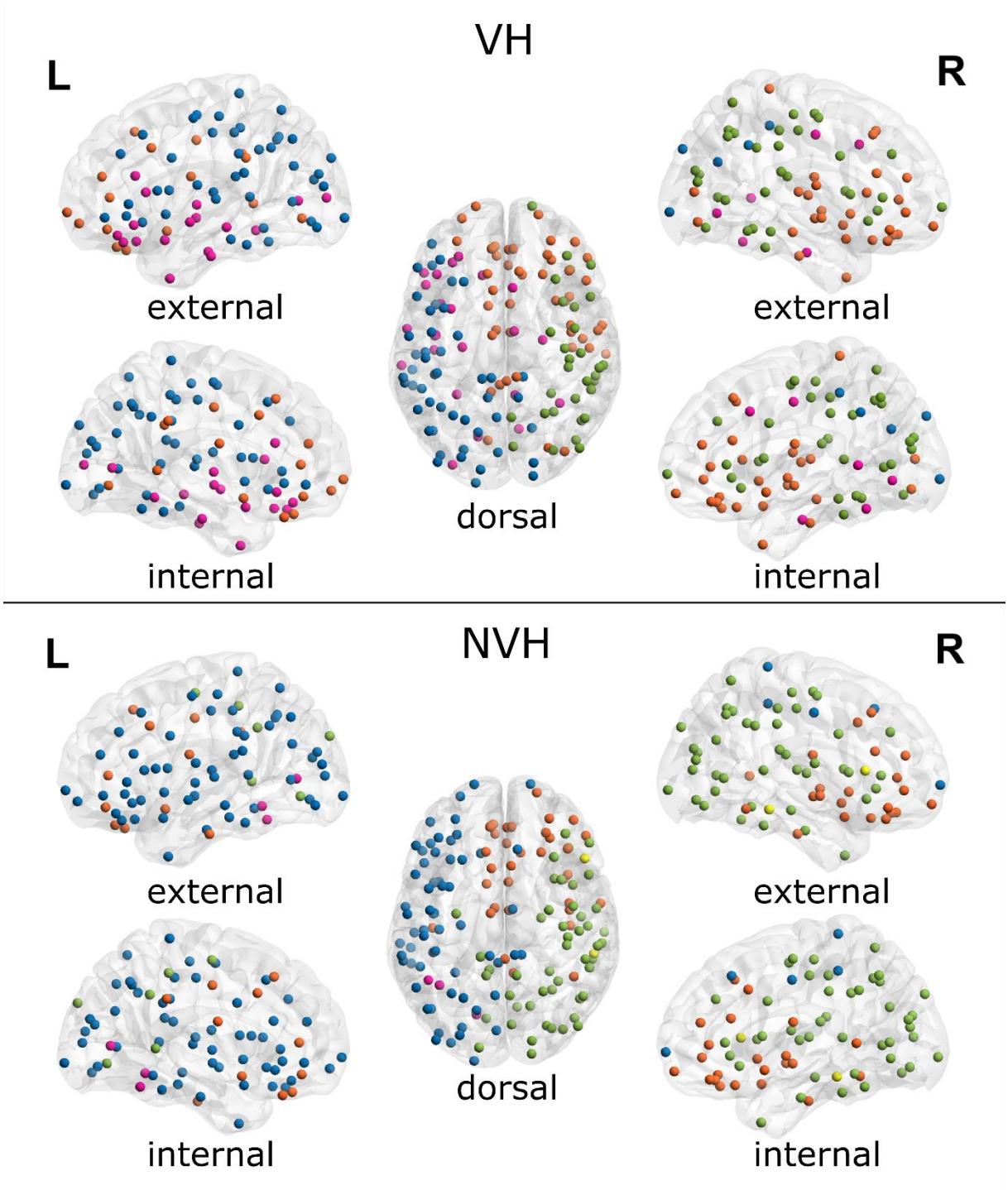

Figure 6.5 – Modular distributions. Top: VH, four modules; bottom: NVH, five modules. Nodes marked with the same colour belong to the same module. Despite two further minor modules in NVH compared to VH, VH shows an additional major module compared to NVH, associated with disruption of left hemisphere modular distribution in VH.

In the EEG-MRI-DTI subsample, NBS analysis reproduced the same alteration pattern as detected in the larger subsample. Specifically, one differential component was detected comprising 18 nodes and 17 edges ($p = 0.038$). Topographical distribution of NBS edges across

modules is shown in Figure 6.6. In the NVH group, 29.41% of NBS edges were connecting nodes belonging to the same module, whilst in VH, i.e. the group in which connections detected with NBS were more affected, that was the case for only 11.76%. This resulted in 17.65% NBS connections being associated with a higher modular disruption in VH. Edges associated with modular disruption in VH include frontal-posterior projections as well as occipital-temporal connectivity.

Distribution within groups of average connectivity of NBS component ($WPLI_{NBS}$) and Q_W values are shown in Figure 6.7. As already found with the larger subsample, $WPLI_{NBS}$ was lower in VH compared to NVH. Q_w was significantly higher in VH compared with NVH ($p = 0.02$).

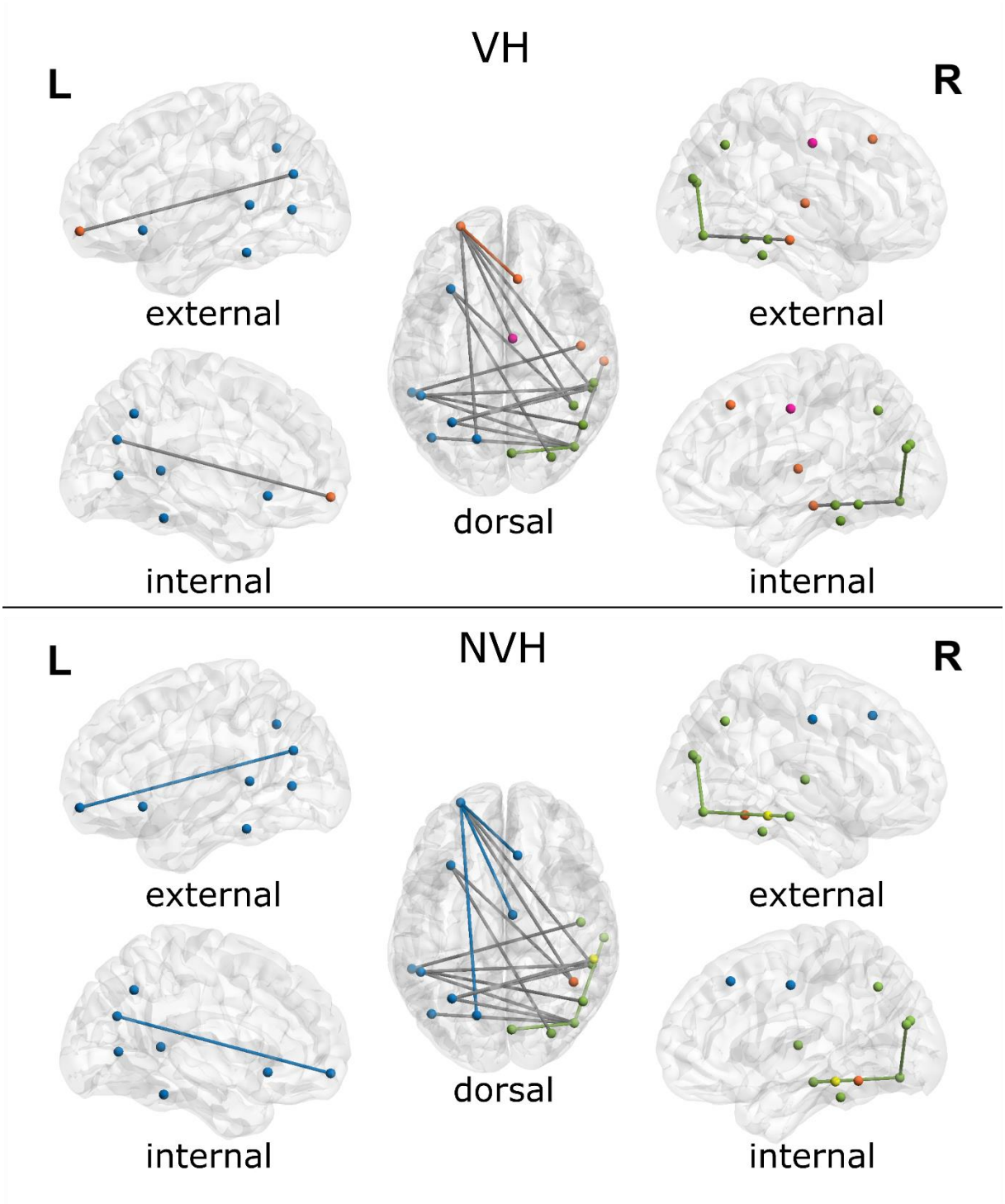

Figure 6.6 - Modular distribution of NBS component. Top: VH group, 11.76% within-module edges; bottom: NVH group, 29.41% within-module edges. Within-module edges are marked with the same colour as the module the connected nodes are part of, based on Figure 6.5. Between-module edges are marked in grey.

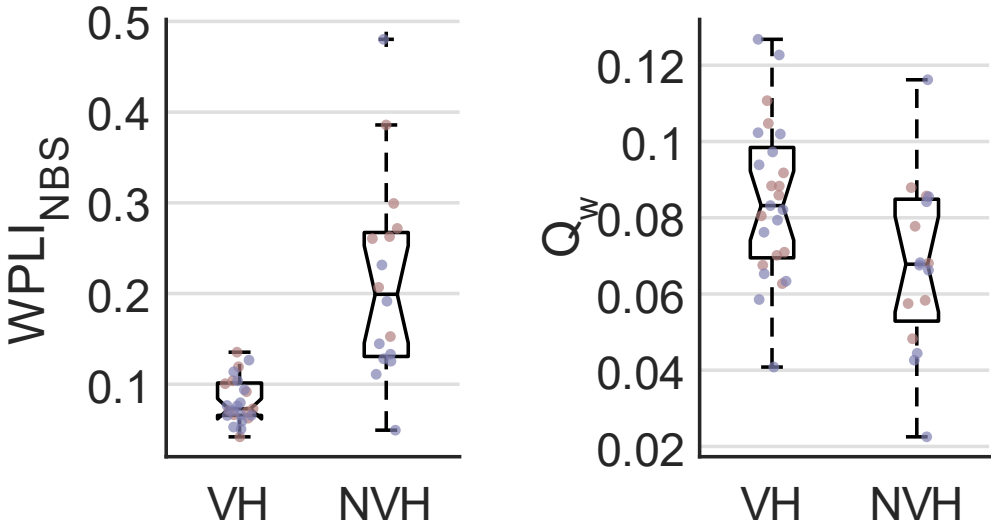

Figure 6.7 – $WPLI_{NBS}$ and modularity (Q_W) distributions in VH and NVH. Both measures are significantly more affected in VH compared with NVH.

6.4.3. Cortical thickness alterations in functionally affected regions

To compare CTh values between groups, nodes corresponding to occipital cortex, IT or PFC were selected among the 11 nodes which showed significantly reduced functional strength in VH compared to NVH. This resulted in selecting seven regions, which comprised left frontomarginal sulcus and gyrus, right inferior- and occipito-temporal lobes, right inferior occipital lobe, right cuneus, left occipital anterior lobe, and left inferior temporal lobe.

Multivariate test proved significant ($p = 0.009$), and among tested regions only the right cuneus showed differential thickness between groups ($p = 0.004$), being lower in NVH compared to VH, as shown in Figure 6.8. Correlation test between cuneus node strength and cortical thickness did not produce any significant result.

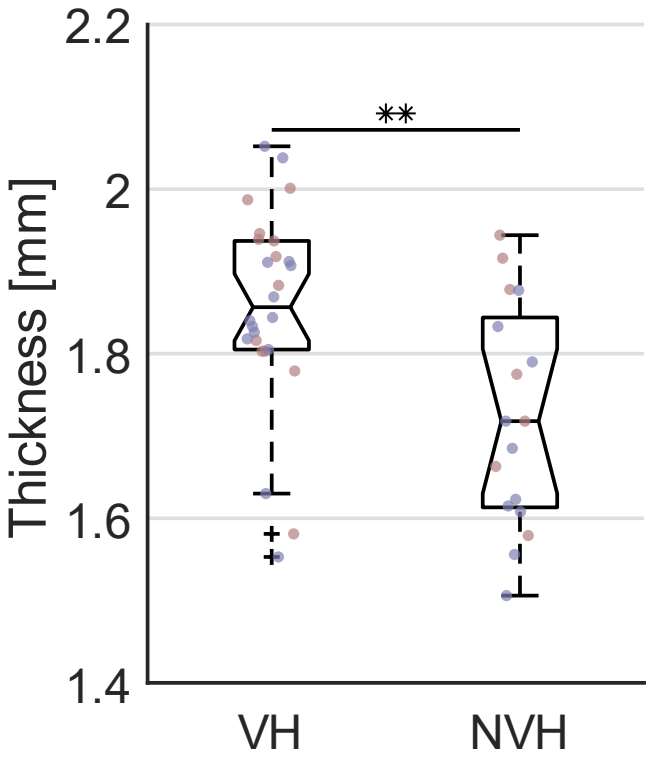

Figure 6.8 – Cortical thickness of right cuneus: comparison between VH and NVH. Cuneus was thinner in NVH group. Red dots: DLB; blue dots: PDD. ** Mann-Whitney U test survived Holm-Bonferroni correction (seven tests).

6.4.4. Thalamus and NBM volumes vs functional connectivity

Multivariate test corrected for MMSE yielded significant result (p = 0.002), and both thalamus and NBM showed a higher degeneration in VH compared to NVH as revealed with ANCOVA tests with MMSE as covariate (post hoc tests yielded respectively p = 0.001 and p = 0.0375). No significant correlation was found between subcortical volumes and $WPLI_{NBS}$ in any of the groups. Distribution of volume values across subjects is shown in Figure 6.9**.**

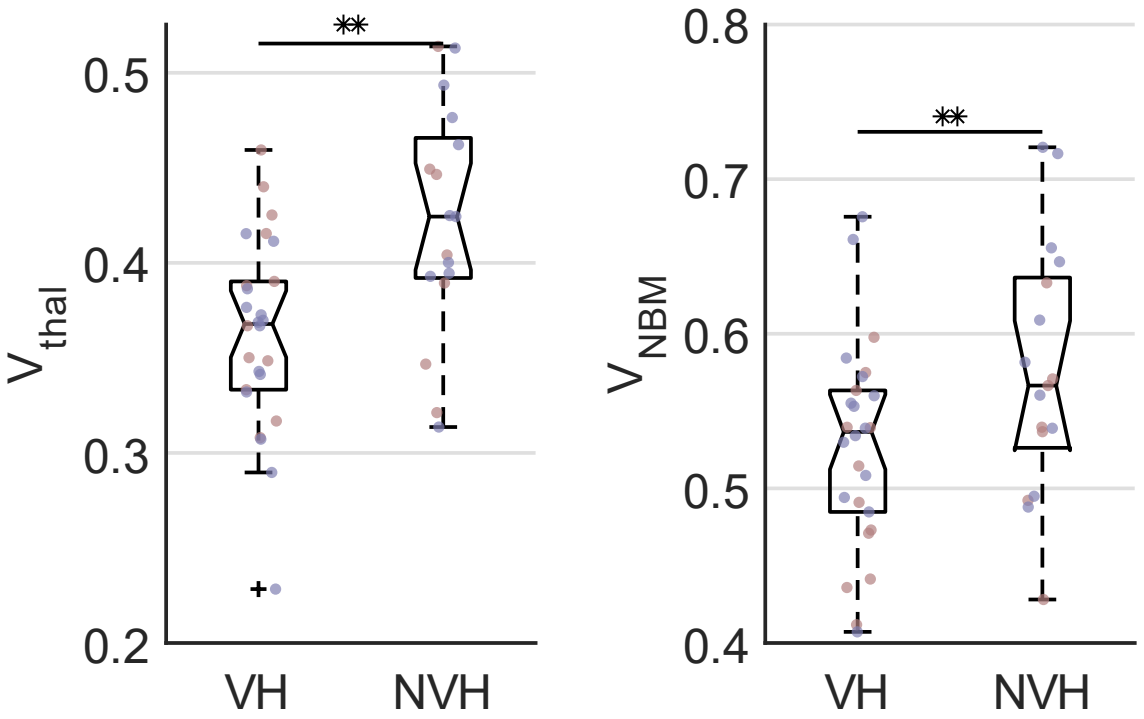

Figure 6.9 – Thalamus (left) and NBM (right) volumes. Both structures showed higher degeneration in VH compared to NVH. Red dots: DLB; blue dots: PDD. ** Mann-Whitney U test survives Holm-Bonferroni correction (2 tests).

6.4.5. Structural vs functional connectivity: outcome of correlation analysis

Comparison of the number of white matter (WM) fibres between groups produced significant outcome for NBM-cortex tract, but not for NBM-thalamus, thalamus-cortex or within cortex. Specifically, the number of fibres projected from the NBM towards functionally affected cortical regions was significantly lower in VH compared to NVH, as shown in Figure 6.10 ($p = 0.023$). In addition, significant correlation was found between average structural connectivity in the same WM tract and $WPLI_{NBS}$ values in VH and NVH as a whole group ($\rho = 0.34$, $p = 0.014$), and it was marked within NVH group ($\rho = 0.60$, $p = 0.008$), but no correlation emerged within the VH group ($\rho = -0.07$, $p = 0.636$). A trend towards significance was also found between $WPLI_{NBS}$ and WM fibres in the thalamus-cortex tract ($\rho = 0.29$, $p = 0.077$). Significant correlation emerged also between Q_W and structural connectivity between thalamus and NBM for NVH group ($\rho = -0.49$, $p = 0.027$, and only a trend towards significance for VH ($\rho = -0.30$, $p = 0.072$). WM-$WPLI_{NBS}$ and WM-Q_w trends are shown in Figure 6.10.

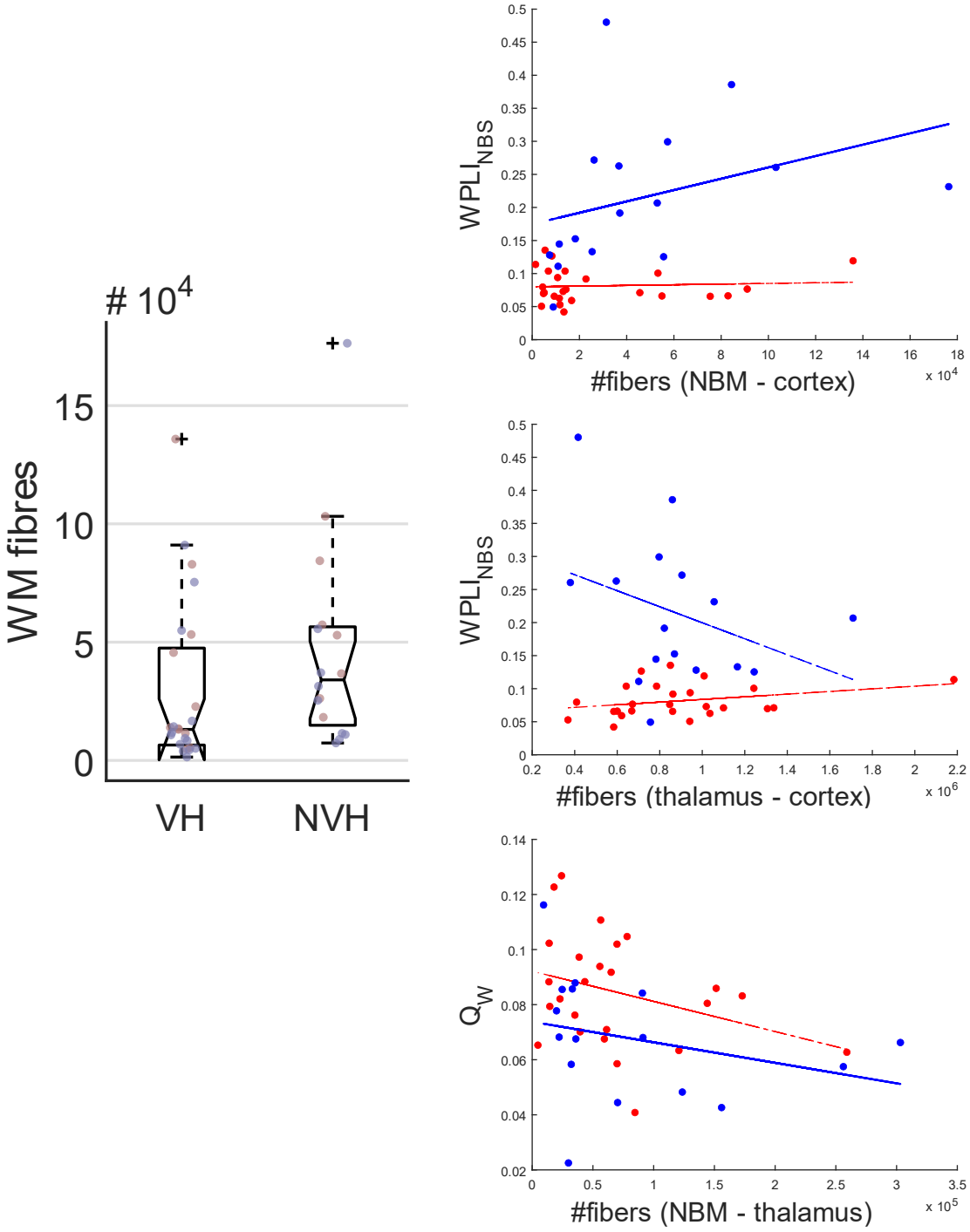

Figure 6.10 – Number of white matter fibres within NBM-cortex tract (left) and structural vs functional connectivity: linear fitting for VH and NVH (right). Left panel: cortical targets are regions which were functionally weakened as detected with NBS; red dots: DLB; blue dots: PDD. Right panel: significant correlation emerges from Spearman rank test between NBM-cortex structural connectivity and $WPLI_{NBS}$ in NVH (ρ = 0.60), and between NBM-thalamus structural connectivity and Q_w in NVH (ρ = -0.49); a trend towards significance was found for $WPLI_{NBS}$ vs thalamus-cortex connectivity (ρ = 0.29) and between Q_w and NBM-thalamus connectivity (ρ = -0.30) in the VH group; thicker line represents significant correlation trend; blue: NVH; red: VH.

6.5. Discussion

The scope of the present chapter was to investigate EEG source network abnormalities at resting state and their correlation with structural features associated with VH clinical condition in Lewy body dementias (LBD), i.e. dementia with Lewy bodies (DLB) and Parkinson's disease dementia (PDD). In line with existing models, areas belonging to visual networks were hypothesised to show altered properties in VH group compared to NVH. Furthermore, it was explored whether VH condition is associated with modular distribution alterations in the functional EEG network. Structural connectivity between functionally affected cortical regions and subcortical regions was also extracted and correlated with functional connectivity measures. This latter analysis was aimed to provide direct evidence of cholinergic involvement in VH-related functional network abnormalities, as speculated in previous studies (Ballard *et al.*, 2000; Harding *et al.*, 2002; Diederich *et al.*, 2005; Shine *et al.*, 2011; Shine *et al.*, 2014; Onofrj *et al.*, 2019).

The NBS analysis detected one differential network component consisting of topographical patterns within the visual ventral network, i.e. occipital cortex, IT and PFC. The most functionally disconnected region within the NBS component in VH was the right cuneus, which paradoxically showed more thinning in NVH group compared to VH. Both thalamus and basal forebrain showed major degeneration in VH, concurring with the idea of cholinergic disruption associated with VH. However, no direct association was found between EEG connectivity and subcortical volumes. As expected, modular distribution was altered in VH, leading to higher network segregation. Specifically, one additional relevant module emerged in VH compared to NVH, and modularity measure was significantly higher in VH. Affected network pattern was also differentially distributed between groups, with 17.65% NBS connections being topographically associated with modular distribution changes between groups. Tractography analysis yielded significantly lower connectivity between NBM and functionally affected cortical regions in VH compared to NVH. Moreover, structural connectivity strength within the same tract was associated with functional cortical connectivity strength in NVH, but not in VH.

The majority of patients in this study were taking cholinesterase inhibitors. As mentioned in section 1.4.2, this likely partially restored EEG activity and network properties towards normative values (Agnoli *et al.*, 1983; Balkan *et al.*, 2003) in the VH group making group differences less distinct. Nevertheless, significant alterations across patient groups emerged.

On the other hand, cholinergic medication might be argued to be the actual cause of absence of visual hallucinations in the NVH group. To exclude this possibility, clinical history of those patients was previously checked, and no record of visual hallucination prior to medication was reported.

6.5.1. The visual ventral network is disconnected in LBD with VH

As detected with NBS, connectivity between occipital cortex, IT and PFC was reduced in VH compared to NVH. Interestingly, the obtained differential topography nicely fits with the PAD model (Collerton *et al.*, 2005) and the computational model by Tsukada *et al.* (2015), according to which VH in LBD are due to a mismatch between top-down, i.e. PFC to IT, and bottom-up streams, i.e. occipital to IT, as described in section 1.2.2. Notably, connectivity with the cuneus was strikingly reduced in VH, in line with reported lower GABA level (Firbank *et al.*, 2018) and glucose metabolism (Pasquier *et al.*, 2002; Perneczky *et al.*, 2008; Gasca-Salas *et al.*, 2016) over the occipital lobe, associated with VH. In fact, cortical electrical activity generation is due to energy consumption by neuron membranes, associated with oxidative metabolism (Ingvar *et al.*, 1979). Hence, EEG activity depends on cerebral metabolism, and abnormal features in this latter are expected to reflect into the first. This seems to be the case in the present analysis and in other studies with PET/EEG combined modality involving clinical conditions which included depression, vascular dementia and AD (Buchan *et al.*, 1997; Larson *et al.*, 1998; Szelies *et al.*, 1999; Dierks *et al.*, 2000; Pizzagalli *et al.*, 2003). From the network perspective, cuneus functional alteration in VH might propagate along the visual ventral network and affect the inferior temporal lobe, whose functional strength also was significantly reduced ($p < 0.05$), although not surviving multiple comparison correction. Frontal projections towards the IT were also affected; these may likely be reflecting dysfunction of top-down visual stream as predicted by the models (Collerton *et al.*, 2005; Tsukada *et al.*, 2015). Specifically, affected connectivity patterns involved the cortical region including the frontomarginal sulcus and gyrus. According to the implemented parcellation, the region is in the inferior part of the frontal pole, continuous to the orbital gyrus (Destrieux *et al.*, 2010), limiting the frontopolar and orbital regions (Luders, 2008). The orbitofrontal cortex is reportedly engaged within the top-down stream; according to the existing visual perception models, a rough version of visual information (Bar, 2003) is projected from the occipital cortex through either dorsal visual

network (Livingstone and Hubel, 1987) or the thalamus (Morris *et al.*, 1999) towards PFC, and OFC activates depending on whether such stimulus can be associated with any information stored in memory, and generates a predictive template (Chaumon *et al.*, 2014). This process rapidly takes place before any visual stimuli is processed through high level visual cortices to reach IT (Bar *et al.*, 2006), where matching between sensory bottom-up and predictive top-down streams takes place, generating an internal image (Bar, 2003; Kveraga *et al.*, 2007). Activation of the frontal areas involved in visual perception mechanism was also reported in another fMRI study, where authors used dynamic casual modelling (DCM) and successfully simulated association between face recognition, activation of frontal areas and effective information flow along the visual ventral network (Summerfield *et al.*, 2006). The present findings may be considered as empirical validation of the implemented models, suggesting that in LBD with VH the information flow stream is also affected at resting-state, being possibly associated with erroneous matching between bottom-up and top-down visual perception streams in the IT.

Notably, reduced interhemispheric connectivity also emerged in the NBS component. Association between reduced interhemispheric connectivity and auditory hallucinations was reported for schizophrenia (Chang *et al.*, 2015; Wigand *et al.*, 2015; Lang *et al.*, 2016), however no study to date reported similar differential topographical patterns in LBD-VH. An EEG study by Mima *et al.* (2001) showed that temporally early coherence between the left and the right occipitotemporal areas is positively correlated with successful object recognition, whilst no significant connectivity enhancement emerged when participants observed meaningless objects. Authors suggested that interhemispheric information flow in visual perception is likely "the first gate of an active attention system" (Mima *et al.*, 2001). In the context of this finding, the NBS topography clearly reproduce such interhemispheric patterns between occipitotemporal areas, suggesting impairment of early functional processes associated with active perception in VH, which already emerges in resting-state.

Moreover, differential topography showed lateralisation towards the right hemisphere. Right cuneus was significantly weakened in VH, whilst no connections from/towards left cuneus were affected, and three different regions within the right IT were affected, against only one within left IT. This result resonates with evidence in literature showing that the right hemisphere pathological features in PD, i.e. left-sided symptoms, are likely associated with

visuo-spatial features, whilst verbal deficits are associated with the left hemisphere (Blonder *et al.*, 1989; Lee *et al.*, 2001; Harris *et al.*, 2003). In fact, perceptual deficits tend to be associated with right hemisphere damage; this has been suggested to be due to different efficiency of the two hemispheres, the right one being mostly involved in processing low-frequency information (Robertson and Ivry, 2000), as it is the one transferred within the top-down stream. From a pathological perspective, reduced node strength within the IT regions might be associated with higher burden of LBs within this region associated with VH, as found by Harding *et al.* (2002).

Interestingly, connectivity between right cuneus and primary auditory cortex was also affected. Although auditory hallucinations are not typical features in LBD, they may emerge among the symptomatic spectrum and are mostly associated with VH (Inzelberg *et al.*, 1998; Ballard *et al.*, 2001b; Tsunoda *et al.*, 2018). However, this aspect is beyond the scope of the present thesis, and future studies will be needed to explore brain network features associated with auditory hallucinations.

6.5.2. Interaction between VAN, DMN and visual network is weakened in VH

Connectivity between visual areas and the middle-posterior cingulate cortex, anterior insula and temporal superior sulcus was shown to be weakened in VH. According to previous research, the posterior part of the cingulate cortex is part of the DMN (Raichle, 2015), whilst anterior insula and temporal superior sulcus, this latter connected to the temporoparietal junction (Krall *et al.*, 2015), belong to the VAN (Vossel *et al.*, 2014; Jimenez *et al.*, 2016). NBS differential component shows that connectivity between areas belonging to the ventral visual network and VAN or DMN areas is reduced in VH, but no alteration emerged in connectivity within or between VAN and DMN. This result may partially contrast the model by Shine *et al.* (2011) according to which overactivation of DMN and VAN causes faulty engagement of DAN and image misperception, as described in section 1.2.2. On the other hand, the approach pursued in the present study may suggest that predicted faulty interaction between attentional and default networks in LBD-VH is mediated by the visual streams, rather than reduced direct connectivity between attentional cortical regions. Unaltered connectivity between attentional networks in VH also appears to contrast with previous studies, where

reduced functional connectivity between attentional networks or higher DMN activation were associated with VH condition (Shine *et al.*, 2014; Yao *et al.*, 2014; Franciotti *et al.*, 2015). This apparent contrast may be due to a different methodological approach having been used. In those studies, functional connectivity analysis was based on hypothesis-based ROIs selection, whilst in the present study affected connectivity patterns emerged from NBS, which is a data driven statistical method (Zalesky *et al.*, 2010) (see section 2.5 for details on its implementation). This leads to speculation that although interaction between attentional and default mode networks and within network connectivity may be altered in VH compared to NVH, such alteration may not be as prominent as the affected interaction between regions within the visual streams, which are more directly involved in visual information processing; hence, altered attentional network patterns in awake resting-state condition would not emerge with the present strategy. An alternative explanation to this contrasting outcome may possibly rely on the condition of interest, i.e. PD in Shine and colleagues' work and PDD+DLB in the present chapter. However, pathological similarities between PD/D and DLB (McKeith, 2007b) and focus in both works on VH symptom regardless of the clinical condition make this scenario less plausible. Reduced functional connectivity with the anterior insula and middle-posterior cingulate cortex is also consistent with previous research showing that GM over anterior insula and hypometabolism over the middle cingulate correlate with the intensity of visual hallucinations in AD and AD-LB mixed pathology condition (Blanc *et al.*, 2014).

6.5.3. Functional network is more segregated in VH compared to NVH

Similar to what was found for DLB versus AD in Chapter 5, LBD patients with VH showed higher functional brain modularity compared to NVH. Although the number of modules was higher in NVH, numerosity was driven by two minor modules comprising respectively three and two nodes (respectively the purple and yellow modules in Figure 6.5). In fact, VH network showed significant modular disruption over the left hemisphere, which comprised two respectively frontal and parieto-occipital modules in VH against one only module in NVH, and featured modular redistribution within central-frontal regions. Disruption of left hemisphere module was also associated with connectivity reduction between PFC and occipital and cingulate cortices as detected with NBS.

To the best of author's knowledge, the present analysis, for the first time, provides evidence of functional network segregation associated with VH in LBD. Modular network organisation has been shown to be crucial for visual perception processing, as different functional mechanisms are allocated to different brain areas (Treisman and Kanwisher, 1998; Zeki and Bartels, 1998; Borowsky *et al.*, 2005) as also described in computational models (Bar, 2003; Bar *et al.*, 2006; Chaumon *et al.*, 2009; Gamond *et al.*, 2011; Chaumon *et al.*, 2014; O'Callaghan *et al.*, 2017). Physiological modular properties of the network are likely disrupted in VH, possibly due to connectivity reduction, as detected in the present study. Specifically, decoupling of areas belonging to certain modules may take place in VH, leading to a higher number of modules. In addition, propensity of the network to organise in modules, i.e. higher modularity, emerges more strongly in VH compared with NVH, possibly due to impairment of long-range connections in VH, as proposed for DLB against AD in section 5.5.1 (Peraza *et al.*, 2018). Based on this hypothesis and differential topographies obtained with NBS and shown in Figure 6.2, affected top-down projections might potentially be driving network segregation in VH. Overall, this analysis shows that visual-related functional subnetwork is a significant factor to effectively assess DLB and PDD network properties, which should not be ignored when analysing functional alterations associated with LB pathology.

6.5.4. Occipital cortex shows higher atrophy in NVH compared to VH

Among visual ventral network nodes which showed lower strength in VH, only the cuneus showed differential CTh between groups. Specifically, CTh was higher in VH compared to NVH, and no significant correlation emerged in any of the groups between cuneus CTh values and functional node strength. As discussed in section 6.5.1, functional alteration within the cuneus are reportedly associated with VH, as also found in the present chapter. Functional brain features are generally associated with respective structural properties, as extensively reported in the literature and discussed in Chapter 1 (Guye *et al.*, 2003; Greicius *et al.*, 2008; Bullmore and Sporns, 2009; Damoiseaux and Greicius, 2009; Honey *et al.*, 2009; Deco and Jirsa, 2012; Stam *et al.*, 2016). Therefore, abnormalities in one would be expected to reflect in the other; however, this seems not to be the case based on the outcome of CTh analysis. Although it would be tempting to interpret cortical thickness preservation as a permissive state of VH generation in LBD, an attempt should be made to discuss this result from the

pathological perspective. As described in section 1.1, cortical atrophy within the medial-temporal lobe is a well reported differential feature in AD against Lewy body pathology associated conditions (Barber *et al.*, 2000b; Burton *et al.*, 2009; Blanc *et al.*, 2015). In the previous chapter, it has been proposed that part of the DLB cohort might include AD-LB mixed pathology cases, which would likely not feature VH (Tiraboschi *et al.*, 2006; Jicha *et al.*, 2010; Toledo *et al.*, 2013; Yoshizawa *et al.*, 2013). Although AD was not reported to show significant cortical thinning over posterior areas, it is possible that mixed pathology cases feature such further structural alteration, possibly associated with attentional rather than visual perception impairment. To test this hypothesis, CTh of right cuneus was computed for HC and AD participants included in the previous chapter. For this analysis, one AD subject was excluded due to cortical segmentation issues which yielded outlying CTh values. This resulted in including structural data from 18 HC and 25 AD. CTh differential patterns between groups were tested with Mann-Whitney U tests ($p < 0.05$, Holm-Bonferroni correction, six tests) based on hypotheses of interest, i.e.: $\mathrm{HC} > \mathrm{AD}$ (one-tailed), $\mathrm{HC} \gtrless \mathrm{VH}$ (two-tailed), $\mathrm{HC} > \mathrm{NVH}$ (one-tailed), $\mathrm{AD} < \mathrm{VH}$ (one-tailed), $\mathrm{AD} \gtrless \mathrm{NVH}$ (two-tailed), $\mathrm{VH} > \mathrm{NVH}$ (one-tailed). As shown in Figure 6.11, cuneus CTh in AD and NVH were significantly lower than VH, and thickness values distributions were not significantly different between AD and NVH. As expected, AD thickness was not significantly lower compared to HC (O'Donovan *et al.*, 2013), whilst a trend towards significance emerged for NVH compared to HC. This outcome provides an evidence of cuneus cortical alteration likely associated with AD-LB mixed pathology, whilst cuneus degeneration seems not featured in pure LBD condition, i.e. patients with VH. This idea also concurs with a previous study assessing more severe cortical atrophy associated with mixed pathology as compared with pure pathology condition (van der Zande *et al.*, 2018), as well as posterior cortical atrophy associated with the “visual dementia” variant of AD (Benson *et al.*, 1988; Crutch *et al.*, 2017).

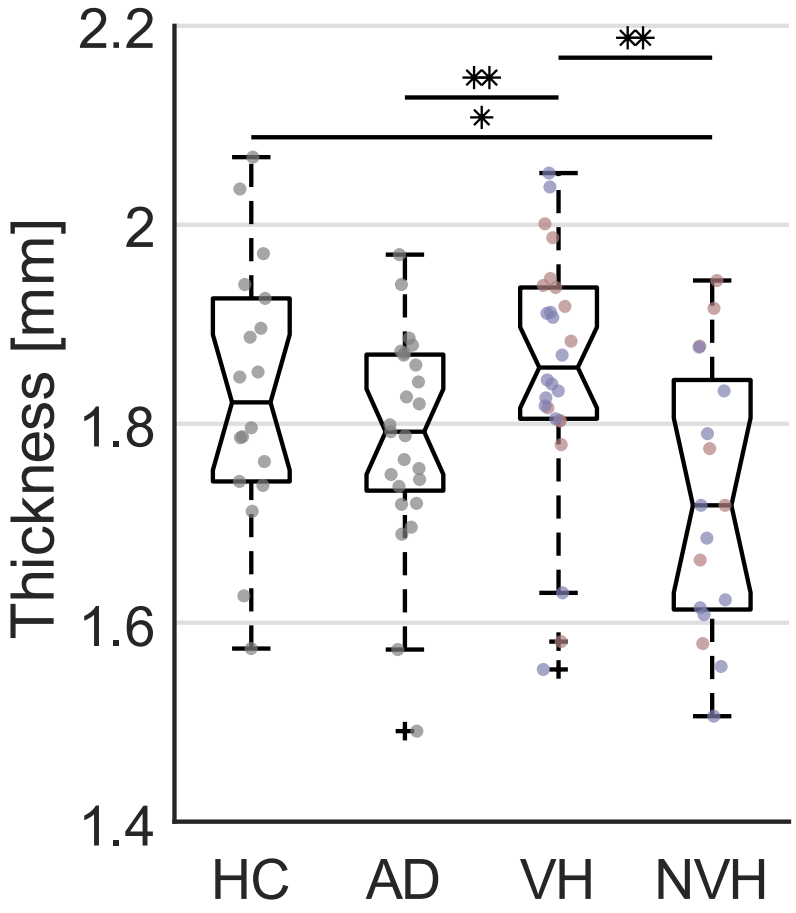

Figure 6.11 – Cuneus cortical thickness, comparison between LBD (VH and NVH), AD and HC. CTh values were not lower in NVH compared to AD, and both groups had reduced CTh compared to VH. Red dots: DLB; blue dots: PDD. * Significant Mann-Whitney U test ($p < 0.05$); ** test survived Holm-Bonferroni correction (six tests).

6.5.5. Subcortical degeneration is not associated with EEG connectivity in LBD

Volume differences between VH and NVH groups emerged for both thalamus and NBM. The thalamus has been reportedly associated with α-band rhythms, possibly having a role in generating such waves throughout the cortex (Berger, 1933; Lopes da Silva *et al.*, 1973; Schürmann *et al.*, 2000; Robinson *et al.*, 2001; Schreckenberger *et al.*, 2004; Roberts and Robinson, 2008), and specifically with visual processing (Reinagel *et al.*, 1999; Kveraga *et al.*, 2007). Functional alteration within the thalamus in LB pathology-related conditions was already reported in an fMRI study including part of the same participant cohort, where functional connectivity between thalamic nuclei and cortex negatively correlated with EEG microstates duration (Schumacher *et al.*, 2019). Onofrj *et al.* (2019) proposed that thalamic

functional dysfunction might be associated with decoupling between DMN and attentional networks, generating short time connectivity states leading to psychotic symptoms in LBD. However, empirical evidence of a correlation between thalamus anatomical degeneration and LBD-VH has not been reported to date. The present study shows a strikingly significant reduction of thalamus volume in VH compared to NVH, in agreement with previous autopsy studies showing pulvinar degeneration in DLB compared to AD (Erskine and Khundakar, 2016; Erskine *et al.*, 2017; Erskine *et al.*, 2019). The present result suggests that such neuronal loss might be specifically associated with VH symptomatic phenotype. However, severity of thalamus degeneration did not correlate with EEG functional connectivity strength within affected NBS component for any of the groups.

NBM volume was also significantly reduced in VH compared with NVH, in line with previous reports (Choi *et al.*, 2012; Shin *et al.*, 2012). This result nicely fits with the idea of cholinergic dysfunction being a driver of VH generation in LBD (Ballard *et al.*, 2000; Harding *et al.*, 2002; Diederich *et al.*, 2005; Shine *et al.*, 2011; Shine *et al.*, 2014; Onofrj *et al.*, 2019), which may be due to degeneration and LB burden over the main cholinergic sources of the brain (Hepp *et al.*, 2017a; Sakai *et al.*, 2019). A recent study which compared NBM volume across dementia types did not find any significant difference between groups (Schumacher *et al.*, 2020b). Comparation of theirs and present results strengthens the hypothesis that NBM neuronal loss might be specifically associated with VH-related pathological features regardless of dementia type. However, NBM atrophy did not correlate with EEG connectivity strength in either groups.

Hence, visual network alterations and subcortical degeneration in VH are either associated with different pathological mechanisms, or, if any effect of the latter exists on the first, that might be mediated by a third feature, e.g. subcortical-cortical white matter fibre tracts.

6.5.6. Cholinergic dysfunction is associated with EEG network abnormalities in VH

Previous studies investigating functional brain abnormalities associated with VH in LBD consistently attributed to the cholinergic system a primary role in the generation of such alterations (Ballard *et al.*, 2000; Harding *et al.*, 2002; Diederich *et al.*, 2005; Shine *et al.*, 2011; Shine *et al.*, 2014; Onofrj *et al.*, 2019). These speculations were suggested by indirect evidences, which included restoration effect of cholinergic medication on EEG features

towards healthier values in DLB (Agnoli *et al.*, 1983; Balkan *et al.*, 2003; Kai *et al.*, 2005), the ability of these to suppress VH (Perry and Perry, 1995) and degeneration of the NBM (Hepp *et al.*, 2017a; Sakai *et al.*, 2019). This latter was also found in the present chapter, where NBM volume was lower in VH compared to NVH. In the present analysis, it has been found that WM projections from the cholinergic cell group in the NBM (Ch4 group in the basal forebrain) towards cortical regions belonging to the functionally affected network component show higher degeneration in VH compared to NVH. This result, together with reduced NBM volume, show that LBD-VH condition is associated with generalised damage of the main source of the cholinergic system. WM degeneration within cholinergic projections towards the cortex was also detected in a study with PD patients (Hepp *et al.*, 2017a), where higher MD was detected in VH compared to NVH for the tracts between NBM and occipital and parietal areas. Authors suggested that such projections might have a key role in aetiology of VH in PD. Main interest of the present chapter was to investigate association between structural and functional connectivity, hence a data driven approach was pursued and GM cortical target ROIs were defined as regions corresponding to the NBS-detected nodes. Interestingly, correlation between cortical functional connectivity and number of NBM-cortex WM fibres emerged in NVH group, but not in VH. This outcome partially resembled the result of WM-DF correlation analysis reported in Chapter 5, where EEG-DTI significant correlation was more consistent in AD than in DLB. In line with the interpretation proposed in that chapter and the outcome of cortical thickness analysis, it is suggested here that NVH patients might include mixed LB-AD pathology cases, where AD component is predominant over LB pathology. In such condition, cholinergic-dependent regulation of functional cortical network connectivity might still persist, whereas they are disrupted in VH, where LBD cases could be associated with either pure LB pathology, i.e. cases with number of fibres $< 2 \cdot 10^4$ as shown in Figure 6.10, or mixed pathology cases with predominant LB pathology, i.e. number of fibres $> 2 \cdot 10^4$. Future studies may specifically aim to assess to which extent a LBD cohort include mixed-pathology cases; to this purpose, hippocampal volume might be extracted, and compared between groups, as hippocampal degeneration is known to be associated with co-existence of AD pathology (Gosche *et al.*, 2002; Carmichael *et al.*, 2012).

Surprisingly, structural connectivity between thalamus and any of the other ROIs was not significantly affected in VH compared to NVH. This outcome apparently contrasts findings from a previous study where correlation between MD within the right thalamic subregion, i.e.

thalamic area projecting towards occipital and parietal areas, and NPI hallucination score were reported in DLB (Delli Pizzi *et al.*, 2014b). However, as discussed above, in the present analysis a data driven approach was pursued, different from the mentioned study. Specifically, in the present analysis thalamus structural alteration was not tested in its subregions separately, whereas fibre tracts from the whole thalamus towards NBM and NBS-detected cortical regions were extracted, number of fibres was compared between groups, and correlation with functional connectivity was tested. Hence, WM alteration in specific thalamic subregions might not necessarily emerge with the present approach. However, investigating such aspect is beyond the scope of the present chapter, as the analysis was aimed to investigate for any functional-structural connectivity relationship associated with the pathological condition rather than thalamic involvement in VH aetiology per se. In fact, although association with α-band connectivity abnormalities and thalamic neuronal loss did not emerge, a subtle correlation trend towards significance was found in VH when testing correlation between the number of fibres in the thalamus-cortex tract and EEG source connectivity strength; this trend did not emerge in NVH. If any causality exists between thalamic degeneration and functional connectivity alterations in VH, it seems that consistent degeneration of thalamic projections is needed to cause significant functional connectivity reduction. Hence, it is possible that a larger cohort sample size might be necessary to obtain enough statistical power so that correlation significance may emerge. As described in section 1.3.1, the thalamus is believed to be the functional source of α-band rhythms in the cortex (Chapman *et al.*, 1962; Mulholland and Runnals, 1962; Klimesch *et al.*, 1998; Jensen and Mazaheri, 2010; Benedek *et al.*, 2014; Wan *et al.*, 2019). Whether significant, the present outcome would show that beside DMN and attentional network alteration as proposed by Onofrj *et al.* (2019), thalamic abnormalities may also affect functional visual network at rest and its interaction with DMN and VAN, as shown with the NBS analysis. This aspect will need to be further explored in future studies.

Cholinergic projections towards the thalamus, i.e. WM fibres in NBM-thalamus tract, were not affected in VH compared to NVH and did not correlate with $WPLI_{NBS}$, whilst significant correlation emerged with Q_w in the NVH group. Disruption of the cholinergic system, and more specifically cholinergic deficit in the right thalamus, was reported to be more severe in LBD compared to AD and associated with cognitive fluctuation severity, together with reduced functional connectivity between thalamus and cortical regions (Ballard *et al.*, 2002; Pimlott *et al.*, 2006; Delli Pizzi *et al.*, 2015b; Schumacher *et al.*, 2019). It is possible that such thalamic

impairment causes the slowing of brain dynamics associated with cognitive dysfunctions (Schumacher *et al.*, 2019) and drives network modular organisation towards higher segregation when VH symptomatology is absent. However, investigation of this pathological aspect is beyond the scope of this thesis.

6.6. Conclusions

In this chapter it has been shown that LBD features different EEG functional network properties depending on whether patients have also developed VH. For the first time differential topography between the two groups was obtained without any prior hypothesis, using data driven approaches instead and successfully validating predictive computational models. The most prominent differential feature consisted of affected visual processing streams in VH compared to NVH, although affected interaction between ventral visual network and DMN or VAN also emerged. The most functionally affected area was the right cuneus, which was also more atrophied in NVH compared to VH, probably due to underlying mixed pathology in NVH condition. Modular organisation of EEG source network is more disrupted when LBD patients also present VH. Correspondingly, modular distribution of the affected network component in VH is altered, within both top-down and bottom-up visual streams. Moreover, thalamus and basal forebrain were expectedly more degenerated in VH compared with NVH, although GM volumes were not correlated with functional cortical connectivity strength. However, the present study provides a direct evidence supporting the hypothesis that disruption of cholinergic projections from the basal forebrain towards the cortex is associated with functional connectivity abnormalities emerging when VH clinical feature develops in LBD. Results of this chapter further validate EEG as an effective tool to investigate pathological insights associated with LBD and, specifically, VH. Potentiality of multiple modalities for investigating functional and structural pathological correlates of LBD was demonstrated, by combining efficiency of EEG methodological approach with widely used structural imaging techniques, e.g. MRI and DTI. Future analysis will need to assess whether VH-related functional and structural biomarkers may be suitable to infer informing features to predict pathological progression at the earliest stage of LBD-associated disease development, e.g. prodromal or MCI-LB.

Chapter 7. Conclusions

The main scope of this thesis was to investigate EEG feature alterations in DLB, with a focus on VH symptom, and their pathological correlate. To this purpose, EEG network and activation features were measured in both sensor and source domain, compared between dementia types and with healthy controls, and correlated with structural measures. Functional and structural network measures were then compared between VH and NVH condition in LBD, and correlation with structural connectivity was tested. Key findings of this study included:

- EEG network features were differentially affected in AD, DLB and PDD. Specifically, α-band measures were altered in LBD, i.e. DLB+PDD, compared to HC, and β-band network was overall more affected in DLB compared to AD.
- The same network feature alterations emerged in the source analysis. In the α-band, differential topographical patterns in AD and DLB against HC matched with attentional networks, and correlated with occipital DF in DLB, but not in AD.
- DLB showed higher network segregation compared to AD in the β-band. Interaction between VAN and DAN was weakened in DLB compared to AD, and differential network pattern strength was associated with integrity of cholinergic projection towards the cortex, more consistently in AD than in DLB.
- Connectivity strength within the visual ventral network and prominently from/toward the cuneus was weaker in VH compared to NVH in LBD. Thalamus and NBM showed more atrophy in VH compared to NVH, but neuronal loss did not correlate with functional connectivity in either groups.
- Integrity of cholinergic projections from the NBM towards the cortex was associated with functional connectivity strength in NVH, but not in VH. Cholinergic deficit in the thalamus was associated with higher network segregation in NVH, with a trend towards significant correlation in VH.

Methodological finding:

- Weighted thresholded graphs yield more consistent network measures across network densities compared to binary graphs.

7.1. General Discussion: Novelties and Strengths

The third chapter of this thesis aimed to explore discriminative EEG network features across dementia types, i.e. AD, DLB and PDD, and between dementia and HC. Previous studies reported differential EEG network measures (Lemstra *et al.*, 2014; van Dellen *et al.*, 2015; Dauwan *et al.*, 2016; Babiloni *et al.*, 2018), however no study to date involved a graph theory analysis also measuring local condition-related functional alterations. In the present analysis, network graphs were obtained through proportional thresholding, and local and global graph features were extracted and compared between participant groups. Results of this analysis revealed that EEG network measures within the α-band accurately discriminate LBD from HC, whilst most β-band network features are differential between DLB and AD. Specifically, DLB showed weaker connectivity and greater network segregation compared to AD, and nodal measure differences were more consistent over posterior and anterior regions. This analysis provided novel evidences showing differential functional network properties between DLB and AD, which were speculated to be associated with differential attentional network alterations. Further aim of this chapter was to contribute to the debate on the most efficient method to obtain network graphs from connectivity matrices (van Wijk *et al.*, 2010; Langer *et al.*, 2013). It was hypothesised here and proved that applying proportional thresholding while preserving graph weights yields more consistent network measures by reducing their dependency on network density (Mehraram *et al.*, 2019). Hence, any graph measure in the following chapter was obtained as its weighted variant.

7.1.1. DLB vs AD

Suitability of EEG as supportive diagnostic tool for dementia and, specifically, DLB, was demonstrated. The following analyses aimed to combine EEG with other brain imaging modalities to obtain pathological insights into the diseases. In the fourth chapter, source localisation was used to reconstruct cortical sources and their corresponding functional network and condition-related abnormalities. To spatially localise the cortical subnetwork involved in such alterations, NBS approach was used (Zalesky *et al.*, 2010), and consistently affected network components between HC, AD and DLB groups were extracted. All differential graph measures detected in the sensor domain analysis were significantly differential also in

the source domain, confirming reliability of EEG as diagnostic biomarker and the potential of EEG-source reconstruction to infer pathological correlates. NBS analysis showed significant alteration of connectivity patterns comprising ventral and dorsal networks in both AD and DLB compared to HC, being more ventrally pronounced in DLB, in agreement with proposed speculations. Interestingly, it has been shown for the first time that average connectivity over the affected subnetwork significantly correlated with DF measured over the posterior cortex in DLB, but not in AD, suggesting that α-band network and posterior activation alterations in DLB might both originate from more severe cholinergic dysfunction in DLB compared to AD (Perry *et al.*, 1991; Tiraboschi *et al.*, 2000; Tiraboschi *et al.*, 2002; Lemstra *et al.*, 2003; Delli Pizzi *et al.*, 2015b). This open question was addressed in the following chapter, and NBS analysis was also used to assess cortical alterations associated with EEG β-band differential features between AD and DLB detected in the sensor domain analysis. As hypothesised, cholinergic regulation of cortical activity was weakened in DLB but still maintained in AD. Modular disruption in DLB compared to AD corresponded to significant functional connectivity reduction over the right hemisphere between dorsal and ventral areas, likely associated with emotional alterations typically emerging in DLB (McKeith *et al.*, 2017). Positive correlation between Q and MMSE suggested that DLB group may likely include mixed-pathology cases, associated with more severe cognitive performance and AD-driven lower modularity. In agreement with the sensor domain analysis, connectivity strength was the most discriminative feature between AD and DLB.

7.1.2. LBD: VH vs NVH

Due to its specificity in discriminating LB pathology from AD (Tiraboschi *et al.*, 2006; Jicha *et al.*, 2010; Toledo *et al.*, 2013; Yoshizawa *et al.*, 2013), functional and structural correlate of VH symptomatic condition were investigated in Chapter 6. With the same approach as implemented in the previous chapter, NBS was used to detect differential network components between VH and NVH. In addition, functional affected regions within NBS components were assessed by measuring individual node strengths and comparing the obtained values between groups. The obtained component consisted of topographical patterns comprising connections between regions belonging to the visual ventral network, i.e. PFC, IT and occipital cortex (Bar, 2003; Bar *et al.*, 2006; Chaumon *et al.*, 2009; Gamond *et al.*,

2011; Chaumon *et al.*, 2014; O'Callaghan *et al.*, 2017), providing the first empirical evidence of developed models of VH in LBD (Collerton *et al.*, 2005; Tsukada *et al.*, 2015). The right cuneus showed the most consistent strength reduction in VH compared to NVH, suggesting that network alterations associated with VH are likely originating from posterior regions. Interestingly, the cuneus showed higher neuronal loss in NVH compared to VH. Post hoc comparison with AD and HC showed that right cuneus thickness in (LBD-)NVH and AD were not significantly different, hence it was speculated that NVH group likely consists of mixed AD-LB pathology cases, in line with previously reported posterior cortical atrophy in such condition (Benson *et al.*, 1988; Crutch *et al.*, 2017). NBM and thalamus featured significant atrophy in VH, although there was no correlation between subcortical GM volume and $WPLI_{NBS}$. On the other hand, correlation between structural and functional connectivity emerged from EEG-DTI combined analysis. Specifically, integrity of cholinergic projections towards the cortex correlated with $WPLI_{NBS}$ in NHV, but not in VH, suggesting that physiological cholinergic regulation of cortical activity might be disrupted in VH. To the best of author's knowledge, this latter result is the first empirical direct evidence of the fact that cholinergic dysfunctions might be the underlying cause of EEG abnormalities in LBD, as consistently speculated in the literature on EEG and dementia (Perry *et al.*, 1991; Ballard *et al.*, 2000; Tiraboschi *et al.*, 2000; Harding *et al.*, 2002; Tiraboschi *et al.*, 2002; Lemstra *et al.*, 2003; Diederich *et al.*, 2005; Shine *et al.*, 2011; Shine *et al.*, 2014; Delli Pizzi *et al.*, 2015b; Onofrj *et al.*, 2019). Instead, when VH is absent, network segregation seems to be likely associated with cognitive dysfunctions, and is apparently driven by cholinergic deficit in the thalamus (Ballard *et al.*, 2002; Pimlott *et al.*, 2006; Delli Pizzi *et al.*, 2015b; Schumacher *et al.*, 2019).

7.2. Limitations

The analyses reported in this thesis present some limitations.

7.2.1. Small sample size

Due to the limited occurrence of DLB compared to other types across dementia cases, the available cohort was imbalanced across groups. This likely biased any diagnosis accuracy analysis such as the ones reported in chapters 3 and 5 to some extent, although proper Python libraries were used to attenuate any sample imbalance effect on classifier trainings. In addition, some of the analyses likely lacked statistical power, which could be increased by including a larger cohort. The reader is referred to section 6.5.6 for an example of correlation trend which did not reach significance likely due to small sample size. Small sample size also produced gender imbalance, with relatively large male cohort compared to female. This was marked in the VH analyses (Chapter 6), where statistical tests could not be corrected for gender distribution imbalance between groups.

7.2.2. EEG has low spatial resolution

As discussed in the first chapter, EEG is emerging as convenient tool for research and diagnostic purpose in neurological diseases. Its advantages rely on its low cost, portability, and non-invasiveness. In addition, compared to fMRI it features high temporal resolution, which makes it suitable to record high frequency electrical activity, such as γ-band oscillations (Freeman and Rogers, 2002; Davidson *et al.*, 2007). In contrast, EEG provides relatively low spatial resolution. Clinical EEG equipment usually features standard 10-20 derivation system comprising 19 scalp electrodes (Jurcak *et al.*, 2007), limiting the accuracy of any source localisation approach (Song *et al.*, 2015). Hence, solutions with higher spatial resolution are often chosen in research, as done in this thesis by analysing high-density EEG data comprising 128 channels (10-5 derivation system). Nevertheless, this is still lower than any resolution reachable with fMRI systems, e.g. 3-4 mm (Glover, 2011).

7.2.3. sLORETA yields smooth source reconstruction

Low spatial resolution is also a weak point of the chosen source localisation technique, hence any interpretation of analyses' results based on spatial information should be read with caution. Generally speaking, there is some inconsistency of connectivity estimates across

source localisation techniques (Mahjoory *et al.*, 2017; Lai *et al.*, 2018). For instance, beamforming method are based on the assumption of uncorrelated sources, whilst this is not the case for MNE approaches (Hämäläinen and Ilmoniemi, 1984; Hämäläinen *et al.*, 1993), likely making this latter more suitable for connectomics analysis. Hincapié *et al.* (2017) showed that connectivity of simulated MEG signals was more accurately reconstructed with beamforming or MNE depending on whether sources were assumed to be respectively point-like or extended cortical patches. Accuracy of combined MEG/EEG source localisation approaches may possibly reduce the influence of this methodological inconsistencies yielding higher precision (Huizenga *et al.*, 2001; Ebersole and Ebersole, 2010).

7.2.4. WPLI cancels true zero-lag connectivity

The main advantage of (W)PLI connectivity measure, especially at the sensor level, is its insensitivity to volume conducted signals, i.e. zero-lag synchronised time-series. However, zero-lag connectivity does not necessarily involve volume conduction, as it may also be due to multiple signals associated with the same (sub)cortical source activation (Roelfsema *et al.*, 1997; Gollo *et al.*, 2014; Colclough *et al.*, 2016). In this latter case, unrecorded connectivity would correspond to a false negative, and possibly relevant topological information might be lost. Moreover, accuracy of phase-based connectivity measures depends on signal-to-noise ratio, which in turn depends on overall signal power (Colclough *et al.*, 2016). However, influence of zero-lag connectivity on network topology and difference between phase-based and correlation measures is beyond of the scope of the present thesis and should be addressed by proper methodological studies.

7.2.5. Lack of connectivity directionality

The EEG network analysis was based on undirected weighted graphs; hence directionality of affected connectivity patterns could not be empirically assessed. Therefore, any assumption of origin and target of connectivity projections was made based on existing speculations, hypotheses, and computational models. Measurement of effective connectivity was not of interest in the present thesis, hence future studies based on effective connectivity measures

will be needed to confirm such assumptions and further prove the validity of, or possibly contradict, the models.

7.2.6. The NBS threshold is arbitrarily chosen

As mentioned in section 2.5, NBS requires choosing a threshold on the single connection t-values before performing a network statistical analysis. The choice of this threshold is a consequence of trials and attempts, as no specific protocol has been proposed yet (Zalesky *et al.*, 2010). Purpose of the research presented in this thesis was to investigate for localised differential network properties, hence t_{th} conservative values were chosen. However, it is possible that sensitivity of NBS may change due to the choice of lower thresholds, leading to either larger network components or no significance at all. This aspect was not investigated and remains a limitation of this work.

7.2.7. Simple and complex hallucinations may have different aetiology

In Chapter 6, patients with simple and complex hallucinations have been grouped together as VH, in order to exclude any visual perception alteration from the NVH group. In fact, NBS yielded consistently affected network component within VH group with no outliers, as shown in Figure 6.2 and Figure 6.3. However, simple and complex hallucinatory features have been suggested to be associated with different pathological mechanisms (Archibald *et al.*, 2011), and other studies chose to include only complex hallucinations in VH group (Delli Pizzi *et al.*, 2014a; Franciotti *et al.*, 2015; Firbank *et al.*, 2018). Due to the small sample size, the extent to which simple hallucination phenomenon influences functional connectivity as compared to complex hallucinations could not be investigated in the present thesis.

7.2.8. DTI data could not be corrected for susceptibility-induced distortions

Differently than T1 MRI recordings, DTI recordings are also sensitive to susceptibility-induced off-resonance fields, which depend on subject head (Graham *et al.*, 2017). To correct for these, an extra unweighted diffusion recording with different acquisition parameters is needed for

each subject. Whilst this was available for subjects from the VEEG-Stim study, this was not the case for the CATFieLD subjects. Therefore, DTI data could not be corrected for susceptibility-related distortions due to data unavailability.

7.3. Conclusions and Future Directions

In this thesis it has been shown that EEG is suitable as indicative diagnostic tool for DLB and its differentiation from AD. Furthermore, combination of multiple modalities, i.e. EEG, MRI, and DTI, allowed to detect differential functional network patterns at the source level between AD and DLB, and their structural correlates. Specifically, it has been experimentally demonstrated that cholinergic dysfunctions generating from the basal forebrain are likely the drivers of detected EEG abnormalities in DLB and, specifically, associated with VH symptom. Moreover, structural and functional features in LBD are significantly influenced by the occurrence of AD-LB mixed-pathology cases, which should be taken in account to correctly interpret obtained results.

7.3.1. EEG as diagnostic tool for MCI-LB?

From the diagnostic perspective, the long-term goals of the research reported in this dissertation is to develop predictive diagnostic tools which can effectively detect the condition type at the earliest disease development stages. Most recent EEG studies have investigated EEG differential features between MCI subtypes, which resonated with the ones between dementia types (Babiloni *et al.*, 2014; Bonanni *et al.*, 2015; Babiloni *et al.*, 2019; Law *et al.*, 2020; Schumacher *et al.*, 2020a). However, graph theory studies and multi-modality approaches have not been pursued to date. It is proposed here for future studies to implement the same methodological pipeline as in the present thesis with an MCI cohort, train a classifier with the obtained EEG features, and test prediction accuracy with the dementia cohort. High classification accuracy would support EEG as a predictive biomarker at the earliest clinical manifestation, and potentially help to better provide effective treatments.

7.3.2. EEG source features to inform targeted medication

From the pathological perspective, cortical and subcortical source localisation and combination with structural data may potentially inform the development and/or prescription of targeted medication. Future studies will need to assess effectiveness of existing treatment to restore localised abnormal disease-related functional and structural features in respective brain areas. In addition, specific medication targeting specific brain areas may be developed to treat individual symptoms such as VH.

7.3.3. EEG subcortical source localisation: is the thalamus functionally altered?

EEG cortical source localisation is becoming widely implemented in most studies involving diverse conditions. However, whether such approach may be suitable to accurately infer activation of subcortical regions is still a matter of research. For instance, Krishnaswamy *et al.* (2017) have proposed spatial source sparsity as an approach to correctly infer both cortical and subcortical activation, successfully extracting thalamus and brainstem signals. More recently, Seeber *et al.* (2019) showed that thalamus α-band activity could correctly be detected with source reconstruction, comparing the obtained signal with intracranial EEG recording from the same area. Although promising, these findings will need to be validated with diverse source localisation techniques, simulated data, and large cohorts before being extensively implemented for diagnostic and pathological research. Once consolidated, such approaches will potentially provide further insights on association between cortical and subcortical activity and their hypothesised and modelled abnormalities in DLB.

References

Aarsland, D., Ballard, C., Larsen, J.P. and McKeith, I. (2001) 'A comparative study of psychiatric symptoms in dementia with Lewy bodies and Parkinson's disease with and without dementia', *Int J Geriatr Psychiatry*, 16(5), pp. 528-36.

Aarsland, D., Ballard, C., Walker, Z., Bostrom, F., Alves, G., Kossakowski, K., Leroi, I., Pozo-Rodriguez, F., Minthon, L. and Londos, E. (2009) 'Memantine in patients with Parkinson's disease dementia or dementia with Lewy bodies: a double-blind, placebo-controlled, multicentre trial', *Lancet Neurol*, 8(7), pp. 613-8.

Achard, S., Salvador, R., Whitcher, B., Suckling, J. and Bullmore, E. (2006) 'A resilient, low-frequency, small-world human brain functional network with highly connected association cortical hubs', *Journal of Neuroscience*, 26(1), pp. 63-72.

Acharya, U.R., Molinari, F., Sree, S.V., Chattopadhyay, S., Ng, K.-H. and Suri, J.S. (2012) 'Automated diagnosis of epileptic EEG using entropies', *Biomedical Signal Processing and Control*, 7(4), pp. 401-408.

Aertsen, A.M., Gerstein, G.L., Habib, M.K. and Palm, G. (1989) 'Dynamics of neuronal firing correlation: modulation of "effective connectivity"', *Journal of Neurophysiology*, 61(5), pp. 900-917.

Agnoli, A., Martucci, N., Manna, V., Conti, L. and Fioravanti, M. (1983) 'Effect of cholinergic and anticholinergic drugs on short-term memory in Alzheimer's dementia: a neuropsychological and computerized electroencephalographic study', *Clinical neuropharmacology*, 6(4), pp. 311-323.

Alexander, A.L., Lee, J.E., Lazar, M. and Field, A.S. (2007) 'Diffusion Tensor Imaging of the Brain', *Neurotherapeutics*, 4(3), pp. 316-329.

Allman, J.M., Watson, K.K., Tetreault, N.A. and Hakeem, A.Y. (2005) 'Intuition and autism: a possible role for Von Economo neurons', *Trends in cognitive sciences*, 9(8), pp. 367-373.

Amari, S.-i., Cichocki, A. and Yang, H.H. (1996) *Advances in neural information processing systems*.

Anderer, P., Roberts, S., Schlögl, A., Gruber, G., Klösch, G., Herrmann, W., Rappelsberger, P., Filz, O., Barbanoj, M.J. and Dorffner, G. (1999) 'Artifact processing in computerized analysis of sleep EEG–a review', *Neuropsychobiology*, 40(3), pp. 150-157.

Anderson, K.L. and Ding, M. (2011) 'Attentional modulation of the somatosensory mu rhythm', *Neuroscience*, 180, pp. 165-80.

Andersson, J.L.R., Graham, M.S., Zsoldos, E. and Sotiropoulos, S.N. (2016) 'Incorporating outlier detection and replacement into a non-parametric framework for movement and distortion correction of diffusion MR images', *Neuroimage*, 141, pp. 556-572.

Andersson, J.L.R. and Sotiropoulos, S.N. (2016) 'An integrated approach to correction for off-resonance effects and subject movement in diffusion MR imaging', *Neuroimage*, 125, pp. 1063-1078.

Andersson, M., Hansson, O., Minthon, L., Rosen, I. and Londos, E. (2008) 'Electroencephalogram variability in dementia with lewy bodies, Alzheimer's disease and controls', *Dement Geriatr Cogn Disord*, 26(3), pp. 284-90.

Angela, J.Y. and Dayan, P. (2002) 'Acetylcholine in cortical inference', *Neural Networks*, 15(4-6), pp. 719-730.

Archibald, N.K., Clarke, M.P., Mosimann, U.P. and Burn, D.J. (2011) 'Visual symptoms in Parkinson's disease and Parkinson's disease dementia', *Mov Disord*, 26(13), pp. 2387-95.

Asaad, G. and Shapiro, B. (1986) 'Hallucinations: theoretical and clinical overview', *The American journal of psychiatry*.

Astolfi, L., Cincotti, F., Mattia, D., Marciani, M.G., Baccala, L.A., de Vico Fallani, F., Salinari, S., Ursino, M., Zavaglia, M., Ding, L., Edgar, J.C., Miller, G.A., He, B. and Babiloni, F. (2007)

'Comparison of different cortical connectivity estimators for high-resolution EEG recordings', *Human Brain Mapping*, 28(2), pp. 143-157.

Avants, B.B., Tustison, N. and Song, G. (2009) 'Advanced normalization tools (ANTS)', *Insight j*, 2(365), pp. 1-35.

Axmacher, N., Henseler, M.M., Jensen, O., Weinreich, I., Elger, C.E. and Fell, J. (2010) 'Cross-frequency coupling supports multi-item working memory in the human hippocampus', *Proceedings of the National Academy of Sciences*, 107(7), pp. 3228-3233.

Baba, M., Nakajo, S., Tu, P.H., Tomita, T., Nakaya, K., Lee, V.M., Trojanowski, J.Q. and Iwatsubo, T. (1998) 'Aggregation of alpha-synuclein in Lewy bodies of sporadic Parkinson's disease and dementia with Lewy bodies', *The American Journal of Pathology*, 152(4), pp. 879-884.

Babiloni, C., Del Percio, C., Lizio, R., Marzano, N., Infarinato, F., Soricelli, A., Salvatore, E., Ferri, R., Bonforte, C., Tedeschi, G., Montella, P., Baglieri, A., Rodriguez, G., Fama, F., Nobili, F., Vernieri, F., Ursini, F., Mundi, C., Frisoni, G.B. and Rossini, P.M. (2014) 'Cortical sources of resting state electroencephalographic alpha rhythms deteriorate across time in subjects with amnesic mild cognitive impairment', *Neurobiol Aging*, 35(1), pp. 130-42.

Babiloni, C., Del Percio, C., Lizio, R., Noce, G., Cordone, S., Lopez, S., Soricelli, A., Ferri, R., Pascarelli, M.T., Nobili, F., Arnaldi, D., Aarsland, D., Orzi, F., Buttinelli, C., Giubilei, F., Onofrj, M., Stocchi, F., Stirpe, P., Fuhr, P., Gschwandtner, U., Ransmayr, G., Caravias, G., Garn, H., Sorpresi, F., Pievani, M., Frisoni, G.B., D'Antonio, F., De Lena, C., Güntekin, B., Hanoğlu, L., Başar, E., Yener, G., Emek-Savaş, D.D., Triggiani, A.I., Franciotti, R., De Pandis, M.F. and Bonanni, L. (2017) 'Abnormalities of cortical neural synchronization mechanisms in patients with dementia due to Alzheimer's and Lewy body diseases: an EEG study', *Neurobiology of Aging*, 55, pp. 143-158.

Babiloni, C., Del Percio, C., Lizio, R., Noce, G., Lopez, S., Soricelli, A., Ferri, R., Nobili, F., Arnaldi, D., Famà, F., Aarsland, D., Orzi, F., Buttinelli, C., Giubilei, F., Onofrj, M., Stocchi, F., Stirpe, P., Fuhr, P., Gschwandtner, U., Ransmayr, G., Garn, H., Fraioli, L., Pievani, M., Frisoni,

G.B., D'Antonio, F., De Lena, C., Güntekin, B., Hanoğlu, L., Başar, E., Yener, G., Emek-Savaş, D.D., Triggiani, A.I., Franciotti, R., Taylor, J.P., Vacca, L., De Pandis, M.F. and Bonanni, L. (2018) 'Abnormalities of resting-state functional cortical connectivity in patients with dementia due to Alzheimer's and Lewy body diseases: an EEG study', *Neurobiology of Aging*, 65, pp. 18-40.

Babiloni, C., Del Percio, C., Pascarelli, M.T., Lizio, R., Noce, G., Lopez, S., Rizzo, M., Ferri, R., Soricelli, A., Nobili, F., Arnaldi, D., Famà, F., Orzi, F., Buttinelli, C., Giubilei, F., Salvetti, M., Cipollini, V., Franciotti, R., Onofrj, M., Stirpe, P., Fuhr, P., Gschwandtner, U., Ransmayr, G., Aarsland, D., Parnetti, L., Farotti, L., Marizzoni, M., D'Antonio, F., De Lena, C., Güntekin, B., Hanoğlu, L., Yener, G., Emek-Savaş, D.D., Triggiani, A.I., Taylor, J.P., McKeith, I., Stocchi, F., Vacca, L., Hampel, H., Frisoni, G.B., De Pandis, M.F. and Bonanni, L. (2019) 'Abnormalities of functional cortical source connectivity of resting-state electroencephalographic alpha rhythms are similar in patients with mild cognitive impairment due to Alzheimer's and Lewy body diseases', *Neurobiology of Aging*, 77, pp. 112-127.

Babiloni, C., Pascarelli, M.T., Lizio, R., Noce, G., Lopez, S., Rizzo, M., Ferri, R., Soricelli, A., Nobili, F., Arnaldi, D., Famà, F., Orzi, F., Buttinelli, C., Giubilei, F., Salvetti, M., Cipollini, V., Bonanni, L., Franciotti, R., Onofrj, M., Stirpe, P., Fuhr, P., Gschwandtner, U., Ransmayr, G., Aarsland, D., Parnetti, L., Farotti, L., Marizzoni, M., D'Antonio, F., De Lena, C., Güntekin, B., Hanoğlu, L., Yener, G., Emek-Savaş, D.D., Triggiani, A.I., Taylor, J.P., McKeith, I., Stocchi, F., Vacca, L., Hampel, H., Frisoni, G.B., De Pandis, M.F. and Del Percio, C. (2020) 'Abnormal cortical neural synchronization mechanisms in quiet wakefulness are related to motor deficits, cognitive symptoms, and visual hallucinations in Parkinson's disease patients: an electroencephalographic study', *Neurobiol Aging*, 91, pp. 88-111.

Balkan, S., Yaras, N., Mihci, E., Dora, B., Agar, A. and YargiÇOglu, P. (2003) 'Effect of donepezil on EEG spectral analysis in Alzheimer's disease', *Acta neurologica belgica*, 103(3), pp. 164-169.

Ballard, C., Aarsland, D., McKeith, I., O'brien, J., Gray, A., Cormack, F., Burn, D., Cassidy, T., Starfeldt, R. and Larsen, J.-P. (2002) 'Fluctuations in attention: PD dementia vs DLB with parkinsonism', *Neurology*, 59(11), pp. 1714-1720.

Ballard, C., Piggott, M., Johnson, M., Cairns, N., Perry, R., McKeith, I., Jaros, E., O'Brien, J., Holmes, C. and Perry, E. (2000) 'Delusions associated with elevated muscarinic binding in dementia with Lewy bodies', *Annals of Neurology*, 48(6), pp. 868-876.

Ballard, C., Walker, M., O'Brien, J., Rowan, E. and McKeith, I. (2001a) 'The characterisation and impact of 'fluctuating'cognition in dementia with Lewy bodies and Alzheimer's disease', *International journal of geriatric psychiatry*, 16(5), pp. 494-498.

Ballard, C.G., O'Brien, J.T., Swann, A.G., Thompson, P., Neill, D. and McKeith, I.G. (2001b) 'The natural history of psychosis and depression in dementia with Lewy bodies and Alzheimer's disease: persistence and new cases over 1 year of follow-up', *The Journal of clinical psychiatry*, 62(1), pp. 46-49.

Bar, M. (2003) 'A Cortical Mechanism for Triggering Top-Down Facilitation in Visual Object Recognition', *Journal of Cognitive Neuroscience*, 15(4), pp. 600-609.

Bar, M., Kassam, K.S., Ghuman, A.S., Boshyan, J., Schmid, A.M., Dale, A.M., Hämäläinen, M.S., Marinkovic, K., Schacter, D.L., Rosen, B.R. and Halgren, E. (2006) 'Top-down facilitation of visual recognition', *Proceedings of the National Academy of Sciences of the United States of America*, 103(2), pp. 449-454.

Barabash, A., Marcos, A., Ancín, I., Vázquez-Alvarez, B., de Ugarte, C., Gil, P., Fernández, C., Encinas, M., López-Ibor, J.J. and Cabranes, J.A. (2009) 'APOE, ACT and CHRNA7 genes in the conversion from amnestic mild cognitive impairment to Alzheimer's disease', *Neurobiology of Aging*, 30(8), pp. 1254-1264.

Barabasi, A.L. and Albert, R. (1999) 'Emergence of scaling in random networks', *Science*, 286(5439), pp. 509-12.

Barber, P.A., Varma, A.R., Lloyd, J.J., Haworth, B., Haworth, J.S.S. and Neary, D. (2000a) 'The electroencephalogram in dementia with Lewy bodies', *Acta Neurologica Scandinavica*, 101(1), pp. 53-56.

Barber, R., Ballard, C., McKeith, I., Gholkar, A. and O'Brien, J. (2000b) 'MRI volumetric study of dementia with Lewy bodies: a comparison with AD and vascular dementia', *Neurology*, 54(6), pp. 1304-1309.

Barnes, J. and David, A.S. (2001) 'Visual hallucinations in Parkinson's disease: a review and phenomenological survey', *J Neurol Neurosurg Psychiatry*, 70(6), pp. 727-33.

Bartos, M., Vida, I. and Jonas, P. (2007) 'Synaptic mechanisms of synchronized gamma oscillations in inhibitory interneuron networks', *Nature Reviews Neuroscience*, 8(1), pp. 45-56.

Basser, P.J. (1995) 'Inferring microstructural features and the physiological state of tissues from diffusion-weighted images', *NMR in Biomedicine*, 8(7), pp. 333-344.

Bauer, M., Kennett, S. and Driver, J. (2012) 'Attentional selection of location and modality in vision and touch modulates low-frequency activity in associated sensory cortices', *J Neurophysiol*, 107(9), pp. 2342-51.

Beach, T.G., Adler, C.H., Lue, L., Sue, L.I., Bachalakuri, J., Henry-Watson, J., Sasse, J., Boyer, S., Shirohi, S., Brooks, R., Eschbacher, J., White, C.L., Akiyama, H., Caviness, J., Shill, H.A., Connor, D.J., Sabbagh, M.N., Walker, D.G. and the Arizona Parkinson's Disease, C. (2009) 'Unified staging system for Lewy body disorders: correlation with nigrostriatal degeneration, cognitive impairment and motor dysfunction', *Acta Neuropathologica*, 117(6), pp. 613-634.

Bechtoldt, H.P., Benton, A.L. and Fogel, M.L. (1962) 'An application of factor analysis in neuropsychology', *The Psychological Record*, 12(2), p. 147.

Behrens, T.E., Berg, H.J., Jbabdi, S., Rushworth, M.F. and Woolrich, M.W. (2007) 'Probabilistic diffusion tractography with multiple fibre orientations: What can we gain?', *Neuroimage*, 34(1), pp. 144-55.

Behrens, T.E., Woolrich, M.W., Jenkinson, M., Johansen-Berg, H., Nunes, R.G., Clare, S., Matthews, P.M., Brady, J.M. and Smith, S.M. (2003a) 'Characterization and propagation of uncertainty in diffusion-weighted MR imaging', *Magn Reson Med*, 50(5), pp. 1077-88.

Behrens, T.E.J., Johansen-Berg, H., Woolrich, M.W., Smith, S.M., Wheeler-Kingshott, C.A.M., Boulby, P.A., Barker, G.J., Sillery, E.L., Sheehan, K., Ciccarelli, O., Thompson, A.J., Brady, J.M. and Matthews, P.M. (2003b) 'Non-invasive mapping of connections between human thalamus and cortex using diffusion imaging', *Nature Neuroscience*, 6(7), pp. 750-757.

Benedek, M., Schickel, R.J., Jauk, E., Fink, A. and Neubauer, A.C. (2014) 'Alpha power increases in right parietal cortex reflects focused internal attention', *Neuropsychologia*, 56, pp. 393-400.

Bennys, K., Rondouin, G., Vergnes, C. and Touchon, J. (2001) 'Diagnostic value of quantitative EEG in Alzheimer's disease', *Neurophysiologie Clinique/Clinical Neurophysiology*, 31(3), pp. 153-160.

Benson, D.F., Davis, R.J. and Snyder, B.D. (1988) 'Posterior cortical atrophy', *Archives of neurology*, 45(7), pp. 789-793.

Berger, H. (1929) 'Über das elektrenkephalogramm des menschen', *Archiv für psychiatrie und nervenkrankheiten*, 87(1), pp. 527-570.

Berger, H. (1933) 'Über das elektrenkephalogramm des menschen', *Archiv für Psychiatrie und Nervenkrankheiten*, 98(1), pp. 231-254.

Bernhardt, B.C., Bonilha, L. and Gross, D.W. (2015) 'Network analysis for a network disorder: the emerging role of graph theory in the study of epilepsy', *Epilepsy & Behavior*, 50, pp. 162-170.

Bernier, R., Aaronson, B. and Kresse, A. (2014) 'EEG mu rhythm in typical and atypical development', *Journal of visualized experiments : JoVE*, (86), p. 51412.

Bertrand, O., Perrin, F. and Pernier, J. (1985) 'A theoretical justification of the average reference in topographic evoked potential studies', *Electroencephalography and Clinical Neurophysiology/Evoked Potentials Section*, 62(6), pp. 462-464.

Betzel, R., Erickson, M., Abell, M., O'Donnell, B., Hetrick, W. and Sporns, O. (2012) 'Synchronization dynamics and evidence for a repertoire of network states in resting EEG', *Frontiers in Computational Neuroscience*, 6(74).

Bhattacharya, B.S., Coyle, D. and Maguire, L.P. (2011) 'A thalamo–cortico–thalamic neural mass model to study alpha rhythms in Alzheimer's disease', *Neural Networks*, 24(6), pp. 631-645.

Binder, J.R., Frost, J.A., Hammeke, T.A., Bellgowan, P., Rao, S.M. and Cox, R.W. (1999) 'Conceptual processing during the conscious resting state: a functional MRI study', *Journal of cognitive neuroscience*, 11(1), pp. 80-93.

Bishop, N.A., Lu, T. and Yankner, B.A. (2010) 'Neural mechanisms of ageing and cognitive decline', *Nature*, 464(7288), pp. 529-535.

Blanc, F., Colloby, S.J., Cretin, B., de Sousa, P.L., Demuynck, C., O'Brien, J.T., Martin-Hunyadi, C., McKeith, I., Philippi, N. and Taylor, J.-P. (2016) 'Grey matter atrophy in prodromal stage of dementia with Lewy bodies and Alzheimer's disease', *Alzheimer's Research & Therapy*, 8(1), p. 31.

Blanc, F., Colloby, S.J., Philippi, N., de Petigny, X., Jung, B., Demuynck, C., Phillipps, C., Anthony, P., Thomas, A., Bing, F., Lamy, J., Martin-Hunyadi, C., O'Brien, J.T., Cretin, B., McKeith, I.,

Armspach, J.P. and Taylor, J.P. (2015) 'Cortical Thickness in Dementia with Lewy Bodies and Alzheimer's Disease: A Comparison of Prodromal and Dementia Stages', *PLoS One*, 10(6), p. e0127396.

Blanc, F., Mahmoudi, R., Jonveaux, T., Galmiche, J., Chopard, G., Cretin, B., Demuynck, C., Martin-Hunyadi, C., Philippi, N., Sellal, F., Michel, J.M., Tio, G., Stackfleth, M., Vandel, P., Magnin, E., Novella, J.L., Kaltenbach, G., Benetos, A. and Sauleau, E.A. (2017) 'Long-term cognitive outcome of Alzheimer's disease and dementia with Lewy bodies: dual disease is worse', *Alzheimers Res Ther*, 9(1), p. 47.

Blanc, F., Noblet, V., Philippi, N., Cretin, B., Foucher, J., Armspach, J.-P., Rousseau, F. and the Alzheimer's Disease Neuroimaging, I. (2014) 'Right Anterior Insula: Core Region of Hallucinations in Cognitive Neurodegenerative Diseases', *PLOS ONE*, 9(12), p. e114774.

Blinowska, K.J., Rakowski, F., Kaminski, M., De Vico Fallani, F., Del Percio, C., Lizio, R. and Babiloni, C. (2017) 'Functional and effective brain connectivity for discrimination between Alzheimer's patients and healthy individuals: A study on resting state EEG rhythms', *Clinical Neurophysiology*, 128(4), pp. 667-680.

Blonder, L.X., Gur, R.E., Gur, R.C., Saykin, A.J. and Hurtig, H.I. (1989) 'Neuropsychological functioning in hemiparkinsonism', *Brain Cogn*, 9(2), pp. 244-57.

Boeve, B.F., Dickson, D.W., Olson, E., Shepard, J., Silber, M., Ferman, T.J., Ahlskog, J. and Benarroch, E. (2007) 'Insights into REM sleep behavior disorder pathophysiology in brainstem-predominant Lewy body disease', *Sleep medicine*, 8(1), pp. 60-64.

Boeve, B.F., Ferman, T.J., Silber, M.H., Lin, S.-C., Tippmann-Peikert, M. and Smith, G.E. (2008) 'P2-219: Polysomnographic evidence of sleep fragmentation and poor sleep efficiency in dementia with Lewy bodies', *Alzheimer's & Dementia: The Journal of the Alzheimer's Association*, 4(4), p. T435.

Boeve, B.F., Silber, M.H., Ferman, T.J., Lin, S.C., Benarroch, E.E., Schmeichel, A.M., Ahlskog, J.E., Caselli, R.J., Jacobson, S., Sabbagh, M., Adler, C., Woodruff, B., Beach, T.G., Iranzo,

A., Gelpi, E., Santamaria, J., Tolosa, E., Singer, C., Mash, D.C., Luca, C., Arnulf, I., Duyckaerts, C., Schenck, C.H., Mahowald, M.W., Dauvilliers, Y., Graff-Radford, N.R., Wszolek, Z.K., Parisi, J.E., Dugger, B., Murray, M.E. and Dickson, D.W. (2013) 'Clinicopathologic correlations in 172 cases of rapid eye movement sleep behavior disorder with or without a coexisting neurologic disorder', *Sleep Med*, 14(8), pp. 754-62.

Bohr, I.J., Kenny, E., Blamire, A., O'Brien, J.T., Thomas, A.J., Richardson, J. and Kaiser, M. (2013) 'Resting-state functional connectivity in late-life depression: higher global connectivity and more long distance connections', *Frontiers in psychiatry*, 3, pp. 116-116.

Bonanni, L., Franciotti, R., Onofrj, V., Anzellotti, F., Mancino, E., Monaco, D., Gambi, F., Manzoli, L., Thomas, A. and Onofrj, M. (2010) 'Revisiting P300 cognitive studies for dementia diagnosis: Early dementia with Lewy bodies (DLB) and Alzheimer disease (AD)', *Neurophysiologie Clinique/Clinical Neurophysiology*, 40(5), pp. 255-265.

Bonanni, L., Perfetti, B., Bifolchetti, S., Taylor, J.P., Franciotti, R., Parnetti, L., Thomas, A. and Onofrj, M. (2015) 'Quantitative electroencephalogram utility in predicting conversion of mild cognitive impairment to dementia with Lewy bodies', *Neurobiol Aging*, 36(1), pp. 434-45.

Bonanni, L., Thomas, A., Tiraboschi, P., Perfetti, B., Varanese, S. and Onofrj, M. (2008) 'EEG comparisons in early Alzheimer's disease, dementia with Lewy bodies and Parkinson's disease with dementia patients with a 2-year follow-up', *Brain*, 131(Pt 3), pp. 690-705.

Bonelli, S., Ransmayr, G., Steffelbauer, M., Lukas, T., Lampl, C. and Deibl, M. (2004) 'L-dopa responsiveness in dementia with Lewy bodies, Parkinson disease with and without dementia', *Neurology*, 63(2), pp. 376-378.

Bonnelle, V., Ham, T.E., Leech, R., Kinnunen, K.M., Mehta, M.A., Greenwood, R.J. and Sharp, D.J. (2012) 'Salience network integrity predicts default mode network function after traumatic brain injury', *Proceedings of the National Academy of Sciences*, 109(12), pp. 4690-4695.

Borowsky, R., Loehr, J., Kelland Friesen, C., Kraushaar, G., Kingstone, A. and Sarty, G. (2005) 'Modularity and intersection of "what", "where" and "how" processing of visual stimuli: a new method of FMRI localization', *Brain Topogr*, 18(2), pp. 67-75.

Braak, H., Tredici, K.D., Rüb, U., de Vos, R.A.I., Jansen Steur, E.N.H. and Braak, E. (2003) 'Staging of brain pathology related to sporadic Parkinson’s disease', *Neurobiology of Aging*, 24(2), pp. 197-211.

Bradley, B.A., Jacob, R.W., Hermance, J.F. and Mustard, J.F. (2007) 'A curve fitting procedure to derive inter-annual phenologies from time series of noisy satellite NDVI data', *Remote sensing of environment*, 106(2), pp. 137-145.

Bradshaw, J., Saling, M., Anderson, V., Hopwood, M. and Brodtmann, A. (2006) 'Higher cortical deficits influence attentional processing in dementia with Lewy bodies, relative to patients with dementia of the Alzheimer's type and controls', *Journal of Neurology, Neurosurgery & Psychiatry*, 77(10), pp. 1129-1135.

Bradshaw, J., Saling, M., Hopwood, M., Anderson, V. and Brodtmann, A. (2004) 'Fluctuating cognition in dementia with Lewy bodies and Alzheimer's disease is qualitatively distinct', *J Neurol Neurosurg Psychiatry*, 75(3), pp. 382-7.

Brasić, J.R. (1998) 'Hallucinations', *Perceptual and motor skills*, 86(3), pp. 851-877.

Brayne, C., Nickson, J., McCracken, C., Gill, C. and Johnson, A. (1998) 'Cognitive function and dementia in six areas of England and Wales: the distribution of MMSE and prevalence of GMS organicity level in the MRC CFA Study', *Psychological Medicine*, 28(2), pp. 319-335.

Brereton, R.G. (2006) 'Consequences of sample size, variable selection, and model validation and optimisation, for predicting classification ability from analytical data', *TrAC Trends in Analytical Chemistry*, 25(11), pp. 1103-1111.

Briel, R.C., McKeith, I.G., Barker, W.A., Hewitt, Y., Perry, R.H., Ince, P.G. and Fairbairn, A.F. (1999) 'EEG findings in dementia with Lewy bodies and Alzheimer's disease', *J Neurol Neurosurg Psychiatry*, 66(3), pp. 401-3.

Brigo, F., Turri, G. and Tinazzi, M. (2015) '123I-FP-CIT SPECT in the differential diagnosis between dementia with Lewy bodies and other dementias', *Journal of the Neurological Sciences*, 359(1), pp. 161-171.

Buchan, R.J., Nagata, K., Yokoyama, E., Langman, P., Yuya, H., Hirata, Y., Hatazawa, J. and Kanno, I. (1997) 'Regional correlations between the EEG and oxygen metabolism in dementia of Alzheimer's type', *Electroencephalography and Clinical Neurophysiology*, 103(3), pp. 409-417.

Bugalho, P., Salavisa, M., Marto, J.P., Borbinha, C. and Alves, L. (2019) 'Polysomnographic data in Dementia with Lewy Bodies: correlation with clinical symptoms and comparison with other α-synucleinopathies', *Sleep medicine*, 55, pp. 62-68.

Bullmore, E. and Sporns, O. (2009) 'Complex brain networks: graph theoretical analysis of structural and functional systems', *Nature Reviews Neuroscience*, 10(3), pp. 186-198.

Burghaus, L., Eggers, C., Timmermann, L., Fink, G.R. and Diederich, N.J. (2012) 'Hallucinations in neurodegenerative diseases', *CNS Neurosci Ther*, 18(2), pp. 149-59.

Burn, D., Emre, M., McKeith, I., De Deyn, P.P., Aarsland, D., Hsu, C. and Lane, R. (2006) 'Effects of rivastigmine in patients with and without visual hallucinations in dementia associated with Parkinson's disease', *Movement disorders: official journal of the Movement Disorder Society*, 21(11), pp. 1899-1907.

Burn, D.J., Rowan, E.N., Minett, T., Sanders, J., Myint, P., Richardson, J., Thomas, A., Newby, J., Reid, J. and O'Brien, J.T. (2003) 'Extrapyramidal features in Parkinson's disease with and without dementia and dementia with Lewy bodies: a cross-sectional comparative study', *Movement disorders: official journal of the Movement Disorder Society*, 18(8), pp. 884-889.

Burton, E.J., Barber, R., Mukaetova-Ladinska, E.B., Robson, J., Perry, R.H., Jaros, E., Kalaria, R.N. and O'Brien, J.T. (2009) 'Medial temporal lobe atrophy on MRI differentiates Alzheimer's disease from dementia with Lewy bodies and vascular cognitive impairment: a prospective study with pathological verification of diagnosis', *Brain*, 132(Pt 1), pp. 195-203.

Buzsáki, G. (2002) 'Theta Oscillations in the Hippocampus', *Neuron*, 33(3), pp. 325-340.

Buzsáki, G. and Wang, X.-J. (2012) 'Mechanisms of gamma oscillations', *Annual review of neuroscience*, 35, pp. 203-225.

Cabral, J., Hugues, E., Sporns, O. and Deco, G. (2011) 'Role of local network oscillations in resting-state functional connectivity', *Neuroimage*, 57(1), pp. 130-139.

Cannas, A., Spissu, A., Floris, G.L., Saddi, M.V., Cossu, G., Melis, M., Tacconi, P., Milia, A., Mascia, M.M. and Giagheddu, M. (2001) 'Chronic delusional hallucinatory psychosis in early-onset Parkinson's disease: drug-induced complication or sign of an idiopathic psychiatric illness?', *Neurological Sciences*, 22(1), pp. 53-54.

Caplan, J., Madsen, J., Schulze-Bonhage, A., Aschenbrenner-Scheibe, R., Newman, E. and Kahana, M. (2003) 'Human theta oscillations related to'. References.

Carmichael, O., Xie, J., Fletcher, E., Singh, B., DeCarli, C. and Initiative, A.s.D.N. (2012) 'Localized hippocampus measures are associated with Alzheimer pathology and cognition independent of total hippocampal volume', *Neurobiology of aging*, 33(6), pp. 1124. e31-1124. e41.

Case, M., Shirinpour, S., Zhang, H., Datta, Y.H., Nelson, S.C., Sadak, K.T., Gupta, K. and He, B. (2017) 'Increased theta band EEG power in sickle cell disease patients', *Journal of pain research*, 11, pp. 67-76.

Catani, M., Jones, D.K., Donato, R. and Ffytche, D.H. (2003) 'Occipito-temporal connections in the human brain', *Brain*, 126(9), pp. 2093-2107.

Cauda, F., Torta, D.M., Sacco, K., D'Agata, F., Geda, E., Duca, S., Geminiani, G. and Vercelli, A. (2013) 'Functional anatomy of cortical areas characterized by Von Economo neurons', *Brain Structure and Function*, 218(1), pp. 1-20.

Chan, P.-C., Lee, H.-H., Hong, C.-T., Hu, C.-J. and Wu, D. (2018) 'REM sleep behavior disorder (RBD) in dementia with Lewy bodies (DLB)', *Behavioural neurology*, 2018.

Chang, X., Xi, Y.B., Cui, L.B., Wang, H.N., Sun, J.B., Zhu, Y.Q., Huang, P., Collin, G., Liu, K., Xi, M., Qi, S., Tan, Q.R., Miao, D.M. and Yin, H. (2015) 'Distinct inter-hemispheric dysconnectivity in schizophrenia patients with and without auditory verbal hallucinations', *Sci Rep*, 5, p. 11218.

Chang, Y.-P., Yang, Y.-H., Lai, C.-L. and Liou, L.-M. (2016) 'Event-Related Potentials in Parkinson's Disease Patients with Visual Hallucination', *Parkinson’s Disease*, 2016, p. 1863508.

Chapman, R.M., Armington, J.C. and Bragdon, H.R. (1962) 'A quantitative survey of kappa and alpha EEG activity', *Electroencephalography and Clinical Neurophysiology*, 14(6), pp. 858-868.

Chaumon, M., Hasboun, D., Baulac, M., Adam, C. and Tallon-Baudry, C. (2009) 'Unconscious contextual memory affects early responses in the anterior temporal lobe', *Brain Research*, 1285, pp. 77-87.

Chaumon, M., Kveraga, K., Barrett, L.F. and Bar, M. (2014) 'Visual predictions in the orbitofrontal cortex rely on associative content', *Cerebral cortex*, 24(11), pp. 2899-2907.

Cho, J.-H., Vorwerk, J., Wolters, C.H. and Knösche, T.R. (2015) 'Influence of the head model on EEG and MEG source connectivity analyses', *NeuroImage*, 110, pp. 60-77.

Choi, S.H., Jung, T.M., Lee, J.E., Lee, S.-K., Sohn, Y.H. and Lee, P.H. (2012) 'Volumetric analysis of the substantia innominata in patients with Parkinson's disease according to cognitive status', *Neurobiology of Aging*, 33(7), pp. 1265-1272.

Christensen, H. (2001) 'What cognitive changes can be expected with normal ageing?', *Australian & New Zealand Journal of Psychiatry*, 35(6), pp. 768-775.

Chu, C.J., Tanaka, N., Diaz, J., Edlow, B.L., Wu, O., Hämäläinen, M., Stufflebeam, S., Cash, S.S. and Kramer, M.A. (2015) 'EEG functional connectivity is partially predicted by underlying white matter connectivity', *NeuroImage*, 108, pp. 23-33.

Colclough, G.L., Woolrich, M.W., Tewarie, P., Brookes, M.J., Quinn, A.J. and Smith, S.M. (2016) 'How reliable are MEG resting-state connectivity metrics?', *Neuroimage*, 138, pp. 284-293.

Collerton, D., Perry, E. and McKeith, I. (2005) 'Why people see things that are not there: a novel perception and attention deficit model for recurrent complex visual hallucinations', *Behavioral and Brain Sciences*, 28(6), pp. 737-757.

Colloby, S.J., Firbank, M.J., Vasudev, A., Parry, S.W., Thomas, A.J. and O'Brien, J.T. (2011) 'Cortical thickness and VBM-DARTEL in late-life depression', *Journal of Affective Disorders*, 133(1), pp. 158-164.

Comon, P. (1994) 'Independent component analysis, a new concept?', *Signal processing*, 36(3), pp. 287-314.

Conti, E., Mitra, J., Calderoni, S., Pannek, K., Shen, K.K., Pagnozzi, A., Rose, S., Mazzotti, S., Scelfo, D., Tosetti, M., Muratori, F., Cioni, G. and Guzzetta, A. (2017) 'Network over-connectivity differentiates autism spectrum disorder from other developmental disorders in toddlers: A diffusion MRI study', *Human brain mapping*, 38(5), pp. 2333-2344.

Corbetta, M., Kincade, J.M., Ollinger, J.M., McAvoy, M.P. and Shulman, G.L. (2000) 'Voluntary orienting is dissociated from target detection in human posterior parietal cortex', *Nature neuroscience*, 3(3), pp. 292-297.

Corbetta, M., Patel, G. and Shulman, G.L. (2008) 'The reorienting system of the human brain: from environment to theory of mind', *Neuron*, 58(3), pp. 306-324.

Corbetta, M. and Shulman, G.L. (2002) 'Control of goal-directed and stimulus-driven attention in the brain', *Nat Rev Neurosci*, 3(3), pp. 201-15.

Corby, J.C. and Kopell, B.S. (1972) 'Differential contributions of blinks and vertical eye movements as artifacts in EEG recording', *Psychophysiology*, 9(6), pp. 640-644.

Cromarty, R.A. (2016) *Investigating attentional function and cognitive fluctuations in Lewy body dementia*. Newcastle University.

Cromarty, R.A., Schumacher, J., Graziadio, S., Gallagher, P., Killen, A., Firbank, M.J., Blamire, A., Kaiser, M., Thomas, A.J., O'Brien, J.T., Peraza, L.R. and Taylor, J.-P. (2018) 'Structural Brain Correlates of Attention Dysfunction in Lewy Body Dementias and Alzheimer's Disease', *Frontiers in aging neuroscience*, 10, pp. 347-347.

Crutch, S.J., Schott, J.M., Rabinovici, G.D., Murray, M., Snowden, J.S., van der Flier, W.M., Dickerson, B.C., Vandenberghe, R., Ahmed, S. and Bak, T.H. (2017) 'Consensus classification of posterior cortical atrophy', *Alzheimer's & Dementia*, 13(8), pp. 870-884.

Cummings, J.L. (1997) 'The Neuropsychiatric Inventory: assessing psychopathology in dementia patients', *Neurology*, 48(5 Suppl 6), pp. 10S-16S.

Dale, A.M., Fischl, B. and Sereno, M.I. (1999) 'Cortical Surface-Based Analysis: I. Segmentation and Surface Reconstruction', *NeuroImage*, 9(2), pp. 179-194.

Dale, A.M., Liu, A.K., Fischl, B.R., Buckner, R.L., Belliveau, J.W., Lewine, J.D. and Halgren, E. (2000) 'Dynamic statistical parametric mapping: combining fMRI and MEG for high-resolution imaging of cortical activity', *Neuron*, 26(1), pp. 55-67.

Damoiseaux, J.S. and Greicius, M.D. (2009) 'Greater than the sum of its parts: a review of studies combining structural connectivity and resting-state functional connectivity', *Brain Structure and Function*, 213(6), pp. 525-533.

daSilva Morgan, K., Elder, G.J., ffytche, D.H., Collerton, D. and Taylor, J.-P. (2018) 'The utility and application of electrophysiological methods in the study of visual hallucinations', *Clinical Neurophysiology*, 129(11), pp. 2361-2371.

Dattola, S., La Foresta, F., Bonanno, L., De Salvo, S., Mammone, N., Marino, S. and Morabito, F.C. (2020) 'Effect of Sensor Density on eLORETA Source Localization Accuracy', in Esposito, A., Faundez-Zanuy, M., Morabito, F.C. and Pasero, E. (eds.) *Neural Approaches to Dynamics of Signal Exchanges*. Singapore: Springer Singapore, pp. 403-414.

Dauwan, M., Hoff, J.I., Vriens, E.M., Hillebrand, A., Stam, C.J. and Sommer, I.E. (2019) 'Aberrant resting-state oscillatory brain activity in Parkinson's disease patients with visual hallucinations: An MEG source-space study', *NeuroImage: Clinical*, 22, p. 101752.

Dauwan, M., Linszen, M.M.J., Lemstra, A.W., Scheltens, P., Stam, C.J. and Sommer, I.E. (2018) 'EEG-based neurophysiological indicators of hallucinations in Alzheimer's disease: Comparison with dementia with Lewy bodies', *Neurobiol Aging*, 67, pp. 75-83.

Dauwan, M., van Dellen, E., van Boxtel, L., van Straaten, E.C.W., de Waal, H., Lemstra, A.W., Gouw, A.A., van der Flier, W.M., Scheltens, P., Sommer, I.E. and Stam, C.J. (2016) 'EEG-directed connectivity from posterior brain regions is decreased in dementia with Lewy bodies: a comparison with Alzheimer's disease and controls', *Neurobiology of Aging*, 41(Supplement C), pp. 122-129.

Davidson, P.R., Jones, R.D. and Peiris, M.T. (2007) 'EEG-based lapse detection with high temporal resolution', *IEEE Transactions on Biomedical Engineering*, 54(5), pp. 832-839.

de Folstein, M. (1975) 'Mini-Mental State Examination'. I. Psychological Assessment Resources(PAR), Ed.) Recuperado de hipocampo ….

de Haan, W., Mott, K., van Straaten, E.C., Scheltens, P. and Stam, C.J. (2012a) 'Activity dependent degeneration explains hub vulnerability in Alzheimer's disease', *PLoS Comput Biol*, 8(8), p. e1002582.

de Haan, W., Pijnenburg, Y.A., Strijers, R.L., van der Made, Y., van der Flier, W.M., Scheltens, P. and Stam, C.J. (2009) 'Functional neural network analysis in frontotemporal dementia and Alzheimer's disease using EEG and graph theory', *BMC neuroscience*, 10(1), p. 101.

de Haan, W., van der Flier, W.M., Koene, T., Smits, L.L., Scheltens, P. and Stam, C.J. (2012b) 'Disrupted modular brain dynamics reflect cognitive dysfunction in Alzheimer's disease', *Neuroimage*, 59(4), pp. 3085-93.

de Munck, J.C. (1989) *A mathematical and physical interpretation of the electromagnetic field of the brain*. Universiteit van Amsterdam.

De Myttenaere, A., Golden, B., Le Grand, B. and Rossi, F. (2016) 'Mean absolute percentage error for regression models', *Neurocomputing*, 192, pp. 38-48.

de Vos, R.A.I., Jansen, E.N.H., Stam, F.C., Ravid, R. and Swaab, D.F. (1995) ''Lewy body disease': clinico-pathological correlations in 18 consecutive cases of Parkinson's disease with and without dementia', *Clinical Neurology and Neurosurgery*, 97(1), pp. 13-22.

Deary, I.J., Corley, J., Gow, A.J., Harris, S.E., Houlihan, L.M., Marioni, R.E., Penke, L., Rafnsson, S.B. and Starr, J.M. (2009) 'Age-associated cognitive decline', *British medical bulletin*, 92(1), pp. 135-152.

Decker, D.A. and Knott, J.R. (1972) 'The EEG in intrinsic supratentorial brain tumors: A comparative evaluation', *Electroencephalography and Clinical Neurophysiology*, 33(3), pp. 303-310.

Deco, G. and Jirsa, V.K. (2012) 'Ongoing Cortical Activity at Rest: Criticality, Multistability, and Ghost Attractors', *The Journal of Neuroscience*, 32(10), pp. 3366-3375.

Delbeuck, X., Van der Linden, M. and Collette, F. (2003) 'Alzheimer' Disease as a Disconnection Syndrome?', *Neuropsychology Review*, 13(2), pp. 79-92.

Delli Pizzi, S., Franciotti, R., Tartaro, A., Caulo, M., Thomas, A., Onofrj, M. and Bonanni, L. (2014a) 'Structural alteration of the dorsal visual network in DLB patients with visual hallucinations: a cortical thickness MRI study', *PLoS One*, 9(1), p. e86624.

Delli Pizzi, S., Franciotti, R., Taylor, J.P., Esposito, R., Tartaro, A., Thomas, A., Onofrj, M. and Bonanni, L. (2015a) 'Structural Connectivity is Differently Altered in Dementia with Lewy Body and Alzheimer's Disease', *Front Aging Neurosci*, 7, p. 208.

Delli Pizzi, S., Franciotti, R., Taylor, J.P., Thomas, A., Tartaro, A., Onofrj, M. and Bonanni, L. (2015b) 'Thalamic Involvement in Fluctuating Cognition in Dementia with Lewy Bodies: Magnetic Resonance Evidences', *Cereb Cortex*, 25(10), pp. 3682-9.

Delli Pizzi, S., Maruotti, V., Taylor, J.-P., Franciotti, R., Caulo, M., Tartaro, A., Thomas, A., Onofrj, M. and Bonanni, L. (2014b) 'Relevance of subcortical visual pathways disruption to visual symptoms in dementia with Lewy bodies', *Cortex*, 59, pp. 12-21.

Delorme, A. and Makeig, S. (2004) 'EEGLAB: an open source toolbox for analysis of single-trial EEG dynamics including independent component analysis', *J Neurosci Methods*, 134(1), pp. 9-21.

Destrieux, C., Fischl, B., Dale, A. and Halgren, E. (2010) 'Automatic parcellation of human cortical gyri and sulci using standard anatomical nomenclature', *NeuroImage*, 53(1), pp. 1-15.

Devanand, D.P. and Levy, S.R. (1995) 'Neuroleptic Treatment of Agitation and Psychosis in Dementia', *Journal of Geriatric Psychiatry and Neurology*, 8(1), pp. S18-S27.

Diederich, N.J., Goetz, C.G. and Stebbins, G.T. (2005) 'Repeated visual hallucinations in Parkinson's disease as disturbed external/internal perceptions: focused review and a new integrative model', *Mov Disord*, 20(2), pp. 130-40.

Dierks, T., Jelic, V., Pascual-Marqui, R.D., Wahlund, L.-O., Julin, P., Linden, D.E.J., Maurer, K., Winblad, B. and Nordberg, A. (2000) 'Spatial pattern of cerebral glucose metabolism

(PET) correlates with localization of intracerebral EEG-generators in Alzheimer's disease', *Clinical Neurophysiology*, 111(10), pp. 1817-1824.

Diestel, R. (1997) 'Graph theory. 1997', *Grad. Texts in Math*, 2.

Dijkstra, E.W. (1959) 'A note on two problems in connexion with graphs', *Numerische mathematik*, 1(1), pp. 269-271.

DiQuattro, N.E. and Geng, J.J. (2011) 'Contextual Knowledge Configures Attentional Control Networks', *The Journal of Neuroscience*, 31(49), pp. 18026-18035.

Donchin, E., Ritter, W. and McCallum, W.C. (1978) 'Cognitive psychophysiology: The endogenous components of the ERP', *Event-related brain potentials in man*, 349, p. 411.

Doppelmayr, M., Klimesch, W., Schwaiger, J., Auinger, P. and Winkler, T. (1998) 'Theta synchronization in the human EEG and episodic retrieval', *Neuroscience Letters*, 257(1), pp. 41-44.

Ebersole, J.S. and Ebersole, S.M. (2010) 'Combining MEG and EEG source modeling in epilepsy evaluations', *J Clin Neurophysiol*, 27(6), pp. 360-71.

Edison, P., Rowe, C.C., Rinne, J.O., Ng, S., Ahmed, I., Kemppainen, N., Villemagne, V.L., O'Keefe, G., Nagren, K., Chaudhury, K.R., Masters, C.L. and Brooks, D.J. (2008) 'Amyloid load in Parkinson's disease dementia and Lewy body dementia measured with [11C]PIB positron emission tomography', *J Neurol Neurosurg Psychiatry*, 79(12), pp. 1331-8.

Eguiluz, V.M., Chialvo, D.R., Cecchi, G.A., Baliki, M. and Apkarian, A.V. (2005) 'Scale-free brain functional networks', *Phys Rev Lett*, 94(1), p. 018102.

Eickhoff, S.B., Stephan, K.E., Mohlberg, H., Grefkes, C., Fink, G.R., Amunts, K. and Zilles, K. (2005) 'A new SPM toolbox for combining probabilistic cytoarchitectonic maps and functional imaging data', *Neuroimage*, 25(4), pp. 1325-1335.

Emre, M., Aarsland, D., Brown, R., Burn, D.J., Duyckaerts, C., Mizuno, Y., Broe, G.A., Cummings, J., Dickson, D.W. and Gauthier, S. (2007) 'Clinical diagnostic criteria for dementia associated with Parkinson's disease', *Movement disorders*, 22(12), pp. 1689-1707.

Engels, M.M., Stam, C.J., van der Flier, W.M., Scheltens, P., de Waal, H. and van Straaten, E.C. (2015) 'Declining functional connectivity and changing hub locations in Alzheimer's disease: an EEG study', *BMC Neurol*, 15, p. 145.

Engels, M.M.A., Yu, M., Stam, C.J., Gouw, A.A., van der Flier, W.M., Scheltens, P., van Straaten, E.C.W. and Hillebrand, A. (2017) 'Directional information flow in patients with Alzheimer's disease. A source-space resting-state MEG study', *NeuroImage: Clinical*, 15, pp. 673-681.

Erskine, D. and Khundakar, A. (2016) 'Stereological approaches to dementia research using human brain tissue', *Journal of chemical neuroanatomy*, 76, pp. 73-81.

Erskine, D., Taylor, J.-P., Thomas, A., Collerton, D., McKeith, I., Khundakar, A., Attems, J. and Morris, C. (2019) 'Pathological Changes to the Subcortical Visual System and its Relationship to Visual Hallucinations in Dementia with Lewy Bodies', *Neuroscience Bulletin*, 35(2), pp. 295-300.

Erskine, D., Thomas, A.J., Attems, J., Taylor, J.P., McKeith, I.G., Morris, C.M. and Khundakar, A.A. (2017) 'Specific patterns of neuronal loss in the pulvinar nucleus in dementia with lewy bodies', *Movement Disorders*, 32(3), pp. 414-422.

Fan, J., McCandliss, B.D., Sommer, T., Raz, A. and Posner, M.I. (2002) 'Testing the efficiency and independence of attentional networks', *J Cogn Neurosci*, 14(3), pp. 340-7.

Fathy, Y.Y., Jonker, A.J., Oudejans, E., de Jong, F.J.J., van Dam, A.-M.W., Rozemuller, A.J.M. and van de Berg, W.D.J. (2019) 'Differential insular cortex subregional vulnerability to α-synuclein pathology in Parkinson's disease and dementia with Lewy bodies', *Neuropathology and Applied Neurobiology*, 45(3), pp. 262-277.

Feige, B., Scheffler, K., Esposito, F., Salle, F.D., Hennig, J. and Seifritz, E. (2005) 'Cortical and Subcortical Correlates of Electroencephalographic Alpha Rhythm Modulation', *Journal of Neurophysiology*, 93(5), pp. 2864-2872.

Fénelon, G., Mahieux, F., Huon, R. and Ziégler, M. (2000) 'Hallucinations in Parkinson's disease: Prevalence, phenomenology and risk factors', *Brain*, 123(4), pp. 733-745.

Ferini-Strambi, L., Marelli, S., Galbiati, A., Rinaldi, F. and Giora, E. (2014) 'REM Sleep Behavior Disorder (RBD) as a marker of neurodegenerative disorders', *Arch Ital Biol*, 152(2-3), pp. 129-146.

Ferman, T.J., Boeve, B.F., Smith, G.E., Lin, S.C., Silber, M.H., Pedraza, O., Wszolek, Z., Graff-Radford, N.R., Uitti, R., Van Gerpen, J., Pao, W., Knopman, D., Pankratz, V.S., Kantarci, K., Boot, B., Parisi, J.E., Dugger, B.N., Fujishiro, H., Petersen, R.C. and Dickson, D.W. (2011) 'Inclusion of RBD improves the diagnostic classification of dementia with Lewy bodies', *Neurology*, 77(9), pp. 875-82.

Ferman, T.J., Smith, G.E., Boeve, B.F., Graff-Radford, N.R., Lucas, J.A., Knopman, D.S., Petersen, R.C., Ivnik, R.J., Wszolek, Z. and Uitti, R. (2006) 'Neuropsychological differentiation of dementia with Lewy bodies from normal aging and Alzheimer's disease', *The Clinical Neuropsychologist*, 20(4), pp. 623-636.

Ffytche, D.H., Creese, B., Politis, M., Chaudhuri, K.R., Weintraub, D., Ballard, C. and Aarsland, D. (2017) 'The psychosis spectrum in Parkinson disease', *Nature reviews. Neurology*, 13(2), pp. 81-95.

Finnigan, S., Wong, A. and Read, S. (2016) 'Defining abnormal slow EEG activity in acute ischaemic stroke: Delta/alpha ratio as an optimal QEEG index', *Clinical Neurophysiology*, 127(2), pp. 1452-1459.

Firbank, M.J., Blamire, A.M., Krishnan, M.S., Teodorczuk, A., English, P., Gholkar, A., Harrison, R.M. and O'Brien, J.T. (2007) 'Diffusion tensor imaging in dementia with Lewy bodies and Alzheimer's disease', *Psychiatry Res*, 155(2), pp. 135-45.

Firbank, M.J., Parikh, J., Murphy, N., Killen, A., Allan, C.L., Collerton, D., Blamire, A.M. and Taylor, J.-P. (2018) 'Reduced occipital GABA in Parkinson disease with visual hallucinations', *Neurology*, 91(7), pp. e675-e685.

Fisch, B.J. and Spehlmann, R. (1999) *Fisch and Spehlmann's EEG primer: basic principles of digital and analog EEG*. Elsevier Health Sciences.

Fischl, B. and Dale, A.M. (2000) 'Measuring the thickness of the human cerebral cortex from magnetic resonance images', *Proceedings of the National Academy of Sciences*, 97(20), pp. 11050-11055.

Fischl, B., Van Der Kouwe, A., Destrieux, C., Halgren, E., Ségonne, F., Salat, D.H., Busa, E., Seidman, L.J., Goldstein, J. and Kennedy, D. (2004) 'Automatically parcellating the human cerebral cortex', *Cerebral cortex*, 14(1), pp. 11-22.

Fjell, A.M., Walhovd, K.B., Westlye, L.T., Østby, Y., Tamnes, C.K., Jernigan, T.L., Gamst, A. and Dale, A.M. (2010) 'When does brain aging accelerate? Dangers of quadratic fits in cross-sectional studies', *NeuroImage*, 50(4), pp. 1376-1383.

Fluss, R., Faraggi, D. and Reiser, B. (2005) 'Estimation of the Youden Index and its associated cutoff point', *Biometrical Journal: Journal of Mathematical Methods in Biosciences*, 47(4), pp. 458-472.

Foldi, N.S., Lobosco, J.J. and Schaefer, L.A. (2002) *Seminars in speech and language*. Copyright© 2002 by Thieme Medical Publishers, Inc., 333 Seventh Avenue, New ….

Fox, M.D., Corbetta, M., Snyder, A.Z., Vincent, J.L. and Raichle, M.E. (2006) 'Spontaneous neuronal activity distinguishes human dorsal and ventral attention systems', *Proceedings of the National Academy of Sciences*, 103(26), pp. 10046-10051.

Franciotti, R., Delli Pizzi, S., Perfetti, B., Tartaro, A., Bonanni, L., Thomas, A., Weis, L., Biundo, R., Antonini, A. and Onofrj, M. (2015) 'Default mode network links to visual

hallucinations: a comparison between Parkinson's disease and multiple system atrophy', *Movement Disorders*, 30(9), pp. 1237-1247.

Franciotti, R., Falasca, N.W., Bonanni, L., Anzellotti, F., Maruotti, V., Comani, S., Thomas, A., Tartaro, A., Taylor, J.-P. and Onofrj, M. (2013) 'Default network is not hypoactive in dementia with fluctuating cognition: an Alzheimer disease/dementia with Lewy bodies comparison', *Neurobiology of aging*, 34(4), pp. 1148-1158.

Franciotti, R., Iacono, D., Della Penna, S., Pizzella, V., Torquati, K., Onofrj, M. and Romani, G. (2006) 'Cortical rhythms reactivity in AD, LBD and normal subjects: a quantitative MEG study', *Neurobiology of aging*, 27(8), pp. 1100-1109.

Franciotti, R., Pilotto, A., Moretti, D.V., Falasca, N.W., Arnaldi, D., Taylor, J.-P., Nobili, F., Kramberger, M., Ptacek, S.G., Padovani, A., Aarlsand, D., Onofrj, M. and Bonanni, L. (2020) 'Anterior EEG slowing in dementia with Lewy bodies: a multicenter European cohort study', *Neurobiology of Aging*, 93, pp. 55-60.

Frantzidis, C.A., Vivas, A.B., Tsolaki, A., Klados, M.A., Tsolaki, M. and Bamidis, P.D. (2014) 'Functional disorganization of small-world brain networks in mild Alzheimer's Disease and amnestic Mild Cognitive Impairment: an EEG study using Relative Wavelet Entropy (RWE)', *Frontiers in aging neuroscience*, 6, p. 224.

Freeman, W.J. and Rogers, L.J. (2002) 'Fine temporal resolution of analytic phase reveals episodic synchronization by state transitions in gamma EEGs', *Journal of neurophysiology*, 87(2), pp. 937-945.

French, I.T. and Muthusamy, K.A. (2018) 'A Review of the Pedunculopontine Nucleus in Parkinson's Disease', *Frontiers in Aging Neuroscience*, 10(99).

Frigerio, R., Fujishiro, H., Ahn, T.-B., Josephs, K.A., Maraganore, D.M., DelleDonne, A., Parisi, J.E., Klos, K.J., Boeve, B.F., Dickson, D.W. and Ahlskog, J.E. (2011) 'Incidental Lewy body disease: Do some cases represent a preclinical stage of dementia with Lewy bodies?', *Neurobiology of Aging*, 32(5), pp. 857-863.

Fuchs, M., Wagner, M., Köhler, T. and Wischmann, H.-A. (1999) 'Linear and nonlinear current density reconstructions', *Journal of clinical Neurophysiology*, 16(3), pp. 267-295.

Fujisawa, S. and Buzsáki, G. (2011) 'A 4 Hz oscillation adaptively synchronizes prefrontal, VTA, and hippocampal activities', *Neuron*, 72(1), pp. 153-165.

Gaig, C. and Tolosa, E. (2009) 'When does Parkinson's disease begin?', *Mov Disord*, 24 Suppl 2, pp. S656-64.

Gallagher, D.A., Parkkinen, L., O'Sullivan, S.S., Spratt, A., Shah, A., Davey, C.C., Bremner, F.D., Revesz, T., Williams, D.R., Lees, A.J. and Schrag, A. (2011) 'Testing an aetiological model of visual hallucinations in Parkinson's disease', *Brain*, 134(Pt 11), pp. 3299-309.

Gallagher, M. and Colombo, P.J. (1995) 'Ageing: the cholinergic hypothesis of cognitive decline', *Current opinion in neurobiology*, 5(2), pp. 161-168.

Galvin, J.E., Price, J.L., Yan, Z., Morris, J.C. and Sheline, Y.I. (2011) 'Resting bold fMRI differentiates dementia with Lewy bodies vs Alzheimer disease', *Neurology*, 76(21), pp. 1797-803.

Gamond, L., George, N., Lemaréchal, J.-D., Hugueville, L., Adam, C. and Tallon-Baudry, C. (2011) 'Early influence of prior experience on face perception', *NeuroImage*, 54(2), pp. 1415-1426.

Gaona, C.M., Sharma, M., Freudenburg, Z.V., Breshears, J.D., Bundy, D.T., Roland, J., Barbour, D.L., Schalk, G. and Leuthardt, E.C. (2011) 'Nonuniform high-gamma (60–500 Hz) power changes dissociate cognitive task and anatomy in human cortex', *Journal of Neuroscience*, 31(6), pp. 2091-2100.

Garrison, K.A., Scheinost, D., Finn, E.S., Shen, X. and Constable, R.T. (2015) 'The (in)stability of functional brain network measures across thresholds', *Neuroimage*, 118, pp. 651-61.

Gasca-Salas, C., Clavero, P., García-García, D., Obeso, J.A. and Rodríguez-Oroz, M.C. (2016) 'Significance of visual hallucinations and cerebral hypometabolism in the risk of

dementia in Parkinson's disease patients with mild cognitive impairment', *Hum Brain Mapp*, 37(3), pp. 968-77.

Giessing, C., Thiel, C.M., Alexander-Bloch, A.F., Patel, A.X. and Bullmore, E.T. (2013) 'Human brain functional network changes associated with enhanced and impaired attentional task performance', *The Journal of neuroscience : the official journal of the Society for Neuroscience*, 33(14), pp. 5903-5914.

GLOOR, P., BALL, G. and SCHAUL, N. (1977) 'Brain lesions that produce delta waves in the EEG', *Neurology*, 27(4), pp. 326-326.

Glover, G.H. (2011) 'Overview of functional magnetic resonance imaging', *Neurosurgery clinics of North America*, 22(2), pp. 133-vii.

Glowniak, J.V., Turner, F.E., Gray, L.L., Palac, R.T., Lagunas-Solar, M.C. and Woodward, W.R. (1989) 'Iodine-123 metaiodobenzylguanidine imaging of the heart in idiopathic congestive cardiomyopathy and cardiac transplants', *Journal of nuclear medicine*, 30(7), pp. 1182-1191.

Goel, V., Brambrink, A.M., Baykal, A., Koehler, R.C., Hanley, D.F. and Thakor, N.V. (1996) 'Dominant frequency analysis of EEG reveals brain's response during injury and recovery', *IEEE Transactions on Biomedical Engineering*, 43(11), pp. 1083-1092.

Goetz, C.G., Pappert, E.J., Blasucci, L.M., Stebbins, G.T., Ling, Z.D., Nora, M.V. and Carvey, P.M. (1998) 'Intravenous levodopa in hallucinating Parkinson's disease patients: high-dose challenge does not precipitate hallucinations', *Neurology*, 50(2), pp. 515-7.

Gola, M., Magnuski, M., Szumska, I. and Wróbel, A. (2013) 'EEG beta band activity is related to attention and attentional deficits in the visual performance of elderly subjects', *International Journal of Psychophysiology*, 89(3), pp. 334-341.

Goljahani, A., D'Avanzo, C., Schiff, S., Amodio, P., Bisiacchi, P. and Sparacino, G. (2012) 'A novel method for the determination of the EEG individual alpha frequency', *NeuroImage*, 60(1), pp. 774-786.

Gollo, L.L., Mirasso, C., Sporns, O. and Breakspear, M. (2014) 'Mechanisms of zero-lag synchronization in cortical motifs', *PLoS Comput Biol*, 10(4), p. e1003548.

Gómez-Tortosa, E., Newell, K., Irizarry, M.C., Albert, M., Growdon, J.H. and Hyman, B.T. (1999) 'Clinical and quantitative pathologic correlates of dementia with Lewy bodies', *Neurology*, 53(6), pp. 1284-1284.

Goodin, D.S., Squires, K.C. and Starr, A. (1978) 'Long latency event-related components of the auditory evoked potential in dementia', *Brain*, 101(4), pp. 635-48.

Gorji, A. and Ghadiri, M.K. (2002) 'History of headache in medieval Persian medicine', *The Lancet Neurology*, 1(8), pp. 510-515.

Gorodnitsky, I.F., George, J.S. and Rao, B.D. (1995) 'Neuromagnetic source imaging with FOCUSS: a recursive weighted minimum norm algorithm', *Electroencephalography and clinical Neurophysiology*, 95(4), pp. 231-251.

Gosche, K., Mortimer, J., Smith, C., Markesbery, W. and Snowdon, D. (2002) 'Hippocampal volume as an index of Alzheimer neuropathology: findings from the Nun Study', *Neurology*, 58(10), pp. 1476-1482.

Graham, M.S., Drobnjak, I., Jenkinson, M. and Zhang, H. (2017) 'Quantitative assessment of the susceptibility artefact and its interaction with motion in diffusion MRI', *PLoS One*, 12(10), p. e0185647.

Graham, R.L. and Hell, P. (1985) 'On the History of the Minimum Spanning Tree Problem', *Annals of the History of Computing*, 7(1), pp. 43-57.

Gramfort, A., Papadopoulo, T., Olivi, E. and Clerc, M. (2010) 'OpenMEEG: opensource software for quasistatic bioelectromagnetics', *BioMedical Engineering OnLine*, 9(1), p. 45.

Grandy, T.H., Werkle-Bergner, M., Chicherio, C., Schmiedek, F., Lövdén, M. and Lindenberger, U. (2013) 'Peak individual alpha frequency qualifies as a stable neurophysiological trait marker in healthy younger and older adults', *Psychophysiology*, 50(6), pp. 570-582.

Grave de Peralta Menendez, R., Murray, M.M., Michel, C.M., Martuzzi, R. and Gonzalez Andino, S.L. (2004) 'Electrical neuroimaging based on biophysical constraints', *NeuroImage*, 21(2), pp. 527-539.

Graziadio, S., Basu, A., Tomasevic, L., Zappasodi, F., Tecchio, F. and Eyre, J.A. (2010) 'Developmental tuning and decay in senescence of oscillations linking the corticospinal system', *J Neurosci*, 30(10), pp. 3663-74.

Grech, R., Cassar, T., Muscat, J., Camilleri, K.P., Fabri, S.G., Zervakis, M., Xanthopoulos, P., Sakkalis, V. and Vanrumste, B. (2008) 'Review on solving the inverse problem in EEG source analysis', *Journal of NeuroEngineering and Rehabilitation*, 5(1), p. 25.

Greicius, M.D., Supekar, K., Menon, V. and Dougherty, R.F. (2008) 'Resting-State Functional Connectivity Reflects Structural Connectivity in the Default Mode Network', *Cerebral Cortex*, 19(1), pp. 72-78.

Grimby, A. (1993) 'Bereavement among elderly people: grief reactions, post-bereavement hallucinations and quality of life', *Acta Psychiatr Scand*, 87(1), pp. 72-80.

Güntekin, B., Emek-Savaş, D.D., Kurt, P., Yener, G.G. and Başar, E. (2013) 'Beta oscillatory responses in healthy subjects and subjects with mild cognitive impairment', *NeuroImage: Clinical*, 3, pp. 39-46.

Guye, M., Parker, G.J.M., Symms, M., Boulby, P., Wheeler-Kingshott, C.A.M., Salek-Haddadi, A., Barker, G.J. and Duncan, J.S. (2003) 'Combined functional MRI and tractography to demonstrate the connectivity of the human primary motor cortex in vivo', *NeuroImage*, 19(4), pp. 1349-1360.

Hagemann, D., Naumann, E. and Thayer, J.F. (2001) 'The quest for the EEG reference revisited: A glance from brain asymmetry research', *Psychophysiology*, 38(5), pp. 847-857.

Hahn, K., Myers, N., Prigarin, S., Rodenacker, K., Kurz, A., Förstl, H., Zimmer, C., Wohlschläger, A.M. and Sorg, C. (2013) 'Selectively and progressively disrupted structural connectivity of functional brain networks in Alzheimer's disease — Revealed by a novel framework to analyze edge distributions of networks detecting disruptions with strong statistical evidence', *NeuroImage*, 81, pp. 96-109.

Hämäläinen, M., Hari, R., Ilmoniemi, R.J., Knuutila, J. and Lounasmaa, O.V. (1993) 'Magnetoencephalography---theory, instrumentation, and applications to noninvasive studies of the working human brain', *Reviews of Modern Physics*, 65(2), pp. 413-497.

Hämäläinen, M. and Ilmoniemi, R. (1984) 'Interpreting measured magnetic fields of the brain: Estimates of current distributions', *Technical Report TKK-F-A559 HUT Finland*, 32.

Hamilton, J.M., Salmon, D.P., Galasko, D., Delis, D.C., Hansen, L.A., Masliah, E., Thomas, R.G. and Thal, L.J. (2004) 'A comparison of episodic memory deficits in neuropathologically-confirmed Dementia with Lewy bodies and Alzheimer's disease', *Journal of the International Neuropsychological Society*, 10(5), pp. 689-697.

Hanoglu, L., Yildiz, S., Polat, B., Demirci, S., Mithat Tavli, A., Yilmaz, N. and Yulug, B. (2016) 'Therapeutic effects of rivastigmine and alfa-lipoic acid combination in the Charles Bonnet Syndrome: electroencephalography correlates', *Current clinical pharmacology*, 11(4), pp. 270-273.

Hanyu, H., Shimizu, S., Hirao, K., Kanetaka, H., Iwamoto, T., Chikamori, T., Usui, Y., Yamashina, A., Koizumi, K. and Abe, K. (2006) 'Comparative value of brain perfusion SPECT and [123 I] MIBG myocardial scintigraphy in distinguishing between dementia with Lewy bodies and Alzheimer’s disease', *European journal of nuclear medicine and molecular imaging*, 33(3), pp. 248-253.

Harding, A.J., Broe, G.A. and Halliday, G.M. (2002) 'Visual hallucinations in Lewy body disease relate to Lewy bodies in the temporal lobe', *Brain*, 125(Pt 2), pp. 391-403.

Hardmeier, M., Hatz, F., Bousleiman, H., Schindler, C., Stam, C.J. and Fuhr, P. (2014) 'Reproducibility of functional connectivity and graph measures based on the phase lag index (PLI) and weighted phase lag index (wPLI) derived from high resolution EEG', *PLoS One*, 9(10), p. e108648.

Harper, L., Fumagalli, G.G., Barkhof, F., Scheltens, P., O'Brien, J.T., Bouwman, F., Burton, E.J., Rohrer, J.D., Fox, N.C. and Ridgway, G.R. (2016) 'MRI visual rating scales in the diagnosis of dementia: evaluation in 184 post-mortem confirmed cases', *Brain*, 139(4), pp. 1211-1225.

Harris, J., Atkinson, E., Lee, A., Nithi, K. and Fowler, M. (2003) 'Hemispace differences in the visual perception of size in left hemiParkinson's disease', *Neuropsychologia*, 41(7), pp. 795-807.

Haufe, S., Nikulin, V.V., Müller, K.-R. and Nolte, G. (2013) 'A critical assessment of connectivity measures for EEG data: A simulation study', *NeuroImage*, 64, pp. 120-133.

Hauk, O., Wakeman, D.G. and Henson, R. (2011) 'Comparison of noise-normalized minimum norm estimates for MEG analysis using multiple resolution metrics', *NeuroImage*, 54(3), pp. 1966-1974.

Heimer, L., De Olmos, J., Alheid, G., Person, J., Sakamoto, N., Shinoda, K., Marksteiner, J. and Switzer, R. (1999) 'Handbook of chemical neuroanatomy, Vol. 15: the primate nervous system, part III'.

Helmholtz, H.v. (1853) 'Ueber einige Gesetze der Vertheilung elektrischer Ströme in körperlichen Leitern, mit Anwendung auf die thierisch-elektrischen Versuche (Schluss.)', *Annalen der Physik*, 165(7), pp. 353-377.

Hepp, D.H., Foncke, E.M.J., Berendse, H.W., Wassenaar, T.M., Olde Dubbelink, K.T.E., Groenewegen, H.J., D J van de Berg, W. and Schoonheim, M.M. (2017a) 'Damaged fiber tracts of the nucleus basalis of Meynert in Parkinson's disease patients with visual hallucinations', *Scientific reports*, 7(1), pp. 10112-10112.

Hepp, D.H., Foncke, E.M.J., Dubbelink, K.T.E.O., Berg, W.D.J.v.d., Berendse, H.W. and Schoonheim, M.M. (2017b) 'Loss of Functional Connectivity in Patients with Parkinson Disease and Visual Hallucinations', *Radiology*, 285(3), pp. 896-903.

Hershey, L.A. and Irwin, D.J. (2018) 'Zonisamide for DLB parkinsonism', *An old drug used in a new context*, 90(8), pp. 349-350.

Higuchi, M., Tashiro, M., Arai, H., Okamura, N., Hara, S., Higuchi, S., Itoh, M., Shin, R.W., Trojanowski, J.Q. and Sasaki, H. (2000) 'Glucose hypometabolism and neuropathological correlates in brains of dementia with Lewy bodies', *Exp Neurol*, 162(2), pp. 247-56.

Hilgetag, C.C. and Goulas, A. (2016) 'Is the brain really a small-world network?', *Brain Structure and Function*, 221(4), pp. 2361-2366.

Hillebrand, A., Tewarie, P., Van Dellen, E., Yu, M., Carbo, E.W., Douw, L., Gouw, A.A., Van Straaten, E.C. and Stam, C.J. (2016) 'Direction of information flow in large-scale resting-state networks is frequency-dependent', *Proceedings of the National Academy of Sciences*, 113(14), pp. 3867-3872.

Hincapié, A.-S., Kujala, J., Mattout, J., Pascarella, A., Daligault, S., Delpuech, C., Mery, D., Cosmelli, D. and Jerbi, K. (2017) 'The impact of MEG source reconstruction method on source-space connectivity estimation: A comparison between minimum-norm solution and beamforming', *NeuroImage*, 156, pp. 29-42.

Hindriks, R., Woolrich, M., Luckhoo, H., Joensson, M., Mohseni, H., Kringelbach, M.L. and Deco, G. (2015) 'Role of white-matter pathways in coordinating alpha oscillations in resting visual cortex', *Neuroimage*, 106, pp. 328-39.

Holm, S. (1979) 'A simple sequentially rejective multiple test procedure', *Scandinavian journal of statistics*, pp. 65-70.

Holroyd, S., Currie, L. and Wooten, G.F. (2001) 'Prospective study of hallucinations and delusions in Parkinson's disease', *J Neurol Neurosurg Psychiatry*, 70(6), pp. 734-8.

Holsheimer, J. and Feenstra, B.W.A. (1977) 'Volume conduction and EEG measurements within the brain: A quantitative approach to the influence of electrical spread on the linear relationship of activity measured at different locations', *Electroencephalography and Clinical Neurophysiology*, 43(1), pp. 52-58.

Honey, C.J., Sporns, O., Cammoun, L., Gigandet, X., Thiran, J.-P., Meuli, R. and Hagmann, P. (2009) 'Predicting human resting-state functional connectivity from structural connectivity', *Proceedings of the National Academy of Sciences*, 106(6), pp. 2035-2040.

Hornykiewicz, O. and Kish, S.J. (1987) 'Biochemical pathophysiology of Parkinson's disease', *Adv Neurol*, 45, pp. 19-34.

Horowitz, M.J. (1975) 'Hallucinations: An information-processing approach', *Hallucinations: Behavior, experience and theory*, pp. 163-196.

Howard, R., Brammer, M., David, A., Woodruff, P. and Williams, S. (1998) 'The anatomy of conscious vision: an fMRI study of visual hallucinations', *Nature neuroscience*, 1(8), pp. 738-742.

Huizenga, H., Van Zuijen, T., Heslenfeld, D.J. and Molenaar, P. (2001) 'Simultaneous MEG and EEG source analysis', *Physics in Medicine & Biology*, 46(7), p. 1737.

Humphries, M.D. and Gurney, K. (2008) 'Network 'Small-World-Ness': A Quantitative Method for Determining Canonical Network Equivalence', *PLOS ONE*, 3(4), p. e0002051.

Huppert, F.A., Brayne, C., Gill, C., Paykel, E.S. and Beardsall, L. (1995) 'CAMCOG—A concise neuropsychological test to assist dementia diagnosis: Socio-demographic determinants

in an elderly population sample', *British Journal of Clinical Psychology*, 34(4), pp. 529-541.

Hyvarinen, A. (1999) *ISCAS'99. Proceedings of the 1999 IEEE International Symposium on Circuits and Systems VLSI (Cat. No. 99CH36349)*. IEEE.

Hyvärinen, A. and Oja, E. (2000) 'Independent component analysis: algorithms and applications', *Neural networks*, 13(4-5), pp. 411-430.

Iizuka, T. and Kameyama, M. (2016) 'Cingulate island sign on FDG-PET is associated with medial temporal lobe atrophy in dementia with Lewy bodies', *Annals of Nuclear Medicine*, 30(6), pp. 421-429.

Imperatori, L.S., Betta, M., Cecchetti, L., Canales-Johnson, A., Ricciardi, E., Siclari, F., Pietrini, P., Chennu, S. and Bernardi, G. (2019) 'EEG functional connectivity metrics wPLI and wSMI account for distinct types of brain functional interactions', *Scientific Reports*, 9(1), p. 8894.

Ingvar, D.H., Rosén, I. and Johannesson, G. (1979) 'EEG Related to Cerebral Metabolism and Blood Flow', *Pharmacopsychiatry*, 12(02), pp. 200-209.

Inzelberg, R., Kipervasser, S. and Korczyn, A.D. (1998) 'Auditory hallucinations in Parkinson's disease', *Journal of Neurology, Neurosurgery & Psychiatry*, 64(4), pp. 533-535.

Iturria-Medina, Y., Canales-Rodríguez, E.J., Melie-García, L., Valdés-Hernández, P.A., Martínez-Montes, E., Alemán-Gómez, Y. and Sánchez-Bornot, J. (2007) 'Characterizing brain anatomical connections using diffusion weighted MRI and graph theory', *Neuroimage*, 36(3), pp. 645-660.

Jackson, C.E. and Snyder, P.J. (2008) 'Electroencephalography and event-related potentials as biomarkers of mild cognitive impairment and mild Alzheimer's disease', *Alzheimers Dement*, 4(1 Suppl 1), pp. S137-43.

Jalili, M. (2016) 'Functional Brain Networks: Does the Choice of Dependency Estimator and Binarization Method Matter?', *Scientific Reports*, 6, p. 29780.

Jalili, M. (2017) 'Graph theoretical analysis of Alzheimer's disease: Discrimination of AD patients from healthy subjects', *Information Sciences*, 384, pp. 145-156.

Jasper, H.H. and Andrews, H.L. (1938) 'Brain potentials and voluntary muscle activity in man', *Journal of Neurophysiology*, 1(2), pp. 87-100.

Jbabdi, S., Sotiropoulos, S.N., Haber, S.N., Van Essen, D.C. and Behrens, T.E. (2015) 'Measuring macroscopic brain connections in vivo', *Nature neuroscience*, 18(11), p. 1546.

Jenkinson, M., Bannister, P., Brady, M. and Smith, S. (2002) 'Improved optimization for the robust and accurate linear registration and motion correction of brain images', *Neuroimage*, 17(2), pp. 825-41.

Jenkinson, M., Beckmann, C.F., Behrens, T.E., Woolrich, M.W. and Smith, S.M. (2012) 'FSL', *Neuroimage*, 62(2), pp. 782-90.

Jensen, O. and Mazaheri, A. (2010) 'Shaping functional architecture by oscillatory alpha activity: gating by inhibition', *Frontiers in human neuroscience*, 4, p. 186.

Jicha, G.A., Schmitt, F.A., Abner, E., Nelson, P.T., Cooper, G.E., Smith, C.D. and Markesbery, W.R. (2010) 'Prodromal clinical manifestations of neuropathologically confirmed Lewy body disease', *Neurobiology of aging*, 31(10), pp. 1805-1813.

Jimenez, A.M., Lee, J., Wynn, J.K., Cohen, M.S., Engel, S.A., Glahn, D.C., Nuechterlein, K.H., Reavis, E.A. and Green, M.F. (2016) 'Abnormal ventral and dorsal attention network activity during single and dual target detection in schizophrenia', *Frontiers in psychology*, 7, p. 323.

Johansen-Berg, H. and Behrens, T.E. (2013) *Diffusion MRI: from quantitative measurement to in vivo neuroanatomy*. Academic Press.

Jones, D.K. (2010) 'Challenges and limitations of quantifying brain connectivity in vivo with diffusion MRI', *Imaging in Medicine*, 2(3), pp. 341–355.

Jones, D.K., Knösche, T.R. and Turner, R. (2013) 'White matter integrity, fiber count, and other fallacies: The do's and don'ts of diffusion MRI', *NeuroImage*, 73, pp. 239-254.

Jordan, K.G. (2004) 'Emergency EEG and continuous EEG monitoring in acute ischemic stroke', *Journal of clinical neurophysiology*, 21(5), pp. 341-352.

Jurcak, V., Tsuzuki, D. and Dan, I. (2007) '10/20, 10/10, and 10/5 systems revisited: their validity as relative head-surface-based positioning systems', *Neuroimage*, 34(4), pp. 1600-1611.

Kai, T., Asai, Y., Sakuma, K., Koeda, T. and Nakashima, K. (2005) 'Quantitative electroencephalogram analysis in dementia with Lewy bodies and Alzheimer's disease', *J Neurol Sci*, 237(1-2), pp. 89-95.

Kaiser, M. (2011) 'A tutorial in connectome analysis: Topological and spatial features of brain networks', *NeuroImage*, 57(3), pp. 892-907.

Kaiser, M., Martin, R., Andras, P. and Young, M.P. (2007) 'Simulation of robustness against lesions of cortical networks', *European Journal of Neuroscience*, 25(10), pp. 3185-3192.

Kamiński, J., Brzezicka, A., Gola, M. and Wróbel, A. (2012) 'Beta band oscillations engagement in human alertness process', *International Journal of Psychophysiology*, 85(1), pp. 125-128.

Kantarci, K., Avula, R., Senjem, M.L., Samikoglu, A.R., Zhang, B., Weigand, S.D., Przybelski, S.A., Edmonson, H.A., Vemuri, P., Knopman, D.S., Ferman, T.J., Boeve, B.F., Petersen, R.C. and Jack, C.R., Jr. (2010) 'Dementia with Lewy bodies and Alzheimer disease: neurodegenerative patterns characterized by DTI', *Neurology*, 74(22), pp. 1814-1821.

Kastner, S., Pinsk, M.A., De Weerd, P., Desimone, R. and Ungerleider, L.G. (1999) 'Increased Activity in Human Visual Cortex during Directed Attention in the Absence of Visual Stimulation', *Neuron*, 22(4), pp. 751-761.

Kertesz, A. (1982) *Western aphasia battery test manual*. Psychological Corp.

Kirino, E. (2007) 'MISMATCH NEGATIVITY CORRELATES WITH DELTA AND THETA EEG POWER IN SCHIZOPHRENIA', *International Journal of Neuroscience*, 117(9), pp. 1257-1279.

Kirov, R., Weiss, C., Siebner, H.R., Born, J. and Marshall, L. (2009) 'Slow oscillation electrical brain stimulation during waking promotes EEG theta activity and memory encoding', *Proceedings of the National Academy of Sciences*, 106(36), pp. 15460-15465.

Klimesch, W., Doppelmayr, M., Russegger, H., Pachinger, T. and Schwaiger, J. (1998) 'Induced alpha band power changes in the human EEG and attention', *Neuroscience Letters*, 244(2), pp. 73-76.

Klimesch, W., Schimke, H. and Schwaiger, J. (1994) 'Episodic and semantic memory: an analysis in the EEG theta and alpha band', *Electroencephalography and Clinical Neurophysiology*, 91(6), pp. 428-441.

Kobayashi, S., Tateno, M., Morii, H., Utsumi, K. and Saito, T. (2009) 'Decreased cardiac MIBG uptake, its correlation with clinical symptoms in dementia with Lewy bodies', *Psychiatry Research: Neuroimaging*, 174(1), pp. 76-80.

Kobeleva, X., Firbank, M., Peraza, L., Gallagher, P., Thomas, A., Burn, D.J., O'Brien, J. and Taylor, J.-P. (2017) 'Divergent functional connectivity during attentional processing in Lewy body dementia and Alzheimer's disease', *Cortex*, 92, pp. 8-18.

Kosaka, K. (1978) 'Lewy bodies in cerebral cortex. Report of three cases', *Acta Neuropathologica*, 42(2), pp. 127-134.

Kosaka, K., Yoshimura, M., Ikeda, K. and Budka, H. (1984) 'Diffuse type of Lewy body disease: progressive dementia with abundant cortical Lewy bodies and senile changes of varying degree--a new disease?', *Clin Neuropathol*, 3(5), pp. 185-92.

Krall, S.C., Rottschy, C., Oberwelland, E., Bzdok, D., Fox, P.T., Eickhoff, S.B., Fink, G.R. and Konrad, K. (2015) 'The role of the right temporoparietal junction in attention and social interaction as revealed by ALE meta-analysis', *Brain structure & function*, 220(2), pp. 587-604.

Krishnaswamy, P., Obregon-Henao, G., Ahveninen, J., Khan, S., Babadi, B., Iglesias, J.E., Hämäläinen, M.S. and Purdon, P.L. (2017) 'Sparsity enables estimation of both subcortical and cortical activity from MEG and EEG', *Proceedings of the National Academy of Sciences*, 114(48), pp. E10465-E10474.

Kurita, A., Murakami, M., Takagi, S., Matsushima, M. and Suzuki, M. (2010) 'Visual hallucinations and altered visual information processing in Parkinson disease and dementia with Lewy bodies', *Mov Disord*, 25(2), pp. 167-71.

Kurita, A., Nakamura, M., Suzuki, M., Mochio, S. and Inoue, K. (2005) 'Visual and auditory event-related potential comparisons between Parkinson's disease with dementia and Alzheimer's disease', *International Congress Series*, 1278, pp. 57-60.

Kveraga, K., Ghuman, A.S. and Bar, M. (2007) 'Top-down predictions in the cognitive brain', *Brain and cognition*, 65(2), pp. 145-168.

Kybic, J., Clerc, M., Abboud, T., Faugeras, O., Keriven, R. and Papadopoulo, T. (2005) 'A common formalism for the Integral formulations of the forward EEG problem', *IEEE Transactions on Medical Imaging*, 24(1), pp. 12-28.

Lai, M., Demuru, M., Hillebrand, A. and Fraschini, M. (2018) 'A comparison between scalp-and source-reconstructed EEG networks', *Scientific reports*, 8(1), pp. 1-8.

Lancichinetti, A. and Fortunato, S. (2012) 'Consensus clustering in complex networks', *Scientific Reports*, 2(1), p. 336.

Lang, X., Wang, L., Zhuo, C.-J., Jia, F., Wang, L.-N. and Wang, C.-L. (2016) 'Reduction of interhemispheric functional connectivity in sensorimotor and visual information processing pathways in schizophrenia', *Chinese medical journal*, 129(20), p. 2422.

Langer, N., Pedroni, A. and Jancke, L. (2013) 'The problem of thresholding in small-world network analysis', *PLoS One*, 8(1), p. e53199.

Langlois, D., Chartier, S. and Gosselin, D. (2010) 'An introduction to independent component analysis: InfoMax and FastICA algorithms', *Tutorials in Quantitative Methods for Psychology*, 6(1), pp. 31-38.

Larson, C.L., Davidson, R.J., Abercrombie, H.C., Ward, R.T., Schaefer, S.M., Jackson, D.C., Holden, J.E. and Perlman, S.B. (1998) 'Relations between PET-derived measures of thalamic glucose metabolism and EEG alpha power', *Psychophysiology*, 35(2), pp. 162-169.

Law, Z.K., Todd, C., Mehraram, R., Schumacher, J., Baker, M.R., LeBeau, F.E., Yarnall, A., Onofrj, M., Bonanni, L. and Thomas, A. (2020) 'The Role of EEG in the Diagnosis, Prognosis and Clinical Correlations of Dementia with Lewy Bodies—A Systematic Review', *Diagnostics*, 10(9), p. 616.

Lee, A., Harris, J., Atkinson, E. and Fowler, M. (2001) 'Evidence from a line bisection task for visuospatial neglect in left hemiparkinson's disease', *Vision Research*, 41(20), pp. 2677-2686.

Lee, J.C. and Tan, D.S. (2006) *Proceedings of the 19th annual ACM symposium on User interface software and technology*. ACM.

Lee, J.E., Park, H.J., Park, B., Song, S.K., Sohn, Y.H., Lee, J.D. and Lee, P.H. (2010a) 'A comparative analysis of cognitive profiles and white-matter alterations using voxel-

based diffusion tensor imaging between patients with Parkinson's disease dementia and dementia with Lewy bodies', *J Neurol Neurosurg Psychiatry*, 81(3), pp. 320-6.

Lee, U., Oh, G., Kim, S., Noh, G., Choi, B. and Mashour, G.A. (2010b) 'Brain networks maintain a scale-free organization across consciousness, anesthesia, and recovery: evidence for adaptive reconfiguration', *Anesthesiology*, 113(5), pp. 1081-91.

Lee, Y.-Y. and Hsieh, S. (2014) 'Classifying different emotional states by means of EEG-based functional connectivity patterns', *PloS one*, 9(4).

Leech, R. and Sharp, D.J. (2014) 'The role of the posterior cingulate cortex in cognition and disease', *Brain*, 137(1), pp. 12-32.

Lega, B.C., Jacobs, J. and Kahana, M. (2012) 'Human hippocampal theta oscillations and the formation of episodic memories', *Hippocampus*, 22(4), pp. 748-761.

Lei, X. and Liao, K. (2017) 'Understanding the Influences of EEG Reference: A Large-Scale Brain Network Perspective', *Frontiers in Neuroscience*, 11(205).

Lemstra, A.W., Eikelenboom, P. and van Gool, W.A. (2003) 'The cholinergic deficiency syndrome and its therapeutic implications', *Gerontology*, 49(1), pp. 55-60.

Lemstra, A.W., van Boxtel, L., van Straaten, E.C.W., de Waal, H., Smits, L., van der Flier, W.M., Scheltens, P., Stam, C. and van Dellen, E. (2014) 'Directed Anterior-To-Posterior Communication in the Brain Is Reversed in Dementia With Lewy Bodies and Is Related To Attention Deficits', *Alzheimer's & Dementia: The Journal of the Alzheimer's Association*, 10(4), p. P349.

Li, R., Wu, X., Fleisher, A.S., Reiman, E.M., Chen, K. and Yao, L. (2012) 'Attention-related networks in Alzheimer's disease: A resting functional MRI study', *Human Brain Mapping*, 33(5), pp. 1076-1088.

Li, Y., Liu, Y., Li, J., Qin, W., Li, K., Yu, C. and Jiang, T. (2009) 'Brain anatomical network and intelligence', *PLoS computational biology*, 5(5), pp. e1000395-e1000395.

Lin, Q.-H., Zheng, Y.-R., Yin, F.-L., Liang, H. and Calhoun, V.D. (2007) 'A fast algorithm for one-unit ICA-R', *Information Sciences*, 177(5), pp. 1265-1275.

Liotti, M. and Tucker, D.M. (1992) 'Right hemisphere sensitivity to arousal and depression', *Brain and Cognition*, 18(2), pp. 138-151.

Lippa, C.F., Duda, J.E., Grossman, M., Hurtig, H.I., Aarsland, D., Boeve, B.F., Brooks, D.J., Dickson, D.W., Dubois, B., Emre, M., Fahn, S., Farmer, J.M., Galasko, D., Galvin, J.E., Goetz, C.G., Growdon, J.H., Gwinn-Hardy, K.A., Hardy, J., Heutink, P., Iwatsubo, T., Kosaka, K., Lee, V.M.-Y., Leverenz, J.B., Masliah, E., McKeith, I.G., Nussbaum, R.L., Olanow, C.W., Ravina, B.M., Singleton, A.B., Tanner, C.M., Trojanowski, J.Q. and Wszolek, Z.K. (2007) 'DLB and PDD boundary issues', *Diagnosis, treatment, molecular pathology, and biomarkers*, 68(11), pp. 812-819.

Liu, A.K.L., Chang, R.C.-C., Pearce, R.K.B. and Gentleman, S.M. (2015) 'Nucleus basalis of Meynert revisited: anatomy, history and differential involvement in Alzheimer's and Parkinson's disease', *Acta neuropathologica*, 129(4), pp. 527-540.

Livingstone, M.S. and Hubel, D.H. (1987) 'Psychophysical evidence for separate channels for the perception of form, color, movement, and depth', *Journal of Neuroscience*, 7(11), pp. 3416-3468.

Lobier, M., Siebenhühner, F., Palva, S. and Palva, J.M. (2014) 'Phase transfer entropy: a novel phase-based measure for directed connectivity in networks coupled by oscillatory interactions', *Neuroimage*, 85, pp. 853-872.

Lobotesis, K., Fenwick, J., Phipps, A., Ryman, A., Swann, A., Ballard, C., McKeith, I. and O'Brien, J. (2001) 'Occipital hypoperfusion on SPECT in dementia with Lewy bodies but not AD', *Neurology*, 56(5), pp. 643-649.

Lopes da Silva, F. (2013) 'EEG and MEG: relevance to neuroscience', *Neuron*, 80(5), pp. 1112-28.

Lopes da Silva, F.H., van Lierop, T.H.M.T., Schrijer, C.F. and Storm van Leeuwen, W. (1973) 'Organization of thalamic and cortical alpha rhythms: Spectra and coherences', *Electroencephalography and Clinical Neurophysiology*, 35(6), pp. 627-639.

Louis, E.D., Goldman, J.E., Powers, J.M. and Fahn, S. (1995) 'Parkinsonian features of eight pathologically diagnosed cases of diffuse Lewy body disease', *Movement disorders: official journal of the Movement Disorder Society*, 10(2), pp. 188-194.

Luck, S.J. (2014) *An introduction to the event-related potential technique*. MIT press.

Luders, H.O. (2008) *Textbook of epilepsy surgery*. CRC Press.

Lytton, W.W. and Sejnowski, T.J. (1991) 'Simulations of cortical pyramidal neurons synchronized by inhibitory interneurons', *J Neurophysiol*, 66(3), pp. 1059-79.

Mack, G.A. and Skillings, J.H. (1980) 'A Friedman-type rank test for main effects in a two-factor ANOVA', *Journal of the American Statistical Association*, 75(372), pp. 947-951.

Mahjoory, K., Nikulin, V.V., Botrel, L., Linkenkaer-Hansen, K., Fato, M.M. and Haufe, S. (2017) 'Consistency of EEG source localization and connectivity estimates', *Neuroimage*, 152, pp. 590-601.

Mak, E., Su, L., Williams, G.B. and O'Brien, J.T. (2014) 'Neuroimaging characteristics of dementia with Lewy bodies', *Alzheimer's research & therapy*, 6(2), pp. 18-18.

Makeig, S. and Onton, J. (2011) 'ERP features and EEG dynamics: an ICA perspective', *Oxford handbook of event-related potential components*.

Mansfield, P. (1984) 'Real-time echo-planar imaging by NMR', *Br Med Bull*, 40(2), pp. 187-90.

Marshall, L., Helgadóttir, H., Mölle, M. and Born, J. (2006) 'Boosting slow oscillations during sleep potentiates memory', *Nature*, 444(7119), pp. 610-3.

Matsui, H., Udaka, F., Tamura, A., Oda, M., Kubori, T., Nishinaka, K. and Kameyama, M. (2005) 'The relation between visual hallucinations and visual evoked potential in Parkinson disease', *Clinical neuropharmacology*, 28(2), pp. 79-82.

Mattila, P.M., Roytta, M., Torikka, H., Dickson, D.W. and Rinne, J.O. (1998) 'Cortical Lewy bodies and Alzheimer-type changes in patients with Parkinson's disease', *Acta Neuropathol*, 95(6), pp. 576-82.

Mazoyer, B., Zago, L., Mellet, E., Bricogne, S., Etard, O., Houdé, O., Crivello, F., Joliot, M., Petit, L. and Tzourio-Mazoyer, N. (2001) 'Cortical networks for working memory and executive functions sustain the conscious resting state in man', *Brain research bulletin*, 54(3), pp. 287-298.

Mazziotta, J., Toga, A., Evans, A., Fox, P., Lancaster, J., Zilles, K., Woods, R., Paus, T., Simpson, G., Pike, B., Holmes, C., Collins, L., Thompson, P., MacDonald, D., Iacoboni, M., Schormann, T., Amunts, K., Palomero-Gallagher, N., Geyer, S., Parsons, L., Narr, K., Kabani, N., Le Goualher, G., Boomsma, D., Cannon, T., Kawashima, R. and Mazoyer, B. (2001) 'A probabilistic atlas and reference system for the human brain: International Consortium for Brain Mapping (ICBM)', *Philosophical transactions of the Royal Society of London. Series B, Biological sciences*, 356(1412), pp. 1293-1322.

McCleery, J., Morgan, S., Bradley, K.M., Noel-Storr, A.H., Ansorge, O. and Hyde, C. (2015) 'Dopamine transporter imaging for the diagnosis of dementia with Lewy bodies', *Cochrane Database of Systematic Reviews*, (1).

McKeith, I. (2007a) 'Dementia with Lewy bodies', in *Handbook of clinical Neurology*. Elsevier, pp. 531-548.

McKeith, I. (2007b) 'Dementia with Lewy bodies and Parkinson's disease with dementia: where two worlds collide', *Pract Neurol*, 7(6), pp. 374-82.

McKeith, I., O'Brien, J., Walker, Z., Tatsch, K., Booij, J., Darcourt, J., Padovani, A., Giubbini, R., Bonuccelli, U., Volterrani, D., Holmes, C., Kemp, P., Tabet, N., Meyer, I. and Reininger, C.

(2007) 'Sensitivity and specificity of dopamine transporter imaging with 123I-FP-CIT SPECT in dementia with Lewy bodies: a phase III, multicentre study', *Lancet Neurol*, 6(4), pp. 305-13.

McKeith, I.G., Boeve, B.F., Dickson, D.W., Halliday, G., Taylor, J.P., Weintraub, D., Aarsland, D., Galvin, J., Attems, J., Ballard, C.G., Bayston, A., Beach, T.G., Blanc, F., Bohnen, N., Bonanni, L., Bras, J., Brundin, P., Burn, D., Chen-Plotkin, A., Duda, J.E., El-Agnaf, O., Feldman, H., Ferman, T.J., Ffytche, D., Fujishiro, H., Galasko, D., Goldman, J.G., Gomperts, S.N., Graff-Radford, N.R., Honig, L.S., Iranzo, A., Kantarci, K., Kaufer, D., Kukull, W., Lee, V.M.Y., Leverenz, J.B., Lewis, S., Lippa, C., Lunde, A., Masellis, M., Masliah, E., McLean, P., Mollenhauer, B., Montine, T.J., Moreno, E., Mori, E., Murray, M., O'Brien, J.T., Orimo, S., Postuma, R.B., Ramaswamy, S., Ross, O.A., Salmon, D.P., Singleton, A., Taylor, A., Thomas, A., Tiraboschi, P., Toledo, J.B., Trojanowski, J.Q., Tsuang, D., Walker, Z., Yamada, M. and Kosaka, K. (2017) 'Diagnosis and management of dementia with Lewy bodies: Fourth consensus report of the DLB Consortium', *Neurology*, 89(1), pp. 88-100.

McKeith, I.G., Dickson, D.W., Lowe, J., Emre, M., O'Brien, J.T., Feldman, H., Cummings, J., Duda, J.E., Lippa, C., Perry, E.K., Aarsland, D., Arai, H., Ballard, C.G., Boeve, B., Burn, D.J., Costa, D., Del Ser, T., Dubois, B., Galasko, D., Gauthier, S., Goetz, C.G., Gomez-Tortosa, E., Halliday, G., Hansen, L.A., Hardy, J., Iwatsubo, T., Kalaria, R.N., Kaufer, D., Kenny, R.A., Korczyn, A., Kosaka, K., Lee, V.M., Lees, A., Litvan, I., Londos, E., Lopez, O.L., Minoshima, S., Mizuno, Y., Molina, J.A., Mukaetova-Ladinska, E.B., Pasquier, F., Perry, R.H., Schulz, J.B., Trojanowski, J.Q. and Yamada, M. (2005) 'Diagnosis and management of dementia with Lewy bodies: third report of the DLB Consortium', *Neurology*, 65(12), pp. 1863-72.

McKeith, I.G., Galasko, D., Kosaka, K., Perry, E., Dickson, D.W., Hansen, L., Salmon, D., Lowe, J., Mirra, S. and Byrne, E. (1996) 'Consensus guidelines for the clinical and pathologic diagnosis of dementia with Lewy bodies (DLB): report of the consortium on DLB international workshop', *Neurology*, 47(5), pp. 1113-1124.

McKellar, P. (1957) *Imagination and thinking: A psychological analysis*. Oxford, England: Basic Books.

McKhann, G.M., Knopman, D.S., Chertkow, H., Hyman, B.T., Jack, C.R., Kawas, C.H., Klunk, W.E., Koroshetz, W.J., Manly, J.J. and Mayeux, R. (2011) 'The diagnosis of dementia due to Alzheimer's disease: Recommendations from the National Institute on Aging-Alzheimer's Association workgroups on diagnostic guidelines for Alzheimer's disease', *Alzheimer's & dementia: the journal of the Alzheimer's Association*, 7(3), pp. 263-269.

McMenamin, B.W., Shackman, A.J., Maxwell, J.S., Bachhuber, D.R.W., Koppenhaver, A.M., Greischar, L.L. and Davidson, R.J. (2010) 'Validation of ICA-based myogenic artifact correction for scalp and source-localized EEG', *NeuroImage*, 49(3), pp. 2416-2432.

Mehraram, R., Kaiser, M., Cromarty, R., Graziadio, S., O'Brien, J.T., Killen, A., Taylor, J.P. and Peraza, L.R. (2019) 'Weighted network measures reveal differences between dementia types: An EEG study', *Hum Brain Mapp*.

Menon, V. and Uddin, L.Q. (2010) 'Saliency, switching, attention and control: a network model of insula function', *Brain Structure and Function*, 214(5-6), pp. 655-667.

Messaritaki, E., Dimitriadis, S.I. and Jones, D.K. (2019) 'Optimization of graph construction can significantly increase the power of structural brain network studies', *NeuroImage*, 199, pp. 495-511.

Mesulam, M.-M. (1990) 'Human brain cholinergic pathways', in *Progress in brain research*. Elsevier, pp. 231-241.

Meunier, D., Achard, S., Morcom, A. and Bullmore, E. (2009) 'Age-related changes in modular organization of human brain functional networks', *Neuroimage*, 44(3), pp. 715-723.

Milo, R., Shen-Orr, S., Itzkovitz, S., Kashtan, N., Chklovskii, D. and Alon, U. (2002) 'Network motifs: simple building blocks of complex networks', *Science*, 298(5594), pp. 824-827.

Mima, T., Oluwatimilehin, T., Hiraoka, T. and Hallett, M. (2001) 'Transient Interhemispheric Neuronal Synchrony Correlates with Object Recognition', *The Journal of Neuroscience*, 21(11), pp. 3942-3948.

Minoshima, S., Foster, N.L., Sima, A.A.F., Frey, K.A., Albin, R.L. and Kuhl, D.E. (2001) 'Alzheimer's disease versus dementia with Lewy bodies: Cerebral metabolic distinction with autopsy confirmation', *Annals of Neurology*, 50(3), pp. 358-365.

Mirandola, L., Mai, R.F., Francione, S., Pelliccia, V., Gozzo, F., Sartori, I., Nobili, L., Cardinale, F., Cossu, M. and Meletti, S. (2017) 'Stereo-EEG: diagnostic and therapeutic tool for periventricular nodular heterotopia epilepsies', *Epilepsia*, 58(11), pp. 1962-1971.

Molloy, S., McKeith, I., O'brien, J. and Burn, D. (2005) 'The role of levodopa in the management of dementia with Lewy bodies', *Journal of Neurology, Neurosurgery & Psychiatry*, 76(9), pp. 1200-1203.

Moretti, D.V., Babiloni, C., Binetti, G., Cassetta, E., Dal Forno, G., Ferreric, F., Ferri, R., Lanuzza, B., Miniussi, C. and Nobili, F. (2004) 'Individual analysis of EEG frequency and band power in mild Alzheimer's disease', *Clinical Neurophysiology*, 115(2), pp. 299-308.

Morillas-Romero, A., Tortella-Feliu, M., Bornas, X. and Putman, P. (2015) 'Spontaneous EEG theta/beta ratio and delta–beta coupling in relation to attentional network functioning and self-reported attentional control', *Cognitive, Affective, & Behavioral Neuroscience*, 15(3), pp. 598-606.

Mormann, F., Lehnertz, K., David, P. and E. Elger, C. (2000) 'Mean phase coherence as a measure for phase synchronization and its application to the EEG of epilepsy patients', *Physica D: Nonlinear Phenomena*, 144(3), pp. 358-369.

Morris, J.S., Öhman, A. and Dolan, R.J. (1999) 'A subcortical pathway to the right amygdala mediating "unseen" fear', *Proceedings of the National Academy of Sciences*, 96(4), pp. 1680-1685.

Moseley, M.E., Cohen, Y., Kucharczyk, J., Mintorovitch, J., Asgari, H.S., Wendland, M.F., Tsuruda, J. and Norman, D. (1990) 'Diffusion-weighted MR imaging of anisotropic water diffusion in cat central nervous system', *Radiology*, 176(2), pp. 439-445.

Mosher, J.C., Lewis, P.S. and Leahy, R.M. (1992) 'Multiple dipole modeling and localization from spatio-temporal MEG data', *IEEE Transactions on Biomedical Engineering*, 39(6), pp. 541-557.

Mosimann, U.P., Collerton, D., Dudley, R., Meyer, T.D., Graham, G., Dean, J.L., Bearn, D., Killen, A., Dickinson, L., Clarke, M.P. and McKeith, I.G. (2008) 'A semi-structured interview to assess visual hallucinations in older people', *Int J Geriatr Psychiatry*, 23(7), pp. 712-8.

Mulholland, T. and Runnals, S. (1962) 'Increased Occurrence of Eeg Alpha During Increased Attention', *The Journal of Psychology*, 54(2), pp. 317-330.

Murphy, N. (2016) *Understanding the temporal dynamics of visual hallucinations in Parkinson's Disease with dementia*. Newcastle University.

Muthukumaraswamy, S. (2013) 'High-frequency brain activity and muscle artifacts in MEG/EEG: a review and recommendations', *Frontiers in human neuroscience*, 7, p. 138.

Nedelska, Z., Schwarz, C.G., Boeve, B.F., Lowe, V.J., Reid, R.I., Przybelski, S.A., Lesnick, T.G., Gunter, J.L., Senjem, M.L., Ferman, T.J., Smith, G.E., Geda, Y.E., Knopman, D.S., Petersen, R.C., Jack, C.R., Jr. and Kantarci, K. (2015) 'White matter integrity in dementia with Lewy bodies: a voxel-based analysis of diffusion tensor imaging', *Neurobiol Aging*, 36(6), pp. 2010-7.

Nelson, A.B., Moisello, C., Lin, J., Panday, P., Ricci, S., Canessa, A., Di Rocco, A., Quartarone, A., Frazzitta, G. and Isaias, I.U. (2017) 'Beta oscillatory changes and retention of motor skills during practice in healthy subjects and in patients with Parkinson's disease', *Frontiers in human neuroscience*, 11, p. 104.

Newman, M.E. (2001) 'Scientific collaboration networks. II. Shortest paths, weighted networks, and centrality', *Physical review E*, 64(1), p. 016132.

Newman, M.E. (2006) 'Modularity and community structure in networks', *Proceedings of the national academy of sciences*, 103(23), pp. 8577-8582.

Nunez, P.L. (1988) 'Methods to estimate spatial properties of dynamic cortical source activity', *Functional brain imaging*, pp. 3-9.

O'Brien, J.T., Colloby, S., Fenwick, J., Williams, E.D., Firbank, M., Burn, D., Aarsland, D. and McKeith, I.G. (2004) 'Dopamine transporter loss visualized with FP-CIT SPECT in the differential diagnosis of dementia with Lewy bodies', *Arch Neurol*, 61(6), pp. 919-25.

O'Donovan, J., Watson, R., Colloby, S.J., Firbank, M.J., Burton, E.J., Barber, R., Blamire, A.M. and O'Brien, J.T. (2013) 'Does posterior cortical atrophy on MRI discriminate between Alzheimer's disease, dementia with Lewy bodies, and normal aging?', *International Psychogeriatrics*, 25(1), pp. 111-119.

O'Callaghan, C., Kveraga, K., Shine, J.M., Adams, R.B. and Bar, M. (2017) 'Predictions penetrate perception: Converging insights from brain, behaviour and disorder', *Consciousness and Cognition*, 47, pp. 63-74.

Oertel, V., Rotarska-Jagiela, A., van de Ven, V.G., Haenschel, C., Maurer, K. and Linden, D.E. (2007) 'Visual hallucinations in schizophrenia investigated with functional magnetic resonance imaging', *Psychiatry Research: Neuroimaging*, 156(3), pp. 269-273.

Ohayon, M.M. (2000) 'Prevalence of hallucinations and their pathological associations in the general population', *Psychiatry Res*, 97(2-3), pp. 153-64.

Oken, B.S. and Chiappa, K.H. (1988) 'Short-term variability in EEG frequency analysis', *Electroencephalography and Clinical Neurophysiology*, 69(3), pp. 191-198.

Onnela, J.-P., Saramäki, J., Kertész, J. and Kaski, K. (2005) 'Intensity and coherence of motifs in weighted complex networks', *Physical Review E*, 71(6), p. 065103.

Onoda, K. and Yamaguchi, S. (2013) 'Small-worldness and modularity of the resting-state functional brain network decrease with aging', *Neuroscience Letters*, 556, pp. 104-108.

Onofrj, M., Espay, A.J., Bonanni, L., Delli Pizzi, S. and Sensi, S.L. (2019) 'Hallucinations, somatic-functional disorders of PD-DLB as expressions of thalamic dysfunction', *Movement Disorders*, 34(8), pp. 1100-1111.

Oostenveld, R., Fries, P., Maris, E. and Schoffelen, J.M. (2011) 'FieldTrip: Open source software for advanced analysis of MEG, EEG, and invasive electrophysiological data', *Comput Intell Neurosci*, 2011, p. 156869.

Oostenveld, R. and Praamstra, P. (2001) 'The five percent electrode system for high-resolution EEG and ERP measurements', *Clinical neurophysiology*, 112(4), pp. 713-719.

Opsahl, T., Agneessens, F. and Skvoretz, J. (2010) 'Node centrality in weighted networks: Generalizing degree and shortest paths', *Social Networks*, 32(3), pp. 245-251.

Organization, W.H. (2012) *Dementia: a public health priority*. World Health Organization.

Ota, M., Sato, N., Ogawa, M., Murata, M., Kuno, S., Kida, J. and Asada, T. (2009) 'Degeneration of dementia with Lewy bodies measured by diffusion tensor imaging', *NMR in Biomedicine: An International Journal Devoted to the Development and Application of Magnetic Resonance In vivo*, 22(3), pp. 280-284.

Palmqvist, S., Hansson, O., Minthon, L. and Londos, E. (2009) 'Practical suggestions on how to differentiate dementia with Lewy bodies from Alzheimer's disease with common cognitive tests', *Int J Geriatr Psychiatry*, 24(12), pp. 1405-12.

Panayiotopoulos, C. (1994) 'Elementary visual hallucinations in migraine and epilepsy', *Journal of Neurology, Neurosurgery & Psychiatry*, 57(11), pp. 1371-1374.

Pao, W.C., Boeve, B.F., Ferman, T.J., Lin, S.-C., Smith, G.E., Knopman, D.S., Graff-Radford, N.R., Petersen, R.C., Parisi, J.E. and Dickson, D.W. (2013) 'Polysomnographic findings in dementia with Lewy bodies', *The neurologist*, 19(1), p. 1.

Pascual-Marqui, R.D. (1999a) 'REPLY TO COMMENTS MADE BY R. GRAVE DE PERALTA MENENDEZ AND SL GOZALEZ ANDINO [10]'.

Pascual-Marqui, R.D. (1999b) 'Review of methods for solving the EEG inverse problem', *International journal of bioelectromagnetism*, 1(1), pp. 75-86.

Pascual-Marqui, R.D. (2002) 'Standardized low-resolution brain electromagnetic tomography (sLORETA): technical details', *Methods Find Exp Clin Pharmacol*, 24 Suppl D, pp. 5-12.

Pascual-Marqui, R.D. (2007) 'Discrete, 3D distributed, linear imaging methods of electric neuronal activity. Part 1: exact, zero error localization', *arXiv preprint arXiv:0710.3341*.

Pasquier, J., Michel, B.F., Brenot-Rossi, I., Hassan-Sebbag, N., Sauvan, R. and Gastaut, J.L. (2002) 'Value of (99m)Tc-ECD SPET for the diagnosis of dementia with Lewy bodies', *Eur J Nucl Med Mol Imaging*, 29(10), pp. 1342-8.

Paulson, G.W. (1997) 'Visual hallucinations in the elderly', *Gerontology*, 43(5), pp. 255-60.

Penttilä, M., Partanen, J.V., Soininen, H. and Riekkinen, P.J. (1985) 'Quantitative analysis of occipital EEG in different stages of Alzheimer's disease', *Electroencephalography and Clinical Neurophysiology*, 60(1), pp. 1-6.

Peraza, L.R., Asghar, A.U.R., Green, G. and Halliday, D.M. (2012) 'Volume conduction effects in brain network inference from electroencephalographic recordings using phase lag index', *Journal of Neuroscience Methods*, 207(2), pp. 189-199.

Peraza, L.R., Cromarty, R., Kobeleva, X., Firbank, M.J., Killen, A., Graziadio, S., Thomas, A.J., O'Brien, J.T. and Taylor, J.P. (2018) 'Electroencephalographic derived network differences in Lewy body dementia compared to Alzheimer's disease patients', *Sci Rep*, 8(1), p. 4637.

Peraza, L.R., Kaiser, M., Firbank, M., Graziadio, S., Bonanni, L., Onofrj, M., Colloby, S.J., Blamire, A., O'Brien, J. and Taylor, J.P. (2014) 'fMRI resting state networks and their association with cognitive fluctuations in dementia with Lewy bodies', *Neuroimage Clin*, 4, pp. 558-65.

Peraza, L.R., Taylor, J.-P. and Kaiser, M. (2015) 'Divergent brain functional network alterations in dementia with Lewy bodies and Alzheimer's disease', *Neurobiology of aging*, 36(9), pp. 2458-2467.

Perkins, N.J. and Schisterman, E.F. (2005) 'The Youden index and the optimal cut-point corrected for measurement error', *Biometrical Journal: Journal of Mathematical Methods in Biosciences*, 47(4), pp. 428-441.

Perneczky, R., Drzezga, A., Boecker, H., Förstl, H., Kurz, A. and Häussermann, P. (2008) 'Cerebral metabolic dysfunction in patients with dementia with Lewy bodies and visual hallucinations', *Dementia and geriatric cognitive disorders*, 25(6), pp. 531-538.

Perriol, M.P., Dujardin, K., Derambure, P., Marcq, A., Bourriez, J.L., Laureau, E., Pasquier, F., Defebvre, L. and Destée, A. (2005) 'Disturbance of sensory filtering in dementia with Lewy bodies: comparison with Parkinson's disease dementia and Alzheimer's disease', *J Neurol Neurosurg Psychiatry*, 76(1), pp. 106-8.

Perry, E.K., McKeith, I., Thompson, P., Marshall, E., Kerwin, J., Jabeen, S., Edwardson, J.A., Ince, P., Blessed, G., Irving, D. and et al. (1991) 'Topography, extent, and clinical relevance of neurochemical deficits in dementia of Lewy body type, Parkinson's disease, and Alzheimer's disease', *Ann N Y Acad Sci*, 640, pp. 197-202.

Perry, E.K. and Perry, R.H. (1995) 'Acetylcholine and hallucinations: disease-related compared to drug-induced alterations in human consciousness', *Brain Cogn*, 28(3), pp. 240-58.

Perry, R.J. and Hodges, J.R. (1999) 'Attention and executive deficits in Alzheimer's disease: A critical review', *Brain*, 122(3), pp. 383-404.

Petcharunpaisan, S., Ramalho, J. and Castillo, M. (2010) 'Arterial spin labeling in neuroimaging', *World journal of radiology*, 2(10), pp. 384-398.

Pezzoli, S., Cagnin, A., Antonini, A. and Venneri, A. (2019) 'Frontal and subcortical contribution to visual hallucinations in dementia with Lewy bodies and Parkinson's disease', *Postgrad Med*, 131(7), pp. 509-522.

Pfurtscheller, G. (2000) 'Spatiotemporal ERD/ERS patterns during voluntary movement and motor imagery', in *Supplements to Clinical neurophysiology*. Elsevier, pp. 196-198.

Pilotto, A., Schiano di Cola, F., Premi, E., Grasso, R., Turrone, R., Gipponi, S., Scalvini, A., Cottini, E., Paghera, B., Garibotto, V., Rizzetti, M.C., Bonanni, L., Borroni, B., Morbelli, S., Nobili, F., Guerra, U.P., Perani, D. and Padovani, A. (2019) 'Extrastriatal dopaminergic and serotonergic pathways in Parkinson's disease and in dementia with Lewy bodies: a 123I-FP-CIT SPECT study', *European Journal of Nuclear Medicine and Molecular Imaging*, 46(8), pp. 1642-1651.

Pimlott, S.L., Piggott, M., Ballard, C., McKeith, I., Perry, R., Kometa, S., Owens, J., Wyper, D. and Perry, E. (2006) 'Thalamic nicotinic receptors implicated in disturbed consciousness in dementia with Lewy bodies', *Neurobiology of disease*, 21(1), pp. 50-56.

Pizzagalli, D.A., Oakes, T.R. and Davidson, R.J. (2003) 'Coupling of theta activity and glucose metabolism in the human rostral anterior cingulate cortex: An EEG/PET study of normal and depressed subjects', *Psychophysiology*, 40(6), pp. 939-949.

Pletnikova, O., West, N., Lee, M.K., Rudow, G.L., Skolasky, R.L., Dawson, T.M., Marsh, L. and Troncoso, J.C. (2005) 'Aβ deposition is associated with enhanced cortical α-synuclein lesions in Lewy body diseases', *Neurobiology of Aging*, 26(8), pp. 1183-1192.

Pokryszko-Dragan, A., Słotwiński, K. and Podemski, R. (2003) 'Modality-specific changes in P300 parameters in patients with dementia of the Alzheimer type', *Med Sci Monit*, 9(4), pp. Cr130-4.

Ponten, S.C., Douw, L., Bartolomei, F., Reijneveld, J.C. and Stam, C.J. (2009) 'Indications for network regularization during absence seizures: Weighted and unweighted graph theoretical analyses', *Experimental Neurology*, 217(1), pp. 197-204.

Prinz, P.N. and Vitiell, M.V. (1989) 'Dominant occipital (alpha) rhythm frequency in early stage Alzheimer's disease and depression', *Electroencephalography and Clinical Neurophysiology*, 73(5), pp. 427-432.

Raghavachari, S., Lisman, J.E., Tully, M., Madsen, J.R., Bromfield, E. and Kahana, M.J. (2006) 'Theta oscillations in human cortex during a working-memory task: evidence for local generators', *Journal of neurophysiology*, 95(3), pp. 1630-1638.

Raichle, M.E. (2015) 'The brain's default mode network', *Annual review of neuroscience*, 38, pp. 433-447.

Rasch, B. and Born, J. (2013) 'About sleep's role in memory', *Physiol Rev*, 93(2), pp. 681-766.

Ray, W. and Cole, H. (1985) 'EEG alpha activity reflects attentional demands, and beta activity reflects emotional and cognitive processes', *Science*, 228(4700), pp. 750-752.

Reinagel, P., Godwin, D., Sherman, S.M. and Koch, C. (1999) 'Encoding of Visual Information by LGN Bursts', *Journal of Neurophysiology*, 81(5), pp. 2558-2569.

Reitan, R.M. (1958) 'Validity of the Trail Making Test as an Indicator of Organic Brain Damage', *Perceptual and Motor Skills*, 8(3), pp. 271-276.

Reuter-Lorenz, P.A. and Cappell, K.A. (2008) 'Neurocognitive aging and the compensation hypothesis', *Current directions in psychological science*, 17(3), pp. 177-182.

Ricci, M., Guidoni, S.V., Sepe-Monti, M., Bomboi, G., Antonini, G., Blundo, C. and Giubilei, F. (2009) 'Clinical findings, functional abilities and caregiver distress in the early stage of dementia with Lewy bodies (DLB) and Alzheimer's disease (AD)', *Archives of Gerontology and Geriatrics*, 49(2), pp. e101-e104.

Ricci, S., Mehraram, R., Tatti, E., Nelson, A.B., Bossini-Baroggi, M., Panday, P., Lin, N. and Ghilardi, M.F. (2019) 'Aging Does Not Affect Beta Modulation during Reaching Movements', *Neural plasticity*, 2019.

Riekkinen, P., Buzsaki, G., Riekkinen, P., Soininen, H. and Partanen, J. (1991) 'The cholinergic system and EEG slow waves', *Electroencephalography and Clinical Neurophysiology*, 78(2), pp. 89-96.

Rizzo, G., Arcuti, S., Copetti, M., Alessandria, M., Savica, R., Fontana, A., Liguori, R. and Logroscino, G. (2018) 'Accuracy of clinical diagnosis of dementia with Lewy bodies: a systematic review and meta-analysis', *Journal of Neurology, Neurosurgery & Psychiatry*, 89(4), pp. 358-366.

Roberts, J. and Robinson, P. (2008) 'Modeling distributed axonal delays in mean-field brain dynamics', *Physical Review E*, 78(5), p. 051901.

Robertson, L.C. and Ivry, R. (2000) 'Hemispheric asymmetries: Attention to visual and auditory primitives', *Current Directions in Psychological Science*, 9(2), pp. 59-63.

Robinson, P., Rennie, C., Wright, J., Bahramali, H., Gordon, E. and Rowe, D. (2001) 'Prediction of electroencephalographic spectra from neurophysiology', *Physical Review E*, 63(2), p. 021903.

Rodriguez, G., Copello, F., Vitali, P., Perego, G. and Nobili, F. (1999) 'EEG spectral profile to stage Alzheimer's disease', *Clinical Neurophysiology*, 110(10), pp. 1831-1837.

Roelfsema, P.R., Engel, A.K., König, P. and Singer, W. (1997) 'Visuomotor integration is associated with zero time-lag synchronization among cortical areas', *Nature*, 385(6612), pp. 157-161.

Roks, G., Korf, E., Van der Flier, W., Scheltens, P. and Stam, C. (2008) 'The use of EEG in the diagnosis of dementia with Lewy bodies', *Journal of Neurology, Neurosurgery & Psychiatry*, 79(4), pp. 377-380.

Rota, M. and Antolini, L. (2014) 'Finding the optimal cut-point for Gaussian and Gamma distributed biomarkers', *Computational Statistics & Data Analysis*, 69, pp. 1-14.

Roth, M., Huppert, F., Mountjoy, C. and Tym, E. (1988) 'Cambridge Cognitive Examination (CAMCOG)', *CAMDEX: The Cambridge Examination for Mental Disorders of the Elderly. Cambridge: Cambridge University*, pp. 19-28.

Rubinov, M., Knock, S.A., Stam, C.J., Micheloyannis, S., Harris, A.W., Williams, L.M. and Breakspear, M. (2009) 'Small-world properties of nonlinear brain activity in schizophrenia', *Hum Brain Mapp*, 30(2), pp. 403-16.

Rubinov, M. and Sporns, O. (2010) 'Complex network measures of brain connectivity: Uses and interpretations', *NeuroImage*, 52(3), pp. 1059-1069.

Sakai, K., Ikeda, T., Ishida, C., Komai, K. and Yamada, M. (2019) 'Delusions and visual hallucinations in a patient with Parkinson's disease with dementia showing pronounced Lewy body pathology in the nucleus basalis of Meynert', *Neuropathology*, 39(4), pp. 319-323.

Sakkalis, V. (2011) 'Review of advanced techniques for the estimation of brain connectivity measured with EEG/MEG', *Computers in Biology and Medicine*, 41(12), pp. 1110-1117.

Salinsky, M., Oken, B. and Morehead, L. (1991) 'Test-retest reliability in EEG frequency analysis', *Electroencephalogr Clin Neurophysiol*, 79(5), pp. 382-392.

Schapira, A.H. and Jenner, P. (2011) 'Etiology and pathogenesis of Parkinson's disease', *Movement Disorders*, 26(6), pp. 1049-1055.

Schneider, J.A., Arvanitakis, Z., Bang, W. and Bennett, D.A. (2007) 'Mixed brain pathologies account for most dementia cases in community-dwelling older persons', *Neurology*, 69(24), pp. 2197-2204.

Schoffelen, J.-M. and Gross, J. (2009) 'Source connectivity analysis with MEG and EEG', *Human Brain Mapping*, 30(6), pp. 1857-1865.

Schreckenberger, M., Lange-Asschenfeld, C., Lochmann, M., Mann, K., Siessmeier, T., Buchholz, H.-G., Bartenstein, P. and Gründer, G. (2004) 'The thalamus as the generator

and modulator of EEG alpha rhythm: a combined PET/EEG study with lorazepam challenge in humans', *NeuroImage*, 22(2), pp. 637-644.

Schultz, G. and Melzack, R. (1991) 'The Charles Bonnet syndrome: 'phantom visual images'', *Perception*, 20(6), pp. 809-25.

Schumacher, J., Peraza, L.R., Firbank, M., Thomas, A.J., Kaiser, M., Gallagher, P., O'Brien, J.T., Blamire, A.M. and Taylor, J.-P. (2019) 'Dysfunctional brain dynamics and their origin in Lewy body dementia', *Brain*, 142(6), pp. 1767-1782.

Schumacher, J., Taylor, J.P., Hamilton, C.A., Firbank, M., Cromarty, R.A., Donaghy, P.C., Roberts, G., Allan, L., Lloyd, J., Durcan, R., Barnett, N., O'Brien, J.T. and Thomas, A.J. (2020a) 'Quantitative EEG as a biomarker in mild cognitive impairment with Lewy bodies', *Alzheimers Res Ther*, 12(1), p. 82.

Schumacher, J., Thomas, A.J., Peraza, L.R., Firbank, M., Cromarty, R., Hamilton, C.A., Donaghy, P.C., O'Brien, J.T. and Taylor, J.-P. (2020b) 'EEG alpha reactivity and cholinergic system integrity in Lewy body dementia and Alzheimer's disease', *Alzheimer's research & therapy*, 12, pp. 1-12.

Schürmann, M., Demiralp, T., Başar, E. and Başar Eroglu, C. (2000) 'Electroencephalogram alpha (8–15 Hz) responses to visual stimuli in cat cortex, thalamus, and hippocampus: a distributed alpha network?', *Neuroscience Letters*, 292(3), pp. 175-178.

Schwartz, G., Davidson, R. and Maer, F. (1975) 'Right hemisphere lateralization for emotion in the human brain: interactions with cognition', *Science*, 190(4211), pp. 286-288.

Scrascia, F., Curcio, G., Ursini, F., Trotta, L., Quintiliani, L., Migliore, S., Altamura, C., Pitocco, F., Altavilla, R., Melgari, J.-M., Quattrocchi, C.C. and Vernieri, F. (2014) 'Relationship among Diffusion Tensor Imaging, EEG Activity, and Cognitive Status in Mild Cognitive Impairment and Alzheimer's Disease Patients', *Journal of Alzheimer's Disease*, 38, pp. 939-950.

Seeber, M., Cantonas, L.-M., Hoevels, M., Sesia, T., Visser-Vandewalle, V. and Michel, C.M. (2019) 'Subcortical electrophysiological activity is detectable with high-density EEG source imaging', *Nature Communications*, 10(1), p. 753.

Selden, N.R., Gitelman, D.R., Salamon-Murayama, N., Parrish, T.B. and Mesulam, M.-M. (1998) 'Trajectories of cholinergic pathways within the cerebral hemispheres of the human brain', *Brain: a journal of neurology*, 121(12), pp. 2249-2257.

Shepard, D. (1968) 'A two-dimensional interpolation function for irregularly-spaced data', *Proceedings of the 1968 23rd ACM national conference*. Association for Computing Machinery, pp. 517–524. Available at: https://doi.org/10.1145/800186.810616.

Shimizu, S., Hanyu, H., Kanetaka, H., Iwamoto, T., Koizumi, K. and Abe, K. (2005) 'Differentiation of Dementia with Lewy Bodies from Alzheimer's Disease Using Brain SPECT', *Dementia and Geriatric Cognitive Disorders*, 20(1), pp. 25-30.

Shimizu, S., Hirose, D., Namioka, N., Kanetaka, H., Hirao, K., Hatanaka, H., Takenoshita, N., Kaneko, Y., Ogawa, Y., Umahara, T., Sakurai, H. and Hanyu, H. (2017) 'Correlation between clinical symptoms and striatal DAT uptake in patients with DLB', *Annals of Nuclear Medicine*, 31(5), pp. 390-398.

Shin, S., Lee, J.E., Hong, J.Y., Sunwoo, M.-K., Sohn, Y.H. and Lee, P.H. (2012) 'Neuroanatomical substrates of visual hallucinations in patients with non-demented Parkinson's disease', *Journal of Neurology, Neurosurgery & Psychiatry*, 83(12), pp. 1155-1161.

Shine, J.M., Halliday, G.H., Carlos, M., Naismith, S.L. and Lewis, S.J. (2012) 'Investigating visual misperceptions in Parkinson's disease: a novel behavioral paradigm', *Movement Disorders*, 27(4), pp. 500-505.

Shine, J.M., Halliday, G.M., Gilat, M., Matar, E., Bolitho, S.J., Carlos, M., Naismith, S.L. and Lewis, S.J.G. (2014) 'The role of dysfunctional attentional control networks in visual misperceptions in Parkinson's disease', *Human Brain Mapping*, 35(5), pp. 2206-2219.

Shine, J.M., Halliday, G.M., Naismith, S.L. and Lewis, S.J. (2011) 'Visual misperceptions and hallucinations in Parkinson's disease: dysfunction of attentional control networks?', *Movement Disorders*, 26(12), pp. 2154-2159.

Shulman, G.L., Ollinger, J.M., Akbudak, E., Conturo, T.E., Snyder, A.Z., Petersen, S.E. and Corbetta, M. (1999) 'Areas involved in encoding and applying directional expectations to moving objects', *Journal of Neuroscience*, 19(21), pp. 9480-9496.

Siegel, M., Donner, T.H., Oostenveld, R., Fries, P. and Engel, A.K. (2008) 'Neuronal Synchronization along the Dorsal Visual Pathway Reflects the Focus of Spatial Attention', *Neuron*, 60(4), pp. 709-719.

Simpson, G.V., Weber, D.L., Dale, C.L., Pantazis, D., Bressler, S.L., Leahy, R.M. and Luks, T.L. (2011) 'Dynamic Activation of Frontal, Parietal, and Sensory Regions Underlying Anticipatory Visual Spatial Attention', *The Journal of Neuroscience*, 31(39), pp. 13880-13889.

Smith, S. (2005) 'EEG in the diagnosis, classification, and management of patients with epilepsy', *Journal of Neurology, Neurosurgery & Psychiatry*, 76(suppl 2), pp. ii2-ii7.

Snyder, A.C., Issar, D. and Smith, M.A. (2018) 'What does scalp electroencephalogram coherence tell us about long-range cortical networks?', *European Journal of Neuroscience*, 48(7), pp. 2466-2481.

Snyder, A.C. and Smith, M.A. (2015) 'Stimulus-dependent spiking relationships with the EEG', *Journal of neurophysiology*, 114(3), pp. 1468-1482.

Soininen, H. and Riekkinen, P.J. (1992) 'EEG in diagnostics and follow-up of Alzheimer's disease', *Acta Neurologica Scandinavica*, 85(139), pp. 36-39.

Song, J., Birn, R.M., Boly, M., Meier, T.B., Nair, V.A., Meyerand, M.E. and Prabhakaran, V. (2014) 'Age-related reorganizational changes in modularity and functional connectivity of human brain networks', *Brain Connect*, 4(9), pp. 662-76.

Song, J., Davey, C., Poulsen, C., Luu, P., Turovets, S., Anderson, E., Li, K. and Tucker, D. (2015) 'EEG source localization: sensor density and head surface coverage', *Journal of neuroscience methods*, 256, pp. 9-21.

Sotiropoulos, S.N. and Zalesky, A. (2019) 'Building connectomes using diffusion MRI: why, how and but', *NMR Biomed*, 32(4), p. e3752.

Spence, S., Shapiro, D. and Zaidel, E. (1996) 'The role of the right hemisphere in the physiological and cognitive components of emotional processing', *Psychophysiology*, 33(2), pp. 112-122.

Sporns, O., Tononi, G. and Kötter, R. (2005) 'The human connectome: a structural description of the human brain', *PLoS computational biology*, 1(4).

Sporns, O. and Zwi, J.D. (2004) 'The small world of the cerebral cortex', *Neuroinformatics*, 2(2), pp. 145-162.

Stam, C.J. (2014) 'Modern network science of neurological disorders', *Nat Rev Neurosci*, 15(10), pp. 683-95.

Stam, C.J., de Haan, W., Daffertshofer, A., Jones, B.F., Manshanden, I., van Cappellen van Walsum, A.M., Montez, T., Verbunt, J.P.A., de Munck, J.C., van Dijk, B.W., Berendse, H.W. and Scheltens, P. (2009) 'Graph theoretical analysis of magnetoencephalographic functional connectivity in Alzheimer's disease', *Brain*, 132(1), pp. 213-224.

Stam, C.J., Jones, B.F., Nolte, G., Breakspear, M. and Scheltens, P. (2007a) 'Small-World Networks and Functional Connectivity in Alzheimer's Disease', *Cerebral Cortex*, 17(1), pp. 92-99.

Stam, C.J., Nolte, G. and Daffertshofer, A. (2007b) 'Phase lag index: assessment of functional connectivity from multi channel EEG and MEG with diminished bias from common sources', *Hum Brain Mapp*, 28(11), pp. 1178-93.

Stam, C.J., Tewarie, P., Van Dellen, E., van Straaten, E.C., Hillebrand, A. and Van Mieghem, P. (2014) 'The trees and the forest: Characterization of complex brain networks with minimum spanning trees', *Int J Psychophysiol*, 92(3), pp. 129-38.

Stam, C.J., van Straaten, E.C.W., Van Dellen, E., Tewarie, P., Gong, G., Hillebrand, A., Meier, J. and Van Mieghem, P. (2016) 'The relation between structural and functional connectivity patterns in complex brain networks', *International Journal of Psychophysiology*, 103, pp. 149-160.

Stefan, H., Bracha, M. and Wolkowitz, O.M. (1989) 'High prevalence of visual hallucinations in research subjects with chronic schizophrenia', *Am J Psychiatry*, 146(4), pp. 526-528.

Stropahl, M., Bauer, A.-K.R., Debener, S. and Bleichner, M.G. (2018) 'Source-Modeling Auditory Processes of EEG Data Using EEGLAB and Brainstorm', *Frontiers in Neuroscience*, 12(309).

Stylianou, M., Murphy, N., Peraza, L.R., Graziadio, S., Cromarty, R., Killen, A., JT, O.B., Thomas, A.J., LeBeau, F.E.N. and Taylor, J.P. (2018) 'Quantitative electroencephalography as a marker of cognitive fluctuations in dementia with Lewy bodies and an aid to differential diagnosis', *Clin Neurophysiol*, 129(6), pp. 1209-1220.

Summerfield, C., Egner, T., Greene, M., Koechlin, E., Mangels, J. and Hirsch, J. (2006) 'Predictive codes for forthcoming perception in the frontal cortex', *Science*, 314(5803), pp. 1311-1314.

Sun, L., Cao, J., na Chu, F., Wang, Z. and Lv, Y. (2014a) 'Dementia with Lewy bodies versus nonconvulsive status epilepticus in the diagnosis of a patient with cognitive dysfunction, complex visual hallucinations and periodic abnormal waves in EEG: a case report', *BMC neurology*, 14(1), p. 112.

Sun, Y., Wong, A.K. and Kamel, M.S. (2009) 'Classification of imbalanced data: A review', *International Journal of Pattern Recognition and Artificial Intelligence*, 23(04), pp. 687-719.

Sun, Y., Yin, Q., Fang, R., Yan, X., Wang, Y., Bezerianos, A., Tang, H., Miao, F. and Sun, J. (2014b) 'Disrupted functional brain connectivity and its association to structural connectivity in amnestic mild cognitive impairment and Alzheimer's disease', *PLoS One*, 9(5), p. e96505.

Szelies, B., Mielke, R., Kessler, J. and Heiss, W.-D. (1999) 'EEG power changes are related to regional cerebral glucose metabolism in vascular dementia', *Clinical Neurophysiology*, 110(4), pp. 615-620.

Tadel, F., Baillet, S., Mosher, J.C., Pantazis, D. and Leahy, R.M. (2011) 'Brainstorm: a user-friendly application for MEG/EEG analysis', *Comput Intell Neurosci*, 2011, p. 879716.

Tarantola, A. (2005) *Inverse problem theory and methods for model parameter estimation*. siam.

Tatti, E., Ricci, S., Mehraram, R., Lin, N., George, S., Nelson, A.B. and Ghilardi, M.F. (2019) 'Beta Modulation Depth Is Not Linked to Movement Features', *Frontiers in Behavioral Neuroscience*, 13(49).

Taylor, J.-P., Firbank, M.J., He, J., Barnett, N., Pearce, S., Livingstone, A., Vuong, Q., McKeith, I.G. and O'Brien, J.T. (2012) 'Visual cortex in dementia with Lewy bodies: magnetic resonance imaging study', *The British Journal of Psychiatry*, 200(6), pp. 491-498.

Taylor, J.-P., McKeith, I.G., Burn, D.J., Boeve, B.F., Weintraub, D., Bamford, C., Allan, L.M., Thomas, A.J. and T O'Brien, J. (2020) 'New evidence on the management of Lewy body dementia', *The Lancet Neurology*, 19(2), pp. 157-169.

Teipel, S.J., Pogarell, O., Meindl, T., Dietrich, O., Sydykova, D., Hunklinger, U., Georgii, B., Mulert, C., Reiser, M.F., Moller, H.J. and Hampel, H. (2009) 'Regional networks underlying interhemispheric connectivity: an EEG and DTI study in healthy ageing and amnestic mild cognitive impairment', *Hum Brain Mapp*, 30(7), pp. 2098-119.

Telesford, Q.K., Joyce, K.E., Hayasaka, S., Burdette, J.H. and Laurienti, P.J. (2011) 'The ubiquity of small-world networks', *Brain Connect*, 1(5), pp. 367-75.

Teunisse, R.J., Cruysberg, J.R., Hoefnagels, W.H., Verbeek, A.L. and Zitman, F.G. (1996) 'Visual hallucinations in psychologically normal people: Charles Bonnet's syndrome', *Lancet*, 347(9004), pp. 794-7.

Theis, F.J., Jung, A., Puntonet, C.G. and Lang, E.W. (2003) 'Linear Geometric ICA: Fundamentals and Algorithms', *Neural Computation*, 15(2), pp. 419-439.

Tiraboschi, P., Hansen, L.A., Alford, M., Merdes, A., Masliah, E., Thal, L.J. and Corey-Bloom, J. (2002) 'Early and widespread cholinergic losses differentiate dementia with Lewy bodies from Alzheimer disease', *Arch Gen Psychiatry*, 59(10), pp. 946-51.

Tiraboschi, P., Hansen, L.A., Alford, M., Sabbagh, M.N., Schoos, B., Masliah, E., Thal, L.J. and Corey-Bloom, J. (2000) 'Cholinergic dysfunction in diseases with Lewy bodies', *Neurology*, 54(2), pp. 407-11.

Tiraboschi, P., Salmon, D.P., Hansen, L.A., Hofstetter, R.C., Thal, L.J. and Corey-Bloom, J. (2006) 'What best differentiates Lewy body from Alzheimer's disease in early-stage dementia?', *Brain*, 129(3), pp. 729-735.

Toledo, J.B., Cairns, N.J., Da, X., Chen, K., Carter, D., Fleisher, A., Householder, E., Ayutyanont, N., Roontiva, A., Bauer, R.J., Eisen, P., Shaw, L.M., Davatzikos, C., Weiner, M.W., Reiman, E.M., Morris, J.C., Trojanowski, J.Q. and the Alzheimer's Disease Neuroimaging, I. (2013) 'Clinical and multimodal biomarker correlates of ADNI neuropathological findings', *Acta Neuropathologica Communications*, 1(1), p. 65.

Tononi, G. and Cirelli, C. (2003) 'Sleep and synaptic homeostasis: a hypothesis', *Brain Res Bull*, 62(2), pp. 143-50.

Traub, R.D., Jefferys, J.G.R. and Whittington, M.A. (1997) 'Simulation of Gamma Rhythms in Networks of Interneurons and Pyramidal Cells', *Journal of Computational Neuroscience*, 4(2), pp. 141-150.

Treisman, A.M. and Kanwisher, N.G. (1998) 'Perceiving visually presented objets: recognition, awareness, and modularity', *Current Opinion in Neurobiology*, 8(2), pp. 218-226.

Tsuboi, Y., Uchikado, H. and Dickson, D.W. (2007) 'Neuropathology of Parkinson's disease dementia and dementia with Lewy bodies with reference to striatal pathology', *Parkinsonism & Related Disorders*, 13, pp. S221-S224.

Tsukada, H., Fujii, H., Aihara, K. and Tsuda, I. (2015) 'Computational model of visual hallucination in dementia with Lewy bodies', *Neural networks*, 62, pp. 73-82.

Tsunoda, N., Hashimoto, M., Ishikawa, T., Fukuhara, R., Yuki, S., Tanaka, H., Hatada, Y., Miyagawa, Y. and Ikeda, M. (2018) 'Clinical Features of Auditory Hallucinations in Patients With Dementia With Lewy Bodies: A Soundtrack of Visual Hallucinations', *The Journal of clinical psychiatry*, 79(3).

Ullsperger, M. and Debener, S. (2010) *Simultaneous EEG and fMRI: recording, analysis, and application*. Oxford University Press.

Urigüen, J.A. and Garcia-Zapirain, B. (2015) 'EEG artifact removal—state-of-the-art and guidelines', *Journal of neural engineering*, 12(3), p. 031001.

Valdes-Hernandez, P.A., Ojeda-Gonzalez, A., Martinez-Montes, E., Lage-Castellanos, A., Virues-Alba, T., Valdes-Urrutia, L. and Valdes-Sosa, P.A. (2010) 'White matter architecture rather than cortical surface area correlates with the EEG alpha rhythm', *Neuroimage*, 49(3), pp. 2328-39.

van Dellen, E., de Waal, H., van der Flier, W.M., Lemstra, A.W., Slooter, A.J., Smits, L.L., van Straaten, E.C., Stam, C.J. and Scheltens, P. (2015) 'Loss of EEG Network Efficiency Is Related to Cognitive Impairment in Dementia With Lewy Bodies', *Mov Disord*, 30(13), pp. 1785-93.

van den Broek, S.P., Reinders, F., Donderwinkel, M. and Peters, M.J. (1998) 'Volume conduction effects in EEG and MEG', *Electroencephalography and Clinical Neurophysiology*, 106(6), pp. 522-534.

van den Heuvel, M.P., de Lange, S.C., Zalesky, A., Seguin, C., Yeo, B.T.T. and Schmidt, R. (2017) 'Proportional thresholding in resting-state fMRI functional connectivity networks and consequences for patient-control connectome studies: Issues and recommendations', *NeuroImage*, 152, pp. 437-449.

van den Heuvel, M.P. and Hulshoff Pol, H.E. (2010) 'Exploring the brain network: A review on resting-state fMRI functional connectivity', *European Neuropsychopharmacology*, 20(8), pp. 519-534.

van den Heuvel, M.P., Stam, C.J., Boersma, M. and Hulshoff Pol, H.E. (2008) 'Small-world and scale-free organization of voxel-based resting-state functional connectivity in the human brain', *NeuroImage*, 43(3), pp. 528-539.

van der Zande, J.J., Steenwijk, M.D., ten Kate, M., Wattjes, M.P., Scheltens, P. and Lemstra, A.W. (2018) 'Gray matter atrophy in dementia with Lewy bodies with and without concomitant Alzheimer's disease pathology', *Neurobiology of Aging*, 71, pp. 171-178.

Van Veen, B.D. and Buckley, K.M. (1988) 'Beamforming: A versatile approach to spatial filtering', *IEEE assp magazine*, 5(2), pp. 4-24.

Van Veen, B.D., van Drongelen, W., Yuchtman, M. and Suzuki, A. (1997) 'Localization of brain electrical activity via linearly constrained minimum variance spatial filtering', *IEEE Trans Biomed Eng*, 44(9), pp. 867-80.

van Wijk, B.C., Stam, C.J. and Daffertshofer, A. (2010) 'Comparing brain networks of different size and connectivity density using graph theory', *PLoS One*, 5(10), p. e13701.

Vann Jones, S.A. and O'Brien, J.T. (2014) 'The prevalence and incidence of dementia with Lewy bodies: a systematic review of population and clinical studies', *Psychol Med*, 44(4), pp. 673-83.

Vecchio, F., Miraglia, F., Curcio, G., Altavilla, R., Scrascia, F., Giambattistelli, F., Quattrocchi, C.C., Bramanti, P., Vernieri, F. and Rossini, P.M. (2015) 'Cortical brain connectivity evaluated by graph theory in dementia: a correlation study between functional and structural data', *J Alzheimers Dis*, 45(3), pp. 745-56.

Vinck, M., Oostenveld, R., van Wingerden, M., Battaglia, F. and Pennartz, C.M. (2011) 'An improved index of phase-synchronization for electrophysiological data in the presence of volume-conduction, noise and sample-size bias', *Neuroimage*, 55(4), pp. 1548-65.

Viola, F.C., Debener, S., Thorne, J. and Schneider, T.R. (2010) 'Using ICA for the analysis of multi-channel EEG data', *Simultaneous EEG and fMRI: Recording, Analysis, and Application: Recording, Analysis, and Application*, pp. 121-133.

Vossel, S., Geng, J.J. and Fink, G.R. (2014) 'Dorsal and ventral attention systems: distinct neural circuits but collaborative roles', *Neuroscientist*, 20(2), pp. 150-9.

Walker, M.P., Ayre, G.A., Cummings, J.L., Wesnes, K., McKeith, I.G., O'Brien, J.T. and Ballard, C.G. (2000) 'Quantifying fluctuation in dementia with Lewy bodies, Alzheimer's disease, and vascular dementia', *Neurology*, 54(8), pp. 1616-1625.

Walker, M.P. and Stickgold, R. (2006) 'Sleep, memory, and plasticity', *Annu Rev Psychol*, 57, pp. 139-66.

Walker, Z., Costa, D.C., Walker, R.W., Shaw, K., Gacinovic, S., Stevens, T., Livingston, G., Ince, P., McKeith, I.G. and Katona, C.L. (2002) 'Differentiation of dementia with Lewy bodies from Alzheimer's disease using a dopaminergic presynaptic ligand', *J Neurol Neurosurg Psychiatry*, 73(2), pp. 134-40.

Walker, Z., Possin, K.L., Boeve, B.F. and Aarsland, D. (2015) 'Lewy body dementias', *The Lancet*, 386(10004), pp. 1683-1697.

Wan, L., Friedman, B.H., Boutros, N.N. and Crawford, H.J. (2008) 'P50 sensory gating and attentional performance', *International Journal of Psychophysiology*, 67(2), pp. 91-100.

Wan, L., Huang, H., Schwab, N., Tanner, J., Rajan, A., Lam, N.B., Zaborszky, L., Li, C.-s.R., Price, C.C. and Ding, M. (2019) 'From eyes-closed to eyes-open: Role of cholinergic projections in EC-to-EO alpha reactivity revealed by combining EEG and MRI', *Human Brain Mapping*, 40(2), pp. 566-577.

Wang, H.F., Yu, J.T., Tang, S.W., Jiang, T., Tan, C.C., Meng, X.F., Wang, C., Tan, M.S. and Tan, L. (2015) 'Efficacy and safety of cholinesterase inhibitors and memantine in cognitive impairment in Parkinson's disease, Parkinson's disease dementia, and dementia with Lewy bodies: systematic review with meta-analysis and trial sequential analysis', *J Neurol Neurosurg Psychiatry*, 86(2), pp. 135-43.

Wang, J., Zuo, X., Dai, Z., Xia, M., Zhao, Z., Zhao, X., Jia, J., Han, Y. and He, Y. (2013a) 'Disrupted Functional Brain Connectome in Individuals at Risk for Alzheimer's Disease', *Biological Psychiatry*, 73(5), pp. 472-481.

Wang, Y., Zhang, X., Huang, J., Zhu, M., Guan, Q. and Liu, C. (2013b) 'Associations Between EEG Beta Power Abnormality and Diagnosis in Cognitive Impairment Post Cerebral Infarcts', *Journal of Molecular Neuroscience*, 49(3), pp. 632-638.

Watanabe, H., Ieda, T., Katayama, T., Takeda, A., Aiba, I., Doyu, M., Hirayama, M. and Sobue, G. (2001) 'Cardiac 123I-meta-iodobenzylguanidine (MIBG) uptake in dementia with Lewy bodies: comparison with Alzheimer's disease', *Journal of Neurology, Neurosurgery & Psychiatry*, 70(6), pp. 781-783.

Watson, R., Blamire, A.M., Colloby, S.J., Wood, J.S., Barber, R., He, J. and O'Brien, J.T. (2012) 'Characterizing dementia with Lewy bodies by means of diffusion tensor imaging', *Neurology*, 79(9), pp. 906-914.

Watts, D.J. and Strogatz, S.H. (1998) 'Collective dynamics of 'small-world'networks', *nature*, 393(6684), p. 440.

Weil, R.S., Lashley, T.L., Bras, J., Schrag, A.E. and Schott, J.M. (2017) 'Current concepts and controversies in the pathogenesis of Parkinson's disease dementia and dementia with Lewy bodies', *F1000Research*, 6.

Weisman, D., Cho, M., Taylor, C., Adame, A., Thal, L.J. and Hansen, L.A. (2007) 'In dementia with Lewy bodies, Braak stage determines phenotype, not Lewy body distribution', *Neurology*, 69(4), pp. 356-359.

Whitham, E.M., Pope, K.J., Fitzgibbon, S.P., Lewis, T., Clark, C.R., Loveless, S., Broberg, M., Wallace, A., DeLosAngeles, D., Lillie, P., Hardy, A., Fronsko, R., Pulbrook, A. and Willoughby, J.O. (2007) 'Scalp electrical recording during paralysis: Quantitative evidence that EEG frequencies above 20Hz are contaminated by EMG', *Clinical Neurophysiology*, 118(8), pp. 1877-1888.

Whittington, M.A. and Traub, R.D. (2003) 'Interneuron Diversity series: Inhibitory interneurons and network oscillations in vitro', *Trends in Neurosciences*, 26(12), pp. 676-682.

Wigand, M., Kubicki, M., Clemm von Hohenberg, C., Leicht, G., Karch, S., Eckbo, R., Pelavin, P.E., Hawley, K., Rujescu, D. and Bouix, S. (2015) 'Auditory verbal hallucinations and the interhemispheric auditory pathway in chronic schizophrenia', *The World Journal of Biological Psychiatry*, 16(1), pp. 31-44.

Williams, D.R. and Lees, A.J. (2005) 'Visual hallucinations in the diagnosis of idiopathic Parkinson's disease: a retrospective autopsy study', *Lancet Neurol*, 4(10), pp. 605-10.

Xia, M., Wang, J. and He, Y. (2013) 'BrainNet Viewer: A Network Visualization Tool for Human Brain Connectomics', *PLOS ONE*, 8(7), p. e68910.

Xu, L., Chiu Cheung, C. and Amari, S.-i. (1998) 'Learned parametric mixture based ICA algorithm1This work was supported by HK RGC Direct Grant CUHK 2050162.1', *Neurocomputing*, 22(1), pp. 69-80.

Xu, T., Cullen, K.R., Mueller, B., Schreiner, M.W., Lim, K.O., Schulz, S.C. and Parhi, K.K. (2016) 'Network analysis of functional brain connectivity in borderline personality disorder using resting-state fMRI', *Neuroimage Clin*, 11, pp. 302-15.

Yao, N., Shek-Kwan Chang, R., Cheung, C., Pang, S., Lau, K.K., Suckling, J., Rowe, J.B., Yu, K., Ka-Fung Mak, H. and Chua, S.E. (2014) 'The default mode network is disrupted in Parkinson's disease with visual hallucinations', *Human brain mapping*, 35(11), pp. 5658-5666.

Yeh, C.H., Jones, D.K., Liang, X., Descoteaux, M. and Connelly, A. (2020) 'Mapping structural connectivity using diffusion MRI: Challenges and opportunities', *Journal of Magnetic Resonance Imaging*.

Yeo, S.S., Chang, P.H. and Jang, S.H. (2013) 'The Ascending Reticular Activating System from Pontine Reticular Formation to the Thalamus in the Human Brain', *Frontiers in Human Neuroscience*, 7(416).

Yoshita, M., Arai, H., Arai, H., Arai, T., Asada, T., Fujishiro, H., Hanyu, H., Iizuka, O., Iseki, E., Kashihara, K., Kosaka, K., Maruno, H., Mizukami, K., Mizuno, Y., Mori, E., Nakajima, K., Nakamura, H., Nakano, S., Nakashima, K., Nishio, Y., Orimo, S., Samuraki, M., Takahashi, A., Taki, J., Tokuda, T., Urakami, K., Utsumi, K., Wada, K., Washimi, Y., Yamasaki, J., Yamashina, S. and Yamada, M. (2015) 'Diagnostic accuracy of 123I-meta-iodobenzylguanidine myocardial scintigraphy in dementia with Lewy bodies: a multicenter study', *PloS one*, 10(3), pp. e0120540-e0120540.

Yoshizawa, H., Vonsattel, J.P.G. and Honig, L.S. (2013) 'Early neuropsychological discriminants for Lewy body disease: an autopsy series', *Journal of Neurology, Neurosurgery & Psychiatry*, 84(12), pp. 1326-1330.

Zaborszky, L., Hoemke, L., Mohlberg, H., Schleicher, A., Amunts, K. and Zilles, K. (2008) 'Stereotaxic probabilistic maps of the magnocellular cell groups in human basal forebrain', *Neuroimage*, 42(3), pp. 1127-1141.

Zalesky, A., Fornito, A. and Bullmore, E.T. (2010) 'Network-based statistic: identifying differences in brain networks', *Neuroimage*, 53(4), pp. 1197-207.

Zeki, S. and Bartels, A. (1998) 'The autonomy of the visual systems and the modularity of conscious vision', *Philos Trans R Soc Lond B Biol Sci*, 353(1377), pp. 1911-4.

Zhong, J., Pan, P., Dai, Z. and Shi, H. (2014) 'Voxelwise meta-analysis of gray matter abnormalities in dementia with Lewy bodies', *Eur J Radiol*, 83(10), pp. 1870-4.

Zhou, Y., Yu, F. and Duong, T. (2014) 'Multiparametric MRI characterization and prediction in autism spectrum disorder using graph theory and machine learning', *PloS one*, 9(6).

Zou, K.H., Yu, C.-R., Liu, K., Carlsson, M.O. and Cabrera, J. (2013) 'Optimal thresholds by maximizing or minimizing various metrics via ROC-type analysis', *Academic radiology*, 20(7), pp. 807-815.

Appendix A. Supplementary Materials for Chapter 3

This appendix contains supplementary information to the study reported in Chapter 3, as also reported in the respective publication (Mehraram *et al.*, 2019).

A. Proportional Thresholding: Binary Measures

Figure A shows the trends of all network measures (excluding C and L in the β-band network, reported in the main manuscript) with respect to the network density.

Spearman correlation test between the network measures and the thresholding level for all frequency ranges and groups together: $\rho_K = 1\ (p = 0); \rho_{K_w} = 0.9105\ (p = 0); \rho_Q = -0.4727\ (p = 0); \rho_{Q_w} = -0.4254\ (p = 0); \rho_\sigma = 0.6424\ (p = 0); \rho_{\sigma_w} = 0.4754\ (p = 0)$.

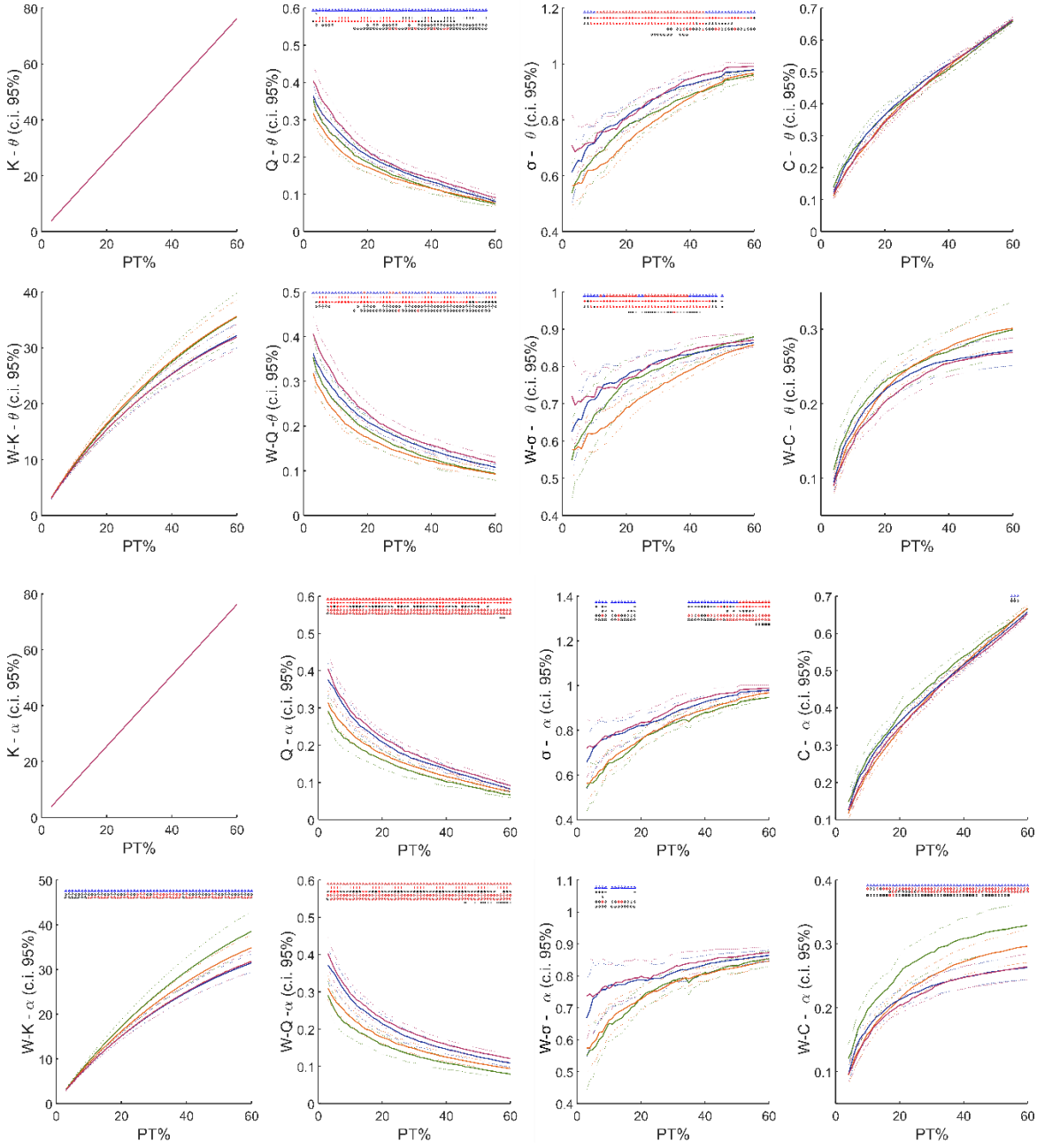

Figure Aa – See caption at Figure Ac.

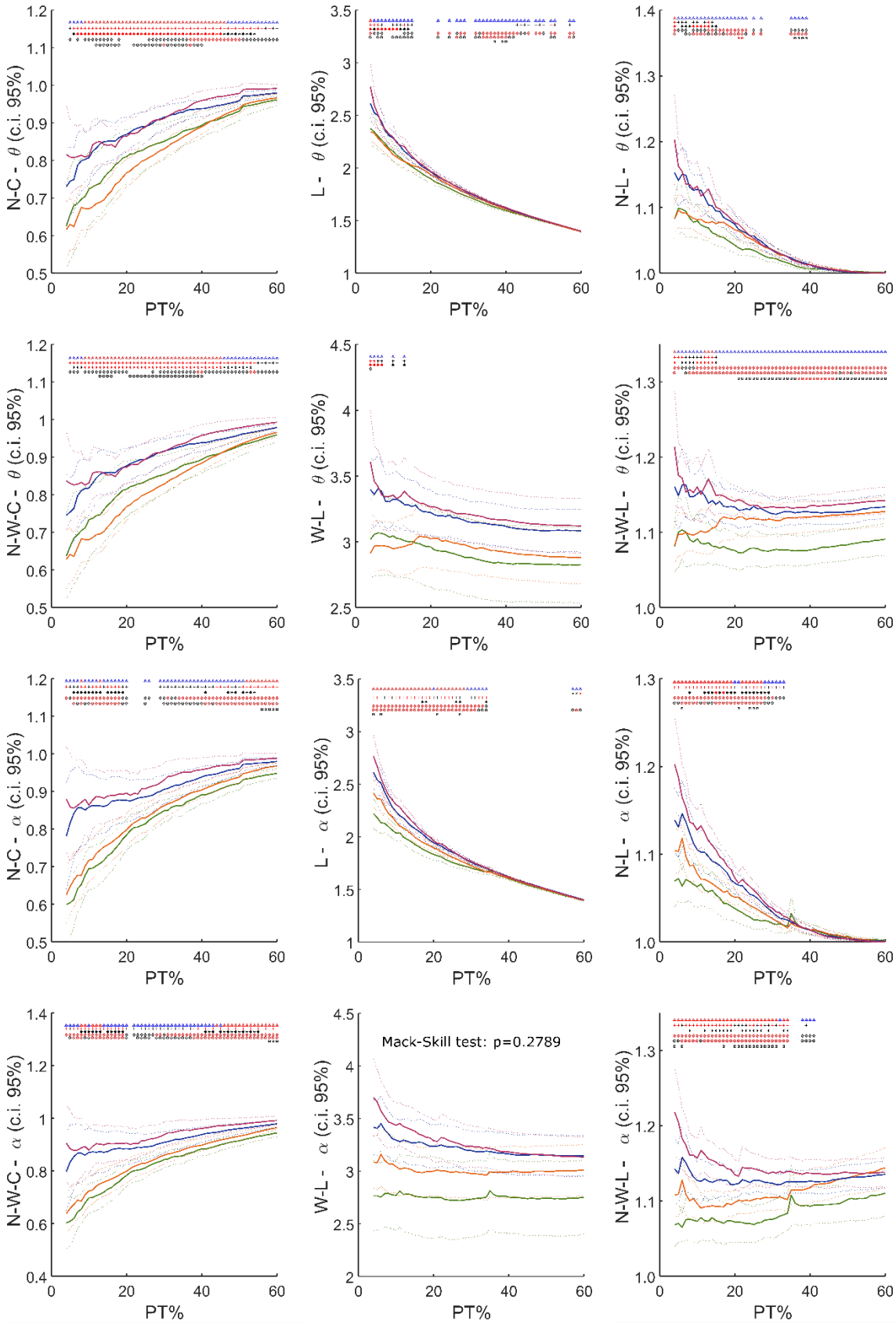

Figure Ab – See caption at Figure Ac.

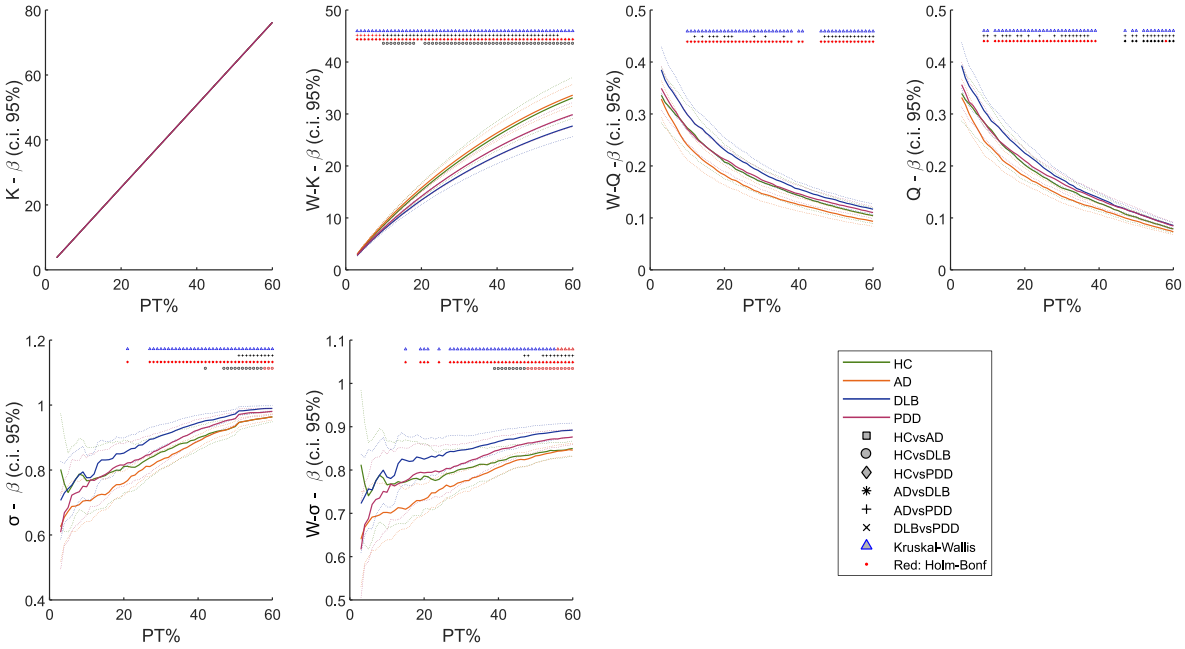

Figure Ac - Dependence of the network measures on the connectivity matrix thresholding level (PT%). Horizontal axis: PT% (range within 3% to 60%); vertical axis: network measure. Markers on top represent results of the one-way Kruskal-Wallis ($p<0.05$) and two-tailed Mann-Whitney U post hoc tests ($p<0.05$) performed at each PT%, as described in the figure's legend (bottom right). Red marker: test survives Holm-Bonferroni correction (Kruskal-Wallis: 60 tests; post hoc test: 6 comparisons). Dotted lines of the same colour delineate 95% confidence interval for each group. Weighted clustering coefficient and characteristic path length plots in the β-band are reported in the main manuscript.

For both binary and weighted characteristic path length measures (clustering coefficient is reported in the main text), their edge-density vs value behaviour curves was modelled as $L_b = ft^g + h$ and $L_w = mt^n + q$, with t= thresholding level; f=-5.27 [-6.206; -4.333]; g=0.09554 [0.07464; 0.1164]; h=6.431 [5.48; 7.381]; m=0.03879 [0.02946; 0.04813]; n=-0.8438 [-0.8974; -0.7902]; q=3.086 [3.063; 3.109] (Figure B and Figure C). The goodness of fit described by the sum of squares error (SSE) was SSE_b=0.01649, SSE_w=0.06544. Numbers in square brackets represent the 95% confidence interval.

By computing the first derivative of the equations with respect to the thresholding level t, the following equations were obtained: $dL_b/dt = fgt^{g-1}$ and $dL_w/dt = mnt^{n-1}$. As in the main text, values of t at which the weighted measure showed lower dependence on PT% compared with the binary measure were searched, i.e. t at which:

$$\frac{dL_w}{dL_b} < 1; \;\; 0 < t \leq 1 \qquad \text{(A)}$$

By computing the ratio in (A) and replacing the corresponding coefficients, the condition in equation (A) is true when $0.0544 < t \leq 1$. Hence the condition expressed in (A) is true for almost all network density values for the characteristic path length.

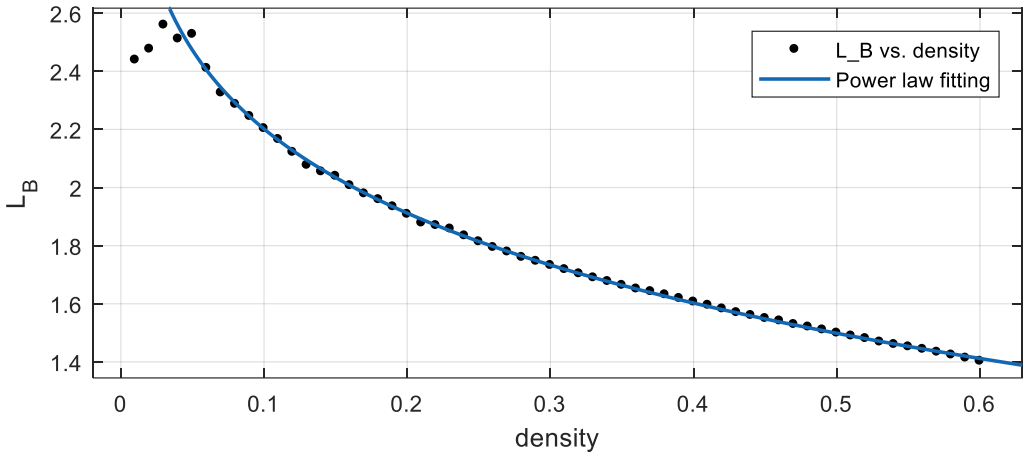

Figure B – Power law fitting curve for the binary characteristic path length L. y-axis: L; x-axis: network density. Black dots: average experimental L across subjects. Blue line: fitting curve.

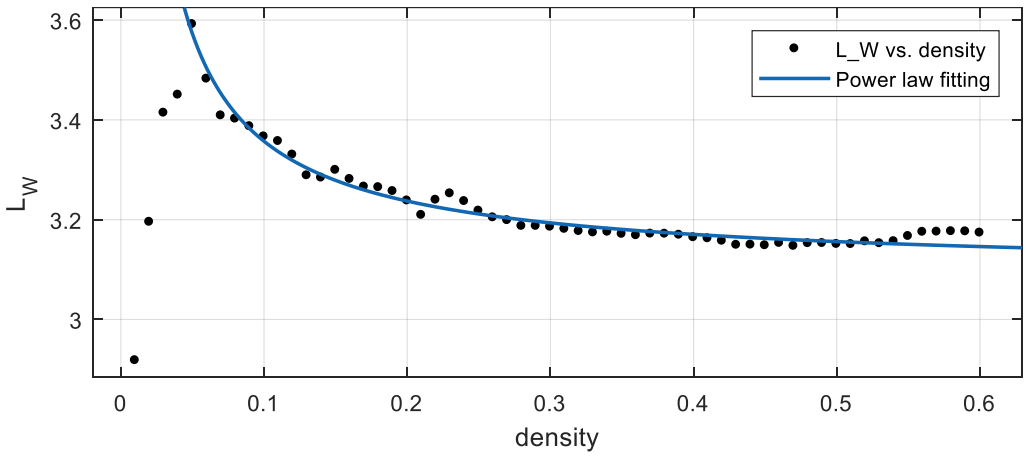

Figure C – Power law fitting curve for the weight-based characteristic path length L. y-axis: W-L; x-axis: network density. Black dots: average experimental L across subjects. Blue line: fitting curve.

B. Network Features: Binary Measures

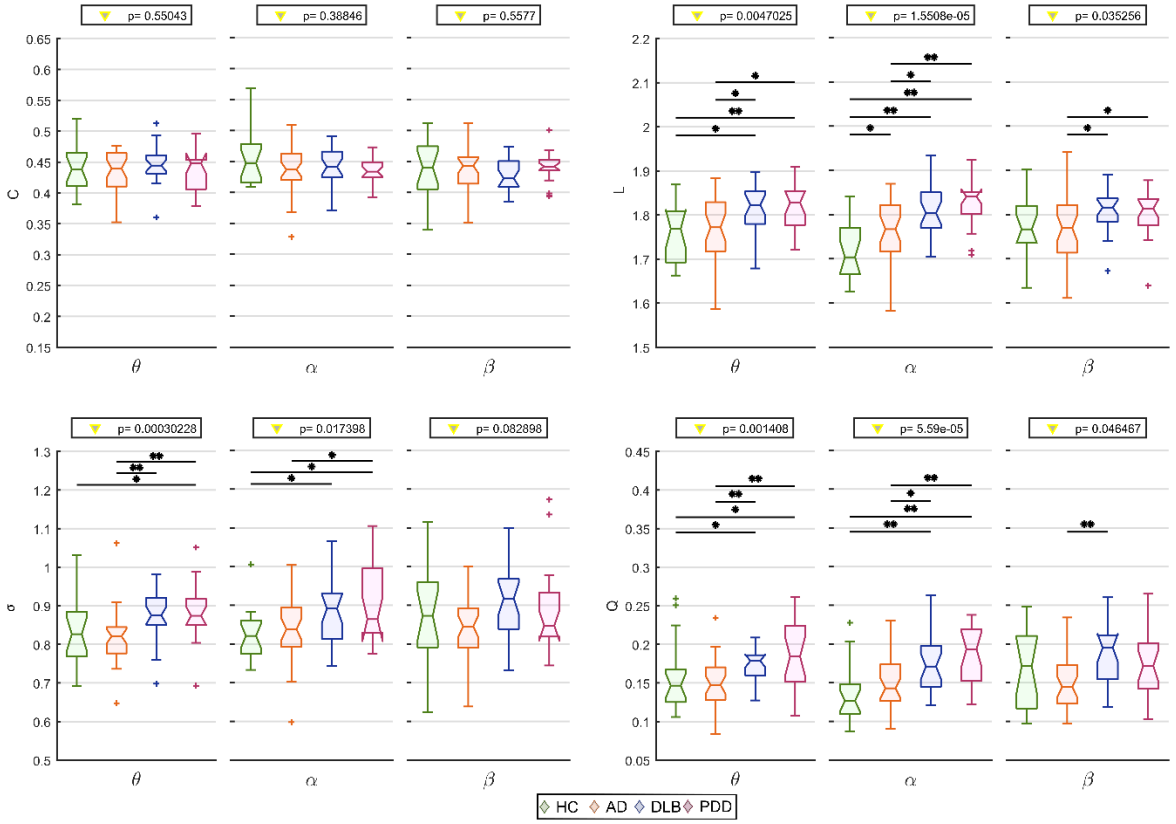

Figure D – Results of the graph theory analysis from the binary network measures. y-axis: network measure; x-axis: frequency band of interest (θ: 4-7.5 Hz, α: 8-13.5 Hz, β: 14-20.5 Hz). Values on top indicate the result of the one-way Kruskal-Wallis test ($p<0.05$); * : significant two-tailed Mann-Whitney U test post hoc test ($p<0.05$); ** : post hoc test survives Holm-Bonferroni correction (6 comparisons).

C. Network Features: Weighted Non-Thresholded (Complete) Matrices

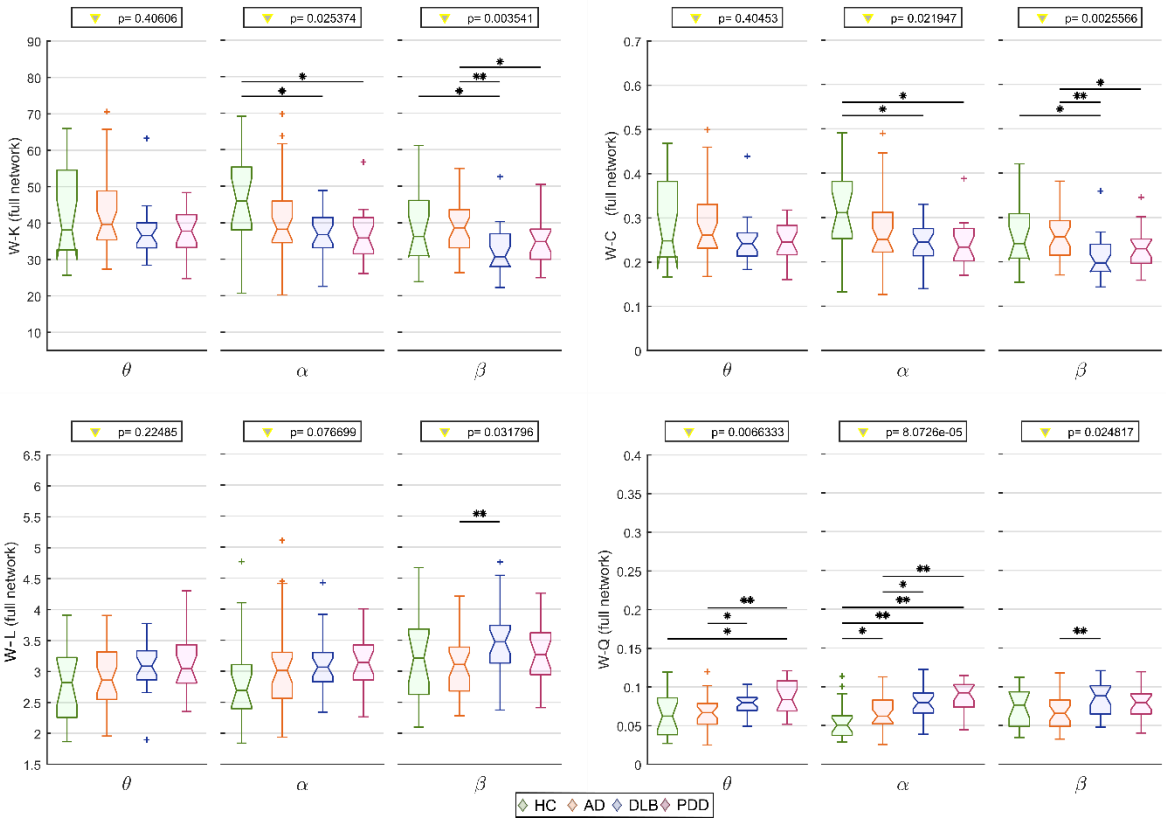

Figure E – Results from the graph theory analysis from the weighted measures computed over non-thresholded networks. x-axis: network measure; y-axis: frequency band of interest (θ: 4-7.5 Hz, α: 8-13.5 Hz, β: 14-20.5 Hz). Values on top indicate the result of the one-way Kruskal-Wallis test ($p<0.05$); * : significant two-tailed Mann-Whitney U test post hoc test ($p<0.05$); ** : post hoc test survives Holm-Bonferroni correction (6 comparisons).

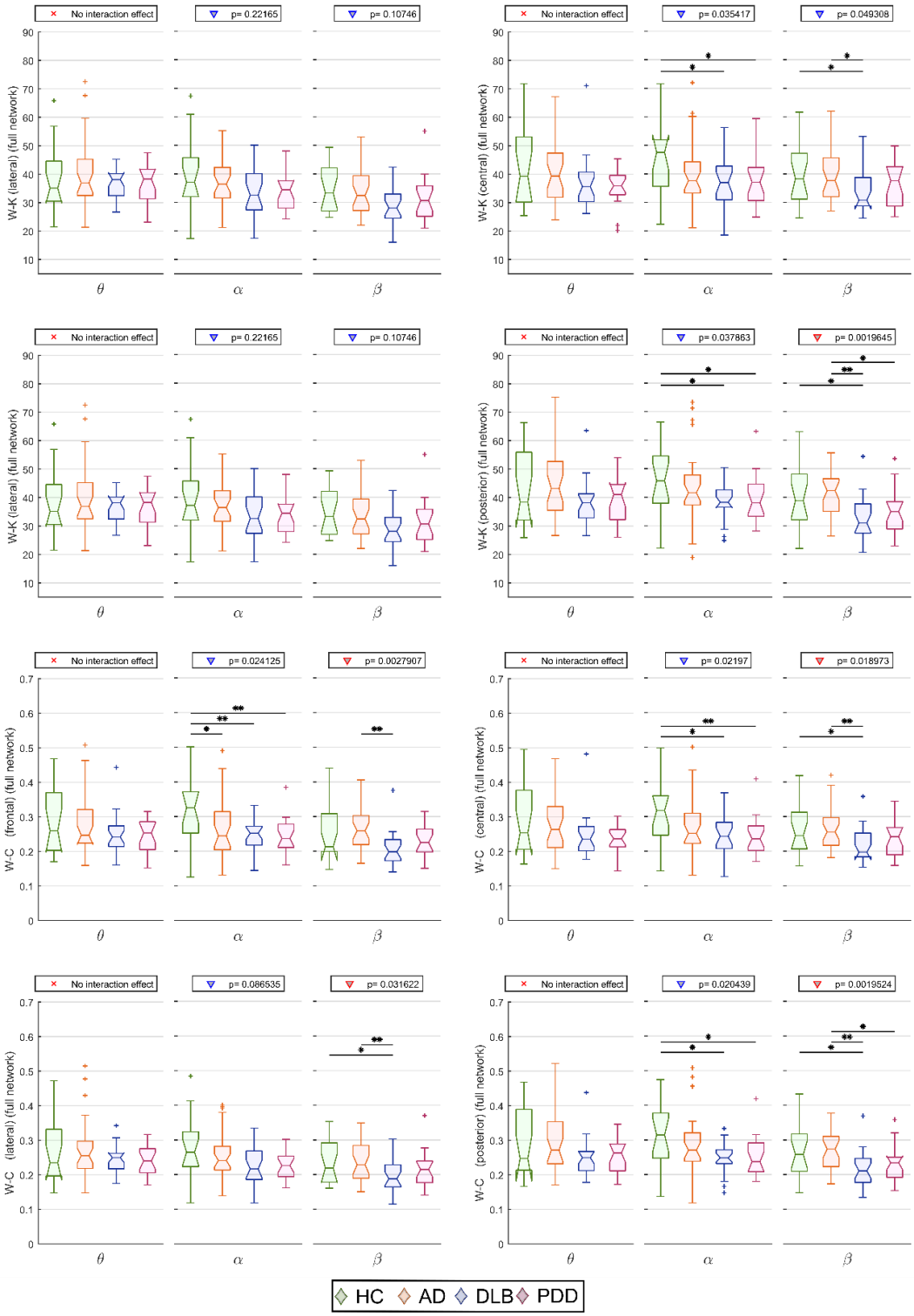

Figure G – Graph theory analysis from local weight-based network measures over non-thresholded matrices. y-axis: local network measure; x-axis: frequency band of interest (θ: 4-7.5 Hz, α: 8-13.5 Hz, β: 14-20.5 Hz). If any interaction was found in the repeated measures ANOVA (within subjects: areas; between subjects: group), the result of the one-way Kruskal-Wallis test ($p<0.05$) is indicated on top. Red triangle: Kruskal-Wallis test survives Holm-Bonferroni correction (4 areas); *significant two-tailed Mann-Whitney U test post hoc test ($p<0.05$); **post hoc test survives Holm-Bonferroni correction (6 comparisons). Top (A): Weighted node degree. Bottom (B): Weighted clustering coefficient.

D. Robustness of The Network: Analysis Outcome for PT% = 10% and PT = 20%

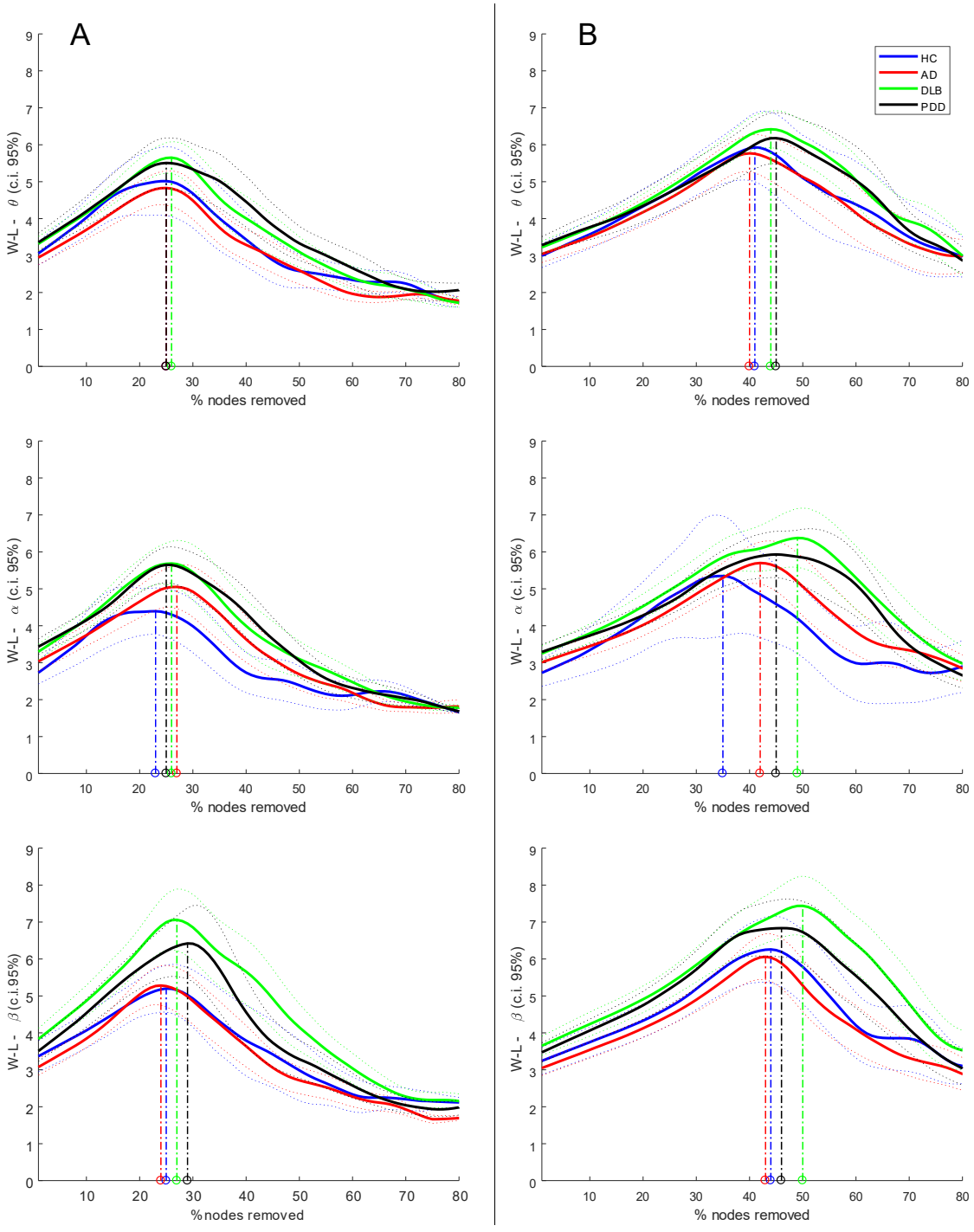

Figure H – Results from the targeted node attack (A: density 10%, bottom row: density 20%). The y-axis shows the weight-based characteristic path length, the x-axis is the percentage of nodes removed from the network.

E. Diagnostic Accuracy: 5 and 7 Folds Classifiers

Figure I shows the results of the random forest classifier using 5 and 7 folds at cross-validation for the scenarios reported in the main text, i.e. DLB vs AD and LBDs vs HC. Similar classification accuracy was found.

5 folds

7 folds

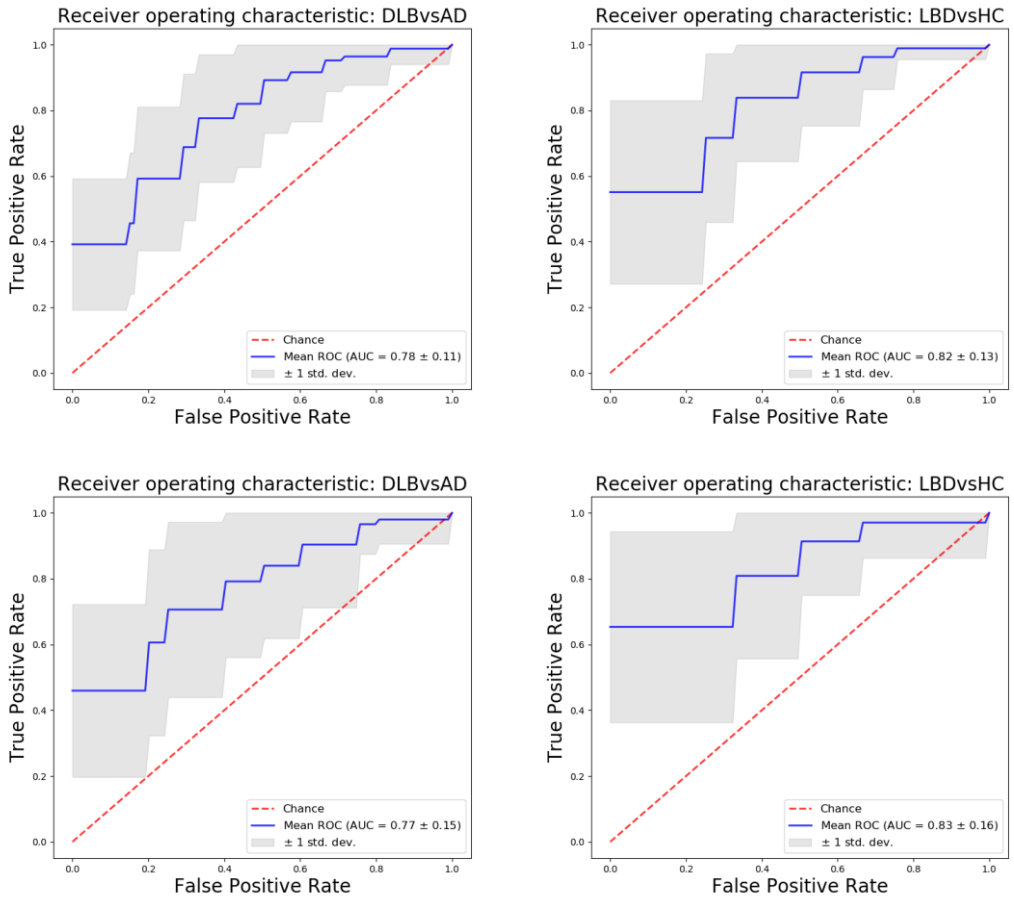

Figure I – Receiver operating characteristic (ROC) curves obtained with random forest classifier and computed for the DLB-vs-AD and dementia-vs-HC scenarios. All weighted network measures were used to train the classifier. Computations were performed using cross-validation with four and seven folds (first and second row respectively) and 10 repetitions; for this the Scikit-Learn framework (version 0.20.1) and the Imbalanced-Learn (version 0.4.3) library in Python were used.

Scenarios which did not yield any significance, i.e. all dementia groups together vs HC group (Figure J) and DLB vs PDD (Figure K), were also tested for exploratory purposes. Classification between all dementia groups together vs HC group was less accurate than LBDs vs HC reported

in the main manuscript. This is since only WPLI measured in the α range was significantly affected in AD compared with HC.

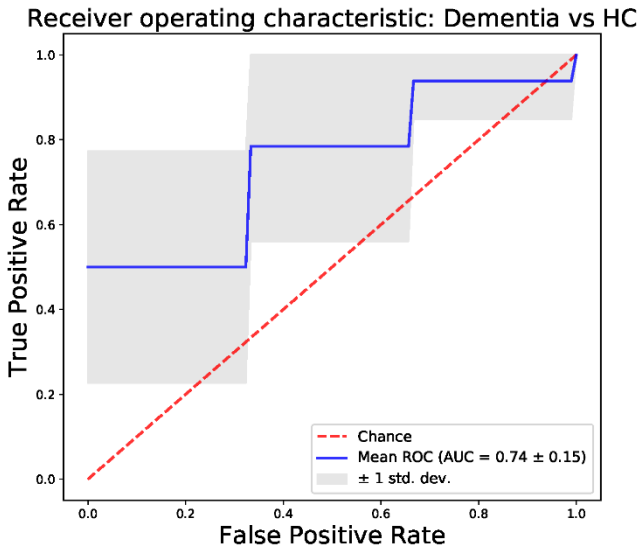

Figure J – Receiver operating characteristic (ROC) curves obtained by the random forest classifier and computed for the dementia-vs-HC scenario. All weighted network measures were used to train the classifier. Computations were performed using cross-validation with six folds and 10 repetitions; for this the Scikit-Learn framework (version 0.20.1) and the Imbalanced-Learn (version 0.4.3) library in Python were used.

The overlapping pathology between PDD and DLB affects the classification between the two groups, which was driven by chance (Figure K).

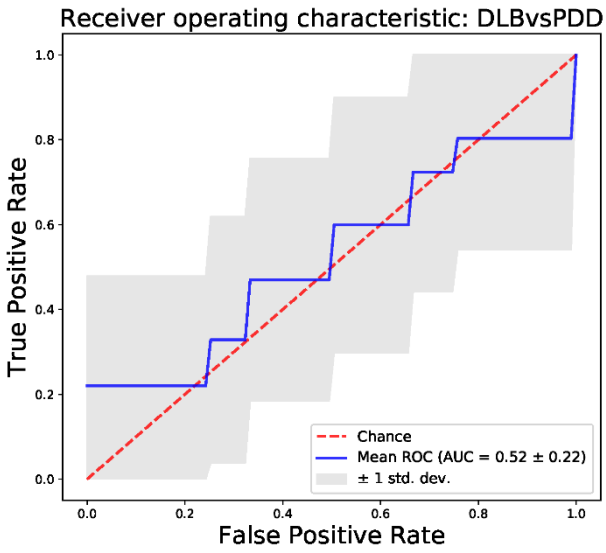

Figure K – Receiver operating characteristic (ROC) curves obtained by the random forest classifier and computed for DLB vs PDD scenario. All (weighted) network measures were used to train the classifier. Computations were performed using cross-validation with six folds and 10 repetitions; for this the Scikit-Learn framework (version 0.20.1) and the Imbalanced-Learn (version 0.4.3) library in Python were used.

Appendix B. MNI Coordinates of Network Nodes from Destrieux Atlas

Label	*x*	*y*	*z*
'Pole_occipital_L'	-16,856895	-100,1667	-5,6742534
'Pole_occipital_R'	18,1147846	-95,929877	-2,8385904
'G_occipital_sup_L'	-13,980972	-92,103146	30,6393072
'S_oc_middle_and_Lunatus_L'	-31,049869	-89,221256	6,53669457
'G_occipital_sup_R'	18,3290267	-87,948505	35,1847473
'G_occipital_middle_L'	-40,138361	-87,491509	13,4534898
'S_oc_sup_and_transversal_L'	-25,742421	-84,568726	20,9439325
'G_and_S_occipital_inf_L'	-38,461317	-83,414618	-11,446184
'G_cuneus_L'	-3,3468657	-81,646603	17,567933
'S_oc_middle_and_Lunatus_R'	37,2338349	-81,03735	9,27653886
'S_oc_sup_and_transversal_R'	30,1793647	-80,346951	22,1792641
'S_collat_transv_post_L'	-24,259606	-79,935652	-7,833175
'G_occipital_middle_R'	46,3450485	-79,025415	15,2361303
'S_collat_transv_post_R'	27,3908389	-78,88232	-8,8665384
'G_cuneus_R'	5,90665408	-78,013931	19,8297602
'G_oc-temp_med-Lingual_L'	-9,5373903	-74,311454	-5,9839477
'G_and_S_occipital_inf_R'	44,2472872	-74,053108	-12,277754
'S_calcarine_L'	-15,496666	-72,070582	4,71003843
'S_parieto_occipital_L'	-15,504848	-69,375785	25,8156653
'G_pariet_inf-Angular_L'	-45,302616	-68,591351	42,2196655
'S_occipital_ant_L'	-43,101425	-68,519245	4,15231965
'G_oc-temp_med-Lingual_R'	9,37101745	-67,3593	-3,6127028
'S_parieto_occipital_R'	17,3258766	-66,76769	27,3665577
'S_calcarine_R'	17,2170709	-66,715428	6,10398333
'S_occipital_ant_R'	47,6111792	-62,243474	4,33894048
'G_parietal_sup_L'	-23,406961	-61,896369	59,818168
'G_pariet_inf-Angular_R'	49,5164272	-60,790665	42,767234
'G_precuneus_L'	-4,134602	-60,289891	43,6100051
'G_precuneus_R'	4,79367477	-60,271867	46,5138273
'S_intrapariet_and_P_trans_L'	-30,657589	-59,100794	41,7982714
'G_parietal_sup_R'	25,1441688	-57,872513	63,2070373
'S_intrapariet_and_P_trans_R'	30,5651545	-56,858196	44,7500326
'S_interm_prim-Jensen_L'	-52,211148	-55,547456	36,9375096
'G_oc-temp_lat-fusifor_L'	-38,018595	-54,096665	-20,14663
'G_oc-temp_lat-fusifor_R'	34,2769577	-51,637045	-20,75457
'S_oc-temp_lat_L'	-44,815804	-51,018649	-11,938669
'S_oc-temp_lat_R'	43,8580055	-48,834051	-14,267307
'S_subparietal_L'	-9,5142274	-48,27462	35,7512872
'S_subparietal_R'	8,9537357	-48,226819	37,5207114
'G_cingul-Post-ventral_R'	7,09224502	-46,656395	5,58728157
'S_oc-temp_med_and_Lingual_L'	-28,407234	-46,364172	-13,258884
'S_oc-temp_med_and_Lingual_R'	29,0422694	-45,597104	-12,87741
'G_cingul-Post-ventral_L'	-7,6501913	-44,821491	3,14298627
'S_interm_prim-Jensen_R'	53,4322737	-43,416018	35,9316095

'S_temporal_sup_L'	-49,801234	-42,712461	7,05405015
'G_temporal_inf_L'	-55,181424	-40,845183	-21,999078
'G_cingul-Post-dorsal_L'	-2,2440024	-40,328792	30,7762786
'G_temp_sup-Plan_tempo_L'	-60,074589	-39,214686	21,6403281
'S_temporal_sup_R'	50,8477299	-38,19845	9,12947461
'G_cingul-Post-dorsal_R'	1,85359023	-38,108126	33,1704614
'G_temporal_inf_R'	55,1884657	-38,095535	-24,232985
'S_cingul-Marginalis_L'	-13,062979	-36,829735	48,9899833
'G_and_S_paracentral_L'	-7,3626139	-36,226501	69,8499747
'G_pariet_inf-Supramar_L'	-61,114305	-35,991977	33,2433335
'G_and_S_paracentral_R'	7,88003389	-35,652382	71,5312243
'S_cingul-Marginalis_R'	11,9953128	-35,555264	49,2884566
'S_temporal_inf_R'	56,0866664	-34,854645	-14,660639
'Lat_Fis-post_L'	-41,857889	-34,072207	19,4094988
'S_postcentral_L'	-40,476822	-33,284302	46,1508686
'S_temporal_inf_L'	-55,519184	-31,191312	-18,6941
'G_pariet_inf-Supramar_R'	58,3919828	-30,067496	37,0142107
'S_postcentral_R'	39,559387	-29,737032	46,4406676
'G_temporal_middle_L'	-62,091079	-28,564557	-11,401692
'G_temp_sup-Plan_tempo_R'	60,8702299	-28,49692	21,4961563
'Lat_Fis-post_R'	40,1730677	-24,817006	18,5783136
'G_postcentral_L'	-47,507469	-24,046153	55,9848725
'S_temporal_transverse_L'	-53,333727	-22,0591	5,73130557
'G_temporal_middle_R'	62,3925978	-21,611309	-15,007033
'G_postcentral_R'	47,0899879	-21,027259	56,1218101
'G_temp_sup-G_T_transv_L'	-47,5505	-20,574775	9,92095113
'S_central_L'	-38,25244	-20,149708	46,0067886
'S_collat_transv_ant_L'	-42,103808	-19,177564	-28,981915
'S_central_R'	37,3316732	-18,272409	46,4338759
'S_temporal_transverse_R'	52,3678114	-18,024797	9,32791289
'S_collat_transv_ant_R'	41,7743007	-17,738935	-29,330809
'G_oc-temp_med-Parahip_L'	-25,057202	-17,490021	-26,242779
'G_oc-temp_med-Parahip_R'	23,8832041	-13,10857	-27,340384
'G_temp_sup-G_T_transv_R'	48,2852039	-12,302355	7,36303752
'G_and_S_subcentral_L'	-57,601796	-10,807142	14,2693463
'S_precentral-sup-part_L'	-27,848176	-10,494424	56,7640435
'G_Ins_lg_and_S_cent_ins_L'	-41,825645	-10,458351	2,23362653
'G_and_S_cingul-Mid-Post_L'	-6,8746307	-10,239292	41,5425646
'S_circular_insula_inf_L'	-41,121354	-10,133728	-5,6777533
'S_pericallosal_R'	4,30568889	-8,4860049	18,3588585
'G_precentral_L'	-43,837353	-8,4417451	54,910341
'S_precentral-sup-part_R'	28,6509131	-8,3610497	56,5433254
'S_circular_insula_inf_R'	41,2795259	-8,1585978	-6,7111148
'G_and_S_cingul-Mid-Post_R'	6,50004415	-7,7839869	43,8611272
'G_and_S_subcentral_R'	57,5925372	-7,347811	13,2478443
'S_pericallosal_L'	-4,3191537	-6,9543949	19,463515
'G_temp_sup-Lateral_L'	-58,757359	-6,301999	-8,2924862
'G_precentral_R'	43,4064661	-6,0062333	54,1418552
'G_Ins_lg_and_S_cent_ins_R'	41,0476219	-4,1843056	-2,0747366

'G_temp_sup-Lateral_R'	60,0830469	-4,1825595	-6,4375975
'S_precentral-inf-part_L'	-44,575172	4,73598383	30,7636279
'Pole_temporal_L'	-32,059063	5,8561879	-42,534359
'S_circular_insula_sup_L'	-36,382066	6,36621618	11,0907429
'S_precentral-inf-part_R'	43,232989	7,0130399	30,9769796
'G_subcallosal_L'	-9,3007413	7,64565551	-13,67521
'G_insular_short_L'	-41,382944	8,3707236	-3,5490326
'G_subcallosal_R'	3,97513351	8,8112282	-10,74926
'G_temp_sup-Plan_polar_L'	-38,32092	8,93823446	-19,277701
'S_circular_insula_sup_R'	36,0867079	10,1757653	9,78910851
'G_temp_sup-Plan_polar_R'	37,8185339	10,644779	-19,135848
'Pole_temporal_R'	32,0010683	10,8225352	-42,322704
'G_front_inf-Opercular_R'	53,0049681	13,2134486	7,86952158
'G_insular_short_R'	40,1523395	13,2278407	-3,9137817
'G_front_inf-Opercular_L'	-52,695732	13,4175965	10,8084564
'G_and_S_cingul-Mid-Ant_L'	-6,3511835	17,120075	36,7664882
'G_and_S_cingul-Mid-Ant_R'	5,64775196	18,6216281	37,9453958
'Lat_Fis-ant-Vertical_L'	-47,339246	20,4408408	9,84885165
'S_front_sup_L'	-24,146665	22,3512719	44,793897
'S_circular_insula_ant_L'	-31,336991	22,5220224	-8,4050156
'Lat_Fis-ant-Vertical_R'	50,3782686	23,1261706	8,80138268
'S_circular_insula_ant_R'	31,7375088	23,9660666	-8,2205039
'S_orbital_med-olfact_L'	-12,789413	26,2275148	-20,002537
'S_orbital_med-olfact_R'	11,3397309	26,5968279	-19,801781
'S_front_inf_L'	-40,559908	26,8651178	19,8092285
'S_front_sup_R'	23,9212788	26,8800996	43,9376926
'G_front_sup_L'	-9,8095551	27,1560262	46,6208742
'G_front_inf-Orbital_L'	-48,374082	27,7471761	-10,024611
'G_front_sup_R'	9,54122583	28,6498217	46,1859897
'S_front_inf_R'	40,022604	29,0828579	20,520266
'Lat_Fis-ant-Horizont_R'	40,7323844	29,6613769	-1,9917581
'G_front_inf-Triangul_L'	-52,34446	30,9573826	2,63543048
'Lat_Fis-ant-Horizont_L'	-43,401756	32,2568612	-4,6294391
'G_rectus_R'	2,87156024	32,3256205	-25,355636
'G_front_inf-Triangul_R'	53,2683917	32,6627652	5,90740657
'G_orbital_L'	-31,042782	34,1044698	-20,590706
'G_orbital_R'	29,1962396	35,6463052	-20,406356
'G_front_middle_L'	-38,591993	35,7733403	33,0580822
'G_front_inf-Orbital_R'	51,1508807	36,9698238	-13,594139
'S_orbital-H_Shaped_L'	-27,354868	37,6675795	-16,42051
'G_rectus_L'	-4,1211068	38,1418317	-23,422932
'G_front_middle_R'	38,6936979	38,2369656	32,078083
'S_orbital-H_Shaped_R'	26,8075877	38,7712856	-16,740152
'S_suborbital_R'	3,15998605	41,9296244	-16,421215
'G_and_S_cingul-Ant_R'	5,85787713	42,3592462	4,55362515
'G_and_S_cingul-Ant_L'	-7,2514034	42,3919445	6,63595362
'S_suborbital_L'	-5,220484	43,9476634	-12,708837
'S_orbital_lateral_L'	-43,648027	45,4283591	-5,5656196
'S_orbital_lateral_R'	43,6923782	46,5803129	-3,1078501

'S_front_middle_L'	-28,307357	47,0646389	19,3032746
'S_front_middle_R'	28,9039738	47,4571278	17,8662803
'G_and_S_frontomargin_L'	-25,310918	60,9520505	-9,0834118
'G_and_S_frontomargin_R'	21,2763927	63,2872608	-11,452679
'G_and_S_transv_frontopol_L'	-16,838447	68,2448486	-2,3301895
'G_and_S_transv_frontopol_R'	17,4681568	68,4477277	0,18827672

Table A – Network node coordinates based on the atlas by (Destrieux *et al.*, 2010). Nodes are computed as mass centroids within each parcellated region.